

Anti-leishmanial Potential of Novel β -carboline Analogues - Synthesis, Screening and Molecular Mechanistic Studies

THESIS

Submitted in partial fulfillment
of the requirements for the degree of
DOCTOR OF PHILOSOPHY

by

Mr. Banoth Karan Kumar

2018PHXF0042P

Under the Supervision of

Prof. S. Murugesan



BITS Pilani

Pilani | Dubai | Goa | Hyderabad

BIRLA INSTITUTE OF TECHNOLOGY AND SCIENCE, PILANI

Pilani Campus

2023

Contents

| | |
|-----------------------|-----------|
| Declaration | i |
| Certificate | ii |
| Acknowledgements | iii-v |
| List of abbreviations | vi-x |
| List of Figures | xi-xiv |
| List of Tables | xv |
| Abstract | xvi-xviii |

| | | |
|------------------|---|---------|
| Chapter 1 | Leishmaniasis – An overview | 1-19 |
| Chapter 2 | Literature review on β -carboline | 20-63 |
| Chapter 3 | Objectives and plan of work | 64-66 |
| Chapter 4 | Design and <i>in-silico</i> prediction of drug-likeness properties | 67-82 |
| Chapter 5 | Synthesis and characterization of the designed analogues | 83-119 |
| Chapter 6 | Anti-leishmanial, cell viability and Trypanothione reductase inhibition assay | 120-146 |
| Chapter 7 | Molecular docking and molecular dynamics studies | 147-175 |
| Chapter 8 | Conclusion and future perspectives | 176-182 |
| Chapter 9 | List of publications and conferences | 183-191 |

| | |
|-----------------|--------------|
| Appendix | Bibliography |
|-----------------|--------------|

Declaration

I hereby declare that the work carried out in this thesis titled "**Anti-leishmanial Potential of Novel β -carboline Analogues - Synthesis, Screening and Molecular Mechanistic Studies**" is an original piece of research work carried out under the guidance of **Prof. S. Murugesan** at BITS-Pilani, Pilani Campus, Pilani, India. This thesis has not been submitted by me for the award of any other degree of any other University/Institute.

Name: **BANOTH KARAN KUMAR**

ID No: **2018PHXF0042P**

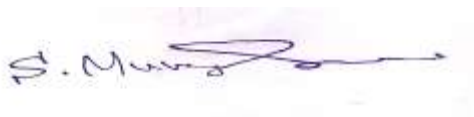
Signature:

Date:

BIRLA INSTITUTE OF TECHNOLOGY AND SCIENCE, PILANI

CERTIFICATE

This is to certify that the thesis entitled “**Anti-leishmanial Potential of Novel β -carboline Analogues - Synthesis, Screening and Molecular Mechanistic Studies**” and submitted by **Mr. Banoth Karan Kumar** ID No. **2018PHXF0042P** for the award of Ph. D. of the institute embodies original work done by him under my supervision.



Signature of the Supervisor:

Name in capital letters: **Prof. S. MURUGESAN**

Designation: **Professor,**

Department of Pharmacy,

Birla Institute of Technology and Science, Pilani

Pilani Campus, Pilani-333031. Rajasthan.

Date: 14-07-2023

Acknowledgements

I would like to present my wholehearted gratitude to my Ph. D. supervisor, **Prof. S. Murugesan**, Professor, Department of Pharmacy, BITS Pilani, Pilani Campus, Pilani for giving me an opportunity to learn and grow under his guidance. He is one of those teachers who believe in bringing out the best of his students. As the saying goes, “*The best teachers are those who show you where to look but don’t tell you what to see*”. He always followed this approach and that helped me to learn and explore things beyond the routine lab work which I believe is going to help me soon. Apart from research, he taught us the value of punctuality, planning, ethics and humility by example. He trained us to think, think and think some more before starting any work. He believed in extensive thought processes and planning before beginning any work. Besides, he was always there to help and advice regarding the work or personal issues whenever required. It won’t be wrong to say that words would not suffice in describing his contribution to my Ph. D.

I will always be grateful to, **Prof. Rafael Balana Fouce**, Professor, University de Leon, Leon, Spain. He was the one who involved in the Leishmanial screening of all our synthesized analogs. Without him, I suppose I would not have been completed this task.

It has been a matter of pride and honour for me to be a student of BITS Pilani. This thesis would not have seen the light of the day without the infrastructural and administrative support from the institute for which I owe a special thanks to **Prof. V. Ramgopal Rao** Vice-Chancellor, BITS Pilani, **Prof. Souvik Bhattacharyya**, Ex-Vice-Chancellor, BITS Pilani, **Prof. Sudhir Kumar Barai**, Director, BITS Pilani, Pilani Campus, **Prof. Sanjay Kumar Verma**, Dean, Administration, BITS Pilani. I wish to extend special thanks to **Prof. Shamik Chakraborty**, Associate Dean, Academic Graduate Studies and Research (AGSR) Division for their administrative support.

I sincerely thank **Prof. Anil Bhanudas Gaikwad**, Professor & Head, **Prof. Anil Jindal**, Convener, Departmental Research Committee (DRC), Department of Pharmacy, BITS Pilani, Pilani Campus, for their timely suggestions, intellectual guidance, and support during various stages of my doctoral program. This thesis work would not have been the same without the scientific inputs, enthusiastic discussions and evaluation from my DAC members, **Prof. Hemant R Jadhav** and **Prof. Atish T Paul**, Department of Pharmacy, BITS Pilani, Pilani Campus.

I would also like to extend my sincere gratitude to the faculty members **Prof. R. Mahesh, Prof. Rajeev Taliyan, Prof. Deepak Chitkara, Prof. Anupama Mittal, Prof. Aniruddha Roy, Dr. Gautam Singhvi, Dr. Murli Manohar Pandey, Dr. Sandeep Sundriyal, Dr. Richa Srivastava** who have supported me during my research and teaching practice. I would also express my gratitude towards **Prof. K.V.G. Chandrasekhar** (BITS Hyderabad) and his scholar **Mr. Adi Narayana** for their constant support in my Ph.D. Journey. I wish to thank all non-teaching staffs **Mr. Rampratap Suthar, Mr. Puran, Mr. Lakshman, Mr. Navin, Mr. Tarachand, Mr. Surendar, Mr. Mukesh** and **Mr. Mahender** for their direct and indirect help and support during my doctoral program.

I would like to make a special mention to **Dr. Penta Ashok** and **Dr. Subhash Chander, Dr. Pritesh Bhat** for taking out time from their busy schedules and helping in setting up the experiments and analysing results whenever I was stuck. I also received great help and support from my juniors in the lab, **Mr, Faheem, Mr. Ala chandu, Mr. Rehman, Ms, Pranali Kuthe.** A constant support from the Master students **Mr. Faheem, Ms, Abhirami, Ms. Samridhi, Ms. Sanchita, Ms, Snehal Jadhav, Ms. Renuka Joshi, Mr. Kishore,** during my work. We had fruitful discussions regarding each other's work, and they made sure that the lab is running smoothly. They also ensured that the lab environment remained jovial, and we enjoyed working together.

I wholeheartedly thank **Dr. Himanshu** and **Mr. Arihant Kumar Singh** for being my roommates besides being my colleagues who made my stay in BITS-Pilani, a wonderful experience. Special thanks to the persons **Ms. Moumita,** and **Ms. Geetika** with them I can discuss the work and vent out our frustrations at times. A steadfast supporter of my professional and personal life is **Ms. Komalatha,** she is the one who encouraged me from the very beginning.

I am happy to acknowledge my senior colleagues, **Dr. Ginson, Dr. Kishan, Dr. Krishna, Dr. Pracheta, Dr. Sudeep, Dr. Saurabh, Dr. Dhanashree, Dr. Vamsi, Dr. Sharath, Ds. Swetha, Ds. Swati, Dr. Violina, Dr. Paramita, Dr. Vishal, Ms. Nikita, Dr. Samrat** who guided me through the thick and thins during my Ph.D. and survival at the department and BITS. I would also like to thank my other colleagues in the department **Mr. Amritansh, Mr. Prabhjeet, Mr. Deepak, Mr. Kedar, Mrs. Ravali Mahipal, Mr. Rupesh, Mr. Imran, and Ds. Tejashree, Ms. Nikitha, Mrs. Urmila Rajesh, Ms. Aishwarya,** for all the memorable moments we spent on the campus. I would also like to mention my lovely juniors **Ms. Kavya, Ms. Vidya, Ms. Manisha, Ms. Sharayu, Ms. Shreya, Mr. Mukesh, Mr. Amit, Mr. Atharva, Mr. Prashant, Ms. Nisha Yadav, Mr. Shubham, Mr. Sai Pradyuth** and **Mr. Shivanshu, Mr. Giriprasad**

for their bright smiles and positive attitudes with which they met me each day and inspired me to keep working.

In granting me the financial assistance for my doctoral research, I would like to thank **Department of Biotechnology - Indo-Spain Bilateral Programme (Ref. No: BT/IN/Spain/39/SM/2017–2018)** and **National Fellowship for Scheduled Tribes (NFST), Ministry of Tribal affairs, Govt of India (Award no- 201920-NFST-TEL-01497)**.

Thanks to the unwavering support and blessings of my family. Everything I own is due to their support. In the first place, I would like to thank my parents, Shri. **Banoth Mangtiya Nayak**, and Mrs. **Banoth Malathi**, for their loyalty, support, and encouragement, as well as for enabling me to write a thesis. Having my father as an inspiration has always been a great source of motivation for me. Special acknowledgement goes to my elder brother **Mr. Banoth Raj Kumar**, and sister Mrs. **Jarpula Swathi Laxman** without which my life would not be what it is. As well as **Mr. Chaved** and **Mr. Tony** for their unstinting love, I want to give my thanks to my nephews.

Banoth Karan Kumar

List of Abbreviations / Symbols

| Abbreviations | |
|----------------------------|---|
| HEPES | (4-(2-hydroxyethyl)-1-piperazineethanesulfonic acid) |
| HEPES | (4-(2-hydroxyethyl)-1-piperazineethanesulfonic acid) |
| EDCI. HCl | 1-Ethyl-3-(3-dimethylaminopropyl)-carbodiimide |
| DTNB | 5,5'-dithio-bis-(2-nitrobenzoic acid) |
| 5-HT | 5-hydroxytryptamine |
| ADMET | Absorption, distribution, metabolism, excretion, toxicity |
| ATP | Adenosine triphosphate |
| ALA | Alanine |
| α | Alpha |
| AmB-D | Amphotericin B deoxycholate |
| Å | Angstrom |
| Log S | Aqueous solubility |
| ARG | Arginine |
| ASN | Asparagine |
| ASP | Aspartic acid |
| <i>B. cereus</i> | <i>Bacillus cereus</i> |
| β | Beta |
| BSA | Bovine serum albumin |
| CaCl₂ | Calcium chloride |
| <i>C. gattii</i> | <i>Cryptococcus gattii</i> |
| CL | Cutaneous leishmaniasis |
| CDK | Cyclin-dependent kinase |
| CDK12 | Cyclin-dependent kinase 12 |
| CYS | Cysteine |
| δ | Delta |
| DENV | Dengue virus |
| DNA | Deoxyribonucleic acid |
| DCM | Dichloromethane |
| DMSO | Dimethyl sulfoxide |
| d | Doublet |
| DNDi | Drugs for Neglected Diseases initiative |

| | |
|------------------------|--|
| DTNB | Ellman's reagent (5,5'-dithiobis-(2-nitrobenzoic acid) |
| <i>E. coli</i> | <i>Escherichia coli</i> |
| EDTA | Ethylenediaminetetraacetic acid |
| XP | Extra precision |
| FAD | Flavin adenine dinucleotide |
| DMEM | Glutamax Dulbecco's modified eagle's medium |
| GLU | Glutamic acid |
| GSK | Glycogen synthase kinase |
| g | Gram |
| EC₅₀ | Half maximal Effective concentration |
| IC₅₀ | Half maximal Inhibitory concentration |
| HSV | <i>Herpes simplex virus</i> |
| HRMS | High resolution mass spectrometry |
| HTS | High throughput screening |
| HIS | Histidine |
| HIV | Human Immunodeficiency Virus |
| HCl | Hydrochloric acid |
| HBA | Hydrogen bond acceptor |
| HBD | Hydrogen bond donor |
| HOBt | Hydroxy benzotriazole |
| IR | Infrared spectroscopy |
| ID | Intradermal |
| IM | Intramuscular |
| Kg | Kilogram |
| <i>L. aethiopica</i> | <i>Leishmania aethiopica</i> |
| <i>L. amazonensis</i> | <i>Leishmania amazonensis</i> |
| <i>L. braziliensis</i> | <i>Leishmania braziliensis</i> |
| <i>L. chagasi</i> | <i>Leishmania chagasi</i> |
| <i>L. donovani</i> | <i>Leishmania donovani</i> |
| LdTR | <i>Leishmania donovani</i> Trypanothione reductase |
| <i>L. guyanensis</i> | <i>Leishmania guyanensis</i> |
| <i>L. infantum</i> | <i>Leishmania infantum</i> |
| <i>L. major</i> | <i>Leishmania major</i> |
| <i>L. mexicana</i> | <i>Leishmania mexicana</i> |

| | |
|-------------------------|--|
| <i>L. panamensis</i> | <i>Leishmania panamensis</i> |
| <i>L. tropica</i> | <i>Leishmania tropica</i> |
| LEU | Leucine |
| LYS | Lysine |
| MgCl₂ | Magnesium chloride |
| MRSA | Methicillin-resistant <i>Staphylococcus aureus</i> |
| MRSE | Methicillin-resistant <i>Staphylococcus epidermidis</i> |
| MET | Methionine |
| μM | Micro molar |
| mg | Milli gram |
| mM | Milli molar |
| mL | Millilitre |
| mmol | Millimole |
| MIC | Minimum inhibitory concentration |
| MAPK | Mitogen-activated protein kinase |
| mol | Mole |
| MD | Molecular dynamics |
| MMGBSA | Molecular mechanics with generalized Born and surface area solvation |
| MWT | Molecular weight |
| MCL | Mucocutaneous leishmaniasis |
| m | Multiplet |
| <i>M. tuberculosis</i> | <i>Mycobacterium tuberculosis</i> |
| nm/sec | Nanomolar/second |
| NTD | Neglected tropical diseases |
| NADPH | Nicotinamide adenine dinucleotide phosphate |
| OD | Optical density |
| OPLS3e | Optimized Potentials for Liquid Simulations 3 |
| ppm | Parts per million |
| PHE | Phenylalanine |
| <i>P. falciparum</i> | <i>Plasmodium falciparum</i> |
| <i>P. knowlesi</i> | <i>Plasmodium knowlesi</i> |
| <i>P. malariae</i> | <i>Plasmodium malariae</i> |
| <i>P. ovale</i> | <i>Plasmodium ovale</i> |

| | |
|-------------------------------------|---|
| <i>P. vivax</i> | <i>Plasmodium vivax</i> |
| PKDL | Post-kala-azar dermal leishmaniasis |
| KCl | Potassium chloride |
| PRO | Proline |
| PDB | Protein data bank |
| PLC | Protein ligand complex |
| ¹H NMR | Proton nuclear magnetic resonance |
| RGY | Radius of Gyration |
| ROS | Reactive oxygen species |
| RCSB | Research Collaboratory for Structural Bioinformatics |
| RESPA | Reversible reference system Propagator Algorithm |
| rt | Room temperature |
| RMSD | Root mean square deviation |
| RMSF | Root mean square fluctuation |
| <i>S. cerevisiae</i> | <i>Saccharomyces cerevisiae</i> |
| <i>S. typhi</i> | <i>Salmonella typhi</i> |
| SI | Selectivity index |
| SIA | Selectivity index of Amastigotes |
| SIP | Selectivity index of Promastigotes |
| SER | Serine |
| s | Singlet |
| NaHCO₃ | Sodium bicarbonate |
| NaCl | Sodium chloride |
| SDS-PAGE | Sodium dodecyl-sulfate polyacrylamide gel electrophoresis |
| NaOH | Sodium hydroxide |
| Na₂SO₄ | Sodium sulfate |
| SASA | Solvent accessible surface area |
| <i>S. aureus</i> | <i>Staphylococcus aureus</i> |
| <i>S. epidermidis</i> | <i>Staphylococcus epidermidis</i> |
| <i>S. pneumoniae</i> | <i>Streptococcus pneumoniae</i> |
| <i>S. pyogenes</i> | <i>Streptococcus pyogenes</i> |
| SAR | Structure activity relationship |
| SC | Sub-cutaneous |
| THF | Tetrahydrofuran |

| | |
|-------------------------|---------------------------|
| TLC | Thin layer chromatography |
| SOCl₂ | Thionyl chloride |
| THR | Threonine |
| t | Triplet |
| <i>T. brucei</i> | <i>Trypanosoma brucei</i> |
| <i>T. cruzi</i> | <i>Trypanosoma cruzi</i> |
| TS2 | Trypanothione |
| TR | Trypanothione reductase |
| TS | Trypanothione synthetase |
| TXNSH | Tryparedoxin |
| TXNP | Tryparedoxin peroxidase |
| TRP | Tryptophan |
| TYR | Tyrosine |
| VAL | Valine |
| VL | Visceral leishmaniasis |
| WHO | World health organization |

List of Figures

| Figure No | Caption | P. No |
|------------------|--|--------------|
| 1.1 | Lifecycle of Leishmaniasis (sandfly and human stages) | 4 |
| 1.2 | Structure of currently marketed drugs for the treatment of Leishmaniasis | 7 |
| 1.3 | Structure of azole antifungals | 8 |
| 1.4 | Structure of antitubercular drugs | 9 |
| 1.5 | Structure of antileishmanial compounds under clinical trials | 10 |
| 2.1 | Structural diversity of carbolines (1a-12a) | 21 |
| 2.2 | Commercialized β -carboline drugs and their pharmacological activity (13a-21a) | 22 |
| 2.3 | Structure of compounds 22a, 23a and 24a | 23 |
| 2.4 | Structure of compounds 25a, 26a and 27a | 23 |
| 2.5 | Structure of compounds 28a and 29a | 24 |
| 2.6 | Structure of compound 30a | 24 |
| 2.7 | Structure of compound 31a | 24 |
| 2.8 | Structure of compound 32a | 25 |
| 2.9 | Structure of compound 33a | 25 |
| 2.10 | Structure of compound 34a | 25 |
| 2.11 | Structure of compound 35a | 26 |
| 2.12 | Structure of compounds 36a, 37a and 38a | 26 |
| 2.13 | Structure of compounds 39a and 40a | 27 |
| 2.14 | Structure of compounds 41a and 42a | 27 |
| 2.15 | Structure of compound 43a | 28 |
| 2.16 | Structure of compounds 44a and 45a | 28 |
| 2.17 | Structure of compounds 46a, 47a and 48a | 29 |
| 2.18 | Structure of compound 49a | 29 |
| 2.19 | Structure of compounds 50a and 51a | 30 |
| 2.20 | Structure of manzamine alkaloids (52a-59a) | 30 |
| 2.21 | Structure of various isolated eudistomins (60a-65a) | 31 |
| 2.22 | Structure of compound 66a | 32 |
| 2.23 | Structure of compounds 67a-69a | 33 |

| | | |
|-------------|---|-----|
| 2.24 | Structure of compounds 70a-73a | 34 |
| 2.25 | Structure of sacleuximine A (74a) | 34 |
| 2.26 | Structure of compound (75a) | 35 |
| 2.27 | Structure of compound (76a) | 36 |
| 2.28 | Structure of compound 77a | 37 |
| 2.29 | Structure of Eudistomin U (78a) and compound 79a | 37 |
| 2.30 | Structure of griseofamine A (80a) and 16-epi-griseofamine A (81a) | 38 |
| 2.31 | Structure of compounds 82a and 83a | 38 |
| 2.32 | Structure of compounds 84a-87a | 39 |
| 2.33 | Structure of compounds 88a-92a | 40 |
| 2.34 | Structure of compound 93a | 41 |
| 2.35 | Structure of compounds 94a-97a | 42 |
| 2.36 | Structure of compounds 98a-101a | 43 |
| 2.37 | Structure of 9 <i>N</i> -methylharmine (102a) and harmol (103a) | 43 |
| 2.38 | Structure of compounds 104a-106a | 44 |
| 2.39 | Structure of compounds 107a-109a | 44 |
| 2.40 | Structure of compounds 110a-112a | 45 |
| 2.41 | Structure of compounds 113a and 114a | 46 |
| 2.42 | Structure of compound 115a | 47 |
| 2.43 | Structure of compounds 116a and 117a-120a | 47 |
| 2.44 | Structure of compounds 121a and 122a | 48 |
| 2.45 | Structure of compound 123a | 48 |
| 2.46 | Structure of compounds 124a-126a | 48 |
| 2.47 | Structure of compound 127a | 49 |
| 2.48 | Structure activity relationship study of β -carboline associated with its anti-leishmanial activity | 51 |
| 4.1 | Previously identified hits molecules | 68 |
| 4.2 | Newly designed analogues | 69 |
| 6.1 | Structure of the potent active molecules against promastigotes | 127 |
| 6.2 | Structure of the significantly active molecules against promastigotes | 127 |
| 6.3 | Structure of the moderately active molecules against promastigotes | 128 |
| 6.4 | Structure of the potent active molecules against amastigotes | 130 |

| | | |
|-------------|--|-----|
| 6.5 | Structure of the significantly active molecules against amastigotes | 131 |
| 6.6 | Structure of the moderately active molecules against amastigotes | 131 |
| 6.7 | Structure of the duly active molecules against both promastigotes and amastigotes | 132 |
| 6.8 | Structure of the potent active molecules against amastigotes with their cell viability value | 133 |
| 6.9 | Lead compounds identified from the previous studies | 138 |
| 6.10 | Structure Activity Relationship studies of the β -carboline analogues | 138 |
| 6.11 | Structure activity relationship study of β -carbolines associated with its Trypanothione reductase inhibitory activity | 143 |
| 7.1 | Superimposed view of FAD molecule in the active site of the target protein (PDB-2JK6) and its re-docked pose in the same target (RMSD – 0.20 Å) | 150 |
| 7.2 | Exposed amino-acid residue interactions (3D and 2D) of the significantly active compounds 68, 72 and 75 in the active site of the target protein PDB:2JK6 | 154 |
| 7.3 | Exposed amino-acid residue interactions (3D and 2D) of the significantly active compounds 77, 91 and 100 in the active site of the target protein PDB:2JK6 | 155 |
| 7.4 | Exposed amino-acid residue interactions (3D and 2D) of the significantly active compounds 78, 70 and standard TR inhibitor in the active site of the target protein PDB:2JK6 | 156 |
| 7.5 | MMGBSA plot of topmost identified hit molecules (compound codes 72, 68, 70, 75, 77, 78, 91, 100) | 157 |
| 7.6 | RMSD plot of protein and ligand of topmost identified hit molecules (compound codes 72, 68, 70, 75, 77, 78, 91, 100) | 158 |
| 7.7 | RMSF plot of topmost identified hit molecules (compound codes 72, 68, 70, 75, 77, 78, 91, 100) | 159 |
| 7.8 | RGY plot of topmost identified hit molecules (compound codes 72, 68, 70, 75, 77, 78, 91, 100) | 160 |
| 7.9 | Time frame analysis of compound 68 at 1, 25, 50, 75 and 100 ns during the Molecular dynamics simulation | 167 |

| | | |
|-------------|---|-----|
| 7.10 | Time frame analysis of compound 72 at 1, 25, 50, 75 and 100 ns during the Molecular dynamics simulation | 168 |
| 7.11 | Time frame analysis of compound 70 at 1, 25, 50, 75 and 100 ns during the Molecular dynamics simulation | 169 |
| 7.12 | Time frame analysis of compound 91 at 1, 25, 50, 75 and 100 ns during the Molecular dynamics simulation | 170 |
| 7.13 | Time frame analysis of compound 100 at 1, 25, 50, 75 and 100 ns during the Molecular dynamics simulation | 170 |
| 7.14 | Time frame analysis of compound 77 at 1, 25, 50, 75 and 100 ns during the Molecular dynamics simulation | 171 |
| 7.15 | Time frame analysis of compound 75 at 1, 25, 50, 75 and 100 ns during the Molecular dynamics simulation | 172 |
| 7.16 | Time frame analysis of compound 78 at 1, 25, 50, 75 and 100 ns during the Molecular dynamics simulation | 173 |
| 8.1 | Pictorial representation of summarized β -carboline analogues with their promastigote and amastigote inhibitory activity spectrum | 181 |

List of Tables

| Table No | Caption | P. No |
|-----------------|--|--------------|
| 1 | The optimum range of physicochemical parameters followed by 95% of the approved drugs | 70 |
| 2 | Forecasted ADME results of the designed analogues of scheme 1 | 73 |
| 3 | Forecasted ADME results of the designed analogues of scheme 2 | 73 |
| 4 | Forecasted ADME results of the designed analogues of scheme 3 | 74 |
| 5 | Forecasted ADME results of the designed analogues of scheme 4 | 74 |
| 6 | Forecasted ADME results of the designed analogues of scheme 5 | 75 |
| 7 | Forecasted ADME results of the designed analogues of scheme 6 | 75 |
| 8 | Forecasted ADME results of the designed analogues of scheme 7 | 76 |
| 9 | Forecasted ADME results of the designed analogues of scheme 8 | 76 |
| 10 | Forecasted toxicity results of the designed analogues of scheme 1 | 77 |
| 11 | Forecasted toxicity results of the designed analogues of scheme 2 | 77 |
| 12 | Forecasted toxicity results of the designed analogues of scheme 3 | 78 |
| 13 | Forecasted toxicity results of the designed analogues of scheme 4 | 78 |
| 14 | Forecasted toxicity results of the designed analogues of scheme 5 | 79 |
| 15 | Forecasted toxicity results of the designed analogues of scheme 6 | 79 |
| 16 | Forecasted toxicity results of the designed analogues of scheme 7 | 80 |
| 17 | Forecasted toxicity results of the designed analogues of scheme 8 | 80 |
| 18 | Results of <i>L. infantum</i> promastigotes inhibition assay | 134 |
| 19 | Results of <i>L. infantum</i> amastigotes inhibition assay | 135 |
| 20 | Results of cell viability assay using human hepatoma (HepG2) cells | 136 |
| 21 | Results of selectivity index of the antileishmanial activities | 137 |
| 22 | Results of Trypanothione reductase inhibition assay | 142 |
| 23 | Molecular docking studies of titled compounds in the active site of target protein (PDB:2JK6) | 152 |
| 24 | 2D interaction of protein-ligand contacts of the potent molecules with target protein (PDB:2JK6) | 162 |
| 25 | Plot of potent ligands protein contacts | 165 |

Abstract

Leishmaniasis is a vector-borne complex disease classed as a neglected tropical disease (NTD) by World Health Organization (WHO). It is caused by the trypanosomatids parasite and transmitted by female sandflies. Leishmaniasis affects 98 nations, mostly low-income developing countries with 0.7 to 1 million new cases annually. Around 350 million people are at risk, 12 million are affected and one million new cases occur every year. Current leishmaniasis pharmacology uses few drugs which were obsolete, had severe adverse effects, and with few exceptions, formulated to be administered parenterally.

β -carboline (*9H*-pyrido-[3,4-*b*]-indole), is an indole alkaloid having a pyridine-indole ring. β -carbolines possess anticancer, antiviral, antibacterial, antifungal, antileishmanial, antithrombotic, anti-inflammatory, etc. effects. In turn, academics, and industry focus on a chemically flexible moiety. Since last decade, researchers have sought a Leishmaniasis vaccine but unfortunately, all results are disappointing. β -carboline analogues may be a potential lead according to the reported works of literature and our findings also agreed. Using β -carboline analogues, the investigations were carried out and found the designed β -carboline analogues as significant anti-leishmanial agents and less toxic with superior Absorption, Distribution, Metabolism, and Excretion (ADME) profiles. The β -carboline was synthesized by Pictet-Spengler reaction using DL-tryptophan and 5-hydroxy tryptophan as the starting materials. The starting materials were initially reacted with thionyl chloride for esterification followed by ring annulation, and conversion of ester to carboxylic acid. Finally, acid amide coupling reaction was done with the aid of coupling agents like *N*-Ethyl-*N'*-(3-dimethylaminopropyl) carbodiimide hydrochloride (EDC hydrochloride) and 1-Hydroxybenzotriazole hydrate (HOBt) with various substituted phenyl piperazines. The synthesized molecules (Total of 128) were characterized by IR, NMR and Mass spectroscopy analytical methods.

The molecules were segregated into the following series, (6-bromo-1-phenyl-*9H*-pyrido-[3,4-*b*]-indol-3-yl)(4-phenylpiperazin-1-yl)-methanone derivatives (**1-16**), (6-nitro-1-phenyl-*9H*-pyrido-[3,4-*b*]-indol-3-yl)(4-phenylpiperazin-1-yl)-methanone derivatives (**17-32**), (6-chloro-1-phenyl-*9H*-pyrido-[3,4-*b*]-indol-3-yl)(4-phenylpiperazin-1-yl)-methanone derivatives (**33-48**), (6-hydroxy-1-phenyl-*9H*-pyrido-[3,4-*b*]-indol-3-yl) (4-phenylpiperazin-1-yl)-methanone derivatives (**49-64**), (6-bromo-9-methyl-1-phenyl-*9H*-pyrido-[3,4-*b*]-indol-3-yl)(4-(4-methoxyphenyl)-piperazin-1-yl)-methanone (**65-80**), (4-(4-methoxyphenyl)-piperazin-1-yl)(9-methyl-6-nitro-1-phenyl-*9H*-pyrido-[3,4-*b*]-indol-3-yl)-methanone (**81-96**), (6-chloro-9-methyl-1-phenyl-*9H*-pyrido-[3,4-*b*]-indol-3-yl)(4-(4-methoxyphenyl)-piperazin-1-yl)-

methanone (**97-112**), (6-hydroxy-9-methyl-1-phenyl-9*H*-pyrido-[3,4-*b*]-indol-3-yl)(4-(*p*-tolyl)piperazin-1-yl)-methanone (**113-128**).

The synthesized compounds were screened for the *in-vitro* anti-leishmanial Promastigote activity (*L. infantum* BCN150 iRFP promastigotes (iRFP-*L. infantum*)), *in-vitro* anti-leishmanial Amastigote activity (*L. infantum* BCN150), cell viability (Human hepatocarcinoma cell HepG2 line (ATCC HB-8065), molecular mechanistic studies by Trypanothione reductase inhibition assay. The critical analysis of screening results offered several intriguing takeaways.

The outcomes of the promastigotes revealed 37 promising molecules. In that 12 molecules are more potent than the standard drug. The compound **72** - $5.20 \pm 0.54 \mu\text{M}$, and compound **60** - $7.59 \pm 2.96 \mu\text{M}$ were potently active molecules. A total of 8 molecules were found significant with the EC_{50} less than $25 \mu\text{M}$. Around 17 moderately active molecules were also identified with EC_{50} in the range of $25\text{-}50 \mu\text{M}$. The results of the amastigote screening discovered 47 promising molecules. In that around 12 molecules are more potent than the standard drug Miltefosine. The compound **70** - $0.46 \pm 0.06 \mu\text{M}$, and compound **77** - $0.45 \pm 0.03 \mu\text{M}$ were potently active molecules. A total of 9 molecules were found significant with the EC_{50} less than $10 \mu\text{M}$. Around 26 moderately active molecules were also identified with EC_{50} in the range of $10\text{-}20 \mu\text{M}$. Around 15 molecules showed dual inhibition against both promastigotes and amastigotes. Among those compounds, compound **9** showed the EC_{50} - $12.68 \pm 8.171 \mu\text{M}$ (promastigotes); $8.52 \pm 0.66 \mu\text{M}$ (amastigotes) and compound **72** with EC_{50} - $5.20 \pm 0.54 \mu\text{M}$ (promastigotes); $1.28 \pm 0.19 \mu\text{M}$ (amastigotes). Out of 128 molecules, around 73 molecules exhibited CC_{50} more than $50 \mu\text{M}$ (Human hepatocarcinoma cells HepG2 line (ATCC HB-8065)). This indicates the screened analogues did not reveal any hepatotoxicity.

A molecular mechanistic exploration study against trypanothione reductase (TR) activity was performed. Compounds **78**, **68**, **81**, **70**, **96** and **88** inhibited TR by $50 \pm 1 \%$, $43 \pm 1 \%$, $38 \pm 5 \%$, $36 \pm 5 \%$, $33 \pm 3 \%$ and $31 \pm 2 \%$, respectively at $50 \mu\text{M}$ tested concentration. Compounds **78**, **68**, **81**, **15** and **109** inhibited TR by $100 \pm 2 \%$, $63 \pm 1 \%$, $61 \pm 1 \%$, $57 \pm 2 \%$ and $47 \pm 1 \%$, respectively at $100 \mu\text{M}$ tested concentration. From the obtained results, it has been presumed that TR is not the only molecular target that the titled β -carboline derivatives are attempting to hit. Hence, further detailed investigations will be required against other possible available targets of leishmaniasis in order to determine the exact molecular target on which the anti-leishmanial β -carboline analogues will act.

Molecular docking and dynamics study was also performed using Trypanothione reductase (PDB:2JK6). Binding free energy (MM-GBSA) calculation study also exposed the same and

these identified hit molecules were in the range of -72.25 to -103.45 Kcal/mol. Molecular dynamics RMSD plot of protein backbone against each ligand was also plotted and the results showed similar fluctuating patterns of the protein with all the ligands during the simulation and the RMSD fluctuated between 2.0 - 5.0 Å.

Amino acids such as PHE365, THR335, CYS57, LYS60, ALA365, PHE367 and ARG287 were actively involved in the tight holding of hit molecules against trypanothione reductase. This is a concluding comment that was obtained from the output of the time frame analysis. These amino acids uncovered several contacts with the studied hit molecules, including hydrogen bonds, aromatic bonds, pi interactions and halogen bonds. In addition to this, several interactions that were mediated by water were also engaged in the process of tightly holding the molecules in the active site of the target protein. Investigations using 100 ns of molecular dynamics simulation revealed that the protein-ligand complexes were stable in the active site. Time frame analysis also revealed vital amino acid residues were involved in the bond formation with the identified hit compounds. Final results showed that these compounds shed light on the field of leishmaniasis drug discovery.



Chapter 1. Leishmaniasis – An overview



Chapter 1. Leishmaniasis – An overview

Leishmaniasis is a complex vector-borne disease classified by World Health Organization (WHO) under the denomination of Neglected Tropical Diseases (NTDs). It is caused by at least 20 species of parasitic protozoa of the Family trypanosomatidae and transmitted by the bites of female sandflies. Depending on the species and regions, leishmaniasis can be zoonotic (mainly rodents and canids are the reservoir hosts) or anthroponotic ¹. Current WHO data indicate that leishmaniasis in its different forms affects 98 countries, predominantly low-income developing countries, with 0.7 to 1 million new cases each year ². More than 350 million people are at risk, around 12 million of whom are infected, with an average annual incidence of one million new cases ³. According to clinical manifestations, leishmaniasis is classified into Cutaneous Leishmaniasis (CL), Visceral Leishmaniasis (VL) and Mucocutaneous Leishmaniasis (MCL). Post-kala-azar dermal leishmaniasis (PKDL) or black fever is usually a sequel of VL that appears as a macular, papular or nodular rash usually on the face, upper arms, trunks and other parts of the body. Leishmaniasis in its various clinical manifestations is responsible for 2.35 million disability-adjusted life years (DALYs) lost ⁴⁻⁶. The species responsible for CL are *Leishmania tropica*, *Leishmania major* and *Leishmania aethiopica* in the Old World, whereas *Leishmania mexicana*, *Leishmania amazonensis* and *Leishmania braziliensis* complexes in the New World. There are currently between 600,000 and 1 million new cases of CL each year. Seventy-five percent of new CL cases are detected in Afghanistan, Brazil, Iran, Iraq and Syria. CL, although non-fatal, is responsible for disfiguring lesions and social stigma ⁷. After the sandfly bite, local edema may be formed, leading to a macule that evolves into a papule and eventually develops into a nodule that grows into necrosis and ulceration. Ulcers can heal, but the remaining wounds are a motif of social repulse even after parasitological treatment ⁸. The clinical manifestations of MCL are typical of the New World and are caused by *L. braziliensis* and to a lesser extent by *L. amazonensis*, *Leishmania guyanensis* and *Leishmania panamensis*. The development of the inflammatory process is similar to CL, but lesions may heal spontaneously only to re-appear in the mucosal tissues of the nose and oral cavity (which may extend to the oropharynx and larynx) thus forming chronic destructive lesions responsible for severe disfigurement ⁹. The most severe form of the disease is visceral leishmaniasis (VL), which is caused by *L. donovani* and *L. infantum* in the Old World and *L. infantum*, *Leishmania chagasi* in the New World, and can be fatal in the absence of drug treatment. This form is endemic in many regions of the world, but more than 90% of the global burden is confined to seven countries: India, Somalia, Kenya, Sudan, South Sudan, Ethiopia and Brazil, where most deaths are accounted for ^{1,6}. Symptoms

Chapter 1. Leishmaniasis – An overview

include weight loss, chronic fever, lymphadenopathy, pancytopenia, muscle atrophy and hepatosplenomegaly, with liver and spleen being palpable in the enlarged abdomen of patients¹⁰.

Host's immunocompetence is very important for the development of leishmaniasis. In this scenario, Leishmania-HIV co-infections are considered as serious complication in 35 countries in the Indian sub-continent, East Africa and Brazil¹¹. A second problem associated with VL is post-kala-azar dermal leishmaniasis (PKDL), a disfiguring skin sequela that is developed by 50% of VL patients in Sudan and 1-3% of VL patients in the Indian sub-continent¹².

A. Leishmaniasis life cycle

Leishmania sp. is a parasitic protist with a digenetic life cycle, which involves one phase in the insect vector and another in the definitive mammalian host species, which can be humans, domestic and wild canids, and other wild animals that can act as reservoirs of the disease. Briefly, the life cycle starts with the ingestion of blood from a naive host by a female phlebotomine infected with *Leishmania*. Upon ingestion, the insect regurgitates some of the ingested blood, thereby inoculating metacyclic (infective) promastigotes (the elongated, flagellated, motile, midgut-resident form of the sandfly), which are phagocytosed by host's neutrophils at the site of the bite^{13,14}. Neutrophils may act by hiding the parasite from the host immune system and facilitating infection by macrophages when they phagocytose the infected apoptotic neutrophils¹⁵. Within the macrophage, promastigotes are transformed into infective amastigotes (rounded, non-flagellated, and non-motile forms present in host phagolysosomes) by the acidic environment and increased temperature of the phagolysosome. The amastigotes divide by binary fission inside the macrophages until they rupture, thus releasing the amastigotes and allowing the surrounding macrophages to phagocytose them. The cycle is completed when a female phlebotomine sandfly ingests blood containing infected cells and the

Chapter 1. Leishmaniasis – An overview

amastigotes transform back to promastigotes inside the insect's hindgut as temperature decreases and pH increases ⁵ (Figure 1.1).

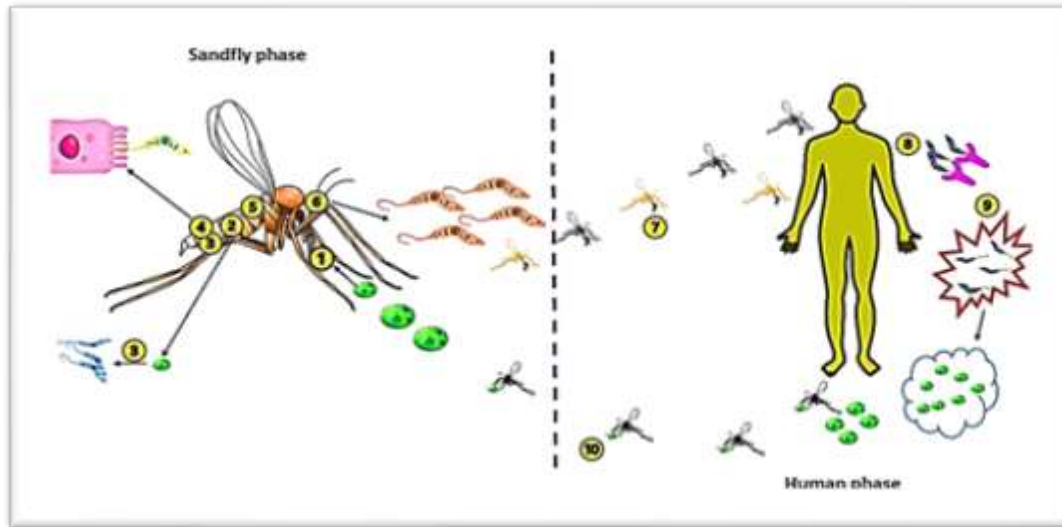


Figure 1.1 Lifecycle of Leishmaniasis (sandfly and human stages)

1. Sandfly sucks blood meal from the infected person in amastigote form **2.** The amastigote form of the parasite travels into the abdominal midgut region of the sandfly **3.** Changes in pH and temperature promote parasite transformation of the amastigote forms to procyclic promastigote form **4.** Procyclic promastigotes convert into nectomonads, which are attached to the microvilli in the midgut region of the sandfly **5.** In the thoracic midgut and stomach valve, the nectomonads transform into haptomads, leptomads, and metacyclic promastigotes **6.** The parasite attaches to the midgut wall and finally migrates back towards the insect mouthparts **7.** The leishmanial infected sandfly bites the healthy human. The site where the sandfly bites are quickly recruited with neutrophils. Recruitment stimulants are proteophosphoglycans secreted in the sandfly saliva and are inoculated along with the parasite into the host during blood meals **8.** A range of macrophage receptors, including complementary receptors (CRs), mannoses, fibronectin receptors, and $\text{Fc}\beta$ receptors ($\text{Fc}\beta\text{R}$), are available to various species of leishmaniasis **9.** Leishmania promastigote acts via its flagellum and various macrophages. This communication provokes intracellular parasite phagocytosis. Low pH, increased temperature, and increased iron absorption induces the parasitophorous vacuole divergence and acidification of promastigote to amastigote. Amastigote parasitophorous vacuole is a very interactive and dynamic organelle to obtain nutrients and additional membranes from the host cell for parasite replication **10.** The amastigote forms are again carried out to the sandflies to infect new hosts

B. Treatment for Leishmaniasis

Vaccination is the most cost-effective method for the prevention of infectious diseases, including parasitic diseases. Prophylaxis protects against disease in the long term and reduces transmission. However, although some countries have effectively used leishmanization in part of their population ¹⁶, none of the vaccines developed against human leishmaniasis have shown remarkable efficacy ¹⁷. This is not the case for canine leishmaniasis where there are marketed vaccines (Leishmune[®], CaniLeish[®]), which showed an effective immunological response for

Chapter 1. Leishmaniasis – An overview

one year¹⁸. The lack of an effective vaccine implies that the main method used to control leishmaniasis when preventive hygiene and vector control measures fail is pharmacotherapy. Current pharmacology against leishmaniasis is based on a handful of chemical compounds (**Figure 1.2**), most of them were outdated, with a multitude of side effects, and, with a few exceptions, formulated to be administered parenterally^{6,18,19}. At present, only one or two of them, at best, would meet the drug target profile requirements to be an antileishmanial drug published by the WHO^{20,21}.

Pentavalent antimonials (Sb^{V}) (Gluca ntime[®], Pentostam[®]) are organometallic derivatives of Sb^{V} that have been used as first-line antileishmanial drugs for 7 decades²². Their mechanism of action is based on interaction with biomolecules containing nitrogen and sulphhydryl ligands (peptides, proteins, enzymes, etc) after the reduction of Sb^{V} to Sb^{III} , which is why they are considered prodrugs²³. It is the only treatment with high success rates for all clinical forms of leishmaniasis, although its overuse has led to the emergence of resistance, especially in the Indian sub-continent²⁴. Sb^{V} -based drugs are repeatedly administered by intramuscular or intravenous routes against VL at a dose of 20 mg/kg body weight, for 30 days with >95% success, but due to the discomfort produced at the site of injection, there is a lack of adherence to treatment with the risk to develop resistances²⁵. These drugs are used locally by intralesional infiltration against Old and New World presentations of CL, although the response varies depending on the species causing the disease²⁶. Despite their efficacy and the large number of lives saved, antimony has a multitude of drawbacks, including high toxicity and side effects, local irritation and pain, cardiac and hepatic alterations, anorexia, nausea, vomiting, myalgia, and arthralgia²⁷. The risk of severe cardiotoxicity precludes its administration in patients over 45 and under 15 years of age²⁸.

Amphotericin B deoxycholate (AMB-D) is a broad-spectrum polyene antifungal drug available since 1960 for the treatment of severe systemic fungal infections²⁹. It has been used as a second-line treatment for VL, thus becoming the treatment of choice in some areas due to the increase in Sb^{V} -resistant strains³⁰. Similarly, to yeasts, the mechanism of action of AMB consists of its selective binding to the parasite's plasma membrane sterols, mainly ergosterol, which creates ion channels that alter the parasite's osmotic balance and the loss of intracellular solutes³¹. AMB is a very effective antileishmanial medication, but it has some drawbacks, such as repeated intravenous administration that requires hospitalization of the patient, unwanted side effects such as fever, myocarditis, nephrotoxicity³², and the poor chemical stability of the drug at high temperatures of many endemic countries³³. AMB has a liposomal version,

Chapter 1. Leishmaniasis – An overview

AmBisome[®], with reduced side effects. It is an expensive but effective treatment and is generally the treatment of choice in pregnant women, HIV-co-infected patients, and other immunocompromised patients³⁴. Single high-dose administration of AmBisome[®] has been the solution to Sb^V resistance problems in the Indian sub-continent, with cure rates above 95%, but not in Africa^{19,27}

Miltefosine (Impavido[®]) is an alkyl phospholipid initially developed as an antineoplastic drug, but it soon demonstrated anti-leishmanial properties. It is the only drug that is administered orally against leishmaniasis³⁵. The mechanism of action is not yet defined but it appears to alter phosphatidylcholine synthesis, inhibit cytochrome c oxidase (decreasing oxygen and ATP available to the parasite that leads to apoptosis-like death), and induces a Th1-type immune response³⁶. A peculiarity of miltefosine is its long half-life (ca. 7 days), which promotes its accumulation during administration³⁷. Miltefosine has side effects such as headache, gastrointestinal disturbances, hepatotoxicity and especially teratogenesis. Therefore, its use should be discontinued in pregnant women or women who expect to become pregnant during treatment³⁸. Allometric dosification of miltefosine in children is required to reach the curative effects described in adults³⁹. Despite the proven efficacy of miltefosine, an increasing number of cases of treatment failure have been reported since its introduction as first-line therapy in the VL elimination program in the Indian sub-continent.⁴⁰

Paromomycin is a broad-spectrum aminoglycoside antibiotic that began to be used in the 1960s as a treatment for leishmaniasis. Its mechanism of action is based on the inhibition of mitochondrial function and interference with protein synthesis⁴¹. In monotherapy there is a risk of resistance and differences in efficacy in different regions, thereby showing high success rates in India but limited efficacy in East Africa⁴². Its efficacy against CL also depends on the species causing the disease⁴³.

Chapter 1. Leishmaniasis – An overview

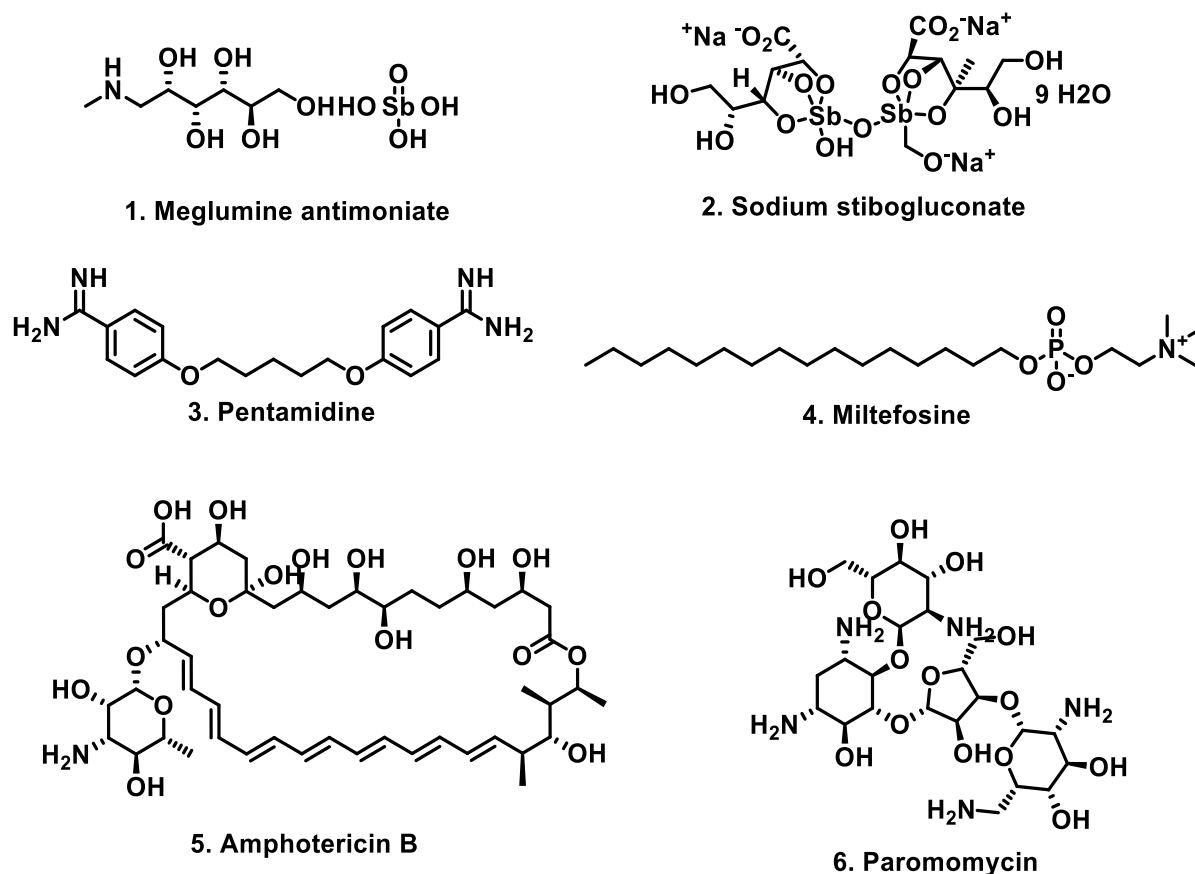


Figure 1.2. Structure of currently marketed drugs for the treatment of Leishmaniasis

Other drugs against leishmaniasis include pentamidine and azole antifungals. Pentamidine is an aromatic diamidine drug consisting of pentane-1,5-diol, which interferes with polyamine synthesis, RNA polymerase activity, enters the protozoal cell binding to transfer RNA and prevents the synthesis of protein, nucleic acids, phospholipids, folates^{44,45}. In the case of *Leishmania*, its use had been almost completely abandoned due to the risk of resistance and severe side effects, but it has recently been recommended for patients co-infected with HIV⁴⁶. The azole antifungals, fluconazole, ketoconazole and itraconazole (**Figure 1.3**) have been mainly used for the treatment of CL⁴⁷. Their mechanism of action is based on the inhibition of the synthesis of lanosterol, an intermediate in the ergosterol synthesis of the parasite⁴⁸. The results show that they are not very effective as monotherapy and should, therefore, they should be used in combination with other drugs such as Miltefosine⁴⁹.

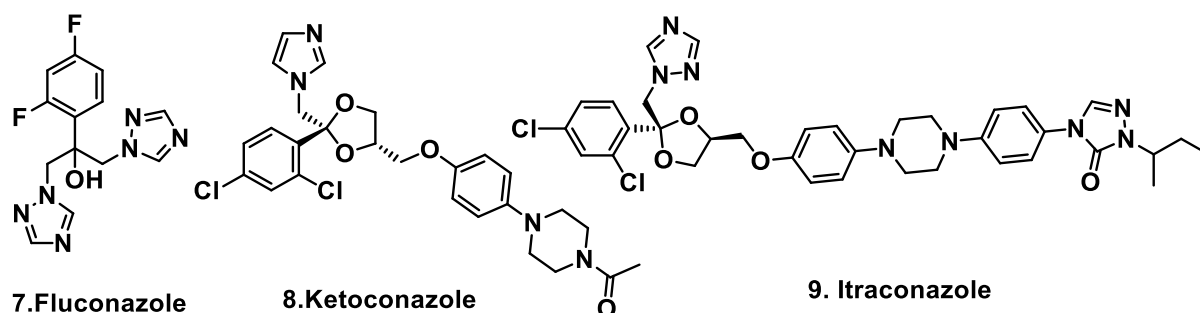


Figure 1.3. Structure of Azole antifungals

To reduce side effects and VL-drugs administration time, the WHO and Drugs for Neglected Diseases initiative (DNDi) have recommended the use of combinations of drugs with different mechanisms of action that facilitate adherence to treatment, thus preventing the emergence of resistant strains. The most common drug used in combination is paromomycin, which is administered intramuscularly together with Sb^V in East Africa. This combination reduces the treatment from 30 to 17 days with an efficacy of more than 95% ⁵⁰.

C. Clinical trials on leishmaniasis

The current situation for the pharmacological management of leishmaniasis in endemic countries is limited to the administration of a reduced number of compounds. Some of them have decreasing efficacy over time due to overuse, some are unaffordable for impoverished countries or chemically unstable, and most of them require repeated parenteral administration over a long period of time, which compromises their adherence. Following the 2012 London Declaration on Neglected Tropical Diseases, the actual results for 2022 were not entirely optimistic for leishmaniasis, including new combination therapies with similar efficacy to previous treatments but with reduced side effects. However, the number of promising chemical species, new drug targets, and High Throughput Screening (HTS) methodologies has grown dramatically so that several molecules, meeting the Target Product Profile for an anti-leishmanial, are currently being evaluated in Phase I clinical trials (**Figure 1.5**)^{20,26,51,52}

Nitroaromatic rings are the privileged pharmacophores of many active antimicrobials, such as the antibiotic metronidazole, the antichagasic drugs benznidazole and nifurtimox, the antitubercular drug pretomanid and the antifungal nifuratel (**Figure 1.4**)^{53,54} From the repositioning campaigns for new anti-tuberculosis drugs, fexinidazole was found to have potent anti-Chagas and anti-sleeping sickness effects and is currently in phase II clinical trials⁵⁵. This molecule has inspired the compound DNDi-0690, which is currently being tested as an oral antileishmanial drug in phase I clinical trials⁵⁶.

Chapter 1. Leishmaniasis – An overview

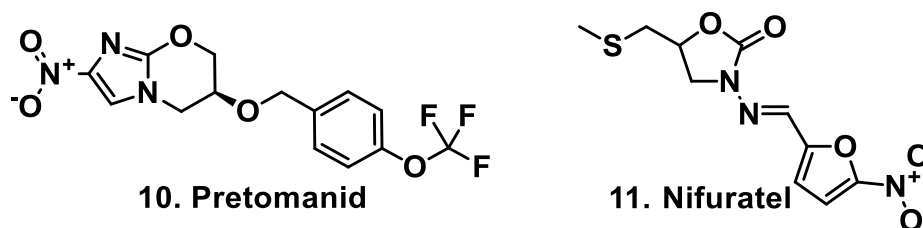
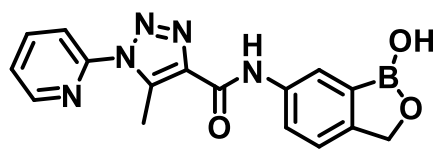
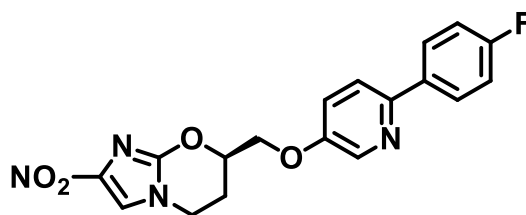


Figure 1.4. Structure of antitubercular drugs

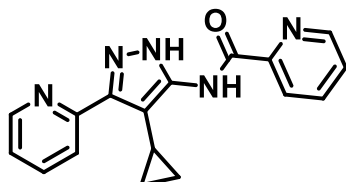
Benzoxaboroles are cyclic boron-containing drugs developed against several infectious diseases, including onychomycosis of the toenails and atopic dermatitis⁵⁷. The 6-carboxamide benzoxaborole, DNDI-6148, was as curative as miltefosine in mice at a minimum dose of 25 mg/kg/d b.i.d. after a 10-day treatment, without toxic side effects⁵². This remarkable efficacy is being currently assessed for first-in-human trials of safety, tolerability, and pharmacokinetics after a single ascending oral dose⁵⁸. GSK3186899 is a pyrazolopyrimidine first identified in a target-based screen against *T. brucei* glycogen synthase kinase (GSK3)⁵⁹. Pyrazolopyrimidines were shown to be strong inhibitors of leishmanial cyclin-dependent kinase 12 (CDK12) with potent anti-leishmanial effects *in vitro*⁶⁰. GSK3186899 administered orally at 25 mg/kg b.i.d for 10 consecutive days produced a 99% reduction in parasite load in a mouse model of VL⁶¹. The good characteristics of GSK3186899 led to its inclusion in Phase I clinical trials. From a mass phenotypic screening of small molecules conducted by Novartis in collaboration with the Wellcome Trust, a set of azabenzoxazole ring compounds led to the identification of GNF6702⁶². Deconvolution studies of this compound showed a strong effect as a reversible inhibitor of the kinetoplastid proteasome and anti-leishmanial effects at sub-micromolar concentrations (Stanley et al., 2019). An azabenzoxazole derivative of GNF6702, called LXE408, administered at 3 mg/kg showed a >99% reduction in parasite load⁶³. Leishmanial proteasome was also identified by GSK and Dundee Drug Discovery as the target of other azabenzoxazole-like compounds. From phenotypic screening, DDD01305143 was found to reduce parasite load by more than 95% *in vivo* in rodents at a dose of 3 mg b.i.d. for 10 consecutive days orally⁶⁴. Both proteasome inhibitors LXE408 and DDD1305143 have been promoted by DNDi to phase I clinical trials against VL. Finally, CpG-D35 is a short synthetic immunomodulatory oligonucleotide that is effective against CL in macaques. After continued parenteral administration, parasite load and lesion size were reduced regardless of the route (ID, IM or SC), hence suggesting that the product induces a systemic immunomodulatory effect that accelerates healing. In addition, the animals developed long-lasting protective memory responses to the parasite⁶⁵.



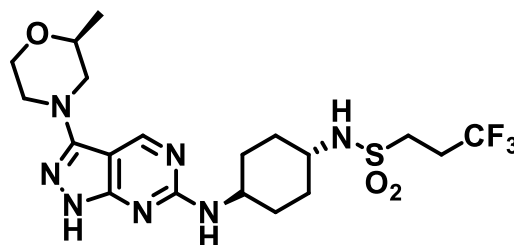
12. DNDi-6148



13. DNDi-0690



14. DNDi-5561



15. GSK-3186899/DD853651

Figure 1.5. Structure of antileishmanial compounds under clinical trials

References

- (1) World Health Organization. *Control of the Leishmaniases.*; 2010.
- (2) *Global Leishmaniasis Surveillance, 2017–2018, and First Report on 5 Additional Indicators*; 2020; Vol. 95.
- (3) World health organization <https://www.who.int/news-room/fact-sheets/detail/leishmaniasis>.
- (4) Burza, S.; Croft, S. L.; Boelaert, M. Leishmaniasis. *Lancet (London, England)* **2018**, 392 (10151), 951–970. [https://doi.org/10.1016/S0140-6736\(18\)31204-2](https://doi.org/10.1016/S0140-6736(18)31204-2).
- (5) Sasidharan, S.; Saudagar, P. Leishmaniasis: Where Are We and Where Are We Heading? *Parasitology Research* **2021**, 120 (5), 1541–1554. <https://doi.org/10.1007/s00436-021-07139-2>.
- (6) Burza, S.; Croft, S. L.; Boelaert, M. Leishmaniasis. *The Lancet* **2018**, 392 (10151), 951–970. [https://doi.org/10.1016/S0140-6736\(18\)31204-2](https://doi.org/10.1016/S0140-6736(18)31204-2).
- (7) Abadías-Granado, I.; Diago, A.; Cerro, P. A.; Palma-Ruiz, A. M.; Gilaberte, Y. Cutaneous and Mucocutaneous Leishmaniasis. *Actas Dermo-sifiliograficas* **2021**. <https://doi.org/10.1016/j.ad.2021.02.008>.
- (8) Torres-Guerrero, E.; Quintanilla-Cedillo, M. R.; Ruiz-Esmenjaud, J.; Arenas, R. Leishmaniasis: A Review. *F1000Research* **2017**, 6 (750), 750. <https://doi.org/10.12688/f1000research.11120.1>.
- (9) Falcão, G. G. V. S. C.; Lins-Kusterer, L.; Leite-Ribeiro, P. M.; Sarmiento, V. A. Orofacial Manifestations of Mucocutaneous Leishmaniasis: A Case Series from Brazil. *F1000Research* **2020**, 8 (756), 756. <https://doi.org/10.12688/f1000research.19056.4>.
- (10) van Griensven, J.; Diro, E. Visceral Leishmaniasis. *Infectious Disease Clinics of North America* **2012**, 26 (2), 309–322. <https://doi.org/10.1016/j.idc.2012.03.005>.
- (11) Lindoso, J. A. L.; Moreira, C. H. V.; Cunha, M. A.; Queiroz, I. T. Visceral Leishmaniasis and HIV Coinfection: Current Perspectives. *HIV/AIDS - Research and Palliative Care*. 2018, pp 193–201. <https://doi.org/10.2147/HIV.S143929>.
- (12) Zijlstra, E. E.; Alves, F.; Rijal, S.; Arana, B.; Alvar, J. Post-Kala-Azar Dermal Leishmaniasis in the Indian Subcontinent: A Threat to the South-East Asia Region Kala-Azar Elimination Programme. *PLoS Neglected Tropical Diseases* **2017**, 11 (11), 1–16. <https://doi.org/10.1371/journal.pntd.0005877>.
- (13) Chaves, M. M.; Lee, S. H.; Kamenyeva, O.; Ghosh, K.; Peters, N. C.; Sacks, D. The Role of Dermis Resident Macrophages and Their Interaction with Neutrophils in the

Chapter 1. Leishmaniasis – An overview

- Early Establishment of Leishmania Major Infection Transmitted by Sand Fly Bite. *PLoS Pathogens* **2020**, *16* (11), 1–24. <https://doi.org/10.1371/journal.ppat.1008674>.
- (14) Passelli, K.; Billion, O.; Tacchini-Cottier, F. The Impact of Neutrophil Recruitment to the Skin on the Pathology Induced by Leishmania Infection. *Frontiers in Immunology* **2021**, *12*, 446. <https://doi.org/10.3389/fimmu.2021.649348>.
- (15) Kupani, M.; Pandey, R. K.; Mehrotra, S. Neutrophils and Visceral Leishmaniasis: Impact on Innate Immune Response and Cross-Talks with Macrophages and Dendritic Cells. *Journal of Cellular Physiology* **2021**, *236* (4), 2255–2267. <https://doi.org/10.1002/jcp.30029>.
- (16) Mohebbali, M.; Nadim, A.; Khamesipour, A. An Overview of Leishmanization Experience: A Successful Control Measure and a Tool to Evaluate Candidate Vaccines. *Acta Tropica* **2019**, *200*, 105173. <https://doi.org/10.1016/j.actatropica.2019.105173>.
- (17) Moafi, M.; Rezvan, H.; Sherkat, R.; Taleban, R. Leishmania Vaccines Entered in Clinical Trials: A Review of Literature. *International Journal of Preventive Medicine* **2019**, *10* (1), 95. https://doi.org/10.4103/ijpvm.IJPVM_116_18.
- (18) Reguera, R. M.; Pérez-Pertejo, Y.; Gutiérrez-Corbo, C.; Domínguez-Asenjo, B.; Ordóñez, C.; García-Estrada, C.; Martínez-Valladares, M.; Balaña-Fouce, R. Current and Promising Novel Drug Candidates against Visceral Leishmaniasis. *Pure and Applied Chemistry* **2019**, *91* (8), 1385–1404. <https://doi.org/10.1515/pac-2018-1102>.
- (19) Sundar, S.; Agrawal, N.; Singh, B. Exploiting Knowledge on Pharmacodynamics-Pharmacokinetics for Accelerated Anti-Leishmanial Drug Discovery/Development. *Expert Opinion on Drug Metabolism and Toxicology* **2019**, *15* (7), 595–612. <https://doi.org/10.1080/17425255.2019.1629417>.
- (20) Balaña-Fouce, R.; Pérez Pertejo, M. Y.; Domínguez-Asenjo, B.; Gutiérrez-Corbo, C.; Reguera, R. M. Walking a Tightrope: Drug Discovery in Visceral Leishmaniasis. *Drug Discovery Today* **2019**, *24* (5), 1209–1216. <https://doi.org/10.1016/j.drudis.2019.03.007>.
- (21) Cruz, I.; Albertini, A.; Barbeitas, M.; Arana, B.; Picado, A.; Ruiz-Postigo, J. A.; Ndung'u, J. M. Target Product Profile for a Point-of-Care Diagnostic Test for Dermal Leishmaniasis. *Parasite Epidemiology and Control* **2019**, *5*, e00103. <https://doi.org/https://doi.org/10.1016/j.parepi.2019.e00103>.
- (22) Frézard, F.; Demicheli, C.; Ribeiro, R. R. Pentavalent Antimonials: New Perspectives for Old Drugs. *Molecules* **2009**, *14* (7), 2317–2336.

Chapter 1. Leishmaniasis – An overview

- <https://doi.org/10.3390/molecules14072317>.
- (23) Shaked-Mishan, P.; Ulrich, N.; Ephros, M.; Zilberstein, D. Novel Intracellular SbV Reducing Activity Correlates with Antimony Susceptibility in *Leishmania Donovanii* *. *Journal of Biological Chemistry* **2001**, *276* (6), 3971–3976. <https://doi.org/https://doi.org/10.1074/jbc.M005423200>.
- (24) Sundar, S.; More, D. K.; Singh, M. K.; Singh, V. P.; Sharma, S.; Makharia, A.; Kumar, P. C. K.; Murray, H. W. Failure of Pentavalent Antimony in Visceral Leishmaniasis in India: Report from the Center of the Indian Epidemic. *Clinical Infectious Diseases* **2000**, *31* (4), 1104–1107. <https://doi.org/10.1086/318121>.
- (25) Bamorovat, M.; Sharifi, I.; Tavakoli Oliae, R.; Jafarzadeh, A.; Khosravi, A. Determinants of Unresponsiveness to Treatment in Cutaneous Leishmaniasis: A Focus on Anthroponotic Form Due to *Leishmania Tropica*. *Frontiers in Microbiology* **2021**, *12*, 1143. <https://doi.org/10.3389/fmicb.2021.638957>.
- (26) Caridha, D.; Vesely, B.; van Bocxlaer, K.; Arana, B.; Mowbray, C. E.; Rafati, S.; Uliana, S.; Reguera, R.; Kreishman-Deitrick, M.; Sciotti, R.; Buffet, P.; Croft, S. L. Route Map for the Discovery and Pre-Clinical Development of New Drugs and Treatments for Cutaneous Leishmaniasis. *International Journal for Parasitology: Drugs and Drug Resistance* **2019**, *11*, 106–117. <https://doi.org/https://doi.org/10.1016/j.ijpddr.2019.06.003>.
- (27) Sundar, S.; Chakravarty, J. Antimony Toxicity. *International Journal of Environmental Research and Public Health* **2010**, *7* (12), 4267–4277. <https://doi.org/10.3390/ijerph7124267>.
- (28) Chappuis, F.; Alirol, E.; Worku, D. T.; Mueller, Y.; Ritmeijer, K. High Mortality among Older Patients Treated with Pentavalent Antimonials for Visceral Leishmaniasis in East Africa and Rationale for Switch to Liposomal Amphotericin B. *Antimicrobial Agents and Chemotherapy* **2011**, *55* (1), 455–456. <https://doi.org/10.1128/AAC.01298-10>.
- (29) Warnock, D. W. Amphotericin B: An Introduction. *Journal of Antimicrobial Chemotherapy* **1991**, *28* (suppl_B), 27–38. https://doi.org/10.1093/jac/28.suppl_B.27.
- (30) Sundar, S.; Chakravarty, J. Leishmaniasis: An Update of Current Pharmacotherapy. *Expert Opinion on Pharmacotherapy* **2013**, *14* (1), 53–63. <https://doi.org/10.1517/14656566.2013.755515>.
- (31) Gray, K. C.; Palacios, D. S.; Dailey, I.; Endo, M. M.; Uno, B. E.; Wilcock, B. C.; Burke, M. D. Amphotericin Primarily Kills Yeast by Simply Binding Ergosterol. *Proceedings*

Chapter 1. Leishmaniasis – An overview

- of the National Academy of Sciences of the United States of America* **2012**, 109 (7), 2234–2239. <https://doi.org/10.1073/pnas.1117280109>.
- (32) Sundar, S.; Singh, A. Chemotherapeutics of Visceral Leishmaniasis : Present and Future Developments. **2021**, No. 2018, 481–489. <https://doi.org/10.1017/S0031182017002116>.
- (33) Hung, C. T.; Lam, F. C.; Perrier, D. G.; Souter, A. A Stability Study of Amphotericin B in Aqueous Media Using Factorial Design. *International Journal of Pharmaceutics* **1988**, 44, 117–123.
- (34) Pagliano, P.; Esposito, S. Visceral Leishmaniosis in Immunocompromised Host: An Update and Literature Review. *Journal of Chemotherapy* **2017**, 29 (5), 261–266. <https://doi.org/10.1080/1120009X.2017.1323150>.
- (35) Palić, S.; Beijnen, J. H.; Dorlo, T. P. C. An Update on the Clinical Pharmacology of Miltefosine in the Treatment of Leishmaniasis. *International Journal of Antimicrobial Agents* **2022**, 59 (1), 106459. <https://doi.org/10.1016/j.ijantimicag.2021.106459>.
- (36) Wadhone, P.; Maiti, M.; Agarwal, R.; Kamat, V.; Martin, S.; Saha, B. Miltefosine Promotes IFN- γ -Dominated Anti-Leishmanial Immune Response. *The Journal of Immunology* **2009**, 182 (11), 7146 LP – 7154. <https://doi.org/10.4049/jimmunol.0803859>.
- (37) Berman, J. Miltefosine to Treat Leishmaniasis. *Expert opinion on pharmacotherapy* **2005**, 6 (8), 1381–1388. <https://doi.org/10.1517/14656566.6.8.1381>.
- (38) Sindermann, H.; Engel, J. Development of Miltefosine as an Oral Treatment for Leishmaniasis. *Transactions of the Royal Society of Tropical Medicine and Hygiene* **2006**, 100 Suppl, S17-20. <https://doi.org/10.1016/j.trstmh.2006.02.010>.
- (39) Dorlo, T. P. C.; Huitema, A. D. R.; Beijnen, J. H.; de Vries, P. J. Optimal Dosing of Miltefosine in Children and Adults with Visceral Leishmaniasis. *Antimicrobial Agents and Chemotherapy* **2012**, 56 (7), 3864–3872. <https://doi.org/10.1128/AAC.00292-12>.
- (40) Rijal, S.; Ostyn, B.; Uranw, S.; Rai, K.; Bhattarai, N. R.; Dorlo, T. P. C.; Beijnen, J. H.; Vanaerschot, M.; Decuypere, S.; Dhakal, S. S.; Das, M. L.; Karki, P.; Singh, R.; Boelaert, M.; Dujardin, J.-C. Increasing Failure of Miltefosine in the Treatment of Kala-Azar in Nepal and the Potential Role of Parasite Drug Resistance, Reinfection, or Noncompliance. *Clinical Infectious Diseases : An official publication of the Infectious Diseases Society of America* **2013**, 56 (11), 1530–1538. <https://doi.org/10.1093/cid/cit102>.
- (41) Davidson, R. N.; den Boer, M.; Ritmeijer, K. Paromomycin. *Transactions of The Royal*

Chapter 1. Leishmaniasis – An overview

- Society of Tropical Medicine and Hygiene* **2009**, *103* (7), 653–660. <https://doi.org/10.1016/j.trstmh.2008.09.008>.
- (42) Hailu, A.; Musa, A.; Wasunna, M.; Balasegaram, M.; Yifru, S.; Mengistu, G.; Hurissa, Z.; Hailu, W.; Weldegebreal, T.; Tesfaye, S.; Makonnen, E.; Khalil, E.; Ahmed, O.; Fadlalla, A.; El-Hassan, A.; Raheem, M.; Mueller, M.; Koummuki, Y.; Rashid, J.; Mbui, J.; Mucee, G.; Njoroge, S.; Manduku, V.; Musibi, A.; Mutuma, G.; Kirui, F.; Lodenyo, H.; Mutea, D.; Kirigi, G.; Edwards, T.; Smith, P.; Muthami, L.; Royce, C.; Ellis, S.; Alobo, M.; Omollo, R.; Kesusu, J.; Owiti, R.; Kinuthia, J.; group, for the L. E. A. P. (LEAP). Geographical Variation in the Response of Visceral Leishmaniasis to Paromomycin in East Africa: A Multicentre, Open-Label, Randomized Trial. *PLOS Neglected Tropical Diseases* **2010**, *4* (10), e709.
- (43) Roatt, B. M.; de Oliveira Cardoso, J. M.; De Brito, R. C. F.; Coura-Vital, W.; de Oliveira Aguiar-Soares, R. D.; Reis, A. B. Recent Advances and New Strategies on Leishmaniasis Treatment. *Applied Microbiology and Biotechnology* **2020**, *104* (21), 8965–8977. <https://doi.org/10.1007/s00253-020-10856-w>.
- (44) Calonge, M.; Johnson, R.; Balaña-Fouce, R.; Ordóñez, D. Effects of Cationic Diamidines on Polyamine Content and Uptake on *Leishmania Infantum* in in Vitro Cultures. *Biochemical Pharmacology* **1996**, *52* (6), 835–841. [https://doi.org/10.1016/0006-2952\(96\)00348-6](https://doi.org/10.1016/0006-2952(96)00348-6).
- (45) Johnson, R.; Cubría, J. C.; Reguera, R. M.; Balaña-Fouce, R.; Ordóñez, D. Interaction of Cationic Diamidines with *Leishmania Infantum* DNA. *Biological Chemistry* **1998**, *379* (7), 925–930. PMID: 9705158.
- (46) Piccica, M.; Lagi, F.; Bartoloni, A.; Zammarchi, L. Efficacy and Safety of Pentamidine Isethionate for Tegumentary and Visceral Human Leishmaniasis: A Systematic Review. *Journal of Travel Medicine* **2021**, *28* (6), taab065. <https://doi.org/10.1093/jtm/taab065>.
- (47) Galvão, E. L.; Pedras, M. J.; Cota, G. F.; Simões, T. C.; Rabello, A. Development and Initial Validation of a Cutaneous Leishmaniasis Impact Questionnaire. *PLOS ONE* **2018**, *13* (8), e0203378. <https://doi.org/10.1371/journal.pone.0203378>
- (48) Hart, D. T.; Lauwers, W. J.; Willemsens, G.; Vanden Bossche, H.; Opperdoes, F. R. Perturbation of Sterol Biosynthesis by Itraconazole and Ketoconazole in *Leishmania Mexicana Mexicana* Infected Macrophages. *Molecular and Biochemical Parasitology* **1989**, *33* (2), 123–134. [https://doi.org/10.1016/0166-6851\(89\)90026-1](https://doi.org/10.1016/0166-6851(89)90026-1).
- (49) Fernández, O. L.; Rosales-Chilama, M.; Quintero, N.; Travi, B. L.; Wetzel, D. M.;

Chapter 1. Leishmaniasis – An overview

- Gómez, M. A.; Saravia, N. G. Potency and Preclinical Evidence of Synergy of Oral Azole Drugs and Miltefosine in an Ex Vivo Model of Leishmania (Viannia) Panamensis Infection. *Antimicrobial Agents and Chemotherapy* **2022**, *66* (1), AAC0142521. <https://doi.org/10.1128/AAC.01425-21>.
- (50) Musa, A.; Khalil, E.; Hailu, A.; Olobo, J.; Balasegaram, M.; Omollo, R.; Edwards, T.; Rashid, J.; Mbui, J.; Musa, B.; Abuzaid, A. A.; Ahmed, O.; Fadlalla, A.; El-Hassan, A.; Mueller, M.; Mucee, G.; Njoroge, S.; Manduku, V.; Mutuma, G.; Apadet, L.; Lodenyo, H.; Mutea, D.; Kirigi, G.; Yifru, S.; Mengistu, G.; Hurissa, Z.; Hailu, W.; Weldegebreal, T.; Tafes, H.; Mekonnen, Y.; Makonnen, E.; Ndegwa, S.; Sagaki, P.; Kimutai, R.; Kesusu, J.; Owiti, R.; Ellis, S.; Wasunna, M. Sodium Stibogluconate (SSG) & Paromomycin Combination Compared to SSG for Visceral Leishmaniasis in East Africa: A Randomised Controlled Trial. *PLoS Neglected Tropical Diseases* **2012**, *6* (6), e1674. <https://doi.org/10.1371/journal.pntd.0001674>.
- (51) SUNDAR, S.; SINGH, A. Chemotherapeutics of Visceral Leishmaniasis: Present and Future Developments. *Parasitology* **2018**, *145* (4), 481–489. <https://doi.org/DOI:10.1017/S0031182017002116>.
- (52) Van Bocxlaer, K.; Caridha, D.; Black, C.; Vesely, B.; Leed, S.; Sciotti, R. J.; Wijnant, G. J.; Yardley, V.; Braillard, S.; Mowbray, C. E.; Ioset, J. R.; Croft, S. L. Novel Benzoxaborole, Nitroimidazole and Aminopyrazoles with Activity against Experimental Cutaneous Leishmaniasis. *International Journal for Parasitology: Drugs and Drug Resistance* **2019**, No. February, 0–1. <https://doi.org/10.1016/j.ijpddr.2019.02.002>.
- (53) Patterson, S.; Wyllie, S. Nitro Drugs for the Treatment of Trypanosomatid Diseases: Past, Present, and Future Prospects. *Trends in Parasitology* **2014**, *30* (6), 289–298. <https://doi.org/10.1016/j.pt.2014.04.003>.
- (54) Domínguez-Asenjo, B.; Gutiérrez-Corbo, C.; Álvarez-Bardón, M.; Pérez-Pertejo, Y.; Balaña-Fouce, R.; Reguera, R. M. Ex Vivo Phenotypic Screening of Two Small Repurposing Drug Collections Identifies Nifuratel as a Potential New Treatment against Visceral and Cutaneous Leishmaniasis. *ACS Infectious Diseases* **2021**, *7* (8), 2390–2401. <https://doi.org/10.1021/acsinfecdis.1c00139>.
- (55) Deeks, E. D. Fexinidazole: First Global Approval. *Drugs* **2019**, *79* (2), 215–220. <https://doi.org/10.1007/s40265-019-1051-6>.
- (56) Thompson, A. M.; O'Connor, P. D.; Marshall, A. J.; Yardley, V.; Maes, L.; Gupta, S.;

Chapter 1. Leishmaniasis – An overview

- Launay, D.; Brailard, S.; Chatelain, E.; Franzblau, S. G.; Wan, B.; Wang, Y.; Ma, Z.; Cooper, C. B.; Denny, W. A. 7-Substituted 2-Nitro-5,6-Dihydroimidazo[2,1- b][1,3]Oxazines: Novel Antitubercular Agents Lead to a New Preclinical Candidate for Visceral Leishmaniasis. *Journal of Medicinal Chemistry* **2017**, *60* (10), 4212–4233. <https://doi.org/10.1021/acs.jmedchem.7b00034>.
- (57) Jinna, S.; Finch, J. Spotlight on Tavaborole for the Treatment of Onychomycosis. *Drug design, Development and Therapy* **2015**, *9*, 6185–6190. <https://doi.org/10.2147/DDDT.S81944>.
- (58) Drugs for Neglected Diseases initiative. *R & D Portfolio DNDi*; 2020.
- (59) Wyllie, S.; Thomas, M.; Patterson, S.; Crouch, S.; De Rycker, M.; Lowe, R.; Gresham, S.; Urbaniak, M. D.; Otto, T. D.; Stojanovski, L.; Simeons, F. R. C.; Manthri, S.; MacLean, L. M.; Zuccotto, F.; Homeyer, N.; Pflaumer, H.; Boesche, M.; Sastry, L.; Connolly, P.; Albrecht, S.; Berriman, M.; Drewes, G.; Gray, D. W.; Ghidelli-Disse, S.; Dixon, S.; Fiandor, J. M.; Wyatt, P. G.; Ferguson, M. A. J.; Fairlamb, A. H.; Miles, T. J.; Read, K. D.; Gilbert, I. H. Cyclin-Dependent Kinase 12 Is a Drug Target for Visceral Leishmaniasis. *Nature* **2018**, *560* (7717), 192–197. <https://doi.org/10.1038/s41586-018-0356-z>.
- (60) Thomas, M.; Brand, S.; De Rycker, M.; Zuccotto, F.; Lukac, I.; Dodd, P. G.; Ko, E.-J.; Manthri, S.; McGonagle, K.; Osuna-Cabello, M.; Riley, J.; Pont, C.; Simeons, F.; Stojanovski, L.; Thomas, J.; Thompson, S.; Viayna, E.; Fiandor, J. M.; Martin, J.; Wyatt, P. G.; Miles, T. J.; Read, K. D.; Marco, M.; Gilbert, I. H. Scaffold-Hopping Strategy on a Series of Proteasome Inhibitors Led to a Preclinical Candidate for the Treatment of Visceral Leishmaniasis. *Journal of Medicinal Chemistry* **2021**, *64* (9), 5905–5930. <https://doi.org/10.1021/acs.jmedchem.1c00047>.
- (61) Thomas, M. G.; De Rycker, M.; Ajakane, M.; Albrecht, S.; Álvarez-Pedraglio, A. I.; Boesche, M.; Brand, S.; Campbell, L.; Cantizani-Perez, J.; Cleghorn, L. A. T.; Copley, R. C. B.; Crouch, S. D.; Daugan, A.; Drewes, G.; Ferrer, S.; Ghidelli-Disse, S.; Gonzalez, S.; Gresham, S. L.; Hill, A. P.; Hindley, S. J.; Lowe, R. M.; Mackenzie, C. J.; Maclean, L.; Manthri, S.; Martin, F.; Miguel-Siles, J.; Nguyen, V. L.; Norval, S.; Osuna-Cabello, M.; Woodland, A.; Patterson, S.; Pena, I.; Quesada-Campos, M. T.; Reid, I. H.; Revill, C.; Riley, J.; Ruiz-Gomez, J. R.; Shishikura, Y.; Simeons, F. R. C.; Smith, A.; Smith, V. C.; Spinks, D.; Stojanovski, L.; Thomas, J.; Thompson, S.; Underwood, T.; Gray, D. W.; Fiandor, J. M.; Gilbert, I. H.; Wyatt, P. G.; Read, K. D.; Miles, T. J.

Chapter 1. Leishmaniasis – An overview

- Identification of GSK3186899/DDD853651 as a Preclinical Development Candidate for the Treatment of Visceral Leishmaniasis. *Journal of Medicinal Chemistry* **2019**, *62* (3), 1180–1202. <https://doi.org/10.1021/acs.jmedchem.8b01218>.
- (62) Khare, S.; Nagle, A. S.; Biggart, A.; Lai, Y. H.; Liang, F.; Davis, L. C.; Barnes, S. W.; Mathison, C. J. N.; Myburgh, E.; Gao, M.-Y.; Gillespie, J. R.; Liu, X.; Tan, J. L.; Stinson, M.; Rivera, I. C.; Ballard, J.; Yeh, V.; Groessl, T.; Federe, G.; Koh, H. X. Y.; Venable, J. D.; Bursulaya, B.; Shapiro, M.; Mishra, P. K.; Spraggon, G.; Brock, A.; Mottram, J. C.; Buckner, F. S.; Rao, S. P. S.; Wen, B. G.; Walker, J. R.; Tuntland, T.; Molteni, V.; Glynne, R. J.; Supek, F. Proteasome Inhibition for Treatment of Leishmaniasis, Chagas Disease and Sleeping Sickness. *Nature* **2016**, *537* (7619), 229–233. <https://doi.org/10.1038/nature19339>.
- (63) Nagle, A.; Biggart, A.; Be, C.; Srinivas, H.; Hein, A.; Caridha, D.; Sciotti, R. J.; Pybus, B.; Kreishman-Deitrick, M.; Bursulaya, B.; Lai, Y. H.; Gao, M.-Y.; Liang, F.; Mathison, C. J. N.; Liu, X.; Yeh, V.; Smith, J.; Lerario, I.; Xie, Y.; Chianelli, D.; Gibney, M.; Berman, A.; Chen, Y.-L.; Jiricek, J.; Davis, L. C.; Liu, X.; Ballard, J.; Khare, S.; Eggimann, F. K.; Luneau, A.; Groessl, T.; Shapiro, M.; Richmond, W.; Johnson, K.; Rudewicz, P. J.; Rao, S. P. S.; Thompson, C.; Tuntland, T.; Spraggon, G.; Glynne, R. J.; Supek, F.; Wiesmann, C.; Molteni, V. Discovery and Characterization of Clinical Candidate LXE408 as a Kinetoplastid-Selective Proteasome Inhibitor for the Treatment of Leishmaniasis. *Journal of Medicinal Chemistry* **2020**, *63* (19), 10773–10781. <https://doi.org/10.1021/acs.jmedchem.0c00499>.
- (64) Wyllie, S.; Brand, S.; Thomas, M.; De Rycker, M.; Chung, C.; Pena, I.; Bingham, R. P.; Bueren-Calabuig, J. A.; Cantizani, J.; Cebrian, D.; Craggs, P. D.; Ferguson, L.; Goswami, P.; Hobrath, J.; Howe, J.; Jeacock, L.; Ko, E.-J.; Korczynska, J.; MacLean, L.; Manthri, S.; Martinez, M. S.; Mata-Cantero, L.; Moniz, S.; Nühs, A.; Osuna-Cabello, M.; Pinto, E.; Riley, J.; Robinson, S.; Rowland, P.; Simeons, F. R. C.; Shishikura, Y.; Spinks, D.; Stojanovski, L.; Thomas, J.; Thompson, S.; Viayna Gaza, E.; Wall, R. J.; Zuccotto, F.; Horn, D.; Ferguson, M. A. J.; Fairlamb, A. H.; Fiandor, J. M.; Martin, J.; Gray, D. W.; Miles, T. J.; Gilbert, I. H.; Read, K. D.; Marco, M.; Wyatt, P. G. Preclinical Candidate for the Treatment of Visceral Leishmaniasis That Acts through Proteasome Inhibition. *Proceedings of the National Academy of Sciences* **2019**, *116* (19), 9318 LP – 9323. <https://doi.org/10.1073/pnas.1820175116>.
- (65) Thacker, S. G.; McWilliams, I. L.; Bonnet, B.; Halie, L.; Beaucage, S.; Rachuri, S.; Dey,

Chapter 1. Leishmaniasis – An overview

R.; Duncan, R.; Modabber, F.; Robinson, S.; Bilbe, G.; Arana, B.; Verthelyi, D. CpG ODN D35 Improves the Response to Abbreviated Low-Dose Pentavalent Antimonial Treatment in Non-Human Primate Model of Cutaneous Leishmaniasis. *PLOS Neglected Tropical Diseases* **2020**, *14* (2), 1–27. <https://doi.org/10.1371/journal.pntd.0008050>.



Chapter 2. Literature review on β -carboline



Chapter 2. Literature review on β -carboline

β -carboline (*9H*-pyrido-[3,4-*b*]-indole), also known as nor-harmane, is a nitrogen-containing heterocycle. β -carboline belongs to the group of indole alkaloids and contains a pyridine ring fused with an indole backbone¹. The structure of β -carboline is like tryptamine, with the ethylamine chain re-connected to the indole nucleus via an extra carbon atom to produce a three-ringed structure². Since its initial discovery in the year 1841, β -carboline alkaloids have been isolated from various sources, principally plants (mainly in *Rutaceae*, *Simaroubaceae*, *Amaranthaceae*, *Caryophyllaceae*, *Rubiaceae* and *Zygophyllaceae*), marine creatures (hydroids, bryozoans, soft corals) and marine sponges³. They also present in microorganisms, insects, food products, alcoholic beverages, tobacco smoke, as well as human tissues and body fluids⁴. Also, β -carbolines display a wide range of unusual biological activities like anticancer^{5,6}, antiviral⁷, antibacterial, antifungal⁸, antileishmanial⁹, antithrombotic, antiinflammatory¹⁰ properties, among others. They also been reported to interact with enzymes and receptors like monoamine oxidase¹¹, topoisomerase I¹², topoisomerase II¹³, mitogen-activated protein kinase (MAPK)¹⁴, cyclin-dependent kinase (CDK)¹⁵, benzodiazepine receptors¹⁶, 5-HT-1 receptors¹⁷, 5-HT-2 receptors¹⁸ and imidazoline receptors¹⁹. Some important β -carboline structures were shown in (Fig-2.1). In turn, a great deal of attention is received by the scientific community (academia and industry) to explore a chemically versatile moiety. To the best of our knowledge, nine β -carboline drugs have been commercialized to date for the treatment of various ailments²⁰ (Fig-2.2).

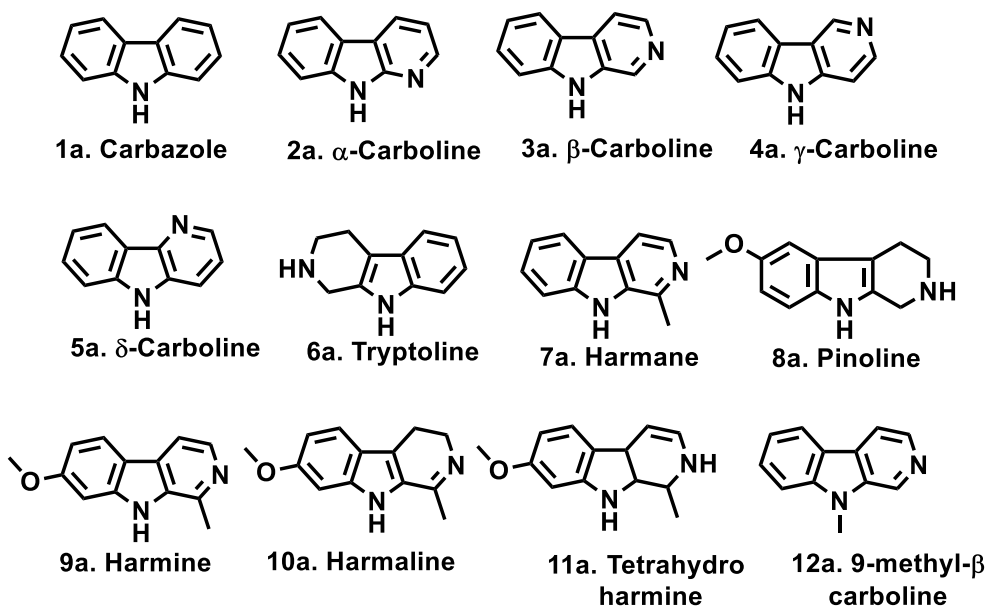


Figure-2.1 Structural diversity of carbolines (1a-12a)

Chapter 2. Literature review on β -carboline

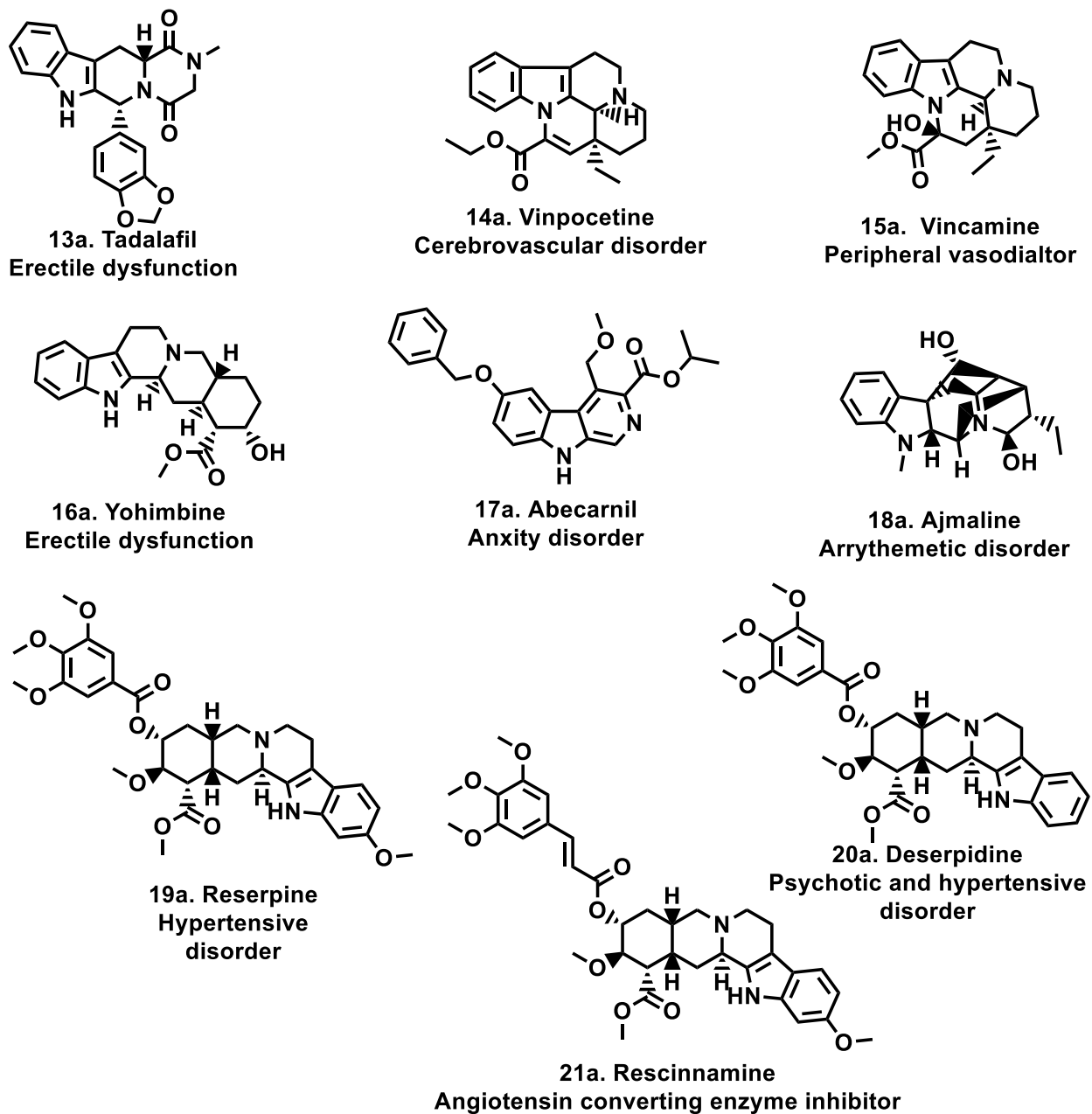


Figure-2.2 Commercialized β -carboline drugs and their pharmacological activity (13a-21a)

Chapter 2. Literature review on β -carboline

2.1. β -carboline derivatives as anti-leishmanial agents

Penta Ashok *et al.* reported the synthesis of piperazinyl- β -carboline-3-carboxamide derivatives and evaluated their anti-leishmanial activity against *Leishmania infantum* and *Leishmania donovani*. Among the reported derivatives, compounds **22a**, **23a**, and **24a** exhibited potent inhibition of promastigotes (EC_{50} 1.59, 1.47, and 3.73 μ M, respectively) and amastigotes (EC_{50} 1.4, 1.9 and 2.6 μ M, respectively) of *L. infantum*²¹.

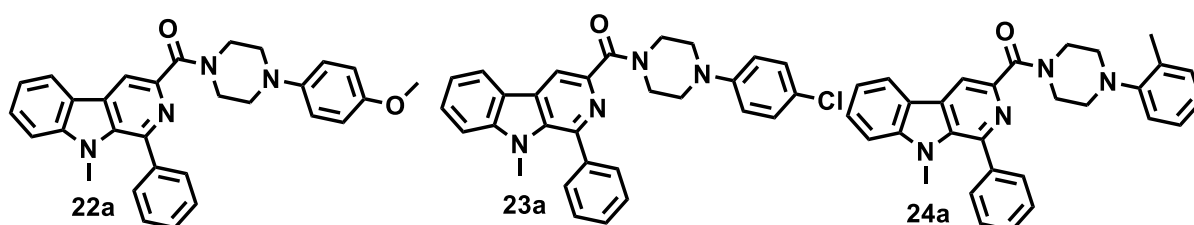


Figure-2.3 Structure of compounds **22a**, **23a** and **24a**

Nitin A. lunagariya *et al.* described the synthesis of 1,3,6-trisubstituted- β -carboline derivatives and evaluated their cytotoxic potential against four human cancer cells, namely A-549, HeLa, Hep G2, and MCF-7 as well as anti-leishmanial activity against promastigotes of *L. donovani* (MHOM/80/IN/Dd8). Among the studied compounds, compounds **25a** and **26a** were found to exhibit moderate inhibition with IC_{50} of 23.5 \pm 9.0 and 68.0 \pm 0.0 μ M, respectively, while compound **27a** was the most active in the tested series with IC_{50} 9.0 \pm 2.8 μ M, suggesting the modification at C-6 was detrimental for anti-leishmanial activity²².

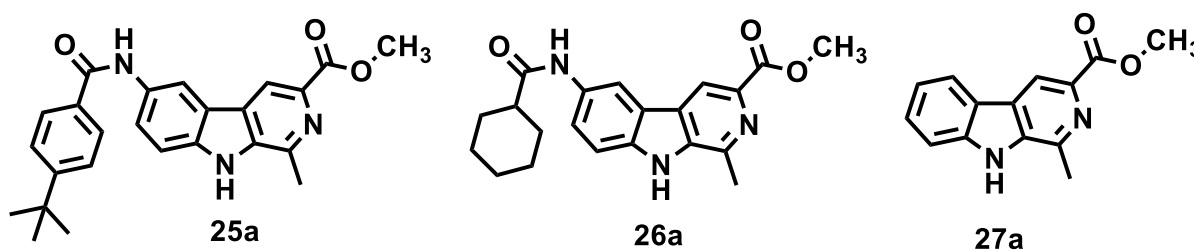


Figure-2.4 Structure of compounds **25a**, **26a** and **27a**

Penta Ashok *et al.* reported the synthesis of (1-phenyl-9*H*-pyrido-[3,4-*b*]-indol-3-yl) (4-phenylpiperazine-1-yl)-methanone derivatives and evaluated them for inhibition activity against *L. infantum* and *L. donovani*. Amongst them, compounds **28a** and **29a** showed the most potent anti-leishmanial activity against the tested strains of Leishmaniasis. The compound **28a** exhibited EC_{50} of 3.47 \pm 2.80 μ M (promastigotes), 2.80 \pm 0.10 μ M (axenic amastigotes) and 4.00 \pm 0.60 μ M (intracellular amastigotes). Another compound **29a** showed EC_{50} 2.89 \pm 0.34 μ M (promastigotes) and 2.80 \pm 0.13 μ M (axenic amastigotes)²³.

Chapter 2. Literature review on β -carboline

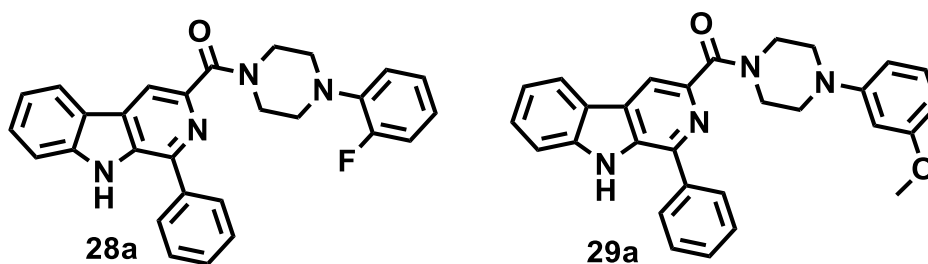


Figure-2.5. Structure of compounds **28a** and **29a**

Ravi Kumar *et al.* reported the synthesis of 2-(pyrimidine-2-yl)-1-phenyl-2,3,4,9-tetrahydro-1H- β -carboline derivatives and evaluated for anti-leishmanial activity against *L. donovani*. Compound **30a** exhibited significant anti-leishmanial activity with an IC_{50} value of 1.93 mg/ml against amastigotes ²⁴.

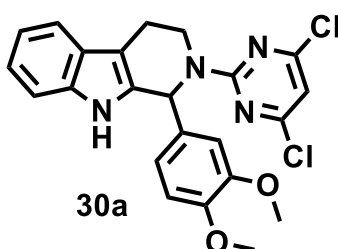


Figure-2.6 Structure of compound **30a**

Vikrant Singh M. Gohil *et al.* reported the anti-leishmanial activity of 1-aryl- β -carboline derivatives against *L. donovani*. Compound **31a** (IC_{50} $2.16 \pm 0.26 \mu\text{M}$) showed notable activity than the standard drug miltefosine (IC_{50} $12.07 \pm 0.82 \mu\text{M}$) ²⁵.

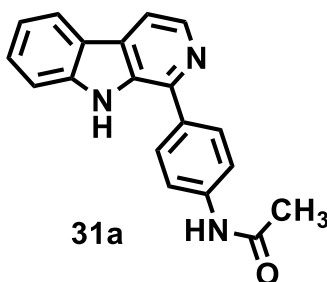


Figure-2.7 Structure of compound **31a**

T. F. Stefanello *et al.* represented the *in-vitro* antileishmanial activity of *N*-butyl-[1-(4-methoxy)-phenyl-9H- β -carboline]-3-carboxamide against *L. amazonensis*. The compound **32a** was active against promastigote, axenic amastigote, and intracellular amastigote forms of *L. amazonensis*, which showed high selectivity for the parasite ²⁶.

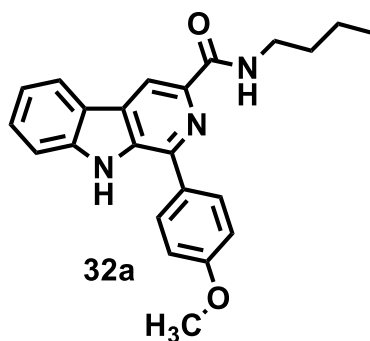


Figure-2.8 Structure of compound **32a**

Penta Ashok *et al.* synthesized and characterized some novel tetrahydro- β -carboline derivatives against transgenic infrared fluorescent *L. infantum* strain. Among the tested analogues, most of the compounds exhibited potent inhibition against both promastigotes (IC_{50} from 1.99 ± 1.40 to $20.69 \pm 0.95 \mu\text{M}$) and amastigote (IC_{50} from 0.67 ± 0.05 to $4.16 \pm 0.008 \mu\text{M}$) forms of *L. infantum*. Moreover, compound **33a** displayed the most potent and selective inhibition of parasite's amastigote form with IC_{50} $0.67 \pm 0.05 \mu\text{M}$ ²⁷.

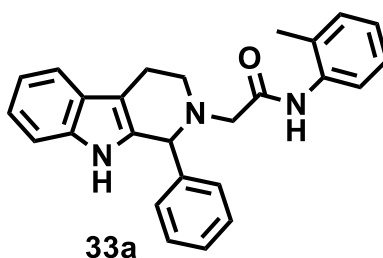


Figure-2.9 Structure of compound **33a**

HélitoVolpato *et al.* studied the effects of *N*-butyl-1-(4-dimethylamino)-phenyl-1,2,3,4-tetrahydro- β -carboline-3-carboxamide and its possible targets against *L. amazonensis*. The results showed that morphological and ultrastructural alterations, depolarization of the mitochondrial membrane, the loss of cell membrane integrity, and an increase in the formation of mitochondrial superoxide anions in *L. amazonensis* treated with compound **34a** ²⁸.

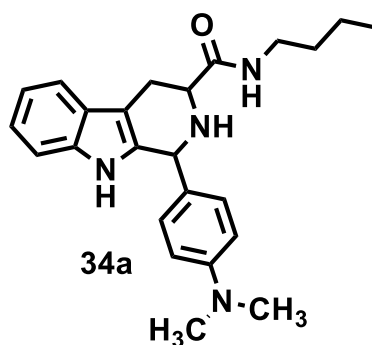


Figure-2.10 Structure of compound **34a**

Chapter 2. Literature review on β -carboline

R. B. Pedroso *et al.* reported the synthesis of 1-substituted- β -carboline-3-carboxamides, 1-substituted- β -carboline-3-carboxylic acid and screened for *in-vitro* activity against *L. amazonensis*. Compound **35a**, (*N*-benzyl-1-(4-methoxy)-phenyl-9*H*- β -carboline-3-carboxamide) exhibited significant activity against promastigotes and axenic amastigote forms with IC_{50} of 2.6 and 1.0 μ M, respectively ²⁹.

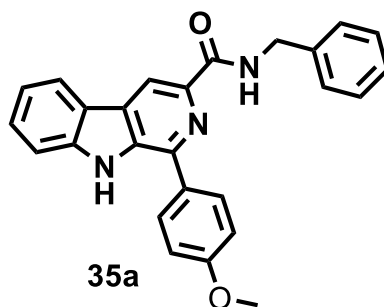


Figure-2.11 Structure of compound **35a**

Shikha S. Chauhan *et al.*, reported a detailed novel β -carboline–quinazolinone hybrids as inhibitors of *L. donovani* trypanothione reductase (LdTR). Among the series of analogues, compounds **36a**, **37a** and **38a** revealed significant *in-vitro* activity against amastigotes with IC_{50} of 4.4, 6.0, 4.3 μ M, and promastigotes with IC_{50} of 3.3, 4.6 and 4.8 μ M, respectively along with an adequate selectivity index (SI) of > 91, 36 and 24. Apart from synthesis and bio-activity, the research group also studied *in-silico* docking studies against the homology modelled target against the LdTR enzyme. The study results revealed that compound **38a** made hydrogen bond interactions with GLU-466 and HIS-461 aminoacid residues, both of which usually participate in the enzymatic process and thus may contribute to its inhibitory potential ³⁰.

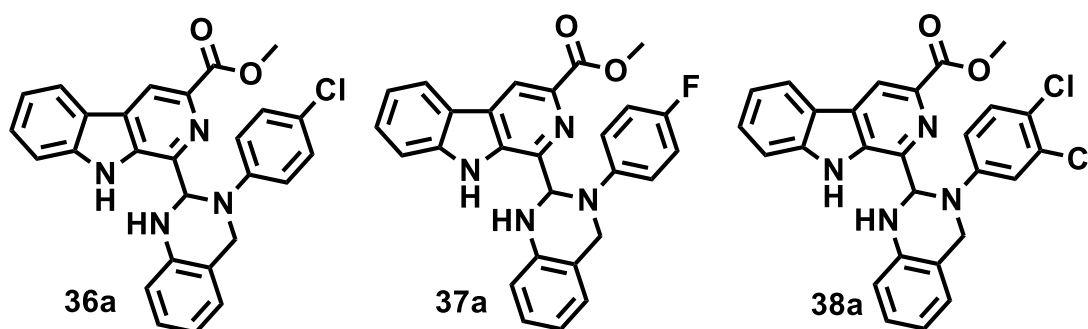


Figure-2.12 Structure of compounds **36a**, **37a** and **38a**

Lilian T. DusmanTonin *et al.* reported a series of 1-phenyl substituted- β -carbolines containing an *N*-butyl carboxamide group at C-3 of the β -carboline nucleus and evaluated *in-vitro* activity against epimastigote forms of *Trypanosoma cruzi* and promastigote forms of *L. amazonensis*. Two derivatives, **39a** and **40a**, presented potent activity against both the tested parasites. The

Chapter 2. Literature review on β -carboline

most active derivative **39a** also showed high selectivity index ratio (SI) for *L. amazonensis* (SI = 2.084)³¹.

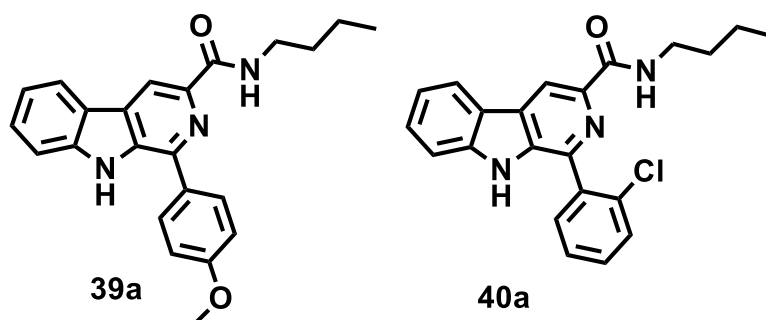


Figure-2.13 Structure of compounds **39a** and **40a**

Ashok *et al.* reported the synthesis and anti-leishmanial activity of (4-aryl piperazine-1-yl) (1-(thiophene-2-yl)-9H-pyrido-[3,4-b]-indol-3-yl)-methanone derivatives against both promastigotes and amastigotes of Leishmanial parasites responsible for visceral (*L. donovani*) and cutaneous (*L. amazonensis*) leishmaniasis. Among the series of synthesized compounds, the compounds **41a** and **42a** were found to exhibit better anti-leishmanial activity than other compounds with IC_{50} values of 8.80 and 7.50 μ M respectively, against the amastigotes of the tested strains³².

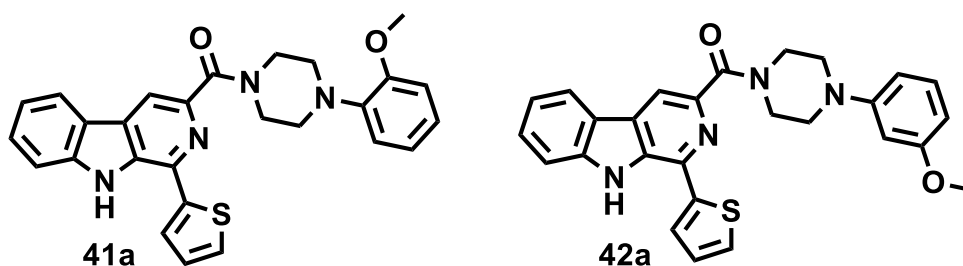


Figure-2.14 Structure of compounds **41a** and **42a**

Pooja Purohit *et al.*, detailed the synthesis of 1,2,3,4-tetrahydro- β -carboline-tetrazole derivatives using Ugi multicomponent reaction, and evaluated the compounds against Leishmaniasis. Among the screened compounds, compound **43a** was found to be the most active with an IC_{50} value of 1.57 μ M against intracellular amastigotes of *L. donovani*, and their activity is comparable with standard drugs miltefosine and sodium stibogluconate. Further, *in-vivo* evaluation of the compound **43a** *L. donovani* golden hamster model at a dose of 50 mg kg^{-1} (i.p for five days) showed $75.04 \pm 7.28\%$ inhibition of splenic parasite burden. Pharmacokinetics of compound **43a** was also studied in the golden Syrian hamster followed with a 50 mg kg^{-1} oral dose, the compound **43a** was detected in hamster serum for up to 24 h. It showed a large volume of distribution ($651.8 L kg^{-1}$), high clearance ($43.2 L h^{-1} kg^{-1}$) and long mean residence time (10 h)³³.

Chapter 2. Literature review on β -carboline

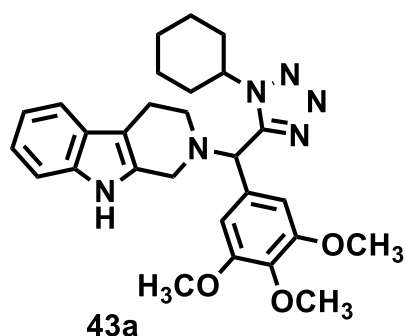


Figure-2.15 Structure of compound **43a**

Paula Baréa *et al.* described the synthesis of a series of novel β -carboline-1,3,5-triazine hybrids and evaluated their *in-vitro* antileishmanial activity against promastigotes and amastigotes forms of *L. amazonensis*. Compounds **44a** and **45a** were found to exhibit potent activity against both amastigotes and promastigotes with IC_{50} values of $1.0 \pm 0.1 \mu\text{M}$ and $1.2 \pm 0.5 \mu\text{M}$, respectively. Mechanism of action studies by scanning electron microscopic technique using promastigotes disclosed that the compound **45a** caused alterations to the cell cycle and produced an increase in lipid storage. This increase in the lipid content may be related to the apoptotic cell death of the parasite ³⁴.

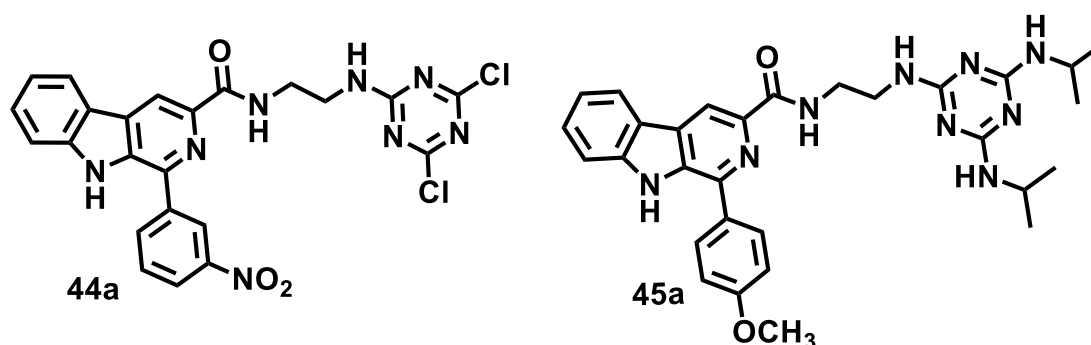


Figure-2.16 Structure of compounds **44a** and **45a**

Irfan Khan *et al.* reported the synthesis and anti-leishmanial screening of some novel β -carboline-peptide and tetrahydro- β -carboline-peptides via natural product inspired molecular hybridization approach. Among the tested compounds, compounds **46a**, **47a** and **48a** revealed significant *in-vitro* anti-leishmanial activity against both promastigotes and intracellular amastigotes of *L. donovani* (IC_{50} 2.43, 3.56 and 7.61 μM , respectively) than the control drug miltefosine ($IC_{50} = 8.2 \mu\text{M}$) with less cytotoxicity when compared with the standard drugs (sodium stibogluconate and Miltefosine). *In-silico* molecular docking studies of the synthesized compounds using the homology modelled LdTR indicated that the compound **47a** showed significant binding free energy when compared with compound **48a** ³⁵.

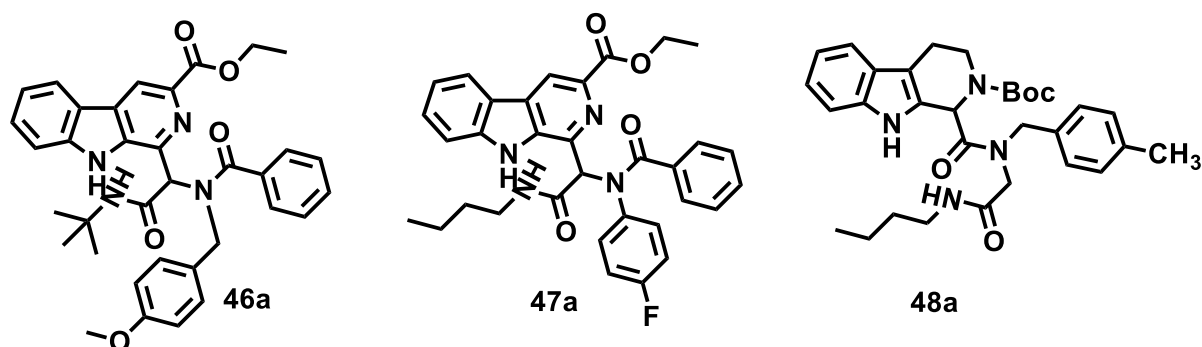


Figure-2.17 Structure of compounds **46a**, **47a** and **48a**

2.2. Phytoconstituents with anti-leishmanial effects

Nature, as an essential source for the discovery of medicinally important compounds and the use of natural products for the treatment of various diseases / infections, is well known from the ages ^{36, 37}. It has been estimated that there are about 250,000 medical plant species in the world. However, the biological activities of only about 6% of them have been screened. Furthermore, only approximately 0.75% of medical herbal compounds have been studied in clinical trials. The significant merits of herbal medicine include their low cost, low incidence of serious adverse effects, and good efficacy. Various bioactive compounds like flavonoids, alkaloids, chalcones, saponins, quinolines, ligans, tannins and terpenoids present in the plant parts, crude extracts, essential oils, and other useful compounds can be a good source for discovering and producing new antileishmanial medicines ³⁸.

Renata S. Gabriel *et al.*, isolated and investigated the effect of the β -carboline-1-propionic acid alkaloid (**49a**) from *Quassiaamara L.*, (Family: *Simaroubaceae*) against *L. amazonensis* and *L. infantum*. The alkaloid was isolated afterward, the liquid-liquid fractionation followed by chromatographic purification of the fraction *Quassiaamara L.*, methanol extract. The isolated β -carboline-1-propionic acid alkaloid (**49a**) exhibited anti-leishmanial activity against both promastigotes and intracellular amastigotes with 50% inhibitory concentrations ranging from 2.7 ± 0.82 to 9.4 ± 0.5 $\mu\text{g/ml}$ and selectivity index >10 . Furthermore, apoptotic *L. amazonensis* (19.5%) and *L. infantum* (40.4%) promastigotes were detected after 5 h incubation with the alkaloid. Moreover, the researchers also studied the inhibition effect on the production of NO by infected macrophages, and the results suggested that the alkaloid displayed a NO-independent mechanism of action for the elimination of intracellular amastigote forms ³⁹.

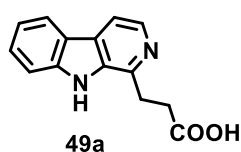


Figure-2.18 Structure of compound **49a**

Chapter 2. Literature review on β -carboline

The harmaline (**50a**), isolated from *Peganumharmala* (Family: *Nitrariaceae*), exhibited amastigote-specific activity (IC_{50} of 1.16 μ M). Harmine (**51a**) isolated from the same plant species also reduced spleen parasite load by approximately 40, 60, 70, and 80% in free, liposomal, niosomal and nanoparticulate forms respectively, when tested in mice model⁴⁰.

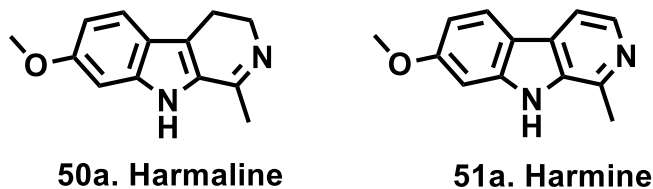


Figure-2.19 Structure of compounds **50a** and **51a**

Manzamines are unique β -carboline alkaloids isolated from Indo-Pacific sponges and characterized by a complicated nitrogen-containing polycyclic system. In 1986, Higa and co-workers first reported manzamine A from the Okinawan sponge of the genus *Haliclona*⁴¹. The full anti-leishmanial effects of the manzamine alkaloids were clearly depicted in the review of Ashok *et al.*, The research group discussed the effects of the manzamine alkaloids (Figure-2.20) as anti-leishmanial agents, their cytotoxicity and the detailed structure-activity relationship⁴².

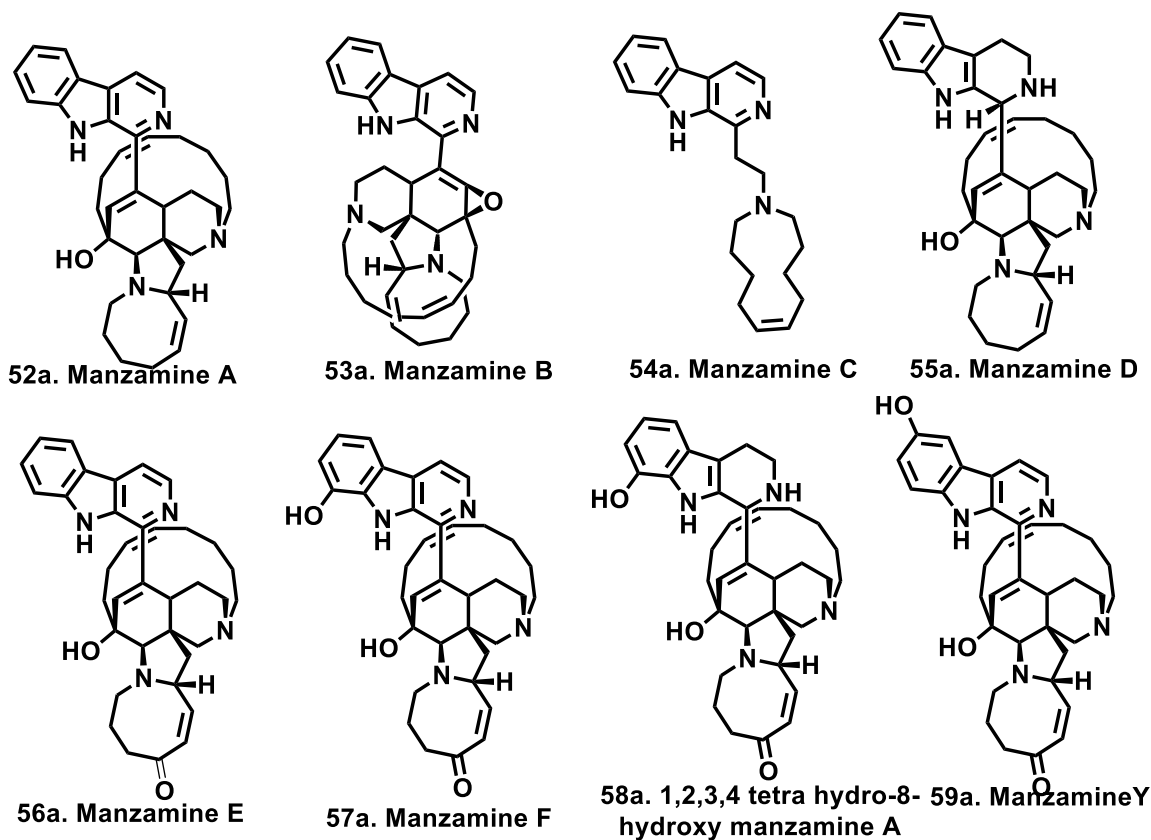


Figure-2.20 Structure of manzamine alkaloids (**52a-59a**)

Chapter 2. Literature review on β -carboline

Eudistomin is also a β -carboline alkaloid isolated from the ascidians (Family: *Ascidacea*). Initially, eudistomin A from *Eudistomao livaceum* was isolated in 1983⁴³; eudistalbins⁴⁴, eudistomidins and other eudistomins⁴⁵ were gradually isolated (Figure 22). The anti-leishmanial activity of these analogues was not reported. Anticancer activity of eudistomin H (**63a**), extracted from *Ascidian Eudistomaviride*, tested against Hela cells, exhibited an IC₅₀ of 0.49 μ g/ml⁴⁶. Antimicrobial studies of eudistomin H (**63a**) revealed the zone of inhibition 7-9 mm⁴⁷.

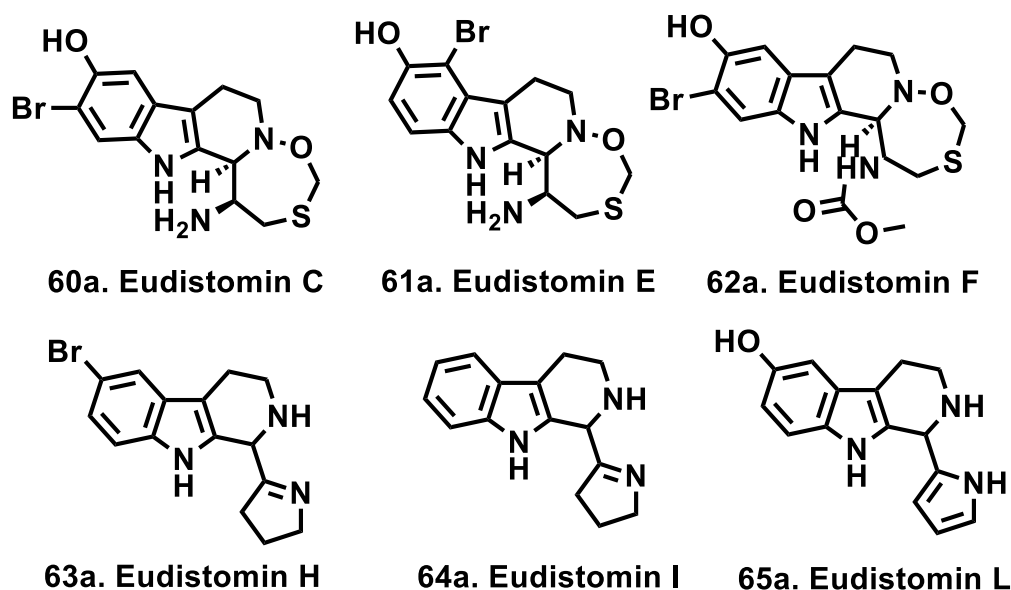


Figure-2.21. Structure of various isolated eudistomins (**60a-65a**)

2.3. Antibacterial activity of β -carboline analogues

Though new antibacterial classes such as oxazolidinones and cyclic lipopeptides have enhanced the available treatment options for extended drug-resistant bacteria, according to WHO reports, there still exists a shortage of molecules in the clinical development pipeline to oppose the current and emerging bacterial resistance. WHO 's priority pathogen list for research and development includes *Mycobacterium tuberculosis* and Gram-negative carbapenem-resistant pathogens *Pseudomonas aeruginosa*, *Acinetobacter baumannii* and *Enterobacteriaceae*. Strategies to overcome the overwhelming antibiotic resistance are related to the development of innovative molecules that do not confer any cross antibiotic resistance, as many of the molecules in the pipeline are me-too drugs or variations of existing classes of drugs⁴⁸⁻⁵⁰.

In 2015, a novel series of diaryl piperazine derivatives were designed and synthesized by Penta Ashok et al. based on the molecular hybridization technique. The synthesized derivatives were tested against *M. tuberculosis* H37Rv strain. Among the tested derivatives, compounds **18-28**

Chapter 2. Literature review on β -carboline

exhibited significant anti-tubercular activity with Minimum Inhibitory Concentration (MIC) values $< 6.25 \mu\text{g/mL}$, with compound **66a** being the most potent of them all with a MIC value of $1.5 \mu\text{g/mL}$ ⁵¹ (Fig. 2.22).

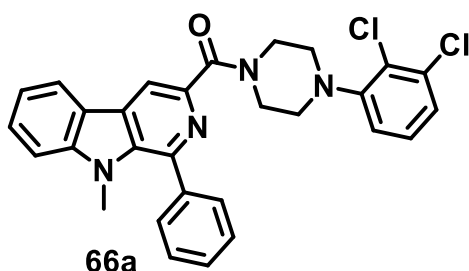


Figure-2.22 Structure of compound **66a**

A series of novel triazole tethered β -carboline derivatives were synthesized and evaluated for their antibacterial activity by Salehi et al. in the year 2016. The synthesized β -carboline derivatives were evaluated against five bacterial strains- *Staphylococcus aureus* (ATCC 25923), *Escherichia coli* (ATCC 25922), *Enterococcus faecalis* (ATCC 29212), *Bacillus cereus* (PTCC 1015) and vancomycin-resistant strain of *Enterococcus faecium* (VREF, ATCC 51559). Among the synthesized β -carboline derivatives, compounds **67a-69a** showed potent antibacterial activity than standard drugs chloramphenicol, vancomycin and cefixime against *E. faecium* (Fig. 2.23). The presence of the bromophenyl group on the fourth position of the triazole nucleus potentiated the antibacterial activity. The synthesized derivatives also showed weak antibacterial activity against *S. aureus*, *B. cereus* and *E. coli*⁵².

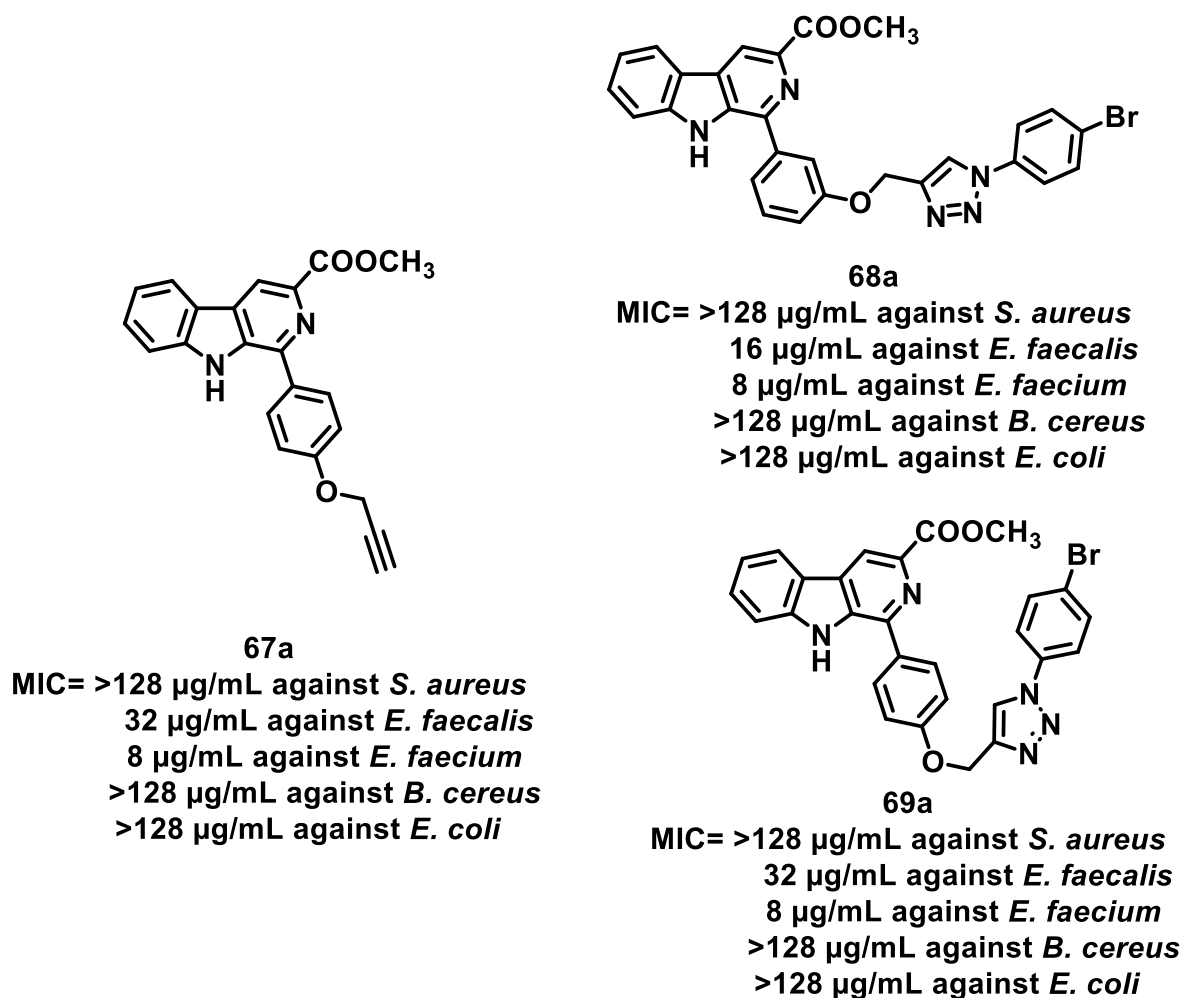


Figure 2.23. Structure of compounds **67a-69a**

Owing to the comprehensive pharmacological profile of canthin-6-one (**70a**) derivatives, a subclass of β -carboline alkaloids, Dai et al. synthesized a series of 3*N*-substituted-canthin-6-one analogues in the year 2016⁵³. The synthesized analogues were tested against two gram-positive bacterial strains - *S. aureus*, *B. cereus* and two gram-negative bacterial strains - *Pseudomonas solanacearum* and *Ralstonia solanacearum*. Among the tested analogues, compounds **71a** and **72a** were found to exhibit better activity (Fig. 2.24). However, compound **73a** was found to exhibit potent activity against *S. aureus* with a MIC value of 0.98 $\mu\text{g/mL}$.

Chapter 2. Literature review on β -carboline

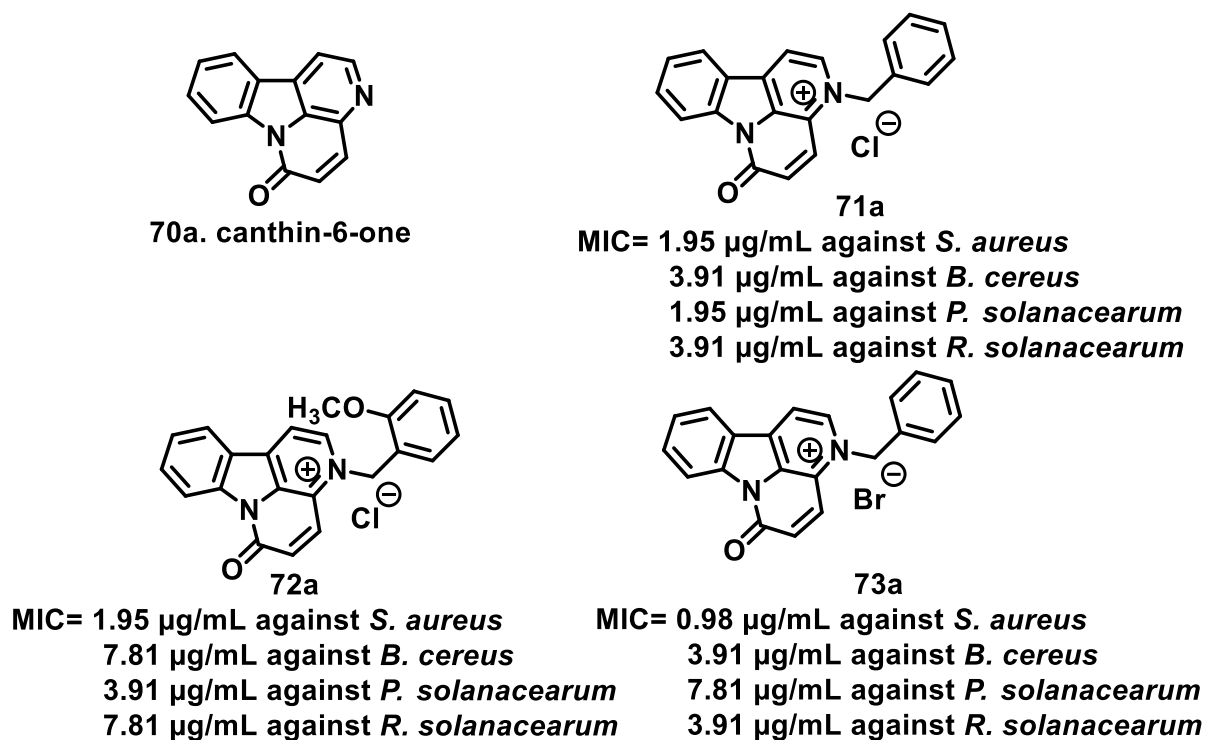
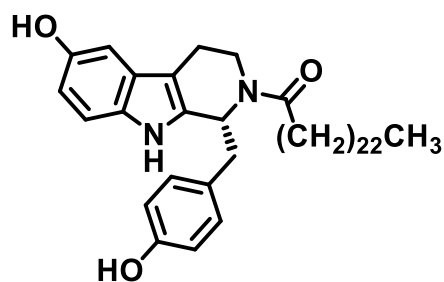


Figure-2.24 Structure of compounds **70a-73a**

In 2017, Samita et al. reported the isolation and structure of Sacleuximine A (**74a**), a natural β -carboline alkaloid from aerial parts of *Triclisia sacleuxii*⁵⁴. It was evaluated for its antibacterial activity against both gram-negative as well as gram-positive strains of bacteria. The obtained results indicate that MIC values ranged between 31.3-125 $\mu\text{g/mL}$ (Fig. 2.25).



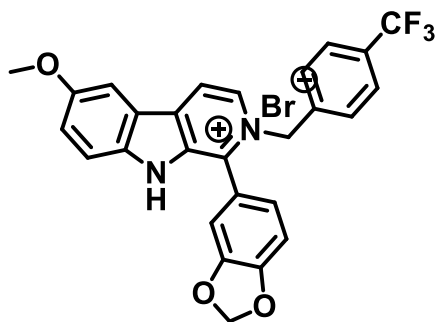
74a. Sacleuximine A
MIC= 125 $\mu\text{g/mL}$ against *E. coli*
31.3 $\mu\text{g/mL}$ against *P. aeruginosa*
62.5 $\mu\text{g/mL}$ against *S. epidermis*

Figure 2.25 Structure of sacleuximine A (**74a**)

Inspired by the antibacterial potential of Harman and their study conducted on canthin-6-one analogues, Dai et al. designed and synthesized a series of quaternized Harman analogues and tested their antibacterial activity *in vitro* and *in vivo*⁵⁵. Among them, compound **75a** showed exceptional bactericidal effect surpassing the effect produced by standard drugs like

Chapter 2. Literature review on β -carboline

fosfomycin and ampicillin with four-fold superiority against Methicillin-Resistant *Staphylococcus aureus* (MRSA) (*S. aureus* ATCC 43300) (Fig. 2.26). To deduce the mechanism of action of compound **75a**, scanning electron microscopy analysis and molecular docking study was performed. It was proposed that compound **75a** might exhibit its activity by disrupting the cell wall and the membrane leading to increased permeability and cell death.



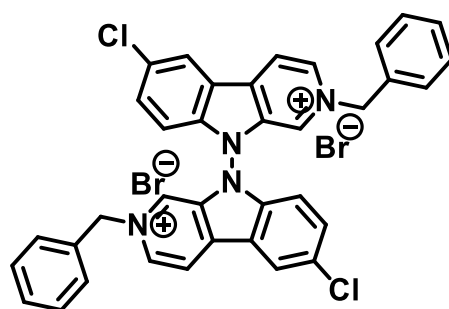
75a

MIC= 25 nmol/mL against *S. aureus*
12.5 nmol/mL against MRSA
25 nmol/mL against *B. cereus*
25 nmol/mL against *B. subtilis*
50 nmol/mL against *E. coli*
25 nmol/mL against *R. solanacearum*

Fig. 2.26 Structure of compound **75a**

In 2018, a series of β -carboline dimers and their N^2 -alkylated analogues were synthesized by Suzuki et al. ⁵⁶. The synthesized β -carboline analogues were evaluated for their *in vitro* antibacterial activity. Compound **76a** exhibited promising antibacterial activity, with its action being more pronounced against *S. aureus* with MIC values ranging from 0.01-0.05 $\mu\text{mol/mL}$. The dimeric form of β -carboline derivatives exhibited better antibacterial activity than their monomeric form (Fig. 2.27).

Chapter 2. Literature review on β -carboline



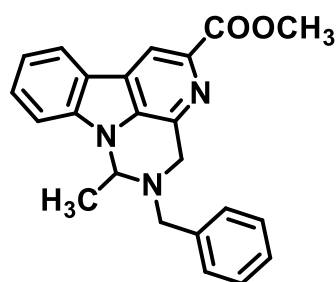
76a

MIC= 0.01 $\mu\text{mol/mL}$ against *Staphylococcus aureus*
0.05 $\mu\text{mol/mL}$ against *Staphylococcus aureus*
0.01 $\mu\text{mol/mL}$ against *Staphylococcus aureus*
0.01 $\mu\text{mol/mL}$ against *Staphylococcus aureus*
0.05 $\mu\text{mol/mL}$ against *Escherichia coli*
>1 $\mu\text{mol/mL}$ against *Pseudomonas aeruginosa*
0.5 $\mu\text{mol/mL}$ against *Acinetobacter baumannii*

Figure 2.27 Structure of compound 76a

Continuing their studies on canthin-6-one analogues, Dai et al. in the year 2018, reported the design and synthesis of novel canthin-6-one derivatives. The synthesized analogues were evaluated for their antibacterial activity against two gram-negative- *E. coli* and *R. solanacearum* and four gram-positive bacteria- *S. aureus*, MRSA, *B. cereus* and *B. subtilis*. Among the 31 derivatives that were assessed, compound **77a** was found to be significantly bioactive with the MIC value of 4 $\mu\text{g/mL}$ (Fig. 2.28). Compound **77a** also exhibited low cytotoxicity against LO2 cells and complied with the Lipinski rule of 5, with all the values being well within the accepted range. Further studies were conducted to explore its mechanism of action. The studies revealed that compound **77a** exerts its antibacterial action by disrupting the cell membrane and by altering the structure of DNA by interacting with it, thus rendering it unrecognizable by DNA topoisomerases leading to cell death⁵⁷.

Chapter 2. Literature review on β -carboline

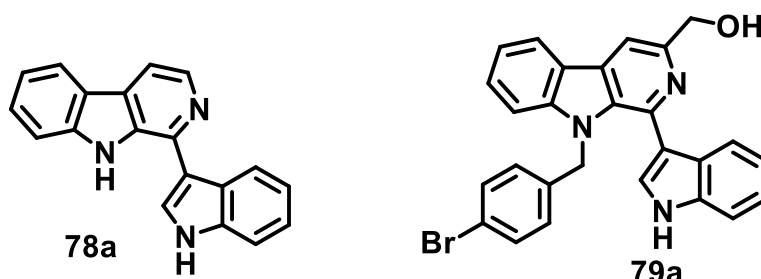


77a

MIC= 12.5 nmol/mL against *S. aureus*
25 nmol/mL against MRSA
25 nmol/mL against *B. cereus*
12.5 nmol/mL against *B. subtilis*
>200 nmol/mL against *E. coli*
25 nmol/mL against *R. solanacearum*

Figure 2.28 Structure of compound 77a

In their effort to increase the antibacterial potency of eudistomin U, a naturally occurring β -carboline analogue found in the marine ascidians, Dai et al. reported the design and synthesis of eudistomin U analogues⁵⁸. The analogues were designed based on the results obtained from the molecular docking study. The analogues were designed by keeping the core of eudistomin U (78a) and substituting with different groups on C-3 and N-9 (Fig. 2.29). The synthesized analogues were evaluated for their antibacterial activity against four bacterial strains (*S. aureus*, MRSA, *B. cereus*, and *R. solanacearum*). Compound 79a stood out from the rest of the analogues with its antibacterial potency surpassing the effect produced by commercially available drugs ciprofloxacin and propineb against MRSA and *R. solanacearum*, respectively. Further studies were conducted to shed light on the mechanism of action of compound 79a. It was proposed that compound 79a might exhibit its damaging effect by disrupting the cell membrane resulting in its entry into the cell and then interfering with the functions of DNA gyrase⁵⁸.



MIC= 3.125 μ mol/L against *S. aureus*
3.125 μ mol/L against MRSA
3.125 μ mol/L against *B. cereus*
1.5625 μ mol/L against *R. solanacearum*

Figure-2.29 Structure of Eudistomin U (78a) and compound 79a

Chapter 2. Literature review on β -carboline

In 2019, Pan et al. reported the total synthesis of Griseofamine A (**80a**), a fungal metabolite produced by *Penicillium griseofulvum* and its diastereomer 16-epi-griseofamine (**81a**)⁵⁹. The synthesized compounds were evaluated for their antibacterial properties against a panel of bacterial strains, which included both gram-positive and gram-negative bacteria. Both the compounds showed selective activity against gram-positive bacteria, including various drug-resistant bacteria like MRSA (ATCC33591), Methicillin-resistant *S. epidermidis* (MRSE) (16-5), Vancomycin-resistant *Enterococci* (VRE) (ATCC51299) with the MIC values ranging between 8-16 $\mu\text{g/mL}$ and 2-8 $\mu\text{g/mL}$ for griseofamine A and 16-epi-griseofamine, respectively. The diastereomer 16-epi-griseofamine was found to be 2-3 times more potent than its counterpart (Fig. 2.30).

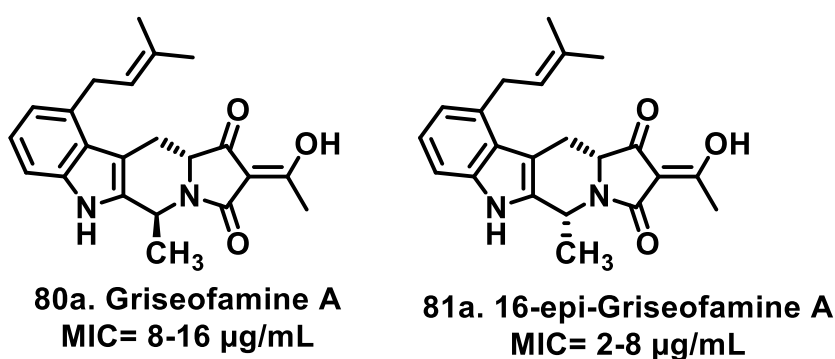


Figure 2.30 Structure of griseofamine A (**80a**) and 16-epi-griseofamine A (**81a**)

A series of imide β -carboline and carbomethoxy β -carboline derivatives were synthesized and evaluated for their antimycobacterial activity by Lopes-Ortiz et al. in the year 2020⁶⁰. Among the compounds evaluated, compounds **82a** and **83a** exhibited better potency than other synthesized analogues, especially against clinically resistant strains of *Mycobacterium* and were safe towards VERO cell lines (Fig. 2.31).

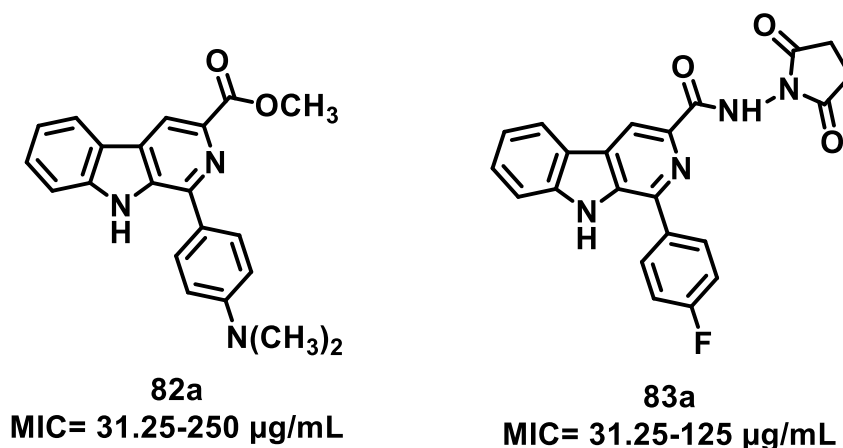


Figure 2.31 Structure of compounds **82a** and **83a**

2.4. Antifungal activity of β -carboline analogues

Fungal infections may be invasive and superficial and the impediment in treatment is due to the presence of common eukaryotic features fungi share with the host organisms, which may lead to potential toxicity, in the case of a common drug target. At present, antifungal agents belong to either one of the five chemical / structural classes: azoles, echinocandins, polyenes pyrimidine and allylamine analogues. Drug development approaches in the recent era target the cell wall, as it is absent in humans. Nevertheless, drug resistance continues to pose a problem, owing to which there is a necessity of new lead molecules⁶¹⁻⁶³.

Harmala alkaloids like harmaline (**84a**), harmine (**85a**), harmalol (**86a**) and their derivatives were evaluated for their *in vitro* antifungal activity against *Cryptococcus neoformans* and *Cryptococcus gattii*. Among the compounds that were screened, 8-nitroharmane (**87a**) was found to be the potent compound with a MIC value of 40 $\mu\text{g/mL}$ against both *C. neoformans* and *C. gattii* fungal strains. It was also evaluated for its cytotoxicity against normal human fibroblasts (MRC-5). 8-nitroharmane exhibited low cytotoxicity with IC_{50} value greater than 50 $\mu\text{g/mL}$ ⁶⁴ (Fig. 2.32).

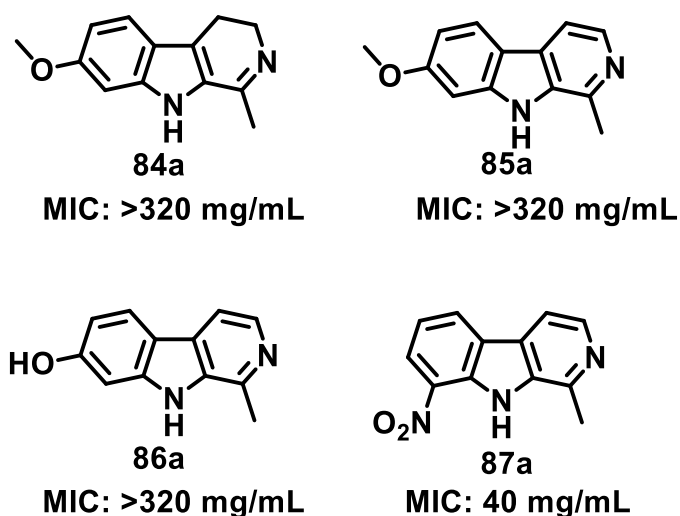


Figure 2.32 Structure of compounds **84a-87a**

Series of β -carboline derivatives were designed, synthesized, and were evaluated against *C. neoformans* for the treatment of cryptococcal meningitis. The synthesized compounds belong to four different scaffolds **88a**, **89a**, **90a** and **91a**. Compound **92a** belonging to scaffold **88a** was found to be the most potent compound with a MIC value of 0.25 $\mu\text{g/mL}$ (Fig. 2.33). Compound **92a** also exhibited potent *in vitro* activity against other fungal pathogens like *Candida albicans*, *Candida gattii*, *Candida glabrata*, among others. The *in vivo* antifungal potential of compound **92a** was evaluated in a murine model of cryptococcal meningitis.

Chapter 2. Literature review on β -carboline

Compound **92a** was found to reduce fungal load in the brain more effectively than the standard drug flucytosine, highlighting its antifungal potency⁶⁵. Further studies were conducted to deduce the mechanism of action of compound **92a**. Microscopic studies revealed that compound **92a** caused abnormal changes in the cell wall and membrane⁶⁵. It was shown that compound **92a** interferes with the cell cycle of *C. neoformans*. Flow cytometric studies revealed that compound **92a** caused cell cycle arrest in the G2/M phase of the cell cycle. Cdc25c/CDK1/Cyclin B pathway plays a prominent role in the homeostasis of the G2/M phase⁶⁶. Compound **92a** caused an upsurge in the levels of Cdc25c and CDK1 in a dose-dependent manner, thus confirming its role in hindering the G2/M phase of the cell cycle⁶⁵.

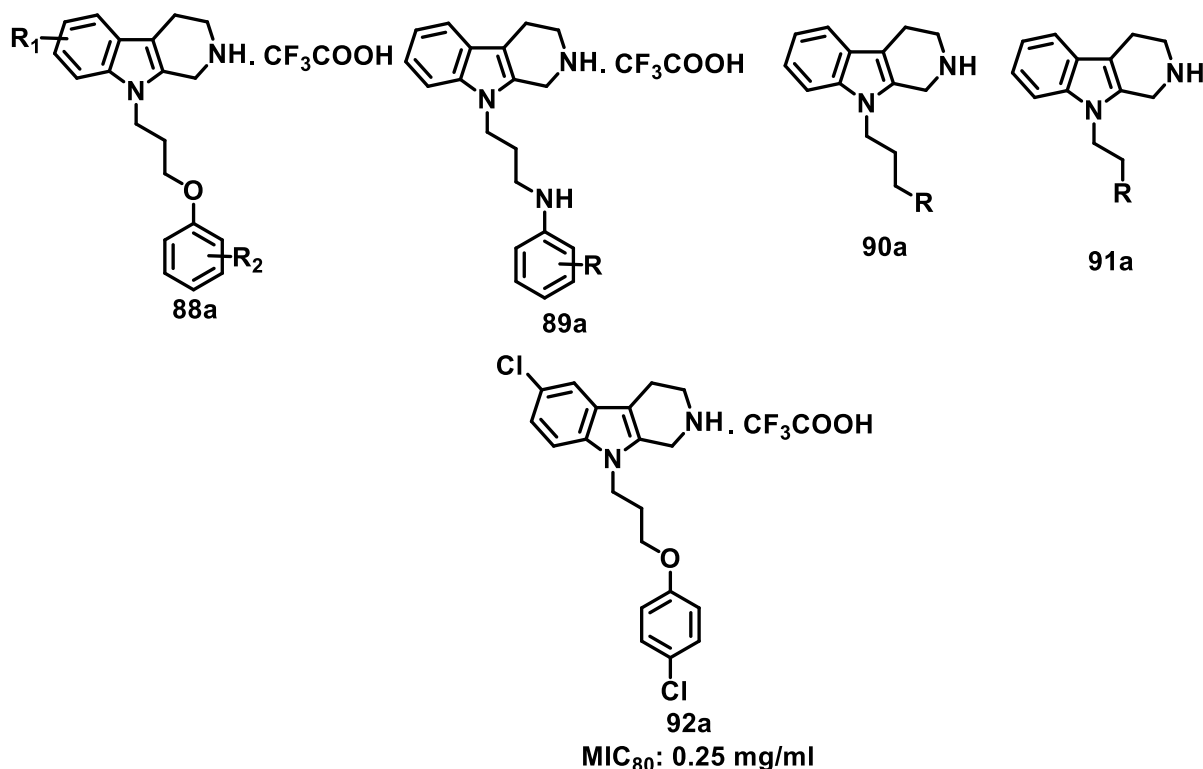
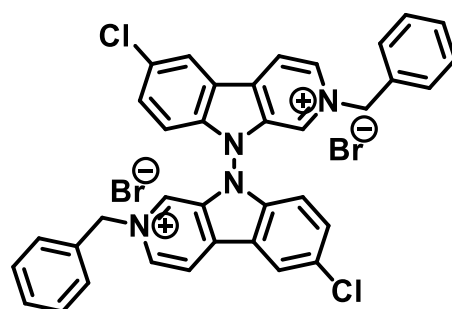


Figure 2.33 Structure of compounds **88a-92a**

Suzuki et al. in the year 2018, synthesized a series of β -carboline dimers and evaluated their antifungal activity against *C. albicans* (GAI 05108), *Candida intermedia* (GAI 15003) and *Candida krusei* (ATCC 14243)⁵⁶. Compound **93a** exhibited MIC values between 0.01-0.5 μ mol/mL, with its antifungal activity being most potent against *C. intermedia* (Fig. 2.34).

Chapter 2. Literature review on β -carboline



93a

MIC= 0.5 $\mu\text{mol/mL}$ against *Candida albicans*
0.01 $\mu\text{mol/mL}$ against *Candida intermedia*
0.5 $\mu\text{mol/mL}$ against *Candida krusei*

Figure 2.34 Structure of compound 93a

2.5. Antiviral activity of β -carboline analogues

Viral diseases account for approximately one-third of the fatalities associated with infectious diseases and the prevalence of long-standing viral infections such as hepatitis and Human immunodeficiency virus (HIV) and the manifestation of new such as coronavirus, drive the need for new antiviral therapy. The FDA has approved around 50 antivirals as of 2014. Antivirals may target the virus or host factors and can be classified into entry inhibitors, nucleoside and non-nucleoside analogues which hamper with viral nucleic acid productions, interferons which block viral protein synthesis and protease inhibitors which impede the maturation of the virions. Despite research focus on antiviral drug development, issues such as upsurge in viral pandemics, lack of complete cures for existing infections, rising resistance and narrow activity spectrum of new antivirals pose a major obstacles during the drug development process⁶⁷⁻⁷⁰.

In 2015, Ashok et al. disclosed the design, synthesis, and *in vitro* antiviral activity of novel β -carboline derivatives against HIV-1⁷¹. Among the β -carboline derivatives that were evaluated, compounds **94a-97a** effectively inhibited the replication of HIV-1 by suppressing the formation of syncytia with compound **95a** being the most potent, with an EC_{50} of 0.53 μM . Furthermore, compound **95a** also inhibited the production of p24 antigen with an EC_{50} value of 1.1 μM (Fig.2.35).

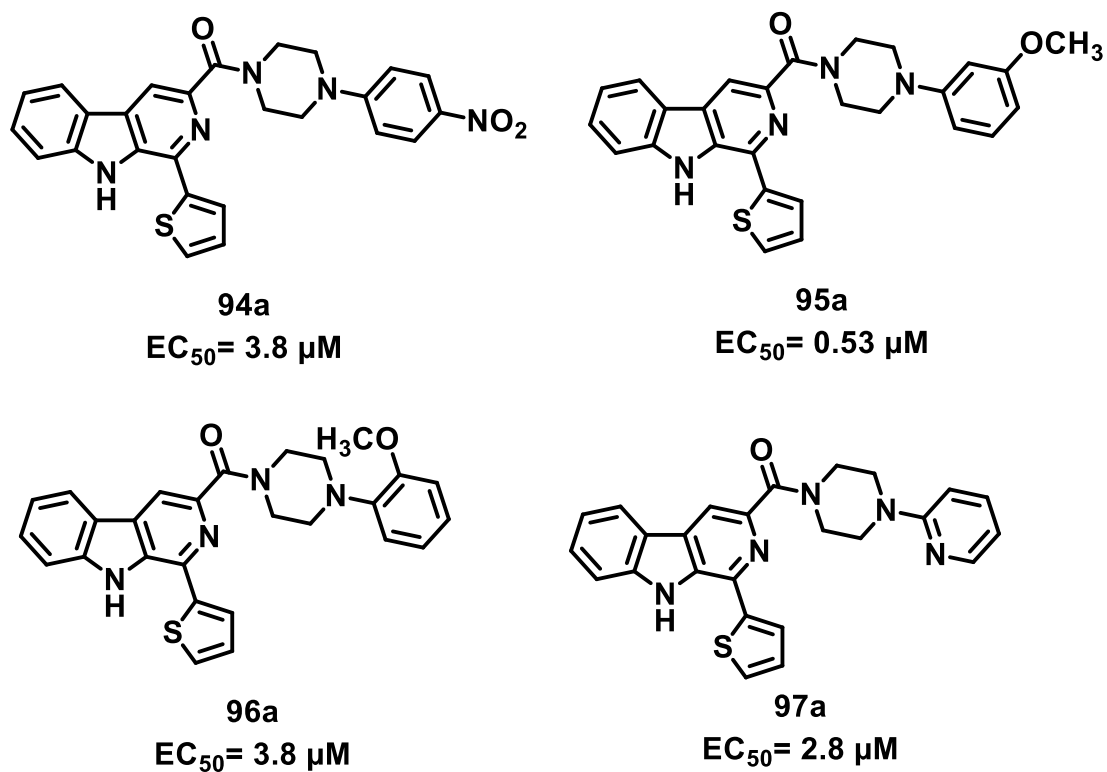


Figure 2.35 Structure of compounds **94a-97a**

In 2015, Ashok et al. reported the design, synthesis of novel β -carboline derivatives⁷². The synthesized analogues were evaluated for their anti-HIV activity against HIV-1 and HIV-2 strains. To the surprise of the authors, compounds **98a-101a** (Fig. 2.36) exhibited selective inhibition of HIV-2 strains with compound **100a** being the most potent of them, all with an EC_{50} value of $2.6 \mu\text{M}$, which was comparable with that of standard drugs - Nevirapine, Lamivudine and Dideoxyinosine. The mechanism for the selective inhibition of HIV-2 strains by the compounds **98a-101a** remains a mystery as the authors ruled out the HIV-2 reverse transcriptase enzyme as a potential target.

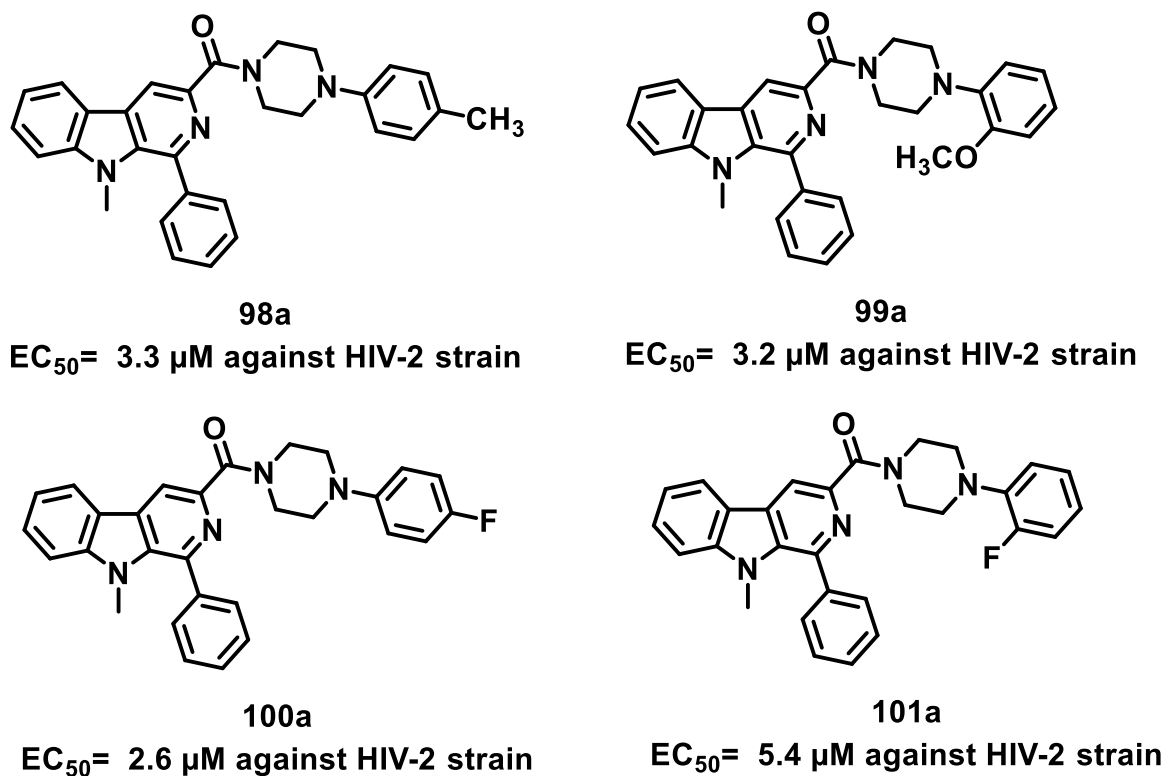
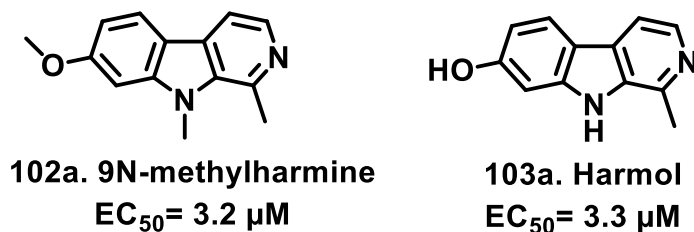


Figure-2.36 Structure of compounds 98a-101a

In 2016, Quintana et al. reported the investigative study conducted on the antiviral capability of some natural and synthetic β -carbolines directed against Dengue virus (DENV)⁷³. Although, a majority of the compounds were found to be inactive or exhibited moderate activity, synthetic derivative 9*N*-methylharmine (**102a**) and a natural β -carboline harmol (**103a**) exhibited a potent inhibitory effect on DENV-2 production with EC₅₀ values of 3.2 μ M and 3.3 μ M, respectively (Fig. 2.37). However, both the compounds failed to exhibit any virucidal activity. Further mechanistic studies revealed that 9*N*-methylharmine prevented the spread of infection by hindering the maturation of the virus and the delivery of viral particles into the extracellular medium.

Figure 2.37 Structure of 9*N*-methylharmine (**102a**) and harmol (**103a**)

In the year 2016, Barbosa et al. reported the synthesis of some novel β -carboline-thiazolidinone hybrids to combat HSV-1 infection⁷⁴. Among the hybrids that were synthesized and evaluated,

Chapter 2. Literature review on β -carboline

compounds **104a-106a** exhibited potent antiviral activity with compound **105a** being the most effective with an EC_{50} value of $0.80 \mu\text{M}$ (Fig. 2.38).

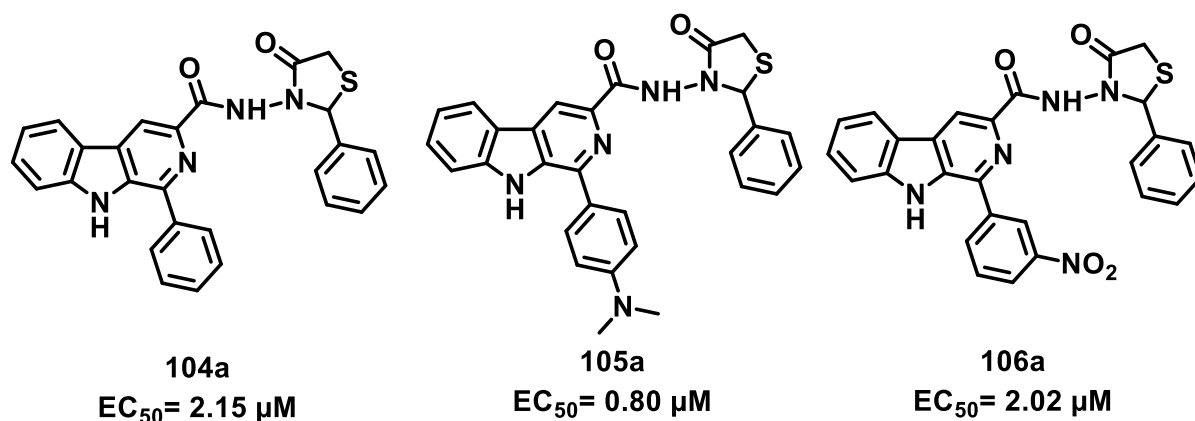


Figure 2.38 Structure of compounds **104a-106a**

In 2018, Gonzalez et al. reported the anti-herpetic properties of some β -carbolines⁷⁵. Among the twenty-one β -carbolines that were evaluated, only three β -carbolines - 9-methyl norharmane (**107a**), 9-methyl harmane (**108a**) and 6-methoxy harmane (**109a**) was very effective in protecting the cells from the cytotoxic effects of Herpes Simplex Virus (HSV) (Fig. 2.39). Compounds **107a-109a** did not possess any virucidal property against the dengue virus, which was consistent with the study reported by Quintana et al.⁷³. Further studies conducted to discover its mechanism of action revealed that these compounds exhibited their activity by affecting the functionality and functionalization of HSV-1 ICP0 (Herpes simplex virus type 1 Infected Cell Protein 0) protein, which plays a vital role in shutting down the host antiviral machinery and in viral replication. The compounds were also found to down-regulate the expression of early and late proteins after penetration of the virus into the cells.

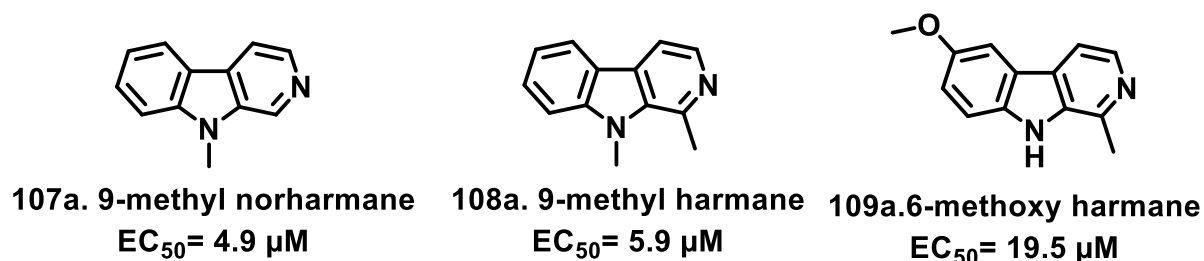


Figure-2.39 Structure of compounds **107a-109a**

2.6. Antimalarial activity of β -carboline analogues

Malaria continues to be a global health concern amassing almost 405,000 deaths out of 228 million cases in 2018 with children under the age of 5 being most vulnerable as they accounted for almost 67 % of the death in the year 2018⁷⁶. Malaria is caused by a parasite belonging to

Chapter 2. Literature review on β -carboline

the genus *Plasmodium* and transmitted to humans by female *Anopheles* mosquitos. Five types of malarial parasites are known to affect humans - *Plasmodium falciparum*, *Plasmodium vivax*, *Plasmodium ovale*, *Plasmodium malariae* and *Plasmodium knowlesi* with *P. falciparum* being the most virulent with high mortality and morbidity⁷⁷. For decades, drugs containing quinoline core such as chloroquine, mefloquine, amodiaquine, among others, have been used for the treatment of malaria. However, widespread resistance to quinolines has suppressed their use clinically. Currently, Artemisinin combination therapy (ACT), a combination of artemisinin with another antimalarial agent to prevent resistance, is the first-line treatment for falciparum malaria. However, recent reports of resistance to ACTs⁷⁸ have underlined the need for the development of novel antimalarial drug candidates and the discovery of novel targets.

Following their initial findings that compound MMV008138 (**110a**) targets the apicoplast of *P. falciparum* and exhibits its antimalarial activity⁷⁹, Yao et al. in the year 2015, determined the active stereoisomer responsible for the activity as mentioned above⁸⁰. The study identified compound **111a** as the active stereoisomer of MMV008138 and exhibited an IC_{50} value of 250 nM, which was comparable to that of MMV008138. Additionally, they synthesized several analogues of compounds and compound **112a** was found to be more potent than compounds with an IC_{50} value of 190 nM (Fig 2.40).

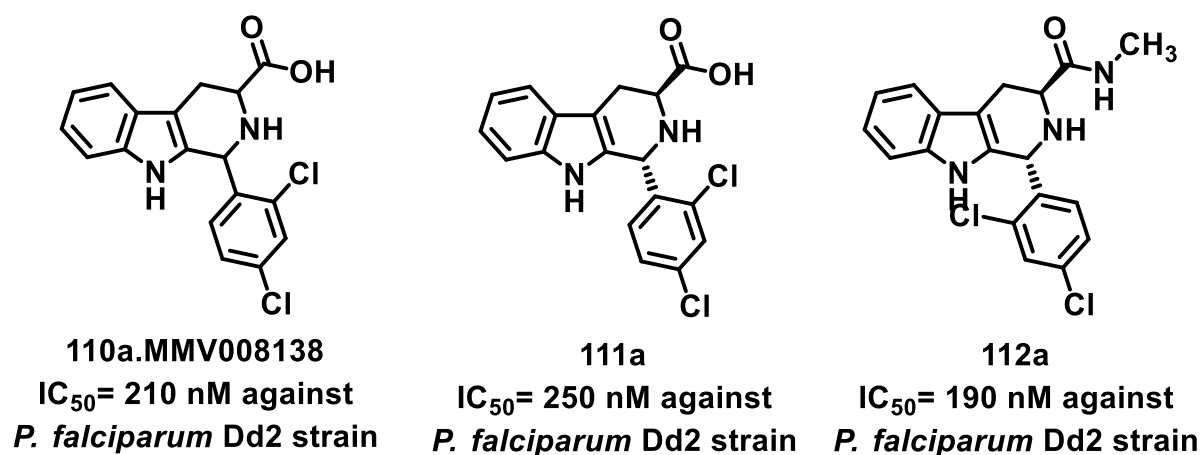


Figure-2.40 Structure of compounds **110a-112a**

Following the report that suggested harmine exhibited potent antimalarial activity by binding to *P. falciparum* heat shock protein 90 (*PfHsp90*) more effectively than the human counterpart⁸¹, Bayih et al. generated a collection of harmine analogues in the year 2016 and determined their ability to bind to *PfHsp90*⁸². *PfHsp90* is a vital chaperone protein that is essential for the growth of malarial parasite during the intraerythrocytic cycle^{83,84}. The life of the malarial parasite has been split between insect stage and the mammalian stage. During transition from

Chapter 2. Literature review on β -carboline

the insect stage to the mammalian stage, the malarial parasite is exposed to a drastic change in temperature. The malarial parasite has developed an internal defence mechanism, i.e., molecular chaperones, to protect against the drastic change in temperature⁸⁵. The malarial parasite was shown to up-regulate the transcription of *PfHsp90* by three to four-fold when cultured around 40 °C. They are involved in normal protein folding and play an essential role in protein trafficking, cell cycle, gene expression and cell differentiation⁸⁶. Structurally, Hsp90 contains a C-terminal substrate-binding domain, a central hinge domain, and the N-terminus ATPase domain⁸⁷. The crystal structure of *PfHsp90* revealed that there are some unique residues in the ATP-binding domain that is different from the Human Hsp90⁸⁸. Considering its essential role in the growth of parasite and structural differences between *PfHsp90* and human Hsp90, *PfHsp90* is an attractive target for drug discovery against malarial parasites. Out of the forty-two analogues that were tested against *PfHsp90* by Bayih et al. compounds **113a** and **114a** turned out to be the most active with IC_{50} values of 12.2 μ M and 23.1 μ M, respectively (Fig. 2.41). Furthermore, compounds **113a** and **114a** exhibited significant antimalarial activity both *in vitro* as well as *in vivo*. Compounds **113a** and **114a** effectively reduced parasitaemia by 51.5% and 56.1% respectively, in *Plasmodium berghei* ANKA strain (chloroquine sensitive, came from ANtwerpen and KAtanga) infected mice model. Compound **114a**, when given in combination with dihydro-artemisinin exhibited better *in vivo* activity profile and also decreased the mortality of mice than either of the compounds when administered alone⁸².

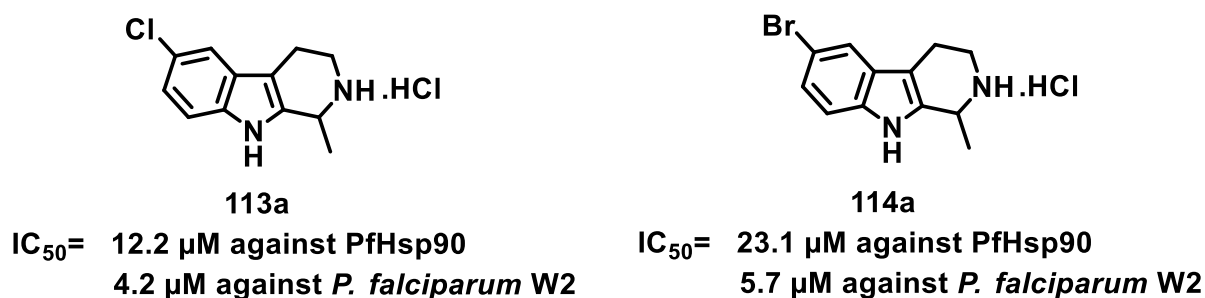
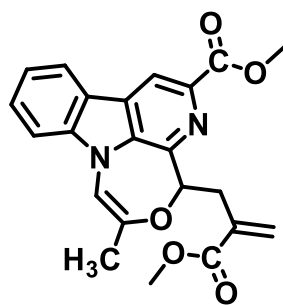


Figure-2.41 Structure of compounds **113a** and **114a**

In 2017, Yadav et al. reported the synthesis and antimalarial activity of β -carboline-fused-1,4-oxaazepine derivatives⁸⁹. Among the analogues that were evaluated, compound **115a** exhibited excellent *in vitro* antimalarial activity against chloroquine-sensitive *P. falciparum* strain 3D7 as well as chloroquine-resistant *P. falciparum* strain K1 with IC_{50} values of 0.57 and 0.72 μ M, respectively. However, compound **115a** did not exhibit any *in vivo* anti-plasmodial effect against multidrug-resistant *P. yoelii*nigeriensis (Fig. 2.42).

Chapter 2. Literature review on β -carboline



115a

IC_{50} = 0.57 μ M against chloroquine sensitive *P. falciparum*
0.72 μ M against chloroquine resistant *P. falciparum*

Figure-2.42 Structure of compound 115a

In continuation of their earlier reports, Ghavami et al. in the year 2018, reported the synthesis and biological studies of MMV008138 **116a** and its analogues on the target Plasmodium falciparum IspD (2-C-methyl-D-erythritol-4-phosphate cytidyltransferase) (*PfIspD*)⁹⁰. Compound **116a** exhibited an IC_{50} value of 44 nM against the target while the other isomers of MMV008138 exhibited weak inhibition. Compound **116a** was also found to be selective only to the *PfIspD* as further studies revealed that it did not affect the human IspD. Compounds **117a -120a** were found to exhibit more potent activity than compound **116a** (Fig 2.43).

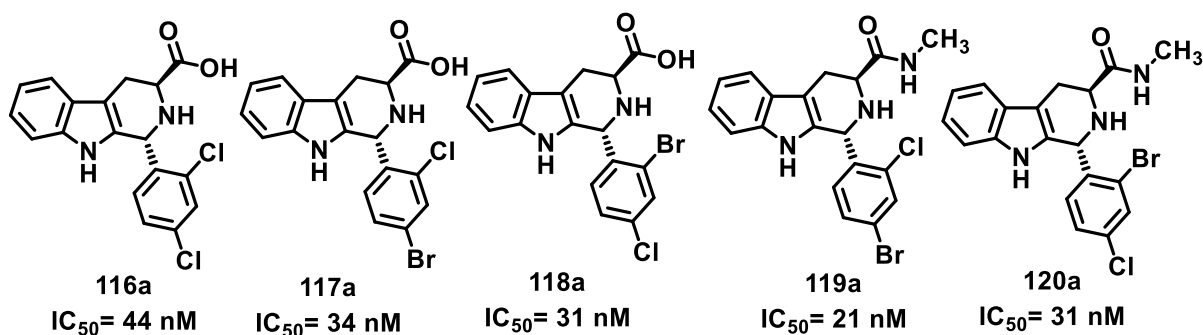


Figure 2.43 Structure of compounds 116a and 117a-120a

In 2018, Gorki et al. reported the synthesis, *in vitro* and *in vivo* antimalarial activity of β -carboline derivatives⁹¹. The synthesized β -carboline analogues were evaluated based on their ability to inhibit the schizont maturation of *P. berghei in vitro*. Two compounds, **121a** and **122a** (Fig. 2.44), exhibited 71.79% and 86.17% inhibition, respectively, at a concentration of 5 μ g/mL and thus were further evaluated for their antimalarial efficacy *in vivo* in the rodent malaria model. However, compound **121a** exhibited better parasite clearance *in vivo* and was more effective in increasing the survivability of the host. Both the compounds were also found to be safe renally and hepatically.

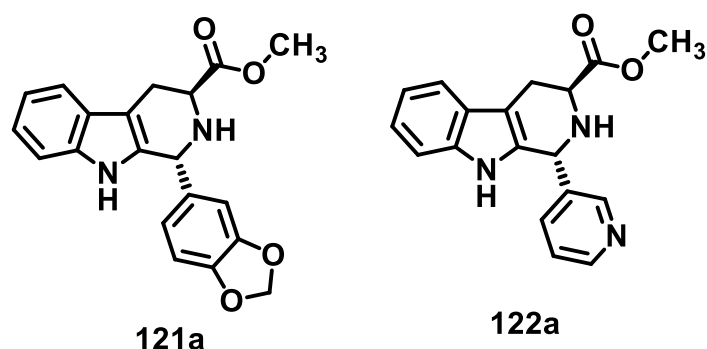
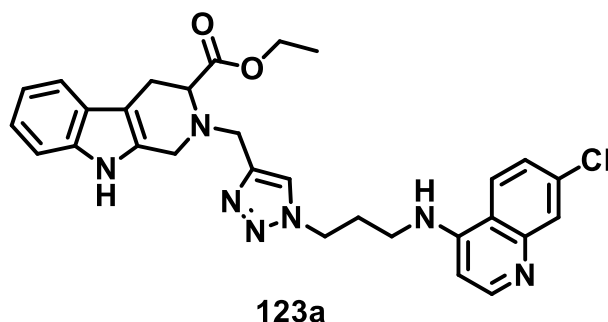


Figure 2.44 Structure of compounds **121a** and **122a**

Sharma et al. in the year 2019, reported the synthesis and anti-plasmodial activity of triazole / acyl hydrazide tethered tetrahydro- β -carboline-aminoquinoline conjugates against chloroquine-resistant *P. falciparum* W2 strain⁹². The synthesized compounds were also evaluated for their toxicity against vero cell lines. Compound **123a** was found to be the most potent, with an IC_{50} value of 0.49 μ M (Fig. 2.45). Compound **123a** was also found to be non-cytotoxic and exhibited a selectivity index of 495.76.



IC_{50} = 0.49 μ M against *P. falciparum*

Figure-2.45 Structure of compound **123a**

In the same year, Pierrot et al. reported the design, synthesis and antimalarial activity of β -carboline analogues against chloroquine-resistant *P. falciparum* K1 strain⁹³. Compounds **124a-126a** exhibited better antimalarial activity than the rest of the analogues with their IC_{50} values lying between 13.8-15.5 μ M (Fig. 2.46).

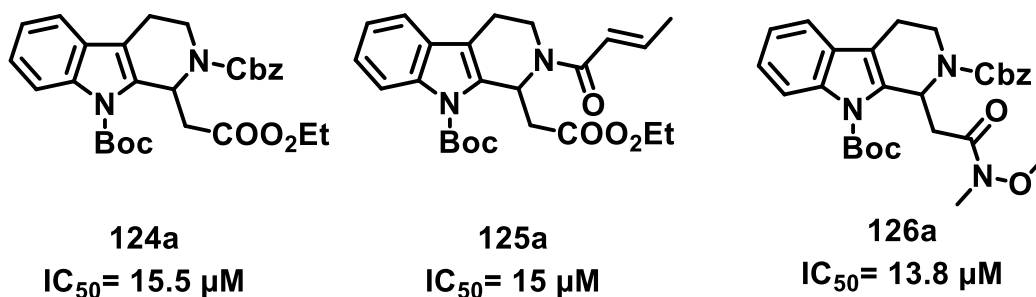


Figure 2.46 Structure of compounds **124a-126a**

Chapter 2. Literature review on β -carboline

2.7. Antitrypanosomal activity of β -carboline analogues

American trypanosomiasis, also known as Chagas disease, is one of the neglected tropical diseases (NTDs), caused by the kinetoplastida protozoan parasite *Trypanosoma cruzi*. It is transmitted to humans when they encounter the feces of infected triatomine bugs, also known as ‘kissing bugs.’ Chagas disease was initially confined only to regions of Latin America. However, it has also spread to other parts of the world like United States of America, Canada, Europe and Asia due to globalization and migration of people infected with *T. cruzi*⁹⁴. Currently, two drugs have been used for treating Chagas disease- benznidazole and nifurtimox. These drugs are highly effective only when they are given at the onset of the acute phase of infection, a phase where people generally do not know whether they are affected with *T. cruzi* or not⁹⁵. They have reduced cure rates, about 20% when the infection reaches the chronic phase⁹⁶. Furthermore, they have several side effects and is contraindicated for patients with kidney or liver dysfunction and pregnant women ushering the need for the development of better drugs. Owing to the promising results of earlier studies of compound **81** against *T. cruzi*^{95,97}, the pathogen responsible for causing Chagas disease, Volpato et al. in the year 2015, did an investigative study to understand the mechanism of action of compound **127a**⁹⁸ (Fig. 2.47). The mechanistic studies revealed that compound **127a** induced structural changes in mitochondria as characterized by increased mitochondrial reactive oxygen species (ROS) and formation of lipid droplets, which might be associated with the opening of permeability transition pore, thus leading to apoptosis. Apart from acting on mitochondria, compound **127a** was also shown to act on the plasma membrane of the parasite. Taken together, compound **127a** induced death in parasite either through necrotic or apoptotic pathways.

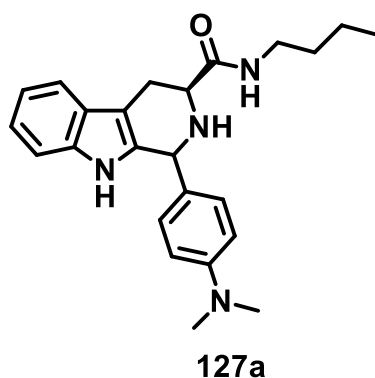


Figure-2.47 Structure of compound **127a**

2.8. Anti-leishmanial structure activity relationship (SAR) studies of β -carbolines

Structure-activity relationship studies are a critical key to many aspects of drug discovery, ranging from primary screening to lead optimization. A collection of molecules and their associated activities were trying to elucidate the details of one or more SARs and subsequently using that information to make structural modifications to optimize some property or activity of the particular moieties⁹⁹.

In this context, the titled β -carboline derivatives were associated with its anti-leishmanial effects. The moiety was well explored, and the library of molecules was already designed, synthesized and many molecules are in the pipeline. The SAR pattern of this moiety helps to identify or modify the existing structure with various substitutions at possible positions to make potent analogues against the neglected tropical disease such as “Leishmaniasis.” The modification of “A” ring at the 6th position with bulkier substituents decreases the anti-leishmanial activity when compared with the unsubstituted analogues at the same position. Tetrahydro- β -carboline nucleus also showed significant anti-leishmanial activity. The structural modifications performed at various positions of “C” ring may improve the potency. Works of the literature indicated that most of the researchers focus on “C” ring only. The modifications on this “C” ring are simple to make and might lead to drastic increase in the anti-leishmanial activity (**Fig 2.48**).

On the second position of β -carboline (**C ring**), substitution with *N*-oxides, small carbon chains, amide substitutions may increase the efficacy. Substitution at the third position with numerous analogues like ortho, para directing phenyl rings, methoxy derivatives of the benzene ring, heterocyclic aldehydes like thiophene, quinoline showed significant anti-leishmanial activity. With various structural modifications at the third position of “C” ring with functional groups such as ester and acid, better anti-leishmanial and anti-cancer activities were observed. Acid derivatives with simple phenyl substitutions enhanced both the anti-cancer and anti-leishmanial activities. Substitution with meta directing functional groups at the phenyl ring (**A**) may decrease the anti-leishmanial efficacy. Methyl substitution at NH of ninth position (**B ring**) increases the anti-leishmanial activity. According to the available data on ring **B**, less research has been explored as an anti-leishmanial agent. To conclude, more precisely, more study may be continued on ring **B**.

Chapter 2. Literature review on β -carboline

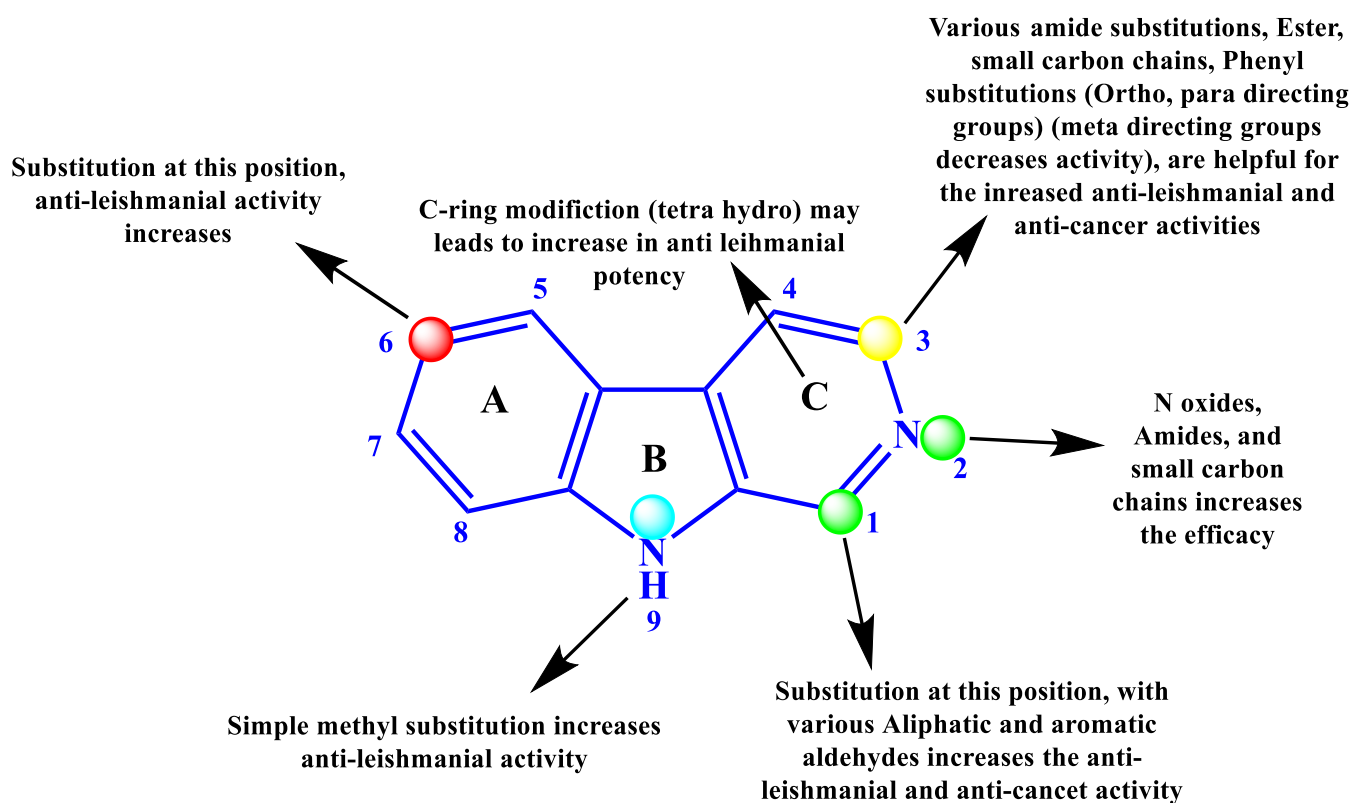


Figure-2.48 Structure activity relationship (SAR) study of β -carboline associated with its anti-leishmanial activity

Chapter 2. Literature review on β -carboline

References

- (1) Cao, R.; Peng, W.; Wang, Z.; Xu, A. Carboline Alkaloids: Biochemical and Pharmacological Functions. *Current Medicinal Chemistry* **2007**, *14* (4), 479–500. <https://doi.org/10.2174/092986707779940998>.
- (2) Dewick, P. M. *Medicinal Natural Products: A Biosynthetic Approach, Second Edition* - Dewick - Wiley Online Library; John Wiley & Sons, Ltd: Chichester, UK, 2002. <https://doi.org/10.1002/0470846275>.
- (3) França, P. H. B.; Barbosa, D. P.; Da Silva, D. L.; Ribeiro, Ê. A. N.; Santana, A. E. G.; Santos, B. V. O.; Barbosa-Filho, J. M.; Quintans, J. S. S.; Barreto, R. S. S.; Quintans, L. J.; De Araújo, J. X. Indole Alkaloids from Marine Sources as Potential Leads against Infectious Diseases. *BioMed Research International* **2014**, *2014*, 1–12. <https://doi.org/10.1155/2014/375423>.
- (4) Piechowska, P.; Zawirska-Wojtasiak, R.; Mildner-Szkudlarz, S. Bioactive β -Carbolines in Food: A Review. *Nutrients* **2019**, *11* (4), 1–10. <https://doi.org/10.3390/nu11040814>.
- (5) Samundeeswari, S.; Chougala, B.; Holiyachi, M.; Shastri, L.; Kulkarni, M.; Dodamani, S.; Jalalpur, S.; Joshi, S.; Dixit, S.; Sunagar, V.; Hunnur, R. Design and Synthesis of Novel Phenyl -1, 4-Beta-Carboline-Hybrid Molecules as Potential Anticancer Agents. *European Journal of Medicinal Chemistry* **2017**, *128*, 123–139. <https://doi.org/10.1016/j.ejmech.2017.01.014>.
- (6) Carvalho, A.; Chu, J.; Meinguet, C.; Kiss, R.; Vandenbussche, G.; Masereel, B.; Wouters, J.; Kornienko, A.; Pelletier, J.; Mathieu, V. A Harmine-Derived Beta-Carboline Displays Anti-Cancer Effects in Vitro by Targeting Protein Synthesis. *European Journal of Pharmacology* **2017**, *805*, 25–35. <https://doi.org/10.1016/j.ejphar.2017.03.034>.
- (7) Brahmabhatt, K. G.; Ahmed, N.; Sabde, S.; Mitra, D.; Singh, I. P.; Bhutani, K. K. Synthesis and Evaluation of β -Carboline Derivatives as Inhibitors of Human Immunodeficiency Virus. *Bioorganic and Medicinal Chemistry Letters* **2010**, *20* (15), 4416–4419. <https://doi.org/10.1016/j.bmcl.2010.06.052>.
- (8) Nenaah, G. Antibacterial and Antifungal Activities of (Beta)-Carboline Alkaloids of Peganum Harmala (L) Seeds and Their Combination Effects. *Fitoterapia* **2010**, *81* (7), 779–782. <https://doi.org/10.1016/j.fitote.2010.04.004>.
- (9) Kam, T. S.; Sim, K. M.; Koyano, T.; Komiyama, K. Leishmanicidal Alkaloids from *Kopsia Griffithii*. *Phytochemistry* **1999**, *50* (1), 75–79. <https://doi.org/10.1016/S0031->

Chapter 2. Literature review on β -carboline

- 9422(98)00492-0.
- (10) Yao, K.; Zhao, M.; Zhang, X.; Wang, Y.; Li, L.; Zheng, M.; Peng, S. A Class of Oral N-[(1S,3S)-1-Methyl-1,2,3,4-Tetrahydro- β -Carboline-3-Carbonyl]-N'-(Amino-Acid-Acyl)Hydrazine: Discovery, Synthesis, in Vitro Anti-Platelet Aggregation/in Vivo Anti-Thrombotic Evaluation and 3D QSAR Analysis. *European Journal of Medicinal Chemistry* **2011**, *46* (8), 3237–3249. <https://doi.org/10.1016/j.ejmech.2011.04.037>.
- (11) Herraiz, T. Identification and Occurrence of β -Carboline Alkaloids in Raisins and Inhibition of Monoamine Oxidase (MAO). *Journal of Agricultural and Food Chemistry* **2007**, *55* (21), 8534–8540. <https://doi.org/10.1021/jf0719151>.
- (12) Sobhani, A. M.; Ebrahimi, A.; Mahmoudian, M. An In Vitro Evaluation of Human DNA Topoisomerase I Inhibition by Peganum Harmala L. Seeds Extract and Its β -Carboline Alkaloids. *J Pharm Pharmaceut Sci.* **2002**, *5* (1), 19–23.
- (13) Deveau, A. M.; Labroli, M. A.; Dieckhaus, C. M.; Barthen, M. T.; Smith, K. S.; MacDonald, T. L. The Synthesis of Amino-Acid Functionalized β -Carbolines as Topoisomerase II Inhibitors. *Bioorganic and Medicinal Chemistry Letters* **2001**, *11* (10), 1251–1255. [https://doi.org/10.1016/S0960-894X\(01\)00136-6](https://doi.org/10.1016/S0960-894X(01)00136-6).
- (14) Trujillo, J. I.; Meyers, M. J.; Anderson, D. R.; Hegde, S.; Mahoney, M. W.; Vernier, W. F.; Buchler, I. P.; Wu, K. K.; Yang, S.; Hartmann, S. J.; Reitz, D. B. Novel Tetrahydro- β -Carboline-1-Carboxylic Acids as Inhibitors of Mitogen Activated Protein Kinase-Activated Protein Kinase 2 (MK-2). *Bioorganic and Medicinal Chemistry Letters* **2007**, *17* (16), 4657–4663. <https://doi.org/10.1016/j.bmcl.2007.05.070>.
- (15) Song, Y.; Kesuma, D.; Wang, J.; Deng, Y.; Duan, J.; Wang, J. H.; Qi, R. Z. Specific Inhibition of Cyclin-Dependent Kinases and Cell Proliferation by Harmine. *Biochemical and Biophysical Research Communications* **2004**, *317* (1), 128–132. <https://doi.org/10.1016/j.bbrc.2004.03.019>.
- (16) Guzman, F.; Cain, M.; Larscheid, P.; Hagen, T.; Cook, J. M.; Schweri, M.; Skolnick, P.; Paul, S. M. Biomimetic Approach to Potential Benzodiazepine. Receptor Agonists and Antagonists. *Journal of Medicinal Chemistry* **1984**, *27* (5), 564–570. <https://doi.org/10.1021/jm00371a002>.
- (17) Glennon, R. A.; Hong, S. S.; Bondarev, M.; Law, H.; Dukat, M.; Rakhit, S.; Power, P.; Fan, E.; Kinneau, D.; Kamboj, R.; Teitler, M.; Herrick-Davis, K.; Smith, C. Binding of O-Alkyl Derivatives of Serotonin at Human 5-HT_{1D} β Receptors. *Journal of Medicinal Chemistry* **1996**, *39* (1), 314–322. <https://doi.org/10.1021/jm950498t>.

Chapter 2. Literature review on β -carboline

- (18) Audia, J. E.; Evrard, D. A.; Murdoch, G. R.; Droste, J. J.; Nissen, J. S.; Schenck, K. W.; Fludzinski, P.; Lucaites, V. L.; Nelson, D. L.; Cohen, M. L. Potent, Selective Tetrahydro- β -Carboline Antagonists of the Serotonin 2B (5HT(2B)) Contractile Receptor in the Rat Stomach Fundus. *Journal of Medicinal Chemistry* **1996**, *39* (14), 2773–2780. <https://doi.org/10.1021/jm960062t>.
- (19) Glennon, R. A.; Grella, B.; Tyacke, R. J.; Lau, A.; Westaway, J.; Hudson, A. L. Binding of β -Carbolines at Imidazoline I2 Receptors: A Structure-Affinity Investigation. *Bioorganic and Medicinal Chemistry Letters* **2004**, *14* (4), 999–1002. <https://doi.org/10.1016/j.bmcl.2003.11.078>.
- (20) Dai, J.; Dan, W.; Schneider, U.; Wang, J. β -Carboline Alkaloid Monomers and Dimers: Occurrence, Structural Diversity, and Biological Activities. *European Journal of Medicinal Chemistry* **2018**, *157*, 622–656. <https://doi.org/10.1016/j.ejmech.2018.08.027>.
- (21) Ashok, P.; Chander, S.; Smith, T. K.; Prakash Singh, R.; Jha, P. N.; Sankaranarayanan, M. Biological Evaluation and Structure Activity Relationship of 9-Methyl-1-Phenyl-9H-Pyrido[3,4-b]Indole Derivatives as Anti-Leishmanial Agents. *Bioorganic Chemistry* **2019**, *84*, 98–105. <https://doi.org/10.1016/j.bioorg.2018.11.037>.
- (22) Lunagariya, N. A.; Gohil, V. M.; Kushwah, V.; Neelagiri, S.; Jain, S.; Singh, S.; Bhutani, K. K. Design, Synthesis and Biological Evaluation of 1,3,6-Trisubstituted β -Carboline Derivatives for Cytotoxic and Anti-Leishmanial Potential. *Bioorganic and Medicinal Chemistry Letters* **2016**, *26* (3), 789–794. <https://doi.org/10.1016/j.bmcl.2015.12.095>.
- (23) Ashok, P.; Chander, S.; Smith, T. K.; Sankaranarayanan, M. Design, Synthesis and Biological Evaluation of Piperazinyl- β -Carbolinederivatives as Anti-Leishmanial Agents Penta. *European Journal of Medicinal Chemistry* **2018**, *150*, 559–566. <https://doi.org/10.1016/j.ejmech.2018.03.022>.
- (24) Kumar, R.; Khan, S.; Verma, A.; Srivastava, S.; Viswakarma, P.; Gupta, S.; Meena, S.; Singh, N.; Sarkar, J.; Chauhan, P. M. S. Synthesis of 2-(Pyrimidin-2-Yl)-1-Phenyl-2,3,4,9-Tetrahydro-1H- β -Carbolines as Antileishmanial Agents. *European Journal of Medicinal Chemistry* **2010**, *45* (8), 3274–3280. <https://doi.org/10.1016/j.ejmech.2010.04.004>.
- (25) Gohil, V. M.; Brahmabhatt, K. G.; Loiseau, P. M.; Bhutani, K. K. Synthesis and Anti-Leishmanial Activity of 1-Aryl- β -Carboline Derivatives against *Leishmania Donovanii*. *Bioorganic and Medicinal Chemistry Letters* **2012**, *22* (12), 3905–3907.

Chapter 2. Literature review on β -carboline

- <https://doi.org/10.1016/j.bmcl.2012.04.115>.
- (26) Stefanello, T. F.; Panice, M. R.; Ueda-Nakamura, T.; Sarragiotto, M. H.; Auzély-Velty, R.; Nakamura, C. V. N -Butyl-[1-(4-Methoxy)Phenyl-9 H - β -Carboline]-3-Carboxamide Prevents Cytokinesis in *Leishmania Amazonensis*. *Antimicrobial Agents and Chemotherapy* **2014**, 58 (12), 7112–7120. <https://doi.org/10.1128/aac.03340-14>.
- (27) Ashok, P.; Chander, S.; Tejería, A.; García-Calvo, L.; Balaña-Fouce, R.; Murugesan, S. Synthesis and Anti-Leishmanial Evaluation of 1-Phenyl-2,3,4,9-Tetrahydro-1 H - β -Carboline Derivatives against *Leishmania Infantum*. *European Journal of Medicinal Chemistry* **2016**, 123, 814–821. <https://doi.org/10.1016/j.ejmech.2016.08.014>.
- (28) Volpato, H.; Desoti, V. C.; Cogo, J.; Panice, M. R.; Sarragiotto, M. H.; Silva, S. de O.; Ueda-Nakamura, T.; Nakamura, C. V. The Effects of N -Butyl-1-(4-Dimethylamino)Phenyl-1,2,3,4-Tetrahydro- β -Carboline-3-Carboxamide against *Leishmania Amazonensis* Are Mediated by Mitochondrial Dysfunction. *Evidence-Based Complementary and Alternative Medicine* **2013**, 1–7. <https://doi.org/10.1155/2013/874367>.
- (29) Pedroso, R. B.; Tonin, L. T. D.; Ueda-Nakamura, T.; Filho, B. P. D.; Sarragiotto, M. H.; Nakamura, C. V. Beta-Carboline-3-Carboxamide Derivatives as Promising Antileishmanial Agents. *Annals of Tropical Medicine and Parasitology* **2012**, 105 (8), 549–557. <https://doi.org/10.1179/2047773211y.0000000005>.
- (30) Chauhan, S. S.; Pandey, S.; Shivahare, R.; Ramalingam, K.; Krishna, S.; Vishwakarma, P.; Siddiqi, M. I.; Gupta, S.; Goyal, N.; Chauhan, P. M. S. Novel β -Carboline-Quinazolinone Hybrid as an Inhibitor of *Leishmania Donovanii* Trypanothione Reductase: Synthesis, Molecular Docking and Bioevaluation. *MedChemComm* **2015**, 6 (2), 351–356. <https://doi.org/10.1039/c4md00298a>.
- (31) Tonin, L. T. D.; Panice, M. R.; Nakamura, C. V.; Rocha, K. J. P.; Santos, A. O. dos; Ueda-Nakamura, T.; Costa, W. F. da; Sarragiotto, M. H. Antitrypanosomal and Antileishmanial Activities of Novel N-Alkyl-(1-Phenylsubstituted- β -Carboline)-3-Carboxamides. *Biomedicine and Pharmacotherapy* **2010**, 64 (6), 386–389. <https://doi.org/10.1016/j.biopha.2010.02.006>.
- (32) Ashok, P.; Chander, S.; Chow, L. M. C.; Wong, I. L. K.; Singh, R. P.; Jha, P. N.; Sankaranarayanan, M. Synthesis and In-Vitro Anti-Leishmanial Activity of (4-Arylpiperazin-1-Yl)(1-(Thiophen-2-Yl)-9H-Pyrido[3,4-b]Indol-3-Yl)Methanone Derivatives. *Bioorganic Chemistry* **2017**, 70, 100–106.

Chapter 2. Literature review on β -carboline

- <https://doi.org/10.1016/j.bioorg.2016.11.013>.
- (33) Purohit, P.; Pandey, A. K.; Singh, D.; Chouhan, P. S.; Ramalingam, K.; Shukla, M.; Goyal, N.; Lal, J.; Chauhan, P. M. S. An Insight into Tetrahydro- β -Carboline–Tetrazole Hybrids: Synthesis and Bioevaluation as Potent Antileishmanial Agents. *MedChemComm* **2017**, 8 (9), 1824–1834. <https://doi.org/10.1039/C7MD00125H>.
- (34) Baréa, P.; Barbosa, V. A.; Bidóia, D. L.; de Paula, J. C.; Stefanello, T. F.; da Costa, W. F.; Nakamura, C. V.; Sarragiotto, M. H. Synthesis, Antileishmanial Activity and Mechanism of Action Studies of Novel β -Carboline-1,3,5-Triazine Hybrids. *European Journal of Medicinal Chemistry* **2018**, 150, 579–590. <https://doi.org/10.1016/j.ejmech.2018.03.014>.
- (35) Khan, I.; Singh, J.; Kumar, V.; Verma, V. P.; Shukla, M.; Dhasmana, A.; Naruka, P. S.; Goswami, A. K.; Ameta, K. L.; Khan, S. A Versatile Pre and Post Ugi Modification for the Synthesis of Natural Product Inspired Fused Peptide-Carboline Scaffolds as Potential Anti-Leishmanial Agents. *ChemistrySelect* **2019**, 4, 12260–12267. <https://doi.org/10.1002/slct.201902441>.
- (36) Oteng Mintah, S.; Asafo-Agyei, T.; Archer, M.-A.; Atta-Adjei Junior, P.; Boamah, D.; Kumadoh, D.; Appiah, A.; Ocloo, A.; Duah Boakye, Y.; Agyare, C. Medicinal Plants for Treatment of Prevalent Diseases. *Pharmacognosy - Medicinal Plants* **2019**, 1–19. <https://doi.org/10.5772/intechopen.82049>.
- (37) Oryan, A. Plant-Derived Compounds in Treatment of Leishmaniasis. *Iranian Journal of Veterinary Research* **2015**, 16 (1), 1–19. <https://doi.org/10.22099/ijvr.2015.2917>.
- (38) Ioset, J.-R. Natural Products for Neglected Diseases: A Review. *Current Organic Chemistry* **2008**, 12 (8), 643–666. <https://doi.org/10.2174/138527208784577394>.
- (39) Gabriel, R. S.; Amaral, A. C. F.; Lima, I. C.; Cruz, J. D.; Garcia, A. R.; Souza, H. A. S.; Adade, C. M.; Vermelho, A. B.; Alviano, C. S.; Alviano, D. S.; Rodrigues, I. A. β -Carboline-1-Propionic Acid Alkaloid: Antileishmanial and Cytotoxic Effects. *Brazilian Journal of Pharmacognosy* **2019**, 2019, 755–762. <https://doi.org/10.1016/j.bjp.2019.08.002>.
- (40) Di Giorgio, C.; Delmas, F.; Ollivier, E.; Elias, R.; Balansard, G.; Timon-David, P. In Vitro Activity of the β -Carboline Alkaloids Harmane, Harmine, and Harmaline toward Parasites of the Species *Leishmania Infantum*. *Experimental Parasitology* **2004**, 106 (3–4), 67–74. <https://doi.org/10.1016/j.exppara.2004.04.002>.
- (41) Sakai, R.; Higa, T.; Jefford, C. W.; Bernardinelli, G. Manzamine A, a Novel Antitumor

Chapter 2. Literature review on β -carboline

- Alkaloid from a Sponge. *Journal of the American Chemical Society* **1986**, *108* (20), 6404–6405. <https://doi.org/10.1021/ja00280a055>.
- (42) Ashok, P.; Lathiya, H.; Murugesan, S. Manzamine Alkaloids as Antileishmanial Agents: A Review. *European Journal of Medicinal Chemistry* **2015**, *97* (1), 928–936. <https://doi.org/10.1016/j.ejmech.2014.07.006>.
- (43) Rinehart, K. L.; Kobayashi, J.; Harbour, G. C.; Hughes, R. G.; Mizesak, S. A.; Scahill, T. A. Eudistomins C, E, K, and L, Potent Antiviral Compounds Containing a Novel Oxathiazepine Ring from the Caribbean Tunicate Eudistoma Olivaceum. *Journal of the American Chemical Society* **1984**, *106* (5), 1524–1526. <https://doi.org/10.1021/ja00317a079>.
- (44) Adesanya, S. A.; Chbani, M.; Pais, M.; Debitus, C. Brominated β -Carbolines from the Marine Tunicate Eudistoma Album. *Journal of Natural Products* **1992**, *55* (4), 525–527. <https://doi.org/10.1021/np50082a025>.
- (45) Netz, N.; Opatz, T. Marine Indole Alkaloids. *Marine Drugs* **2015**, *13* (8), 4814–4914. <https://doi.org/10.3390/md13084814>.
- (46) Rajesh, R. P.; Annappan, M. Anticancer Effects of Brominated Indole Alkaloid Eudistomin H from Marine Ascidian Eudistoma Viride against Cervical Cancer Cells (HeLa). *Anticancer Research* **2015**, *35* (1), 283–294. PMID: 25550562.
- (47) Rajesh, R. P.; Murugan, A. Spectroscopic Identification of Brominated, Non-Brominated Alkaloids and Evaluation of Antimicrobial Activity of Eudistomin-I, Eudistomin H, from Green Ascidian Eudistoma Viride. *Journal of Applied Pharmaceutical Science* **2019**, *9* (2), 116–123. <https://doi.org/10.7324/JAPS.2019.90216>.
- (48) Organization, W. H. *Antibacterial Agents in Clinical Development: An Analysis of the Antibacterial Clinical Development Pipeline, Including Tuberculosis*; World Health Organization, 2017.
- (49) Theuretzbacher, U.; Bush, K.; Harbarth, S.; Paul, M.; Rex, J. H.; Tacconelli, E.; Thwaites, G. E. Critical Analysis of Antibacterial Agents in Clinical Development. *Nature Reviews Microbiology* **2020**, *18*, 286. <https://doi.org/10.1038/s41579-020-0340-0>
- (50) Rex, J. H.; Lynch, H. F.; Cohen, I. G.; Darrow, J. J.; Outterson, K. Designing Development Programs for Non-Traditional Antibacterial Agents. *Nature communications* **2019**, *10* (1), 3416. <https://doi.org/10.1038/s41467-019-11303-9>.

Chapter 2. Literature review on β -carboline

- (51) Penta, A.; Franzblau, S.; Wan, B.; Murugesan, S. Design, Synthesis and Evaluation of Diarylpiperazine Derivatives as Potent Anti-Tubercular Agents. *European Journal of Medicinal Chemistry* **2015**, *105*, 238–244. <https://doi.org/10.1016/j.ejmech.2015.10.024>.
- (52) Salehi, P.; Babanezhad-Harikandei, K.; Bararjanian, M.; Al-Harrasi, A.; Esmaeili, M. A.; Aliahmadi, A. Synthesis of Novel 1,2,3-Triazole Tethered 1,3-Disubstituted β -Carboline Derivatives and Their Cytotoxic and Antibacterial Activities. *Medicinal Chemistry Research* **2016**, *25* (9), 1895–1907. <https://doi.org/10.1007/s00044-016-1622-y>.
- (53) Dai, J. K.; Dan, W. J.; Li, N.; Du, H. T.; Zhang, J. W.; Wang, J. R. Synthesis, in Vitro Antibacterial Activities of a Series of 3-N-Substituted Canthin-6-Ones. *Bioorganic and Medicinal Chemistry Letters* **2016**, *26* (2), 580–583. <https://doi.org/10.1016/j.bmcl.2015.11.070>.
- (54) Samita, F.; Ochieng, C. O.; Owuor, P. O.; Manguro, L. O. A.; Midiwo, J. O. Isolation of a New β -Carboline Alkaloid from Aerial Parts of *Triclisia Sacleuxii* and Its Antibacterial and Cytotoxicity Effects. *Natural Product Research* **2017**, *31* (5), 529–536. <https://doi.org/10.1080/14786419.2016.1201666>.
- (55) Dai, J.; Dan, W.; Ren, S.; Shang, C.; Wang, J. Design, Synthesis and Biological Evaluations of Quaternization Harman Analogues as Potential Antibacterial Agents. *European Journal of Medicinal Chemistry* **2018**, *160*, 23–36. <https://doi.org/10.1016/j.ejmech.2018.10.012>.
- (56) Suzuki, K.; Nomura, I.; Ninomiya, M.; Tanaka, K.; Koketsu, M. Synthesis and Antimicrobial Activity of β -Carboline Derivatives with N 2 -Alkyl Modifications. *Bioorganic and Medicinal Chemistry Letters* **2018**, *28* (17), 2976–2978. <https://doi.org/10.1016/j.bmcl.2018.06.050>.
- (57) Dai, J.; Dan, W.; Li, N.; Wang, R.; Zhang, Y.; Li, N.; Wang, R.; Wang, J. Synthesis and Antibacterial Activity of C2 or C5 Modified and D Ring Rejiggered Canthin-6-One Analogues. *Food Chemistry* **2018**, *253*, 211–220. <https://doi.org/10.1016/j.foodchem.2018.01.166>.
- (58) Dai, J.; Dan, W.; Li, N.; Wang, J. Computer-Aided Drug Discovery: Novel 3,9-Disubstituted Eudistomin U Derivatives as Potent Antibacterial Agents. *European Journal of Medicinal Chemistry* **2018**, *157*, 333–338. <https://doi.org/10.1016/j.ejmech.2018.08.001>.

Chapter 2. Literature review on β -carboline

- (59) Pan, X.; Liu, Z. Total Synthesis and Antibacterial Activity Evaluation of Griseofamine A and 16- Epi-Griseofamine A. *Organic Letters* **2019**, *21* (7), 2393–2396. <https://doi.org/10.1021/acs.orglett.9b00672>.
- (60) Lopes-Ortiz, M. A.; Panice, M. R.; Borges de Melo, E.; Ataíde Martins, J. P.; Baldin, V. P.; Agostinho Pires, C. T.; Caleffi-Ferracioli, K. R.; Dias Siqueira, V. L.; Bertin de Lima Scodro, R.; Sarragiotto, M. H.; Cardoso, R. F. Synthesis and Anti-Mycobacterium Tuberculosis Activity of Imide- β -Carboline and Carbomethoxy- β -Carboline Derivatives. *European Journal of Medicinal Chemistry* **2020**, *187*, 111935. <https://doi.org/10.1016/j.ejmech.2019.111935>.
- (61) Lima, S. L.; Colombo, A. L.; de Almeida Junior, J. N. Fungal Cell Wall: Emerging Antifungals and Drug Resistance. *Frontiers in Microbiology* **2019**, *10*, 2573. <https://doi.org/10.3389/fmicb.2019.02573>.
- (62) Campoy, S.; Adrio, J. L. Antifungals. *Biochemical Pharmacology* **2017**, *133*, 86–96. <https://doi.org/10.1016/j.bcp.2016.11.019>
- (63) Prasad, R.; Shah, A. H.; Rawal, M. K. Antifungals: Mechanism of Action and Drug Resistance. In *Yeast Membrane Transport*; Springer, 2016; pp 327–349.
- (64) Cruz, K. S.; Lima, E. S.; Silva, M. D. J. A. Da; Souza, E. S. De; Montoia, A.; Pohlit, A. M.; Souza, J. V. B. De. Screening and Antifungal Activity of a β -Carboline Derivative against *Cryptococcus Neoformans* and *C. Gattii*. *International Journal of Microbiology* **2019**, *2019*, 7157845. <https://doi.org/10.1155/2019/7157845>.
- (65) Tu, J.; Li, Z.; Jiang, Y.; Ji, C.; Han, G.; Wang, Y.; Liu, N.; Sheng, C. Discovery of Carboline Derivatives as Potent Antifungal Agents for the Treatment of Cryptococcal Meningitis. *Journal of Medicinal Chemistry* **2019**, *62* (5), 2376–2389. <https://doi.org/10.1021/acs.jmedchem.8b01598>.
- (66) Xu, P.; Zhou, Z.; Xiong, M.; Zou, W.; Deng, X.; Ganaie, S. S.; Kleiboeker, S.; Peng, J.; Liu, K.; Wang, S.; Ye, S. Q.; Qiu, J. Parvovirus B19 NS1 Protein Induces Cell Cycle Arrest at G2-Phase by Activating the ATR-CDC25C-CDK1 Pathway. *PLoS Pathogens* **2017**, *13* (3), e1006266. <https://doi.org/10.1371/journal.ppat.1006266>.
- (67) Vardanyan, R.; Hruby, V. Chapter 34 - Antiviral Drugs; Vardanyan, R., Hruby, V. B. T.-S. of B.-S. D., Eds.; Academic Press: Boston, 2016; pp 687–736. <https://doi.org/https://doi.org/10.1016/B978-0-12-411492-0.00034-1>.
- (68) Clercq, E. De. Antivirals and Antiviral Strategies. *Nature Reviews Microbiology* **2004**, *2* (9), 704–720. <https://doi.org/10.1038/nrmicro975>.

Chapter 2. Literature review on β -carboline

- (69) Edagwa, B. J.; Gendelman, H. E. Broad-Spectrum Antivirals. *Nature Materials* **2018**, *17* (2), 114–116. <https://doi.org/10.1038/nmat5064>.
- (70) Kaufmann, S. H. E.; Dorhoi, A.; Hotchkiss, R. S.; Bartenschlager, R. Host-Directed Therapies for Bacterial and Viral Infections. *Nature Reviews Drug Discovery* **2018**, *17* (1), 35–56. <https://doi.org/10.1038/nrd.2017.162>.
- (71) Ashok, P.; Lu, C. L.; Chander, S.; Zheng, Y. T.; Murugesan, S. Design, Synthesis, and Biological Evaluation of 1-(Thiophen-2-Yl)-9H-Pyrido[3,4-b]Indole Derivatives as Anti-HIV-1 Agents. *Chemical Biology and Drug Design* **2015**, *85* (6), 722–728. <https://doi.org/10.1111/cbdd.12456>.
- (72) Ashok, P.; Chander, S.; Balzarini, J.; Pannecouque, C.; Murugesan, S. Design, Synthesis of New β -Carboline Derivatives and Their Selective Anti-HIV-2 Activity. *Bioorganic and Medicinal Chemistry Letters* **2015**, *25* (6), 1232–1235. <https://doi.org/10.1016/j.bmcl.2015.01.058>.
- (73) Quintana, V. M.; Piccini, L. E.; Panozzo Z enere, J. D.; Damonte, E. B.; Ponce, M. A.; Castilla, V. Antiviral Activity of Natural and Synthetic β -Carbolines against Dengue Virus. *Antiviral Research* **2016**, *134*, 26–33. <https://doi.org/10.1016/j.antiviral.2016.08.018>.
- (74) Barbosa, V. A.; Bar ea, P.; Mazia, R. S.; Ueda-Nakamura, T.; Costa, W. F. da; Foglio, M. A.; Goes Ruiz, A. L. T.; Carvalho, J. E. de; Vendramini-Costa, D. B.; Nakamura, C. V.; Sarragiotto, M. H. Synthesis and Evaluation of Novel Hybrids β -Carboline-4-Thiazolidinones as Potential Antitumor and Antiviral Agents. *European Journal of Medicinal Chemistry* **2016**, *124*, 1093–1104. <https://doi.org/10.1016/j.ejmech.2016.10.018>.
- (75) Gonzalez, M. M.; Cabrerizo, F. M.; Baiker, A.; Erra-Balsells, R.; Osterman, A.; Nitschko, H.; Vizoso-Pinto, M. G. β -Carboline Derivatives as Novel Antivirals for Herpes Simplex Virus. *International Journal of Antimicrobial Agents* **2018**, *52* (4), 459–468. <https://doi.org/10.1016/j.ijantimicag.2018.06.019>.
- (76) Ashley, E. A.; Pyae Phyo, A.; Woodrow, C. J. Malaria. *The Lancet* **2018**, *391* (10130), 1608–1621. [https://doi.org/10.1016/S0140-6736\(18\)30324-6](https://doi.org/10.1016/S0140-6736(18)30324-6).
- (77) Krungkrai, J.; Krungkrai, S. R. Antimalarial Qinghaosu/Artemisinin: The Therapy Worthy of a Nobel Prize. *Asian Pacific Journal of Tropical Biomedicine*. Hainan Medical University May 2016, pp 371–375. <https://doi.org/10.1016/j.apjtb.2016.03.010>.
- (78) Dondorp, A. M.; Nosten, F.; Yi, P.; Das, D.; Phyo, A. P.; Tarning, J.; Lwin, K. M.;

Chapter 2. Literature review on β -carboline

- Ariey, F.; Hanpithakpong, W.; Lee, S. J.; Ringwald, P.; Silamut, K.; Imwong, M.; Chotivanich, K.; Lim, P.; Herdman, T.; An, S. S.; Yeung, S.; Singhasivanon, P.; Day, N. P. J.; Lindegardh, N.; Socheat, D.; White, N. J. Artemisinin Resistance in Plasmodium Falciparum Malaria. *New England Journal of Medicine* **2009**, *361* (5), 455–467. <https://doi.org/10.1056/NEJMoa0808859>.
- (79) Bowman, J. D.; Merino, E. F.; Brooks, C. F.; Striepen, B.; Carlier, P. R.; Cassera, M. B. Antiapicoplast and Gametocytocidal Screening to Identify the Mechanisms of Action of Compounds within the Malaria Box. *Antimicrobial Agents and Chemotherapy* **2014**, *58* (2), 811–819. <https://doi.org/10.1128/AAC.01500-13>.
- (80) Yao, Z. K.; Krai, P. M.; Merino, E. F.; Simpson, M. E.; Slebodnick, C.; Cassera, M. B.; Carlier, P. R. Determination of the Active Stereoisomer of the MEP Pathway-Targeting Antimalarial Agent MMV008138, and Initial Structure-Activity Studies. *Bioorganic and Medicinal Chemistry Letters* **2015**, *25* (7), 1515–1519. <https://doi.org/10.1016/j.bmcl.2015.02.020>.
- (81) Shahinas, D.; MacMullin, G.; Benedict, C.; Crandall, I.; Pillaid, D. R. Harmine Is a Potent Antimalarial Targeting Hsp90 and Synergizes with Chloroquine and Artemisinin. *Antimicrobial Agents and Chemotherapy* **2012**, *56* (8), 4207–4213. <https://doi.org/10.1128/AAC.00328-12>.
- (82) Bayih, A. G.; Folefoc, A.; Mohon, A. N.; Eagon, S.; Anderson, M.; Pillai, D. R. In Vitro and in Vivo Anti-Malarial Activity of Novel Harmine-Analog Heat Shock Protein 90 Inhibitors: A Possible Partner for Artemisinin. *Malaria Journal* **2016**, *15* (1), 1–11. <https://doi.org/10.1186/s12936-016-1625-7>.
- (83) Banumathy, G.; Singh, V.; Pavithra, S. R.; Tatu, U. Heat Shock Protein 90 Function Is Essential for Plasmodium Falciparum Growth in Human Erythrocytes. *Journal of Biological Chemistry* **2003**, *278* (20), 18336–18345. <https://doi.org/10.1074/jbc.M211309200>.
- (84) Pavithra, S. R.; Banumathy, G.; Joy, O.; Singh, V.; Tatu, U. Recurrent Fever Promotes Plasmodium Falciparum Development in Human Erythrocytes. *Journal of Biological Chemistry* **2004**, *279* (45), 46692–46699. <https://doi.org/10.1074/jbc.M409165200>.
- (85) Acharya, P.; Kumar, R.; Tatu, U. Chaperoning a Cellular Upheaval in Malaria: Heat Shock Proteins in Plasmodium Falciparum. *Molecular and Biochemical Parasitology* **2007**, *153* (2), 85–94. <https://doi.org/10.1016/j.molbiopara.2007.01.009>.
- (86) Su, X. zhuan; Wellems, T. E. Sequence, Transcript Characterization and Polymorphisms

Chapter 2. Literature review on β -carboline

- of a Plasmodium Falciparum Gene Belonging to the Heat-Shock Protein (HSP) 90 Family. *Gene* **1994**, *151* (1–2), 225–230. [https://doi.org/10.1016/0378-1119\(94\)90661-0](https://doi.org/10.1016/0378-1119(94)90661-0).
- (87) Cowen, L. E.; Lindquist, S. Cell Biology: Hsp90 Potentiates the Rapid Evolution of New Traits: Drug Resistance in Diverse Fungi. *Science* **2005**, *309* (5744), 2185–2189. <https://doi.org/10.1126/science.1118370>.
- (88) Corbett, K. D.; Berger, J. M. Structure of the ATP-Binding Domain of Plasmodium Falciparum Hsp90. *Proteins: Structure, Function and Bioinformatics* **2010**, *78* (13), 2738–2744. <https://doi.org/10.1002/prot.22799>.
- (89) Yadav, V. D.; Srivastava, K.; Tripathi, R.; Batra, S. Synthesis of β -Carboline-Fused 1,4-Oxazepines and Their Assessment as Antiplasmodial Agents. *Tetrahedron* **2017**, *73* (38), 5680–5689. <https://doi.org/10.1016/j.tet.2017.08.003>.
- (90) Ghavami, M.; Merino, E. F.; Yao, Z.-K.; Elahi, R.; Simpson, M. E.; Fernández-Murga, M. L.; Butler, J. H.; Casasanta, M. A.; Krai, P. M.; Totrov, M. M.; Slade, D. J.; Carlier, P. R.; Cassera, M. B. Biological Studies and Target Engagement of the 2-C-Methyl-d-Erythritol 4-Phosphate Cytidylyltransferase (IspD)-Targeting Antimalarial Agent (1 R,3 S)-MMV008138 and Analogs. *ACS Infectious Diseases* **2018**, *4* (4), 549–559. <https://doi.org/10.1021/acsinfecdis.7b00159>.
- (91) Gorki, V.; Singh, R.; Walter, N. S.; Bagai, U.; Salunke, D. B. Synthesis and Evaluation of Antiplasmodial Efficacy of β -Carboline Derivatives against Murine Malaria. *ACS Omega* **2018**, *3*, 13200–13210. <https://doi.org/10.1021/acsomega.8b01833>.
- (92) Sharma, B.; Kaur, S.; Legac, J.; Rosenthal, P. J.; Kumar, V. Bioorganic & Medicinal Chemistry Letters Acyl Hydrazide Integrated Tetrahydro- β -Carboline-4-Aminoquinoline Conjugates. *Bioorganic and Medicinal Chemistry Letters* **2019**, 126810. <https://doi.org/10.1016/j.bmcl.2019.126810>.
- (93) Pierrot, D.; Sinou, V.; Bun, S. S.; Parzy, D.; Taudon, N.; Rodriguez, J.; Ollivier, E.; Bonne, D. Design and Synthesis of Simplified Speciophylline Analogues and β -Carbolines as Active Molecules against Plasmodium Falciparum. *Drug Development Research* **2019**, *80* (1), 133–137. <https://doi.org/10.1002/ddr.21494>.
- (94) World Health Organisation (WHO). *Chagas Disease (Also Known as American Trypanosomiasis)*; 2021.
- (95) Valdez, R. H.; Tonin, L. T. D.; Ueda-Nakamura, T.; Filho, B. P. D.; Morgado-Diaz, J. A.; Sarragiotto, M. H.; Nakamura, C. V. Biological Activity of 1,2,3,4-Tetrahydro- β -

Chapter 2. Literature review on β -carboline

- Carboline-3-Carboxamides against *Trypanosoma Cruzi*. *Acta Tropica* **2009**, *110* (1), 7–14. <https://doi.org/10.1016/j.actatropica.2008.11.008>.
- (96) Sales, P. A.; Molina, I.; Murta, S. M. F.; Sánchez-Montalvá, A.; Salvador, F.; Corrêa-Oliveira, R.; Carneiro, C. M. Experimental and Clinical Treatment of Chagas Disease: A Review. *American Journal of Tropical Medicine and Hygiene*. American Society of Tropical Medicine and Hygiene **2017**, pp 1289–1303. <https://doi.org/10.4269/ajtmh.16-0761>.
- (97) Valdez, R. H.; Tonin, L. T. D.; Ueda-Nakamura, T.; Silva, S. O.; Dias Filho, B. P.; Kaneshima, E. N.; Yamada-Ogatta, S. F.; Yamauchi, L. M.; Sarragiotto, M. H.; Nakamura, C. V. In Vitro and in Vivo Trypanocidal Synergistic Activity of N-Butyl-1-(4-Dimethylamino)Phenyl-1,2,3,4-Tetrahydro- β -Carboline-3- Carboxamide Associated with Benznidazole. *Antimicrobial Agents and Chemotherapy* **2012**, *56* (1), 507–512. <https://doi.org/10.1128/AAC.05575-11>.
- (98) Volpato, H.; Desoti, V. C.; Valdez, R. H.; Ueda-Nakamura, T.; Silva, S. de O.; Sarragiotto, M. H.; Nakamura, C. V. Mitochondrial Dysfunction Induced by N-Butyl-1-(4-Dimethylamino)Phenyl-1,2,3,4-Tetrahydro- β -Carboline-3-Carboxamide Is Required for Cell Death of *Trypanosoma Cruzi*. *PLOS ONE* **2015**, *10* (6), e0130652. <https://doi.org/10.1371/journal.pone.0130652>.
- (99) Guha, R. *In Silico Models for Drug Discovery*; Kortagere, S., Ed.; Methods in Molecular Biology; Humana Press: Totowa, NJ, 2013; Vol. 993. <https://doi.org/10.1007/978-1-62703-342-8>.



Chapter 3. Objectives and Plan of work



Chapter 3. Objectives and Plan of work

Gaps in existing research

A high number of unmet medical needs persist for the deadly neglected tropical diseases of visceral, cutaneous and mucocutaneous leishmaniasis. Unfortunately, the treatment options available for these diseases have only marginally improved within the past century. Due to development of resistance to the current treatments and extensive toxicity, current treatments face therapeutic limitations. In addition, many anti-leishmanial drugs are ineffective in eliminating the parasite from all infected individuals and are only effective against certain species. Most of the molecules currently being used clinically are characterized by high levels of toxicity, resistance and unwanted side effects. Furthermore, they are expensive and decade old as well. From the past decade onwards, several researchers are trying to find out a suitable vaccine for the treatment of Leishmaniasis but all the outcomes are not satisfactory. The existing literature suggested that β -carboline analogues may emerge as a promising lead. Similarly, our earlier findings as well as our continued interest also suggested as much. Therefore, we currently explored the options of finding more potent and less toxic compounds for the treatment of leishmaniasis with better ADMET profiles, using β -carboline analogues.

Objective: To Design, Synthesis and Study of novel β -carboline analogues as potential anti-leishmanial agents

Plan of work

3.1. Design and *in-silico* ADMET prediction studies

Based upon the reported literatures as well as rational approach, novel β -carboline analogues were designed as antileishmanial agents. Computational prediction of physicochemical, Drug likeness and Absorption, Distribution, Metabolism, Excretion and Toxicity (ADMET) properties of the designed analogues was performed using appropriate software and online tools.

3.2. Synthesis and characterization of the designed molecules

Several reaction conditions were evaluated for optimization of the reaction and final optimized conditions were used for the synthesis of the designed titled compounds. The synthesized compounds were characterized by physicochemical evaluation. Preliminary methods like melting point and thin layer chromatography were performed for the synthesized compounds. Synthesized compounds were further purified by various techniques like washing with suitable solvents, column chromatography and re-crystallization techniques as per the requirement. The

Chapter 3. Objectives and Plan of work

structure of the synthesized compounds was further confirmed by IR, ¹H NMR and Mass spectral analysis.

3.3. Evaluation of anti-leishmanial activity and cell-viability studies

The synthesized compounds were screened for

3.3.1 *In-vitro* anti-leishmanial Promastigote activity (*L. infantum* BCN150 iRFP promastigotes (iRFP-*L. infantum*))

3.3.2. *In-vitro* anti-leishmanial Amastigote activity (*L. infantum* BCN150)

3.3.3. Cell-viability study (Human hepatocarcinoma cell HepG2 line (ATCC HB-8065))

3.4: Structure-Activity Relationship studies

The Structure-Activity Relationship (SAR) was derived for the synthesized molecules by analyzing their anti-leishmanial screening data. Based on the obtained activity spectrum, the outcome was compiled concisely to conclude the major contribution sites of the selected molecule.

3.5. Molecular mechanistic studies

One of the probable targets was shortlisted based on the reported literature and it was Trypanothione reductase (TR). The TR inhibition assay was performed (Bradford method) for the identified hits from the above-mentioned studies (promastigote and amastigote assays).

3.6. Molecular docking studies

Docking studies was performed for the compounds which exhibited potent activity ($EC_{50} < 1 \mu\text{M}$ against amastigote forms from each series) during anti-leishmanial screening to presume their putative binding modes as well as interaction pattern against the selected target of Trypanothione reductase (PDB-2JK6).

3.7. Molecular mechanics with generalized Born and surface area (MMGBSA) solvation studies

Molecular mechanics with generalized Born and surface area (MMGBSA) solvation studies were carried out for the potent molecules ($EC_{50} < 1 \mu\text{M}$ against amastigote forms from each series).

3.8. Molecular dynamics studies

To find out the stability of the protein-ligand complexes of molecular docking studies, a 100 ns molecular dynamics study was conducted for the docked complexes.

3.9. Time frame analysis

Every 25 ns of the molecular dynamics simulation of the identified hit molecules were critically investigated for their conformational changes in the active site of the target.



**Chapter 4. Design and *In-silico* Prediction of
Drug-likeness Properties**



Materials and methods

Design of novel β -carboline analogues

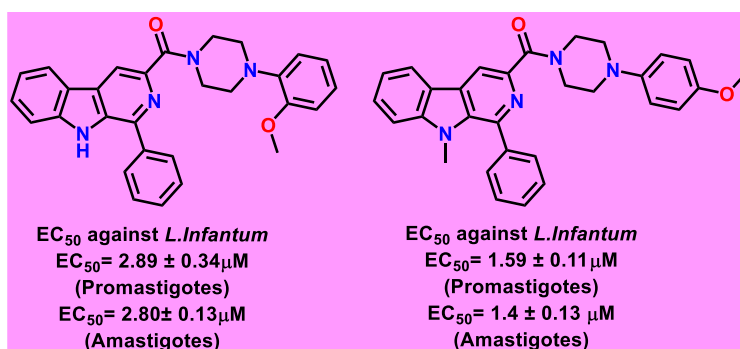


Figure 4.1. Previously identified hits molecules

As the investigation begin with the previously identified hit molecules named (4-(2-methoxyphenyl)-piperazin-1-yl) (1-phenyl-9H-pyrido-[3,4-b]-indol-3-yl)-methanone which revealed EC₅₀ of 2.80 μ M, and the other hit (4-(4-methoxyphenyl)-piperazin-1-yl) (9-methyl-1-phenyl-9H-pyrido-[3,4-b]-indol-3-yl)-methanone revealed an EC₅₀ of 1.4 μ M against the amastigotes (**Figure 4.1.**). This was laid an interest in further modification of the β -carboline scaffold. The existing literatures also revealed the same, that the alteration of these molecules with various substitutions may help in the increased amount of anti-leishmanial activities. The investigation was further proceeded with the substitutions like Nitro, Bromo, Chloro and hydroxy at the 6th position as there were no reports available as on date. As depicted in **Figure 4.2**, the modifications were made. Benzaldehyde, chloro benzaldehyde, methoxy benzaldehyde and thiophene aldehydes were introduced in the 1st position. Similarly substituted Phenyl piperazines were incorporated at 3rd position to produce novel compounds.

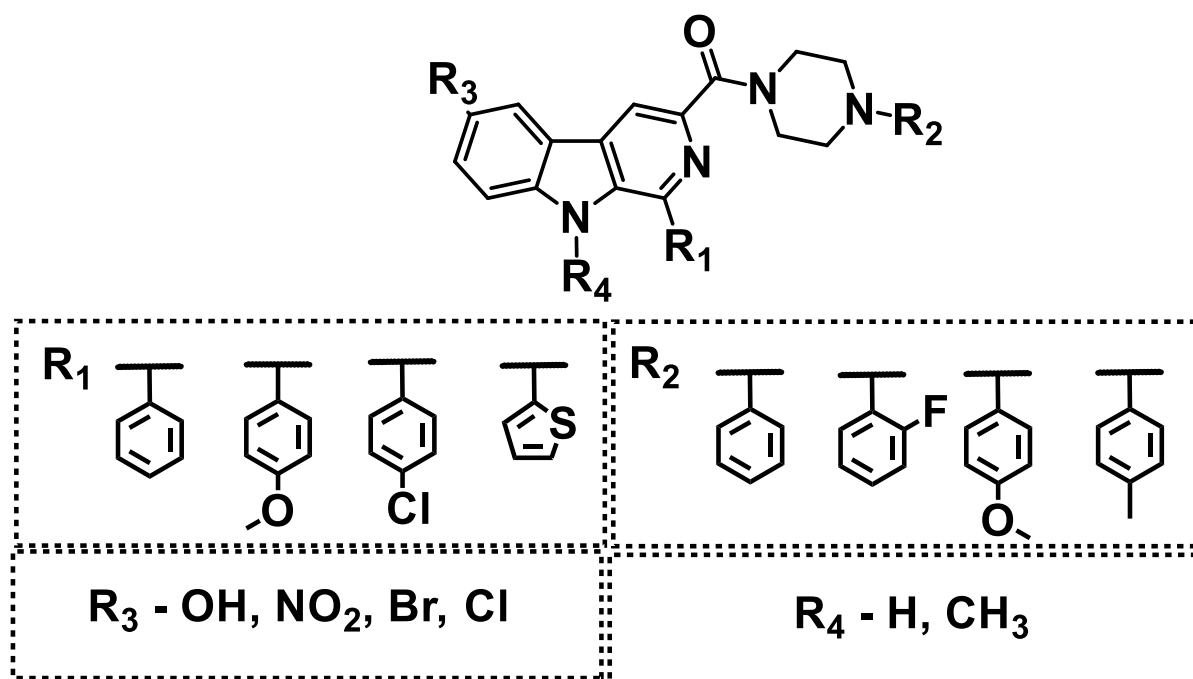


Figure 4.2. Newly designed analogues

***In-silico* prediction of drug-likeness properties**

***In-silico* predicted physico-chemical parameters:** The physicochemical parameters of the designed compounds were *in silico* predicted using the Qikprop module of Schrodinger. The diverse parameters predicted were molecular weight (M.Wt.), total solvent accessible surface area (SASA), number of hydrogen bond donor (HBD), number of hydrogen bond acceptor (HBA), octanol / water partition coefficient (log P), aqueous solubility (Log S), predicted apparent Caco-2 cell permeability in nm/sec (PCaco) and number of rotatable bonds (Rot). The toxicity parameters were predicted using Data warrior¹.

Prediction of pharmacokinetic parameters (ADMET) of the designed analogues:

Physicochemical and pharmacokinetic (absorption, distribution, metabolism, excretion, and toxicity, abbreviated as ADMET) properties play a very crucial role in the discovery and development of new drugs. Currently available approved drugs in the market possess a balance of desirable ADMET properties (**Table 1**) and intrinsic potency. Moreover, the calculation of ADMET profile of all new compounds using *in-vivo* model is a very challenging, time-consuming, and costly task. To predict the drug-likeness behaviour of the designed compounds, their physicochemical and ADMET properties were *in-silico* predicted using the Qikprop module of Schrödinger¹⁴⁻¹⁶. The predicted results of the ADME and toxicity profiles are presented in **tables 2 to 9**.

Chapter 4. Design and Prediction of Drug-likeness Properties

Table 1. The optimum range of physicochemical parameters followed by 95% of the approved drugs

| S. No | Molecular descriptor | Optimum range |
|-------|--|-------------------------|
| 1 | Molecular weight (MW) | 130 to 725 |
| 2 | Estimated number of hydrogen bonds that would be donated by the solute to water molecules in an aqueous solution | 0 to 6 |
| 3 | Estimated number of hydrogen bonds that would be accepted by the solute from water molecules in an aqueous solution | 2 to 20 |
| 4 | Octanol/water partition coefficient (log P) | -2 to 6.5 |
| 5 | Number of violations of Lipinski's rule of five. The rules are MW < 500, logPo/w < 5, donor HB ≤ 5, accept HB ≤ 10. Compounds that satisfy these rules are considered drug-like. (The "five" refers to the limits, which are multiples of 5) | Maximum is 4 |
| 6 | Predicted aqueous solubility, log S. S in mol dm ⁻³ is the concentration of the solute in a saturated solution that is in equilibrium with the crystalline solid | -6.5 to 0.5 |
| 7 | Predicted apparent Caco-2 cell permeability in nm/sec. Caco-2 cells are a model for the gut- blood barrier | <25 poor, >500 great |
| 8 | Number of likely metabolic reactions | 1 to 8 |
| 9 | Number of violations of Jorgensen's rule of three. The three rules are: log S > -5.7, PCaco > 22 nm/s, # Primary Metabolites < 7. Compounds with fewer (and preferably no) violations of these rules are more likely to be orally available | Maximum is 3 |

Drug-likeness assessment: All designed titled compounds (128), substituted (4-phenylpiperazin-1-yl) (9*H*-pyrido-[3,4-*b*]-indol-3-yl)-methanone analogues were analysed for their potential as drug candidates. Drug-likeness properties like absorption, distribution, metabolism, excretion (ADME) were assessed using Lipinski's rule of five. **Table 2 to 9** shows the predicted properties or descriptors of the titled analogues considered for the rule of five, along with their ranges. Several substituted (4-phenylpiperazin-1-yl) (9*H*-pyrido-[3,4-*b*]-indol-3-yl)-methanone analogues aimed at pharmacological applications exhibited significant drug-like properties without violating Lipinski's rule of five.

From the predicted ADME results of compounds **1-16 (scheme 1)**, it can be seen that all the compounds have slightly increased molecular weight and Log P values than the prescribed limit by LOR5 (< 500 Da and log P < 5, respectively). In addition, these compounds were having low solubility profile as the log S value were < -5.7. However, Caco-2 permeability was observed to be greater and a smaller number of primary metabolites (0-2) were seen.

Chapter 4. Design and Prediction of Drug-likeness Properties

From the predicted ADME results of compounds **17-32 (scheme 2)**, it can be seen that all the compounds violated at least one rule from LOR5 marginally; either the molecular weight of the compounds were greater than 500 Da, or log P values were >5 (between 5.26 - 6.18). However, these compounds have slightly improved log P profile compared to scheme-1 compounds, as the values were close to 5. In addition, the Caco-2 cell permeability values were good and have low solubility profile.

Most of the compounds of **scheme 3 (compound 33-48)** have significant ADME profile as the molecular weight was between 470-530 Da, slightly higher than acceptable range, and have high Log P values. Around 50% compounds of scheme-3 have two marginal violations, majorly due to higher Log P values. The only violation observed in case of JOR3 is the low solubility profile.

All the compounds in **scheme 4** were shown to have molecular weight in the acceptable range (~500 Da) and the Log P of 5 with ± 1 deviations. Only three compounds (**56, 58** and **64**) among 16 (**compound 49-64**) had two violations which was mostly due to Log P values. In case of JOR3, the compounds have shown poor solubility profile while Caco-2 cell permeability and primary metabolites result were significant.

In case of compounds **65-80 (scheme 5)**, all the compounds have molecular weight between 520-590 Da and no H-bond donors were present. The Log P values were higher than the normal (between 6.9 – 7.6) and therefore showed two marginal violations of LOR5. The solubility profile was also poor while Caco-2 cell permeability was between 3280-3700 indicating higher permeability. Less number of primary metabolites were observed (between 0-2) and therefore showed only one violation in JOR3.

For compounds **81-96 (scheme 6)**, the molecular weight, satisfy the LOR5 as the range was between 505 – 557 Da, and further has high Log P values, showing two marginal violations. While, in JOR3, only solubility profile was found to be poor.

The compounds synthesized through **scheme 7 (97-112)** has molecular weight ranging between 480 – 545 Da and log P between 6.8-8.2 showing two marginal violations of LOR5, while in case of JOR3, one violation was seen as the solubility profile was low (between -10.63 - 8.64).

The compounds under **scheme 8 (113-128)**, most of the molecules has acceptable molecular weight obeying LOR5, and also acceptable donor hydrogen bonds, while the acceptor hydrogen bonds are slightly higher with ± 2.5 deviation, and therefore showed one violation in LOR5. In case of JOR3, one violation was seen as the observed solubility profile was poor.

Chapter 4. Design and Prediction of Drug-likeness Properties

From the analysis of all 128 compounds, it is clear that the molecules have low water solubility as the Log S values were very low (acceptable range is <-2.5). Although, the observed violations are marginal as per LOR5 and JOR3 rules but all these observed drug-like parameters were within the acceptable range that has been followed by 95% of the approved drugs in the market. Hence, these titled study compounds can be considered for further exploration.

The bioavailability of drug molecules can be predicted using the "rule of three", which Jorgenson implemented. A compound is orally viable if it complies with some, or all parameters listed under Jorgensen rule of three. It depends on the absorption and liver first-pass metabolism processes for a compound's bioavailability. Permeability, solubility, interactions with gut wall metabolism and transporter enzymes are factors that primarily signify the absorption of any compound. According to Jorgensen's r03, the QikProp predicted values were within the limit as shown in the below mentioned tables.

QikProp has also predicted a possible number of metabolic reactions that can readily take place after any molecules enter the body. These metabolic reactions were used to determine whether the molecules can easily access the target site after entering the body or not. A total of two metabolic reactions were estimated to be possible for each of the titled compounds (For 95% of drugs, there will be between 1 and 8 metabolic reactions). Although, some compounds were likely to undergo up to 3 metabolic reactions due to their complexity, suggesting that the compound may be used as drug candidates with better bioavailability profile. PCaco permeability was excellent for the forecasted molecules. Hence, all the substituted (4-phenylpiperazin-1-yl) (9H-pyrido-[3,4-b]-indol-3-yl)-methanone analogues discovered in this work displayed potential drug-like properties.

Toxicity prediction: All the designed compounds consisting of substituted (4-phenylpiperazin-1-yl) (9H-pyrido-[3,4-b]-indol-3-yl)-methanone analogues had their potential as therapeutic candidates. With the assistance of Data Warrior, toxicology predictions were carried out, and the metrics used were mutagenicity, tumorigenicity, reproductive impact and irritant skin sensitivity (**Table 10 to 17**). None of the titled compounds exhibited any harmful effects. In conclusion, these molecules do not pose any health risks during the development phase of drug discovery.

Chapter 4. Design and Prediction of Drug-likeness Properties

Table 2. Forecasted ADME results of the designed analogues of scheme 1

| Comp. code | LIPINSKI RULE OF FIVE | | | | JORGENSEN RULE OF THREE | | | | |
|------------|-----------------------|----------|-----------|----------|-------------------------|--------|---------|-------|--------------------------|
| | MW | Donor HB | Accept HB | Log Po/w | Rule of five violations | Log S | PCaco | Metab | Rule of three violations |
| 1 | 541.45 | 1 | 5.75 | 6.75 | 2 | -9.13 | 2681.76 | 1 | 1 |
| 2 | 529.41 | 1 | 5.00 | 6.89 | 2 | -9.19 | 2907.38 | 0 | 1 |
| 3 | 525.45 | 1 | 5.00 | 6.97 | 2 | -9.50 | 2643.89 | 1 | 1 |
| 4 | 541.45 | 1 | 5.75 | 6.85 | 2 | -9.23 | 2740.81 | 1 | 1 |
| 5 | 541.45 | 1 | 5.75 | 6.75 | 2 | -9.11 | 2640.43 | 1 | 1 |
| 6 | 559.44 | 1 | 5.75 | 6.97 | 2 | -9.40 | 2826.92 | 1 | 1 |
| 7 | 555.47 | 1 | 5.75 | 7.11 | 2 | -9.79 | 2780.26 | 2 | 1 |
| 8 | 571.47 | 1 | 6.50 | 6.90 | 2 | -9.41 | 2802.09 | 2 | 1 |
| 9 | 559.89 | 1 | 5.00 | 7.47 | 2 | -10.25 | 2643.40 | 1 | 1 |
| 10 | 575.89 | 1 | 5.75 | 7.23 | 2 | -9.81 | 2641.52 | 1 | 1 |
| 11 | 563.86 | 1 | 5.00 | 7.40 | 2 | -10.01 | 2969.21 | 0 | 1 |
| 12 | 575.89 | 1 | 5.75 | 7.36 | 2 | -10.00 | 2741.68 | 1 | 1 |
| 13 | 547.47 | 1 | 5.75 | 6.63 | 2 | -9.05 | 2774.35 | 2 | 1 |
| 14 | 535.43 | 1 | 5.00 | 6.81 | 2 | -9.30 | 3064.29 | 1 | 1 |
| 15 | 531.47 | 1 | 5.00 | 6.86 | 2 | -9.48 | 2787.82 | 2 | 1 |
| 16 | 547.47 | 1 | 5.75 | 6.77 | 2 | -9.18 | 3006.44 | 2 | 1 |

Table 3. Forecasted ADME results of the designed analogues of scheme 2

| Comp. comp | LIPINSKI RULE OF FIVE | | | | JORGENSEN RULE OF THREE | | | | |
|------------|-----------------------|----------|-------------|----------|-------------------------|-------|--------|-------|--------------------------|
| | MW | Donor HB | Acceptor HB | Log Po/w | Rule of five violations | Log S | PCaco | Metab | Rule of three violations |
| 17 | 521.57 | 1 | 6.75 | 5.77 | 2 | -8.99 | 316.05 | 3 | 1 |
| 18 | 537.57 | 1 | 7.50 | 5.54 | 2 | -8.33 | 340.56 | 3 | 1 |
| 19 | 491.55 | 1 | 6.00 | 5.68 | 1 | -8.78 | 316.07 | 2 | 1 |
| 20 | 507.55 | 1 | 6.75 | 5.52 | 2 | -8.49 | 335.14 | 2 | 1 |
| 21 | 511.97 | 1 | 6.00 | 5.87 | 2 | -8.89 | 330.78 | 1 | 1 |
| 22 | 505.58 | 1 | 6.00 | 6.00 | 2 | -9.35 | 316.07 | 3 | 1 |
| 23 | 525.54 | 1 | 6.75 | 5.68 | 2 | -8.67 | 337.22 | 2 | 1 |
| 24 | 525.99 | 1 | 6.00 | 6.18 | 2 | -9.53 | 315.80 | 2 | 1 |
| 25 | 529.96 | 1 | 6.00 | 6.12 | 2 | -9.24 | 371.68 | 1 | 1 |
| 26 | 541.99 | 1 | 6.75 | 6.01 | 2 | -9.22 | 333.82 | 2 | 1 |
| 27 | 497.57 | 1 | 6.00 | 5.57 | 1 | -8.75 | 332.77 | 3 | 1 |
| 28 | 483.54 | 1 | 6.00 | 5.26 | 1 | -8.17 | 333.08 | 2 | 1 |
| 29 | 501.53 | 1 | 6.00 | 5.52 | 2 | -8.54 | 374.45 | 2 | 1 |
| 30 | 513.57 | 1 | 6.75 | 5.44 | 2 | -8.60 | 358.84 | 3 | 1 |
| 31 | 497.57 | 1 | 6.00 | 5.57 | 1 | -8.75 | 332.73 | 3 | 1 |
| 32 | 477.52 | 1 | 6.00 | 5.38 | 1 | -8.15 | 330.53 | 1 | 1 |

Chapter 4. Design and Prediction of Drug-likeness Properties

Table 4. Forecasted ADME results of the designed analogues of scheme 3

| Comp. comp | LIPINSKI RULE OF FIVE | | | | JORGENSEN RULE OF THREE | | | | |
|------------|-----------------------|----------|-------------|----------|-------------------------|--------|---------|-------|--------------------------|
| | MW | Donor HB | Acceptor HB | Log Po/w | Rule of five violations | Log S | PCaco | Metab | Rule of three violations |
| 33 | 497.00 | 1 | 5.75 | 6.74 | 1 | -9.14 | 2802.03 | 1 | 1 |
| 34 | 484.96 | 1 | 5.00 | 6.82 | 1 | -9.13 | 2970.38 | 0 | 1 |
| 35 | 481.00 | 1 | 5.00 | 6.89 | 1 | -9.40 | 2643.38 | 1 | 1 |
| 36 | 497.00 | 1 | 5.75 | 6.79 | 1 | -9.15 | 2805.59 | 1 | 1 |
| 37 | 497.00 | 1 | 5.75 | 6.69 | 1 | -9.09 | 2652.30 | 1 | 1 |
| 38 | 514.99 | 1 | 5.75 | 6.91 | 2 | -9.32 | 2844.55 | 1 | 1 |
| 39 | 511.02 | 1 | 5.75 | 7.04 | 2 | -9.69 | 2779.16 | 2 | 1 |
| 40 | 527.02 | 1 | 6.50 | 6.74 | 2 | -8.95 | 2741.90 | 2 | 1 |
| 41 | 472.99 | 1 | 5.00 | 6.49 | 1 | -8.85 | 2784.20 | 1 | 1 |
| 42 | 487.02 | 1 | 5.00 | 6.79 | 1 | -9.37 | 2792.58 | 2 | 1 |
| 43 | 503.02 | 1 | 5.75 | 6.66 | 2 | -9.23 | 2993.75 | 2 | 1 |
| 44 | 490.98 | 1 | 5.00 | 6.73 | 1 | -9.19 | 3058.71 | 1 | 1 |
| 45 | 503.02 | 1 | 5.75 | 6.62 | 2 | -9.01 | 2820.25 | 2 | 1 |
| 46 | 519.40 | 1 | 5.00 | 7.33 | 2 | -9.90 | 2968.80 | 0 | 1 |
| 47 | 515.44 | 1 | 5.00 | 7.40 | 2 | -10.18 | 2640.79 | 1 | 1 |
| 48 | 531.44 | 1 | 5.75 | 7.23 | 2 | -9.86 | 2793.87 | 1 | 1 |

Table 5. Forecasted ADME results of the designed analogues of scheme 4

| Comp. comp | LIPINSKI RULE OF FIVE | | | | JORGENSEN RULE OF THREE | | | | |
|------------|-----------------------|----------|-------------|----------|-------------------------|-------|--------|-------|--------------------------|
| | MW | Donor HB | Acceptor HB | Log Po/w | Rule of five violations | Log S | PCaco | Metab | Rule of three violations |
| 49 | 462.55 | 2 | 5.75 | 5.71 | 1 | -8.46 | 901.44 | 2 | 1 |
| 50 | 466.51 | 2 | 5.75 | 5.57 | 1 | -8.09 | 904.39 | 1 | 1 |
| 51 | 478.55 | 2 | 6.50 | 5.49 | 1 | -8.09 | 897.18 | 2 | 1 |
| 52 | 448.52 | 2 | 5.75 | 5.38 | 1 | -7.85 | 890.52 | 1 | 1 |
| 53 | 478.55 | 2 | 6.50 | 5.47 | 1 | -8.05 | 844.74 | 2 | 1 |
| 54 | 496.54 | 2 | 6.50 | 5.63 | 1 | -8.21 | 865.36 | 2 | 1 |
| 55 | 492.58 | 2 | 6.50 | 5.77 | 1 | -8.60 | 848.68 | 3 | 1 |
| 56 | 508.58 | 2 | 7.25 | 5.49 | 2 | -7.91 | 832.11 | 3 | 1 |
| 57 | 482.97 | 2 | 5.75 | 5.81 | 1 | -8.49 | 808.37 | 1 | 1 |
| 58 | 500.96 | 2 | 5.75 | 6.06 | 2 | -8.82 | 903.20 | 1 | 1 |
| 59 | 454.55 | 2 | 5.75 | 5.22 | 1 | -7.73 | 849.43 | 2 | 1 |
| 60 | 468.57 | 2 | 5.75 | 5.51 | 1 | -8.30 | 849.33 | 3 | 1 |
| 61 | 472.54 | 2 | 5.75 | 5.48 | 1 | -8.16 | 926.31 | 2 | 1 |
| 62 | 484.57 | 2 | 6.50 | 5.40 | 1 | -8.19 | 911.88 | 3 | 1 |
| 63 | 482.97 | 2 | 5.75 | 5.81 | 1 | -8.49 | 808.37 | 1 | 1 |
| 64 | 512.99 | 2 | 6.50 | 5.98 | 2 | -8.83 | 892.21 | 2 | 1 |

Chapter 4. Design and Prediction of Drug-likeness Properties

Table 6. Forecasted ADME results of the designed analogues of scheme 5

| Comp. comp | LIPINSKI RULE OF FIVE | | | | JORGENSEN RULE OF THREE | | | | |
|------------|-----------------------|----------|-------------|----------|-------------------------|-------|---------|-------|--------------------------|
| | MW | Donor HB | Acceptor HB | Log Po/w | Rule of five violations | Log S | PCaco | Metab | Rule of three violations |
| 65 | 555.47 | 0 | 5.75 | 7.04 | 2 | -8.95 | 3289.42 | 1 | 1 |
| 66 | 525.45 | 0 | 5.00 | 6.94 | 2 | -8.62 | 3516.53 | 0 | 1 |
| 67 | 539.47 | 0 | 5.00 | 7.26 | 2 | -9.20 | 3519.77 | 1 | 1 |
| 68 | 543.44 | 0 | 5.00 | 7.20 | 2 | -9.10 | 3417.70 | 0 | 1 |
| 69 | 573.46 | 0 | 5.75 | 7.33 | 2 | -9.44 | 3465.00 | 1 | 1 |
| 70 | 585.50 | 0 | 6.50 | 7.26 | 2 | -9.30 | 3689.55 | 2 | 1 |
| 71 | 569.50 | 0 | 5.75 | 7.32 | 2 | -9.36 | 3477.30 | 2 | 1 |
| 72 | 585.50 | 0 | 6.50 | 7.12 | 2 | -9.18 | 3279.53 | 2 | 1 |
| 73 | 573.92 | 0 | 5.00 | 7.76 | 2 | -9.96 | 3522.37 | 1 | 1 |
| 74 | 589.92 | 0 | 5.75 | 7.54 | 2 | -9.72 | 3291.55 | 1 | 1 |
| 75 | 577.88 | 0 | 5.00 | 7.71 | 2 | -9.87 | 3417.95 | 0 | 1 |
| 76 | 589.92 | 0 | 5.75 | 7.57 | 2 | -9.58 | 3568.76 | 1 | 1 |
| 77 | 561.50 | 0 | 5.75 | 7.13 | 2 | -9.40 | 3713.91 | 2 | 1 |
| 78 | 549.46 | 0 | 5.00 | 7.16 | 2 | -9.35 | 3670.86 | 1 | 1 |
| 79 | 545.50 | 0 | 5.00 | 7.24 | 2 | -9.65 | 3283.19 | 2 | 1 |
| 80 | 561.50 | 0 | 5.75 | 7.07 | 2 | -9.37 | 3659.76 | 2 | 1 |

Table 7. Forecasted ADME results of the designed analogues of scheme 6

| Comp. comp | LIPINSKI RULE OF FIVE | | | | JORGENSEN RULE OF THREE | | | | |
|------------|-----------------------|----------|-------------|----------|-------------------------|-------|--------|-------|--------------------------|
| | MW | Donor HB | Acceptor HB | Log Po/w | Rule of five violations | Log S | PCaco | Metab | Rule of three violations |
| 81 | 521.57 | 0 | 6.75 | 5.71 | 2 | -8.16 | 394.24 | 2 | 1 |
| 82 | 521.57 | 0 | 6.75 | 5.73 | 2 | -8.00 | 446.63 | 2 | 1 |
| 83 | 505.58 | 0 | 6.00 | 5.95 | 2 | -8.42 | 424.05 | 2 | 1 |
| 84 | 509.54 | 0 | 6.00 | 5.87 | 2 | -8.30 | 413.46 | 1 | 1 |
| 85 | 539.57 | 0 | 6.75 | 5.93 | 2 | -8.43 | 427.70 | 2 | 1 |
| 86 | 551.60 | 0 | 7.50 | 5.79 | 2 | -8.10 | 427.00 | 3 | 1 |
| 87 | 535.60 | 0 | 6.75 | 5.98 | 2 | -8.44 | 441.74 | 3 | 1 |
| 88 | 551.60 | 0 | 7.50 | 5.77 | 2 | -8.16 | 417.60 | 3 | 1 |
| 89 | 556.02 | 0 | 6.75 | 6.23 | 2 | -8.67 | 446.42 | 2 | 1 |
| 90 | 540.02 | 0 | 6.00 | 6.43 | 2 | -9.12 | 433.72 | 2 | 1 |
| 91 | 543.98 | 0 | 6.00 | 6.37 | 2 | -9.00 | 421.48 | 1 | 1 |
| 92 | 540.02 | 0 | 6.00 | 6.44 | 2 | -9.14 | 431.68 | 2 | 1 |
| 93 | 527.60 | 0 | 6.75 | 5.79 | 2 | -8.51 | 459.36 | 3 | 1 |
| 94 | 515.56 | 0 | 6.00 | 5.82 | 2 | -8.51 | 449.32 | 2 | 1 |
| 95 | 511.60 | 0 | 6.00 | 5.91 | 2 | -8.75 | 410.64 | 3 | 1 |
| 96 | 527.60 | 0 | 6.75 | 5.74 | 2 | -8.48 | 458.58 | 3 | 1 |

Chapter 4. Design and Prediction of Drug-likeness Properties

Table 8. Forecasted ADME results of the designed analogues of scheme 7

| Comp. comp | LIPINSKI RULE OF FIVE | | | | JORGENSEN RULE OF THREE | | | | |
|------------|-----------------------|----------|-------------|----------|-------------------------|--------|---------|-------|--------------------------|
| | MW | Donor HB | Acceptor HB | Log Po/w | Rule of five violations | Log S | PCaco | Metab | Rule of three violations |
| 97 | 511.02 | 0 | 5.75 | 6.96 | 2 | -8.82 | 3282.79 | 1 | 1 |
| 98 | 481.00 | 0 | 5.00 | 6.86 | 1 | -8.49 | 3509.42 | 0 | 1 |
| 99 | 495.02 | 0 | 5.00 | 7.18 | 1 | -9.07 | 3523.19 | 1 | 1 |
| 100 | 498.99 | 0 | 5.00 | 7.12 | 1 | -8.98 | 3440.90 | 0 | 1 |
| 101 | 529.01 | 0 | 5.75 | 7.21 | 2 | -9.20 | 3568.98 | 1 | 1 |
| 102 | 511.02 | 0 | 5.75 | 6.92 | 2 | -8.64 | 3483.62 | 1 | 1 |
| 103 | 525.05 | 0 | 5.75 | 7.24 | 2 | -9.24 | 3469.65 | 2 | 1 |
| 104 | 541.05 | 0 | 6.50 | 7.04 | 2 | -9.06 | 3299.63 | 2 | 1 |
| 105 | 529.47 | 0 | 5.00 | 8.01 | 2 | -10.63 | 3514.04 | 1 | 1 |
| 106 | 545.47 | 0 | 5.75 | 7.47 | 2 | -9.61 | 3285.29 | 1 | 1 |
| 107 | 533.43 | 0 | 5.00 | 7.63 | 2 | -9.75 | 3446.97 | 0 | 1 |
| 108 | 515.44 | 0 | 5.00 | 7.36 | 2 | -9.26 | 3505.55 | 0 | 1 |
| 109 | 487.02 | 0 | 5.00 | 6.84 | 1 | -8.92 | 3289.59 | 1 | 1 |
| 110 | 505.01 | 0 | 5.00 | 7.07 | 2 | -9.22 | 3673.29 | 1 | 1 |
| 111 | 501.05 | 0 | 5.00 | 7.16 | 2 | -9.52 | 3283.25 | 2 | 1 |
| 112 | 517.04 | 0 | 5.75 | 7.00 | 2 | -9.25 | 3655.31 | 2 | 1 |

Table 9. Forecasted ADME results of the designed analogues of scheme 8

| Comp. comp | LIPINSKI RULE OF FIVE | | | | JORGENSEN RULE OF THREE | | | | |
|------------|-----------------------|----------|-------------|----------|-------------------------|-------|---------|-------|--------------------------|
| | MW | Donor HB | Acceptor HB | Log Po/w | Rule of five violations | Log S | PCaco | Metab | Rule of three violations |
| 113 | 476.58 | 1 | 5.75 | 6.05 | 1 | -8.34 | 1053.58 | 2 | 1 |
| 114 | 480.54 | 1 | 5.75 | 6.01 | 1 | -8.31 | 1031.75 | 1 | 1 |
| 115 | 492.58 | 1 | 6.50 | 5.92 | 1 | -8.22 | 1018.12 | 2 | 1 |
| 116 | 462.55 | 1 | 5.75 | 5.75 | 1 | -7.81 | 1030.79 | 1 | 1 |
| 117 | 492.58 | 1 | 6.50 | 5.92 | 1 | -8.27 | 1015.33 | 2 | 1 |
| 118 | 510.57 | 1 | 6.50 | 6.13 | 2 | -8.57 | 1064.89 | 2 | 1 |
| 119 | 506.60 | 1 | 6.50 | 6.24 | 2 | -8.87 | 1010.61 | 3 | 1 |
| 120 | 522.60 | 1 | 7.25 | 6.03 | 2 | -8.56 | 1046.39 | 3 | 1 |
| 121 | 497.00 | 1 | 5.75 | 6.33 | 1 | -8.79 | 1017.75 | 1 | 1 |
| 122 | 514.99 | 1 | 5.75 | 6.50 | 2 | -8.99 | 1030.22 | 1 | 1 |
| 123 | 468.57 | 1 | 5.75 | 5.72 | 1 | -8.14 | 1002.43 | 2 | 1 |
| 124 | 482.60 | 1 | 5.75 | 6.03 | 1 | -8.71 | 1001.57 | 3 | 1 |
| 125 | 486.56 | 1 | 5.75 | 5.95 | 1 | -8.46 | 1113.83 | 2 | 1 |
| 126 | 498.60 | 1 | 6.50 | 5.89 | 1 | -8.52 | 1115.79 | 3 | 1 |
| 127 | 497.00 | 1 | 5.75 | 6.33 | 1 | -8.79 | 1017.75 | 1 | 1 |
| 128 | 527.02 | 1 | 6.50 | 6.38 | 2 | -8.98 | 981.47 | 2 | 1 |

Chapter 4. Design and Prediction of Drug-likeness Properties

Table 10. Forecasted toxicity results of the designed analogues of scheme 1

| Comp. code | Mutagenicity | Tumorigenicity | Reproductive effect | Irritant | Skin sensitization |
|------------|--------------|----------------|---------------------|----------|--------------------|
| 1 | None | None | None | None | None |
| 2 | None | None | None | None | None |
| 3 | None | None | None | None | None |
| 4 | None | None | None | None | None |
| 5 | None | None | None | None | None |
| 6 | None | None | None | None | None |
| 7 | None | None | None | None | None |
| 8 | None | None | None | None | None |
| 9 | None | None | None | None | None |
| 10 | None | None | None | None | None |
| 11 | None | None | None | None | None |
| 12 | None | None | None | None | None |
| 13 | None | None | None | None | None |
| 14 | None | None | None | None | None |
| 15 | None | None | None | None | None |

None of the compounds from scheme 1 were observed to have toxicity and hence, theoretically can be considered as safe.

Table 11. Forecasted toxicity results of the designed analogues of scheme 2

| Comp. code | Mutagenicity | Tumorigenicity | Reproductive effect | Irritant | Skin sensitization |
|------------|--------------|----------------|---------------------|----------|--------------------|
| 17 | None | None | None | None | None |
| 18 | None | None | None | None | None |
| 19 | None | None | None | None | None |
| 20 | None | None | None | None | None |
| 21 | None | None | None | None | None |
| 22 | None | None | None | None | None |
| 23 | None | None | None | None | None |
| 24 | None | None | None | None | None |
| 25 | None | None | None | None | None |
| 26 | None | None | None | None | None |
| 27 | None | None | None | None | None |
| 28 | None | None | None | None | None |
| 29 | None | None | None | None | None |
| 30 | None | None | None | None | None |
| 31 | None | None | None | None | None |
| 32 | None | None | None | None | None |

None of the compounds from scheme 2 were observed to have toxicity and hence, theoretically can be considered as safe.

Chapter 4. Design and Prediction of Drug-likeness Properties

Table 12. Forecasted toxicity results of the designed analogues of scheme 3

| Comp. code | Mutagenicity | Tumorigenicity | Reproductive effect | Irritant | Skin sensitization |
|-------------------|---------------------|-----------------------|----------------------------|-----------------|---------------------------|
| 33 | None | None | None | None | None |
| 34 | None | None | None | None | None |
| 35 | None | None | None | None | None |
| 36 | None | None | None | None | None |
| 37 | None | None | None | None | None |
| 38 | None | None | None | None | None |
| 39 | None | None | None | None | None |
| 40 | None | None | None | None | None |
| 41 | None | None | None | None | None |
| 42 | None | None | None | None | None |
| 43 | None | None | None | None | None |
| 44 | None | None | None | None | None |
| 45 | None | None | None | None | None |
| 46 | None | None | None | None | None |
| 47 | None | None | None | None | None |
| 48 | None | None | None | None | None |

None of the compounds from scheme 3 were observed to have toxicity and hence, theoretically can be considered as safe.

Table 13. Forecasted toxicity results of the designed analogues of scheme 4

| Comp. code | Mutagenicity | Tumorigenicity | Reproductive effect | Irritant | Skin sensitization |
|-------------------|---------------------|-----------------------|----------------------------|-----------------|---------------------------|
| 49 | None | None | None | None | None |
| 50 | None | None | None | None | None |
| 51 | None | None | None | None | None |
| 52 | None | None | None | None | None |
| 53 | None | None | None | None | None |
| 54 | None | None | None | None | None |
| 55 | None | None | None | None | None |
| 56 | None | None | None | None | None |
| 57 | None | None | None | None | None |
| 58 | None | None | None | None | None |
| 59 | None | None | None | None | None |
| 60 | None | None | None | None | None |
| 61 | None | None | None | None | None |
| 62 | None | None | None | None | None |
| 63 | None | None | None | None | None |
| 64 | None | None | None | None | None |

None of the compounds from scheme 4 were observed to have toxicity and hence, theoretically can be considered as safe.

Chapter 4. Design and Prediction of Drug-likeness Properties

Table 14. Forecasted toxicity results of the designed analogues of scheme 5

| Comp. code | Mutagenicity | Tumorigenicity | Reproductive effect | Irritant | Skin sensitization |
|-------------------|---------------------|-----------------------|----------------------------|-----------------|---------------------------|
| 65 | None | None | None | None | None |
| 66 | None | None | None | None | None |
| 67 | None | None | None | None | None |
| 68 | None | None | None | None | None |
| 69 | None | None | None | None | None |
| 70 | None | None | None | None | None |
| 71 | None | None | None | None | None |
| 72 | None | None | None | None | None |
| 73 | None | None | None | None | None |
| 74 | None | None | None | None | None |
| 75 | None | None | None | None | None |
| 76 | None | None | None | None | None |
| 77 | None | None | None | None | None |
| 78 | None | None | None | None | None |
| 79 | None | None | None | None | None |
| 80 | None | None | None | None | None |

None of the compounds from scheme 5 were observed to have toxicity and hence, theoretically can be considered as safe.

Table 15. Forecasted toxicity results of the designed analogues of scheme 6

| Comp. code | Mutagenicity | Tumorigenicity | Reproductive effect | Irritant | Skin sensitization |
|-------------------|---------------------|-----------------------|----------------------------|-----------------|---------------------------|
| 81 | None | None | None | None | None |
| 82 | None | None | None | None | None |
| 83 | None | None | None | None | None |
| 84 | None | None | None | None | None |
| 85 | None | None | None | None | None |
| 86 | None | None | None | None | None |
| 87 | None | None | None | None | None |
| 88 | None | None | None | None | None |
| 89 | None | None | None | None | None |
| 90 | None | None | None | None | None |
| 91 | None | None | None | None | None |
| 92 | None | None | None | None | None |
| 93 | None | None | None | None | None |
| 94 | None | None | None | None | None |
| 95 | None | None | None | None | None |
| 96 | None | None | None | None | None |

None of the compounds from scheme 6 were observed to have toxicity and hence, theoretically can be considered as safe.

Chapter 4. Design and Prediction of Drug-likeness Properties

Table 16. Forecasted toxicity results of the designed analogues of scheme 7

| Comp. code | Mutagenicity | Tumorigenicity | Reproductive effect | Irritant | Skin sensitization |
|-------------------|---------------------|-----------------------|----------------------------|-----------------|---------------------------|
| 97 | None | None | None | None | None |
| 98 | None | None | None | None | None |
| 99 | None | None | None | None | None |
| 100 | None | None | None | None | None |
| 101 | None | None | None | None | None |
| 102 | None | None | None | None | None |
| 103 | None | None | None | None | None |
| 104 | None | None | None | None | None |
| 105 | None | None | None | None | None |
| 106 | None | None | None | None | None |
| 107 | None | None | None | None | None |
| 108 | None | None | None | None | None |
| 109 | None | None | None | None | None |
| 110 | None | None | None | None | None |
| 111 | None | None | None | None | None |
| 112 | None | None | None | None | None |

None of the compounds from scheme 7 were observed to have toxicity and hence, theoretically can be considered as safe.

Table 17. Forecasted toxicity results of the designed analogues of scheme 8

| Comp. code | Mutagenicity | Tumorigenicity | Reproductive effect | Irritant | Skin sensitization |
|-------------------|---------------------|-----------------------|----------------------------|-----------------|---------------------------|
| 113 | None | None | None | None | None |
| 114 | None | None | None | None | None |
| 115 | None | None | None | None | None |
| 116 | None | None | None | None | None |
| 117 | None | None | None | None | None |
| 118 | None | None | None | None | None |
| 119 | None | None | None | None | None |
| 120 | None | None | None | None | None |
| 121 | None | None | None | None | None |
| 122 | None | None | None | None | None |
| 123 | None | None | None | None | None |
| 124 | None | None | None | None | None |
| 125 | None | None | None | None | None |
| 126 | None | None | None | None | None |
| 127 | None | None | None | None | None |
| 128 | None | None | None | None | None |

None of the compounds from scheme 8 were observed to have toxicity and hence, theoretically can be considered as safe.

References

- (1) Sander, T.; Freyss, J.; Von Korff, M.; Rufener, C. DataWarrior: An Open-Source Program for Chemistry Aware Data Visualization and Analysis. *Journal of Chemical Information and Modeling* **2015**, *55* (2), 460–473. <https://doi.org/10.1021/ci500588j>.
- (2) Schrödinger Release 2019-1: Maestro, Schrödinger, LLC, New York, NY, 2019.
- (3) Conners, R.; Schambach, F.; Read, J.; Cameron, A.; Sessions, R. B.; Vivas, L.; Easton, A.; Croft, S. L.; Brady, R. L. Mapping the Binding Site for Gossypol-like Inhibitors of Plasmodium Falciparum Lactate Dehydrogenase. *Molecular and Biochemical Parasitology* **2005**, *142* (2), 137–148. <https://doi.org/10.1016/j.molbiopara.2005.03.015>.
- (4) Schrödinger Release 2019-1: LigPrep, Schrödinger, LLC, New York, NY, 2019. Schrödinger Release 2019-1: LigPrep, Schrödinger, LLC, New York, NY, 2019.
- (5) Schrödinger Release 2019-1: Schrödinger Suite 2019-1 Protein Preparation Wizard; Epik, Schrödinger, LLC, New York, NY, 2019.
- (6) *Schrödinger Release 2020-4: Desmond Molecular Dynamics System, D. E. Shaw Research, New York, NY, 2020. Maestro-Desmond Interoperability Tools, Schrödinger, New York, NY, 2020.*
- (7) Mark, P.; Nilsson, L. Structure and Dynamics of the TIP3P, SPC, and SPC/E Water Models at 298 K. *Journal of Physical Chemistry A* **2001**, *105* (43), 9954–9960. <https://doi.org/10.1021/jp003020w>.
- (8) Jorgensen, W. L.; Maxwell, D. S.; Tirado-Rives, J. Development and Testing of the OPLS All-Atom Force Field on Conformational Energetics and Properties of Organic Liquids. *Journal of the American Chemical Society* **1996**, *118* (45), 11225–11236. <https://doi.org/10.1021/ja9621760>.
- (9) Berne, M. T. and B. J. G. J. M. Reversible Multiple Time Scale Molecular Dynamics. *The Journal of Physical Chemistry* **1993**, *97* (51), 13429–13434. <https://doi.org/10.1021/j100153a002>.
- (10) Cheng, A.; Merz, K. M. Application of the Nosé–Hoover Chain Algorithm to the Study of Protein Dynamics. *The Journal of Physical Chemistry* **1996**, *100* (5), 1927–1937. <https://doi.org/10.1021/jp951968y>.
- (11) Kalibaeva, G.; Ferrario, M.; Ciccotti, G. Constant Pressure-Constant Temperature Molecular Dynamics: A Correct Constrained NPT Ensemble Using the Molecular Virial. *Molecular Physics* **2003**, *101* (6), 765–778.

Chapter 4. Design and Prediction of Drug-likeness Properties

<https://doi.org/10.1080/0026897021000044025>.

- (12) Kumar, B. K.; Faheem; Sekhar, K. V. G. C.; Ojha, R.; Prajapati, V. K.; Pai, A.; Murugesan, S. Pharmacophore Based Virtual Screening, Molecular Docking, Molecular Dynamics and MM-GBSA Approach for Identification of Prospective SARS-CoV-2 Inhibitor from Natural Product Databases. *Journal of Biomolecular Structure and Dynamics* **2022**, *40* (30), 1363–1386. <https://doi.org/10.1080/07391102.2020.1824814>.
- (13) Karan Kumar, B.; Faheem; Balana Fouce, R.; Melcon-Fernandez, E.; Perez-Pertejo Yolanda, Y.; Reguera, R. M.; Adinarayana, N.; Chandra Sekhar, K. V. G.; Vanaparthi, S.; Murugesan, S. Design, Synthesis and Evaluation of Novel β -Carboline Ester Analogues as Potential Anti-Leishmanial Agents. *Journal of Biomolecular Structure and Dynamics* **2022**, *40* (23), 12592-12607. <https://doi.org/10.1080/07391102.2021.1973564>.
- (14) QikProp Descriptors and Properties PISA. **2015**, 2–4.
- (15) Ganesan, M. S.; Raja, K. K.; Murugesan, S.; Kumar, B. K.; Rajagopal, G.; Thirunavukkarasu, S. Synthesis, Biological Evaluation, Molecular Docking, Molecular Dynamics and DFT Studies of Quinoline-Fluoroproline Amide Hybrids. *Journal of Molecular Structure* **2020**, *1217*, 128360. <https://doi.org/10.1016/j.molstruc.2020.128360>.
- (16) van de Waterbeemd, H.; Gifford, E. ADMET in Silico Modelling: Towards Prediction Paradise? *Nature Reviews Drug Discovery* **2003**, *2* (3), 192–204. <https://doi.org/10.1038/nrd1032>.



Chapter 5. Synthesis and Characterization of the designed analogues



Chapter 5. Synthesis and Characterization of the designed analogues

Materials and methods

All solvents and reagents purchased from Sigma or Merck companies were used as received without further purification. The solvent system used throughout the experimental work for running Thin Layer Chromatography (TLC) was ethyl acetate and hexane mixture to monitor the reaction. Column chromatography was performed using silica gel (100–200 mesh), SRL, India) as stationary phase and a mixture of ethyl acetate and hexane as mobile phase. Melting points were uncorrected and were determined in an open capillary tube on a Precision Buchi B530 (Flawil, Switzerland) melting point apparatus. IR spectra of the synthesized compounds were recorded using an ATR spectrophotometer (Bruker, alpha-II). ¹H spectra were recorded on a Bruker DPX-400 spectrometer (Bruker India Scientific Pvt. Ltd., Mumbai) using TMS as an internal standard (chemical shifts in δ , ppm), HRMS were recorded on Agilent Technologies 6545 Q-TOF LC/MS.

Chemistry:

The synthetic scheme for β -carboline piperazine derivatives was represented in Scheme 1 to 8. The titled compounds were synthesized using DL-Tryptophan as starting material. For the hydroxy series, 5-hydroxy tryptophan was used as starting material. Initial esterification of DL-Tryptophan using thionyl chloride to get an ethyl ester of tryptophan, was followed by Pictet-Spengler reaction in presence of trifluoroacetic acid to obtain tricyclic ethyl-2,3,4,9-tetrahydro-1-phenyl-1*H*-pyrido-[3,4-*b*]-indole-3-carboxylate. Upon oxidation with sulphur and xylene, ethyl-1-phenyl-9*H*-pyrido-[3,4-*b*]-indole-3-carboxylate was obtained and is continued by 9-*N*-methylation with methyl iodide in presence of potassium hydroxide to acquire ethyl-9-methyl-1-phenyl-9*H*-pyrido-[3,4-*b*]-indole-3-carboxylate for the schemes-4 to 8 and this step was not performed in scheme-1. For the nitration process, sodium nitrate was used with trifluoro acetic acid. Further alkaline ester hydrolysis of the above obtained compound produced 9-methyl-1-phenyl-9*H*-pyrido-[3,4-*b*]-indole-3-carboxylic acid and (1-phenyl-9*H*-pyrido-[3,4-*b*]-indole-3-carboxylic acid. The carboxylic acid key intermediate was treated with appropriate amines (aryl-substituted piperazines) in presence of coupling agent 1-ethyl-3-(3-dimethylaminopropyl)-carbodiimide hydrochloride (EDCI) and hydroxy benzotriazole (HOBt) to obtain the desired products.

Synthesis of ethyl 2-amino-3-(1*H*-indol-3-yl)-propionate:

To a solution of DL-tryptophan (1) (5 g, 0.0245 mol) in 50 mL of ethanol, SOCl₂ (5.32 mL, 0.073 mol) was added drop wise at 0 °C. Subsequently, the reaction mixture was refluxed for 1 h. After completion of reaction as monitored by TLC, solvent was evaporated in-vacuo and

Chapter 5. Synthesis and Characterization of the designed analogues

the residue obtained was dissolved in ethyl acetate. Organic layer was washed twice with NaHCO₃ solution. The separated organic layer was dried over Na₂SO₄ and concentrated under vacuum¹.

Synthesis of ethyl-2,3,4,9-tetrahydro-1-substituted-1*H*-pyrido-[3,4-*b*]-indole-3-carboxylate:

To the mixture of ethyl 2-amino-3-(1*H*-indol-3-yl)-propanoate (2) (5 g, 0.022 mol) and benzaldehyde (2) (2.2 mL, 0.022 mol) in 100 mL of dichloromethane, 2.5 mL of trifluoroacetic acid was added drop wise at 0 °C for 10 min. Then, reaction mixture was stirred at room temperature for 3 h. After completion of reaction as monitored by TLC, the reaction mixture was poured into saturated NaHCO₃ solution. Organic layer was separated and washed twice with brine solution, dried over Na₂SO₄ and concentrated under vacuum².

Synthesis of ethyl 1-substituted-9*H*-pyrido-[3,4-*b*]-indole-3-carboxylate:

To a solution of ethyl-2,3,4,9-tetrahydro-1-phenyl-1*H*-pyrido-[3,4-*b*]-indole-3-carboxylate (3) (4 g, 0.013 mol) in 100 mL of dry xylene, sulphur (5.15 g, 0.039 mol) was added and the reaction mixture was stirred and refluxed at 100 °C for 24 h. After completion of reaction as monitored by TLC, the solvent was evaporated in-vacuo, the residue was dissolved in ethyl acetate and washed twice with 50 mL of distilled water. The separated organic layer was dried over Na₂SO₄ and concentrated under vacuum to get the desired product^{3,4}.

Synthesis of ethyl 6-bromo-9*H*-pyrido-[3,4-*b*]-indole-3-carboxylate:

To a solution of compound 4 (0.10 mmol) in ethyl acetate (250 mL), a solution of *N*-bromo succinimide (15.7 g, 0.12 mmol) in ethyl acetate (300 mL) was added, and the mixture was refluxed for 12 h. Progress of the reaction was monitored by thin layer chromatography, after completion of the reaction, cooled to room temperature, the reaction mixture was washed with 0.1 M NaOH, the organic phase was collected and dried under vacuum to give the desired compound.

Synthesis of substituted 9*H*-pyrido-[3,4-*b*]-indole-3-carboxylic acid:

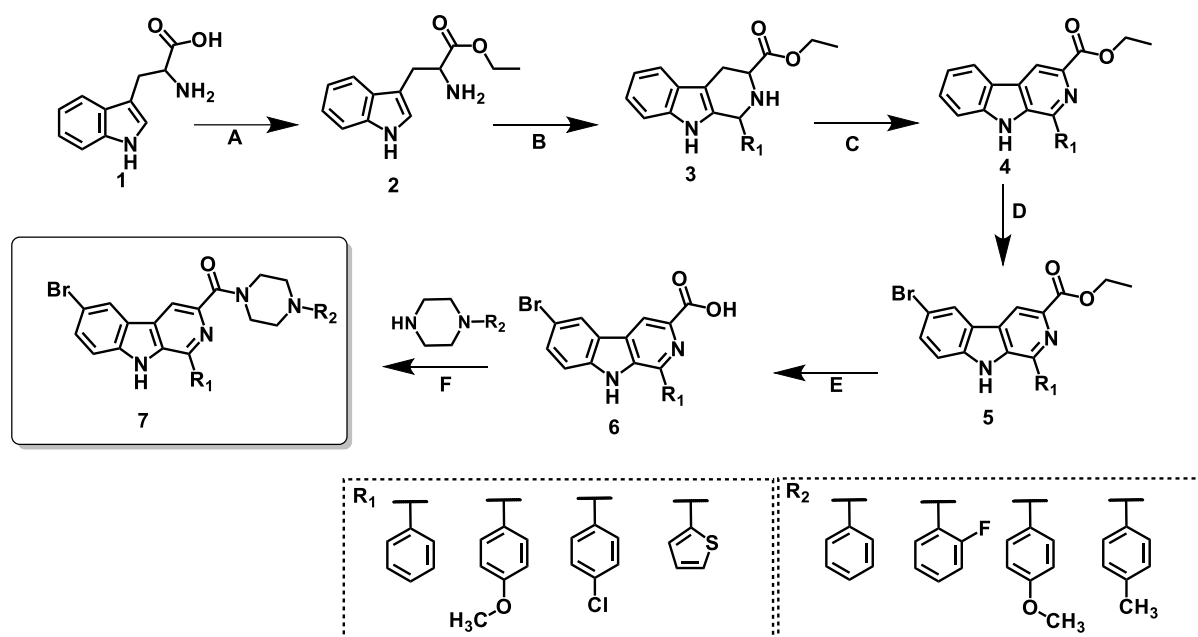
To a solution of ethyl-6-bromo-9*H*-pyrido-[3,4-*b*]-indole-3-carboxylate (5) (3 g, 0.01 mol) in ethanol water (1:1) mixture, NaOH (1.2 g, 0.03 mol) was added and refluxed for 30 min. After completion of reaction as monitored by TLC, ethanol from the reaction mixture was removed under vacuum and neutralized with dil. HCl. Then, the reaction mixture was extracted with ethyl acetate (2 x 30 mL), collected organic layer was dried over Na₂SO₄ and concentrated under vacuum.

Synthesis of ((6-bromo-1-phenyl-9H-pyrido-[3,4-b]-indol-3-yl) (4-phenylpiperazin-1-yl)-methanone:

To a stirred solution of 1-phenyl-9H-pyrido-[3,4-b]-indole-3-carboxylic acid (6) (0.29 g, 1 mmol) in dry THF, HOBt (0.16 g, 1.2 mmol) and EDCI. HCl (0.23 g, 1.2 mmol) were added and continued stirring for 30 min. To the reaction mixture, 1-phenylpiperazine (1 mmol) was added under ice cold temperature and the reaction mixture was further stirred at room temperature for 6 h. After completion of reaction as monitored by TLC, solvent was evaporated under vacuum. Reaction mixture was extracted with ethyl acetate (2 x 20 mL), collected organic layer was dried over Na₂SO₄ and concentrated under vacuum to get desired compound. The obtained crude product was passed through short bed of silica gel (100-200) by using ethyl acetate and n-hexane mixture as mobile phase to obtain analytically pure compound.

Synthesis of (6-bromo-1-phenyl-9H-pyrido-[3,4-b]-indol-3-yl) (4-phenylpiperazin-1-yl)-methanone derivatives:

To a solution of the compound 4 (0.10 mmol) in ethyl acetate (250 mL), a solution of *N*-bromo succinimide (15.7 g, 0.12 mmol) in ethyl acetate (300 mL) was added, and the mixture was refluxed for 2 h. Progress of the reaction was monitored by thin layer chromatography, after completion of the reaction, cooled to room temperature, the reaction mixture was washed with 0.1 M NaOH, the organic phase was collected and dried under vacuum to give the desired compound.



Scheme 1: Reagents and conditions: (A) SOCl_2 , ethanol, $0\text{ }^\circ\text{C}$, reflux, 1 h (B) Aromatic aldehydes, trifluoroacetic acid, DCM, rt, 3 h (C) Sulfur, Xylene, $100\text{ }^\circ\text{C}$, reflux 24 h (D), *N*-bromo succinimide, ethyl acetate, reflux, 24 h (E) NaOH, ethanol: water (1:1), rt, 45 min, (F) THF, EDCl, HCl, HOBt, Phenyl piperazine, rt, overnight

Characterized data for 6-bromo substituted compounds of scheme 1:

(6-bromo-1-phenyl-9H-pyrido-[3,4-*b*]-indol-3-yl) (4-(4-methoxyphenyl)-piperazin-1-yl)-methanone (1): Pale yellow solid, Melting point $180\text{-}182\text{ }^\circ\text{C}$, Yield 72 %, IR $\nu_{\text{max}}/\text{cm}$: 3229, 1620, 1557, 1492, 1433, ^1H NMR (400 MHz, Chloroform-*d*) δ 8.78 (s, 1H), 8.44 (s, 1H), 8.18 (d, $J = 7.6\text{ Hz}$, 1H), 7.80-7.84 (m 3H), 7.74 (d, $J = 7.8\text{ Hz}$, 1H), 7.62-7.56 (m, 2H), 7.38-7.34 (m, 2H), 7.15-7.08 (m, 4H), 7.03-6.97 (m, 2H), 4.19-4.00 (m, 3H), 3.26-3.17 (m, 4H), ^{13}C NMR (101 MHz, Chloroform-*d*) δ 168.60, 152.20, 151.68, 147.25, 146.78, 132.12, 129.23, 126.54, 128.14, 115.35, 113.35, 55.80, 26.60, 49.65. ESI MS (m/z): calculated for $\text{C}_{29}\text{H}_{25}\text{BrN}_4\text{O}_2$, 504.12, found 505.18 $[\text{M}+\text{H}]^+$, 506.20 $[\text{M}+2]^+$

(6-bromo-1-phenyl-9H-pyrido-[3,4-*b*]-indol-3-yl) (4-(2-fluorophenyl)-piperazin-1-yl)-methanone (2): Pale yellow solid, Melting point $185\text{-}187\text{ }^\circ\text{C}$, Yield 61 %, IR $\nu_{\text{max}}/\text{cm}$: 3228, 1620, 1587, 1490, 1433, ^1H NMR (400 MHz, Chloroform-*d*) 8.57 (s, 1H), 8.09 (d, $J = 7.5, 1.0\text{ Hz}$, 1H), 7.88 – 7.82 (m, 2H), 7.53 – 7.45 (m, 2H), 7.30 – 7.24 (m, 1H), 7.07 – 7.02 (m, 3H), 6.84 – 6.75 (m, 2H), 4.04 – 3.91 (m, 4H), 3.84 (s, 3H), 3.18. (d, $J = 30.1\text{ Hz}$, 3H), ^{13}C NMR (101 MHz, Chloroform-*d*) δ 169.60, 152.21, 154.67, 146.25, 145.79, 133.12, 123.24, 122.54, 128.14, 116.35, 113.75, 54.81, 55.61, 49.64. ESI MS (m/z): calculated for $\text{C}_{28}\text{H}_{22}\text{BrFN}_4\text{O}$, 528.15, found 529.25 $[\text{M}+\text{H}]^+$, 530.26 $[\text{M}+2]^+$

(6-bromo-1-phenyl-9H-pyrido-[3,4-b]-indol-3-yl) (4-(p-tolyl)-piperazin-1-yl)-methanone (3): White solid, Melting point 210-212 °C, Yield 68 %, IR $\nu_{\text{max}}/\text{cm}$: 3234, 1620, 1533, 1480, ^1H NMR (400 MHz, Chloroform-*d*) δ 8.53 (s, 1H), 8.39 (s, 1H), 7.98 – 7.82 (m, 2H), 7.57 – 7.48 (m, 2H), 7.40 – 7.26 (m, 3H), 7.07 – 7.02 (m, 4H), 6.84 – 6.75 (m, 2H), 4.04 – 3.91 (m, 4H), 3.84 (s, 3H), 3.18. (s, $J = 30.1$ Hz, 3H). ESI MS (m/z): calculated for $\text{C}_{29}\text{H}_{25}\text{BrN}_4\text{O}$, 524.55, found 525.65 $[\text{M}+\text{H}]^+$, 526.35 $[\text{M}+2]^+$

(6-bromo-1-phenyl-9H-pyrido-[3,4-b]-indol-3-yl) (4-(2-methoxyphenyl)-piperazin-1-yl)-methanone (4): White solid, Yield 60%, Melting point 230-232 °C, IR $\nu_{\text{max}}/\text{cm}$: 3228, 1620, 1587, 1490, 1433, ^1H NMR (400 MHz, Chloroform-*d*) δ 8.51 (s, 1H), 8.37 (s, 1H), 8.09 (d, $J = 7.3$, 1.0 Hz, 1H), 7.88 – 7.86 (m, 4H), 7.53 – 7.45 (m, 2H), 7.30 – 7.24 (m, 2H), 7.09 – 7.02 (m, 4H), 6.85 – 6.75 (m, 2H), 4.04 – 3.94 (m, 3H), 3.18. (d, $J = 30.1$ Hz, 4H). ESI MS (m/z): calculated for $\text{C}_{29}\text{H}_{25}\text{BrN}_4\text{O}_2$, 540.12, found 541.85 $[\text{M}+\text{H}]^+$, 542.22 $[\text{M}+2]^+$

(6-bromo-1-(4-methoxyphenyl)-9H-pyrido-[3,4-b]-indol-3-yl) (4-phenylpiperazin-1-yl)-methanone (5): White solid, Yield 59%. Melting point 150-152 °C, IR $\nu_{\text{max}}/\text{cm}$: 3218, 1630, 1587, 1467, 1443, ^1H NMR (400 MHz, Chloroform-*d*) δ 8.61 (s, 1H), 8.31 (s, 1H), 8.09 (d, $J = 7.5$, 1.0 Hz, 1H), 7.87 – 7.89 (m, 2H), 7.56 – 7.45 (m, 2H), 7.30 – 7.24 (m, 2H), 7.08 – 7.02 (m, 4H), 6.84 – 6.75 (m, 2H), 4.04 – 3.91 (m, 4H), 3.84 (s, 3H), 3.18. (d, $J = 30.1$ Hz, 3H). ESI MS (m/z): calculated for $\text{C}_{29}\text{H}_{25}\text{BrN}_4\text{O}_2$, 540.15, found 541.35 $[\text{M}+\text{H}]^+$, 542.22 $[\text{M}+2]^+$

(6-bromo-1-(4-methoxyphenyl)-9H-pyrido-[3,4-b]-indol-3-yl) (4-(2-fluorophenyl)-piperazin-1-yl)-methanone (6): White solid, Yield 60%, Melting point 160-162 °C, IR $\nu_{\text{max}}/\text{cm}$: 3218, 1630, 1587, 1467, 1443, ^1H NMR (400 MHz, Chloroform-*d*) δ 8.51 (s, 1H), 8.37 (s, 1H), 8.09 (d, $J = 7.3$, 1.0 Hz, 1H), 7.81 – 7.86 (m, 2H), 7.53 – 7.45 (m, 2H), 7.30 – 7.24 (m, 2H), 7.09 – 7.02 (m, 4H), 6.85 – 6.75 (m, 3H), 4.04 – 3.94 (m, 3H), 3.18. (d, $J = 30.1$ Hz, 4H). ESI MS (m/z): calculated for $\text{C}_{29}\text{H}_{24}\text{BrFN}_4\text{O}_2$, 558.11, found 559.25 $[\text{M}+\text{H}]^+$, 560.33 $[\text{M}+2]^+$

(6-bromo-1-(4-methoxyphenyl)-9H-pyrido-[3,4-b]-indol-3-yl) (4-(p-tolyl)-piperazin-1-yl)-methanone (7): Yellow solid, Yield 69%, Melting point 173-175 °C, IR $\nu_{\text{max}}/\text{cm}$: 3218, 1630, 1587, 1467, 1443, ^1H NMR (400 MHz, Chloroform-*d*) δ 8.53 (s, 1H), 8.33 (s, 1H), 8.10 (d, $J = 7.3$, 1.0 Hz, 1H), 7.84 – 7.86 (m, 2H), 7.52 – 7.43 (m, 2H), 7.31 – 7.24 (m, 2H), 7.09 – 7.02 (m, 4H), 6.85 – 6.75 (m, 2H), 4.04 – 3.94 (m, 3H), 3.18. (d, $J = 30.1$ Hz, 4H). ^{13}C NMR (101 MHz, Chloroform-*d*) δ 179.50, 158.29, 157.66, 149.25, 145.78, 132.12, 124.33, 126.54, 128.14, 125.37, 114.34, 55.88, 56.70, 52.45. ESI MS (m/z): calculated for $\text{C}_{30}\text{H}_{27}\text{BrN}_4\text{O}_2$, 554.13, found 555.95 $[\text{M}+\text{H}]^+$, 556.22 $[\text{M}+2]^+$

(6-bromo-1-(4-methoxyphenyl)-9H-pyrido-[3,4-b]-indol-3-yl) (4-(4-methoxyphenyl)-piperazin-1-yl)-methanone (8): White solid, Yield 69 %, Melting point 155-157 °C, IR $\nu_{\text{max/cm}}$: 3223, 1662, 1518, 1431, 725, $^1\text{H NMR}$ (400 MHz, Chloroform-*d*) δ 8.41 (s, 1H), 8.03 – 7.95 (m, 2H), 7.69 – 7.62 (m, 3H), 7.59 (d, $J = 1.8$ Hz, 2H), 7.28 (s, 1H), 6.99 – 6.84 (m, 7H), 4.06 (t, $J = 5.1$ Hz, 2H), 3.79 (d, $J = 1.9$ Hz, 3H), 3.50 (q, $J = 7.0$ Hz, 2H), 3.16 (d, $J = 5.8$ Hz, 4H). ESI MS (m/z): calculated for $\text{C}_{30}\text{H}_{27}\text{BrN}_4\text{O}_3$, 570.13, found 571.65 $[\text{M}+\text{H}]^+$, 572.56 $[\text{M}+2]^+$

(6-bromo-1-(4-chlorophenyl)-9H-pyrido-[3,4-b]-indol-3-yl) (4-(p-tolyl)-piperazin-1-yl)-methanone (9): Off white solid, Yield 60%, Melting point 171-173 °C, IR $\nu_{\text{max/cm}}$: 3228, 1620, 1587, 1490, 1433, $^1\text{H NMR}$ (400 MHz, Chloroform-*d*) δ 8.51 (s, 1H), 8.37 (s, 1H), 8.09 (d, $J = 7.3, 1.0$ Hz, 1H), 7.88 – 7.86 (m, 2H), 7.53 – 7.45 (m, 2H), 7.30 – 7.24 (m, 2H), 7.09 – 7.02 (m, 4H), 6.85 – 6.75 (m, 2H), 4.04 – 3.94 (m, 3H), 3.18. (d, $J = 30.1$ Hz, 4H). ESI MS (m/z): calculated for $\text{C}_{29}\text{H}_{24}\text{BrClN}_4\text{O}$, 559.89, found 560.85 $[\text{M}+\text{H}]^+$, 561.25 $[\text{M}+2]^+$, 563.26 $[\text{M}+4]^+$

(6-bromo-1-(4-chlorophenyl)-9H-pyrido-[3,4-b]-indol-3-yl) (4-(4methoxyphenyl)-piperazin-1-yl)-methanone (10): Yellow solid, Yield 60%, Melting point 128-130 °C, IR $\nu_{\text{max/cm}}$: 3209, 1614, 1550, 1508, $^1\text{H NMR}$ (400 MHz, Chloroform-*d*) δ 8.54 (s, 1H), 8.37 (s, 1H), 8.09 (d, $J = 7.8, 1.0$ Hz, 1H), 7.88 – 7.85 (m, 2H), 7.53 – 7.45 (m, 2H), 7.32 – 7.24 (m, 1H), 7.07 – 7.02 (m, 3H), 6.84 – 6.75 (m, 2H), 4.04 – 3.91 (m, 4H), 3.80 (s, 3H), 3.18. (d, $J = 30.1$ Hz, 4H). ESI MS (m/z): calculated for $\text{C}_{29}\text{H}_{24}\text{BrClN}_4\text{O}_2$, 574.18, found 575.28 $[\text{M}+\text{H}]^+$, 576.77 $[\text{M}+2]^+$, 578.89 $[\text{M}+4]^+$

(6-bromo-1-(4-chlorophenyl)-9H-pyrido-[3,4-b]-indol-3-yl) (4-(2-fluorophenyl)-piperazin-1-yl)-methanone (11): Yellow solid, Yield 59%, Melting point 146-148 °C, IR $\nu_{\text{max/cm}}$: 3223, 1662, 1518, 1431, 735, $^1\text{H NMR}$ (400 MHz, Chloroform-*d*) δ 8.61 (s, 1H), 8.31 (s, 1H), 8.09 (d, $J = 7.5, 1.0$ Hz, 1H), 7.87 – 7.89 (m, 2H), 7.56 – 7.45 (m, 2H), 7.30 – 7.24 (m, 2H), 7.08 – 7.02 (m, 4H), 6.84 – 6.75 (m, 2H), 4.04 – 3.91 (m, 3H), 3.84 (s, 2H), 3.18. (d, $J = 30.1$ Hz, 2H). ESI MS (m/z): calculated for $\text{C}_{28}\text{H}_{21}\text{BrClFN}_4\text{O}$, 562.06, found 563.09 $[\text{M}+\text{H}]^+$

(6-bromo-1-(4-chlorophenyl)-9H-pyrido-[3,4-b]-indol-3-yl) (4-(2-methoxyphenyl)-piperazin-1-yl)-methanone (12): Yellow solid, Yield 68%, Melting point 138-140 °C, IR $\nu_{\text{max/cm}}$: 3213, 1635, 1518, 1431, 729, $^1\text{H NMR}$ (400 MHz, Chloroform-*d*) δ 8.53 (s, 1H), 8.39 (s, 1H), 8.09 (d, $J = 7.3, 1.0$ Hz, 1H), 7.98 – 7.82 (m, 2H), 7.57 – 7.48 (m, 2H), 7.40 – 7.26 (m, 3H), 7.07 – 7.02 (m, 4H), 6.84 – 6.75 (m, 2H), 4.04 – 3.91 (m, 3H), 3.86 (s, 3H), 3.18. (d,

$J = 30.1$ Hz, 3H). ESI MS (m/z): calculated for $C_{29}H_{24}BrClN_4O_2$, 574.08, found 575.15 $[M+H]^+$, 576.67 $[M+2]^+$, 578.86 $[M+4]^+$

(6-bromo-1-(thiophen-2-yl)-9H-pyrido-[3,4-*b*]-indol-3-yl) (4-(4-methoxyphenyl)-

piperazin-1-yl)-methanone (13): Yellow solid, Yield 61%, Melting point 123-125 °C, IR ν_{max}/cm : 3220, 1612, 1558, 1520, 748, 1H NMR (400 MHz, Chloroform-*d*) 8.57 (s, 1H), 8.09 (d, $J = 7.5$, 1.0 Hz, 1H), 7.88 – 7.82 (m, 2H), 7.53 – 7.45 (m, 2H), 7.30 – 7.24 (m, 1H), 7.07 – 7.02 (m, 3H), 6.84 – 6.75 (m, 2H), 4.04 – 3.91 (m, 4H), 3.84 (s, 3H), 3.18. (d, $J = 30.1$ Hz, 4H). ESI MS (m/z): calculated for $C_{27}H_{23}BrN_4O_2S$, 546.07, found 547.35 $[M+H]^+$, 548.09 $[M+2]^+$

(6-bromo-1-(thiophen-2-yl)-9H-pyrido-[3,4-*b*]-indol-3-yl) (4-(2-fluorophenyl)-piperazin-

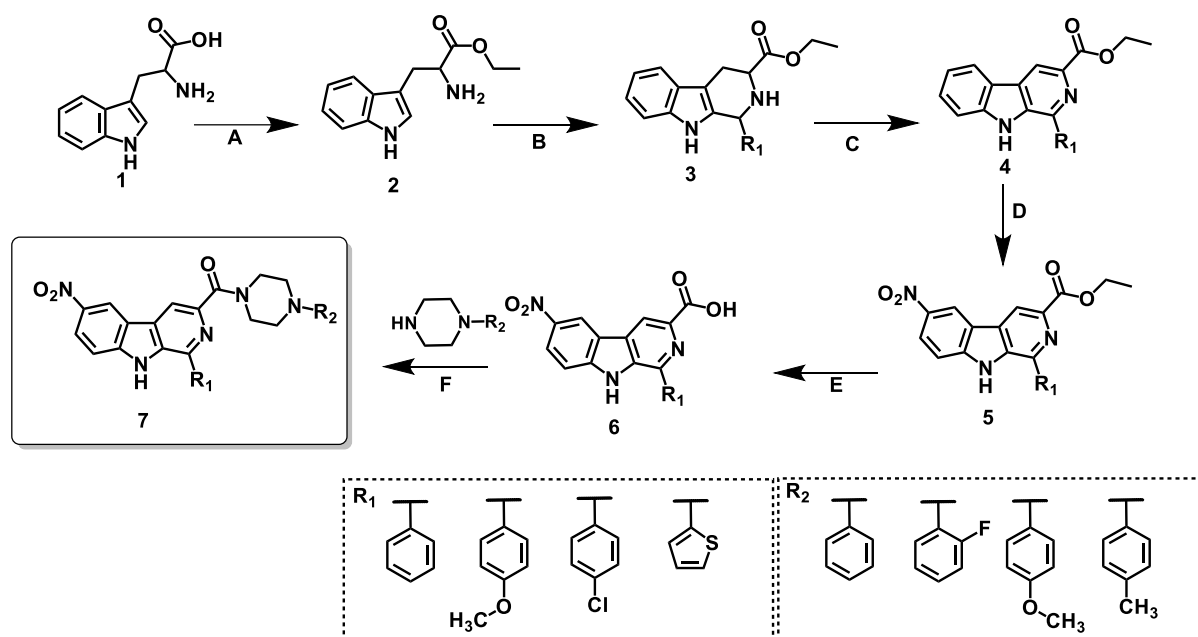
1-yl)-methanone (14): White solid, Yield 62%, Melting point 167-169 °C, IR ν_{max}/cm : 3153, 1652, 1515, 1469, 720, 1H NMR (400 MHz, Chloroform-*d*) δ 8.20 (s, 1H), 7.5 – 7.38 (m, 9H), 7.02 – 6.89 (m, 3H), 3.10-3.01 (m, 4H), 2.10 – 2.05 (m, 2H), 1.36 – 1.21 (m, 4H). ^{13}C NMR (101 MHz, Chloroform-*d*) δ 170.67, 154.21, 151.69, 144.26, 141.78, 131.17, 128.23, 122.54, 120.14, 115.57, 112.37, 54.88, 52.60, 48.67. ESI MS (m/z): calculated for $C_{26}H_{20}BrFN_4OS$, 534.05, found 535.65 $[M+H]^+$, 536.86 $[M+2]^+$

(6-bromo-1-(thiophen-2-yl)-9H-pyrido-[3,4-*b*]-indol-3-yl) (4-(*p*-tolyl)-piperazin-1-yl)-

methanone (15): Pale yellow solid, Yield 65%, Melting point 179-181 °C, IR ν_{max}/cm : 3159, 1610, 1588, 723, 1H NMR (400 MHz, Chloroform-*d*) δ 8.56 (s, 1H), 8.37 (s, 1H), 8.10 (d, $J = 7.4$, 1.0 Hz, 1H), 7.84 – 7.86 (m, 3H), 7.53 – 7.45 (m, 4H), 7.35 – 7.24 (m, 2H), 7.09 – 7.02 (m, 4H), 6.85 – 6.75 (m, 2H), 4.04 – 3.94 (m, 3H), 3.18. (d, $J = 30.1$ Hz, 4H). ESI MS (m/z): calculated for $C_{27}H_{23}BrN_4OS$, 530.85, found 531.75 $[M+H]^+$, 532.67 $[M+2]^+$

(6-bromo-1-(thiophen-2-yl)-9H-pyrido-[3,4-*b*]-indol-3-yl)(4-(2-methoxyphenyl)-

piperazin-1-yl)-methanone (16): Pale yellow solid, Yield 79%, Melting point 190-192°C, IR ν_{max}/cm : 3263, 1656, 1541, 1508, 1H NMR (400 MHz, Chloroform-*d*) δ 8.85 (s, 1H), 8.12 (d, $J = 7.8$ Hz, 1H), 8.01-7.91 (m, 2H), 7.65-7.54 (m, 4H), 7.54 (t, $J = 7.4$ Hz, 1H), 7.38-7.31 (m, 1H), 7.22-7.20 (m, 2H), 7.11-7.00 (m, 2H), 4.10-4.00 (m, 3H), 3.38 (s, 3H), 3.10-3.01 (m, 3H). ESI MS (m/z): calculated for $C_{27}H_{23}BrN_4O_2S$, 546.07, found 547.16 $[M+H]^+$. 548.89 $[M+2]^+$



Scheme 2: Reagents and conditions: (A) SOCl₂, ethanol, 0 °C, reflux, 1 h (B) Aromatic aldehydes, trifluoroacetic acid, DCM, rt, 3 h (C) Sulfur, xylene, 100 °C, reflux 24 h (D) Trifluoroacetic acid, sodium nitrite, 0 °C, 24 h (E) NaOH, ethanol: water (1:1), rt, 45 min (F) THF, EDCI, HCl, HOBt, Phenylpiperazine, rt, overnight

Synthesis of ethyl-6-nitro-1-phenyl-9H-pyrido-[3,4-b]-indole-3-carboxylate: The initial steps up to step 4 was common and already incorporated above. Only the step of nitration was mentioned here. To the compound (4) (620 mg, 2.75 mmol) and sodium nitrate (351 mg, 4.13 mmol) and trifluoroacetic acid (20 mL) was added dropwise at 0°C and then the reaction mixture was allowed to stir for 24 h. After, the reaction mixture was neutralized by adding sodium bicarbonate solution then extracted with ethyl acetate and concentrate it to get the desired nitro substituted product.

Characterized data for 6-Nitro substituted compounds of scheme 2:

(1-(4-methoxyphenyl)-6-nitro-9H-pyrido-[3,4-b]-indol-3-yl) (4-(p-tolyl)-piperazin-1-yl)-methanone (17): Pale yellow solid, Yield 68%, Melting point 160-162 °C, IR ν_{max} /cm: 3234, 1625, 1546, 1510, 1255, ¹H NMR (400 MHz, Chloroform-*d*) δ 8.57 (s, 1H), 8.37 (s, 1H), 8.09 (d, *J* = 7.8, 1.0 Hz, 1H), 7.88 – 7.82 (m, 2H), 7.53 – 7.45 (m, 2H), 7.30 – 7.24 (m, 1H), 7.07 – 7.02 (m, 3H), 6.84 – 6.75 (m, 2H), 4.04 – 3.91 (m, 4H), 3.84 (s, 3H), 3.18 (d, *J* = 30.1 Hz, 4H), 3.21 (s, 3H). ESI MS (*m/z*): calculated for C₃₀H₂₇N₅O₄, 521.21, found 522.56 [M+H]⁺

(1-(4-methoxyphenyl)-6-nitro-9H-pyrido-[3,4-b]-indol-3-yl) (4-(4-methoxyphenyl)-piperazin-1-yl)-methanone (18): Yellow solid, Yield 60%, Melting point 155-157 °C, IR ν_{max} /cm: 3220, 1635, 1546, 1520, 1255, ¹H NMR (400 MHz, Chloroform-*d*) δ 8.6 (s, 1H), 8.37 (s, 1H), 8.09 (d, *J* = 7.9, 1.0 Hz, 1H), 7.89 – 7.82 (m, 2H), 7.53 – 7.45 (m, 2H), 7.30 – 7.24

Chapter 5. Synthesis and Characterization of the designed analogues

(m, 1H), 7.07 – 7.02 (m, 3H), 6.94 – 6.75 (m, 2H), 4.04 – 3.91 (m, 4H), 3.84 (s, 3H), 3.18. (d, $J = 30.1$ Hz, 4H), 3.8 (s, 3H). ESI MS (m/z): calculated for $C_{30}H_{27}N_5O_5$, 537.20, found 538.55 [M+H]⁺

(6-nitro-1-phenyl-9H-pyrido-[3,4-b]-indol-3-yl) (4-(p-tolyl)-piperazin-1-yl)-methanone (19): Yellow solid, Yield 68%, Melting point 190-192 °C, IR ν_{max}/cm : 3244, 1615, 1547, 1511, 1256, ¹H NMR (400 MHz, Chloroform-*d*) δ 8.56 (s, 1H), 8.37 (s, 1H), 8.09 (d, $J = 7.3$, 1.0 Hz, 1H), 7.88 – 7.82 (m, 2H), 7.53 – 7.45 (m, 2H), 7.30 – 7.24 (m, 2H), 7.07 – 7.02 (m, 4H), 6.84 – 6.75 (m, 2H), 4.04 – 3.91 (m, 4H), 3.84 (s, 3H), 3.18. (d, $J = 30.1$ Hz, 3H). ¹³C NMR (101 MHz, Chloroform-*d*) δ 171.50, 152.210, 150.68, 148.85, 146.88, 133.72, 129.83, 126.54, 122.14, 111.35, 110.35, 54.80, 56.70, 49.35. ESI MS (m/z): calculated for $C_{29}H_{25}N_5O_3$, 491.20, found 492.92 [M+H]

(4-(4-methoxyphenyl)-piperazin-1-yl) (6-nitro-1-phenyl-9H-pyrido-[3,4-b]-indol-3-yl)-methanone (20): White solid, Yield 59%, Melting point 145-147 °C, IR ν_{max}/cm : 3234, 1625, 1546, 1510, 1255, ¹H NMR (400 MHz, Chloroform-*d*) δ 8.61 (s, 1H), 8.37 (s, 1H), 8.09 (d, $J = 7.3$, 1.0 Hz, 1H), 7.88 – 7.86 (m, 2H), 7.53 – 7.68 (m, 2H), 7.30 – 7.24 (m, 2H), 7.09 – 7.02 (m, 4H), 6.84 – 6.75 (m, 2H), 4.04 – 3.91 (m, 4H), 3.84 (s, 3H), 3.28. (d, $J = 30.1$ Hz, 3H). ESI MS (m/z): calculated for $C_{29}H_{25}N_5O_4$, 507.19, found 508.24 [M+H]⁺

(1-(4-chlorophenyl)-piperazin-1-yl) (6-nitro-1-phenyl-9H-pyrido-[3,4-b]-indol-3-yl)-methanone (21): Gray solid, Yield 60%, Melting point 122-124 °C, IR ν_{max}/cm : 3228, 1620, 1587, 1490, 1433, ¹H NMR (400 MHz, Chloroform-*d*) δ 8.51 (s, 1H), 8.37 (s, 1H), 8.09 (d, $J = 7.3$, 1.0 Hz, 1H), 7.88 – 7.86 (m, 2H), 7.53 – 7.45 (m, 2H), 7.30 – 7.24 (m, 2H), 7.09 – 7.02 (m, 4H), 6.85 – 6.75 (m, 2H), 4.04 – 3.94 (m, 3H), 3.18. (d, $J = 30.1$ Hz, 4H). ESI MS (m/z): calculated for $C_{28}H_{22}ClN_5O_3$, 511.14, found 512.46 [M+H]⁺, 513.54 [M+2]⁺

(6-nitro-1-(p-tolyl)-9H-pyrido-[3,4-b]-indol-3-yl) (4-(p-tolyl)-piperazin-1-yl)-methanone (22): Yellow solid, Yield 69%, Melting point 112-114 °C, IR ν_{max}/cm : 3203, 1610, 1588, 1481, ¹H NMR (400 MHz, Chloroform-*d*) δ 8.53 (s, 1H), 8.37 (s, 1H), 8.10 (d, $J = 7.3$, 1.0 Hz, 1H), 7.84 – 7.86 (m, 2H), 7.53 – 7.45 (m, 2H), 7.30 – 7.24 (m, 2H), 7.09 – 7.02 (m, 4H), 6.85 – 6.75 (m, 2H), 4.04 – 3.94 (m, 3H), 3.56 (s, 3H), 3.18. (d, $J = 30.1$ Hz, 4H). ¹³C NMR (101 MHz, Chloroform-*d*) δ 173.77, 151.23, 151.67, 144.26, 141.78, 131.17, 129.23, 122.54, 121.14, 117.57, 113.37, 55.88, 52.60, 48.67. ESI MS (m/z): calculated for $C_{30}H_{27}N_5O_3$, 505.21, found 506.56 [M+H]⁺

(4-(2-fluorophenyl)-piperazin-1-yl) (1-(4-methoxyphenyl)-6-nitro-9H-pyrido-[3,4-b]-indol-3-yl)-methanone (23): Yellow solid, Yield 69%, Melting point 116-118 °C, IR

Chapter 5. Synthesis and Characterization of the designed analogues

ν_{\max}/cm : 3184, 1624, 1595, 1489, 1319, $^1\text{H NMR}$ (400 MHz, Chloroform-*d*) δ 8.57 (s, 1H), 8.37 (s, 1H), 8.09 (d, $J = 7.8$, 1.0 Hz, 1H), 7.88 – 7.82 (m, 2H), 7.53 – 7.45 (m, 2H), 7.30 – 7.24 (m, 1H), 7.07 – 7.02 (m, 3H), 6.84 – 6.75 (m, 2H), 4.04 – 3.91 (m, 4H), 3.84 (s, 3H), 3.18. (d, $J = 30.1$ Hz, 3H). ESI MS (m/z): calculated for $\text{C}_{29}\text{H}_{24}\text{FN}_5\text{O}_4$, 525.18, found 526.46 $[\text{M}+\text{H}]^+$

(1-(4-chlorophenyl)-6-nitro-9H-pyrido-[3,4-*b*]-indol-3-yl) (4-(*p*-tolyl)-piperazin-1-yl)-methanone (24): Yellow solid, Yield 54%, Melting point 122-124 °C, IR ν_{\max}/cm : 3234, 1625, 1546, 1510, 1255, $^1\text{H NMR}$ (400 MHz, Chloroform-*d*) δ 8.8 (s, 1H), 8.37 (s, 1H), 8.09 (d, $J = 7.9$, 1.0 Hz, 1H), 7.89 – 7.82 (m, 2H), 7.53 – 7.45 (m, 2H), 7.30 – 7.24 (m, 1H), 7.07 – 7.02 (m, 3H), 6.94 – 6.75 (m, 2H), 4.04 – 3.91 (m, 4H), 3.18. (d, $J = 30.1$ Hz, 4H), 3.84 (s, 3H). $^{13}\text{C NMR}$ (101 MHz, Chloroform-*d*) δ 168.70, 152.30, 151.68, 147.25, 149.78, 132.12, 129.23, 125.54, 124.14, 115.35, 113.35, 55.80, 56.60, 50.75. ESI MS (m/z): calculated for $\text{C}_{29}\text{H}_{24}\text{ClN}_5\text{O}_3$, 525.16, found 526.76 $[\text{M}+\text{H}]^+$, 527.89 $[\text{M}+2]^+$

(1-(4-chlorophenyl)-6-nitro-9H-pyrido-[3,4-*b*]-indol-3-yl) (4-(2-fluorophenyl)-piperazin-1-yl)-methanone (25): Yellow solid, Yield 59%, Melting point 152-154 °C, IR ν_{\max}/cm : 3174, 1626, 1556, 1487, 1431, $^1\text{H NMR}$ (400 MHz, Chloroform-*d*) δ 8.59 (s, 1H), 8.37 (s, 1H), 8.09 (d, $J = 7.8$, 1.0 Hz, 1H), 7.89 – 7.82 (m, 2H), 7.53 – 7.45 (m, 2H), 7.30 – 7.24 (m, 1H), 7.07 – 7.02 (m, 3H), 6.86 – 6.75 (m, 2H), 4.07 – 3.91 (m, 4H), 3.15. (d, $J = 30.1$ Hz, 4H). ESI MS (m/z): calculated for $\text{C}_{28}\text{H}_{21}\text{ClFN}_5\text{O}_3$, 529.13, found 530.16 $[\text{M}+\text{H}]^+$, 531.89 $[\text{M}+2]^+$

(1-(4-chlorophenyl)-6-nitro-9H-pyrido-[3,4-*b*]-indol-3-yl) (4-(4-methoxyphenyl)-piperazin-1-yl)-methanone (26): Yellow solid, Yield 60%, Melting point 120-122 °C, IR ν_{\max}/cm : 3209, 1614, 1550, 1508, $^1\text{H NMR}$ (400 MHz, Chloroform-*d*) δ 8.54 (s, 1H), 8.37 (s, 1H), 8.09 (d, $J = 7.8$, 1.0 Hz, 1H), 7.88 – 7.85 (m, 2H), 7.53 – 7.45 (m, 2H), 7.32 – 7.24 (m, 1H), 7.07 – 7.02 (m, 3H), 6.84 – 6.75 (m, 2H), 4.04 – 3.91 (m, 4H), 3.80 (s, 3H), 3.18. (d, $J = 30.1$ Hz, 4H). ESI MS (m/z): calculated for $\text{C}_{29}\text{H}_{24}\text{ClN}_5\text{O}_4$, 541.15, found 542.33 $[\text{M}+\text{H}]^+$, 543.23 $[\text{M}+2]^+$

(6-nitro-1-(thiophen-2-yl)-9H-pyrido-[3,4-*b*]-indol-3-yl) (4-(*p*-tolyl)-piperazin-1-yl)-methanone (27): White solid, Yield 55%, Melting point 187-189 °C, IR ν_{\max}/cm : 3203, 1610, 1588, 1481, $^1\text{H NMR}$ (400 MHz, Chloroform-*d*) δ 8.61 (s, 1H), 8.37 (s, 1H), 8.10 (d, $J = 7.3$, 1.0 Hz, 1H), 7.78 – 7.86 (m, 2H), 7.53 – 7.45 (m, 2H), 7.30 – 7.24 (m, 2H), 7.09 – 7.02 (m, 2H), 6.85 – 6.75 (m, 2H), 4.04 – 3.94 (m, 3H), 3.85 (s, 3H), 3.18. (d, $J = 30.1$ Hz, 4H). ESI MS (m/z): calculated for $\text{C}_{27}\text{H}_{23}\text{N}_5\text{O}_3\text{S}$, 497.15, found 498.53 $[\text{M}+\text{H}]^+$

(6-nitro-1-(thiophen-2-yl)-9H-pyrido-[3,4-*b*]-indol-3-yl) (4-phenylpiperazin-1-yl)-methanone (28): Off solid, Yield 60%, Melting point 180-182 °C, IR ν_{\max}/cm : 3201, 1614,

Chapter 5. Synthesis and Characterization of the designed analogues

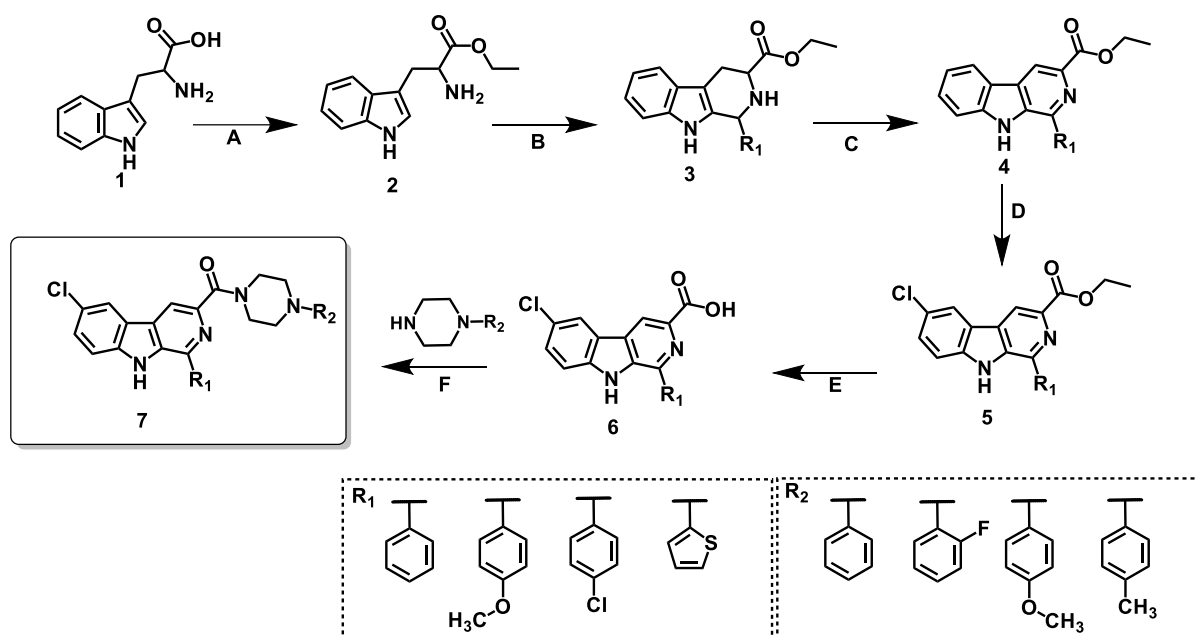
1560, 1510, ¹H NMR (400 MHz, Chloroform-*d*) δ 8.54 (s, 1H), 8.37 (s, 1H), 8.09 (d, *J* = 7.8, 1.0 Hz, 1H), 7.88 – 7.85 (m, 2H), 7.53 – 7.45 (m, 2H), 7.32 – 7.24 (m, 1H), 7.07 – 7.02 (m, 3H), 6.84 – 6.75 (m, 2H), 4.04 – 3.91 (m, 4H), 3.18. (d, *J* = 30.1 Hz, 4H). ESI MS (*m/z*): calculated for C₂₆H₂₁N₅O₃S, 483.14, found 484.63 [M+H]⁺

(4-(2-fluorophenyl)-piperazin-1-yl) (6-nitro-1-(thiophen-2-yl)-9H-pyrido-[3,4-b]-indol-3-yl)-methanone (29): Pale yellow solid, Yield 69%, Melting point 187-189 °C, IR *v*_{max}/cm: 3184, 1624, 1595, 1489, 1319, ¹H NMR (400 MHz, Chloroform-*d*) δ 8.57 (s, 1H), 8.37 (s, 1H), 8.09 (d, *J* = 7.8, 1.0 Hz, 1H), 7.88 – 7.82 (m, 2H), 7.53 – 7.45 (m, 2H), 7.30 – 7.24 (m, 1H), 7.07 – 7.02 (m, 3H), 6.84 – 6.75 (m, 2H), 4.04 – 3.91 (m, 4H), 3.25. (d, *J* = 30.1 Hz, 3H). ESI MS (*m/z*): calculated for C₂₆H₂₀FN₅O₃S, 501.13, found 502.19 [M+H]⁺

(4-(4-methoxyphenyl)-piperazin-1-yl) (6-nitro-1-(thiophen-2-yl)-9H-pyrido-[3,4-b]-indol-3-yl)-methanone (30): White solid, Yield 59 %, Melting point 178-180 °C, IR *v*_{max}/cm: 3223, 1662, 1518, 1431, ¹H NMR (400 MHz, Chloroform-*d*) δ 8.41 (s, 1H), 8.03 – 7.95 (m, 2H), 7.69 – 7.62 (m, 3H), 7.59 (d, *J* = 1.8 Hz, 2H), 7.28 (s, 1H), 6.99 – 6.84 (m, 3H), 4.06 (t, *J* = 5.1 Hz, 2H), 3.79 (d, *J* = 1.9 Hz, 3H), 3.50 (q, *J* = 7.0 Hz, 2H), 3.16 (d, *J* = 5.8 Hz, 4H). ¹³C NMR (101 MHz, Chloroform-*d*) δ 164.60, 153.28, 152.68, 145.27, 146.79, 131.18, 128.23, 122.54, 122.14, 115.75, 113.35, 55.80, 51.63, 48.67. ESI MS (*m/z*): calculated for C₂₇H₂₃N₅O₄S, 513.15, found 514.75 [M+H]⁺

(6-nitro-1-(thiophen-2-yl)-9H-pyrido-[3,4-b]-indol-3-yl) (4-(*p*-tolyl)-piperazin-1-yl)-methanone (31): White solid, Yield 59%, Melting point 148-150 °C, IR *v*_{max}/cm: 3234, 1685, 1547, 1541, 1256, ¹H NMR (400 MHz, Chloroform-*d*) δ 8.56 (s, 1H), 8.37 (s, 1H), 7.88 – 7.82 (m, 2H), 7.53 – 7.45 (m, 2H), 7.30 – 7.24 (m, 2H), 7.07 – 7.02 (m, 4H), 6.84 – 6.75 (m, 2H), 4.04 – 3.91 (m, 3H), 3.84 (s, 3H), 3.18. (d, *J* = 30.1 Hz, 3H). ESI MS (*m/z*): calculated for C₂₇H₂₃N₅O₃S, 497.15, found 498.18 [M+H]⁺

(6-nitro-1-phenyl-9H-pyrido-[3,4-b]-indol-3-yl) (4-phenylpiperazin-1-yl)-methanone (32): White solid, Yield 59%, Melting point 177-179 °C, ¹H NMR (400 MHz, Chloroform-*d*) δ 8.61 (s, 1H), 8.31 (s, 1H), 8.09 (d, *J* = 7.5, 1.0 Hz, 1H), 7.87 – 7.89 (m, 2H), 7.56 – 7.45 (m, 2H), 7.30 – 7.24 (m, 2H), 7.08 – 7.02 (m, 4H), 6.84 – 6.75 (m, 2H), 4.04 – 3.91 (m, 4H), 3.18. (d, *J* = 30.1 Hz, 3H). ESI MS (*m/z*): calculated for C₂₈H₂₃N₅O₃, 477.18, found 478.74 [M+H]⁺



Scheme 3: Reagents and conditions: (A) SOCl_2 , ethanol, 0°C , reflux, 1 h (B) Aromatic aldehydes, trifluoroacetic acid, DCM, rt, 3 h (C) Sulfur, xylene, 100°C , reflux 24 h (D), *N*-chlorosuccinimide, ethyl acetate, reflux, 24 h (E) NaOH, ethanol: water (1:1), rt, 45 min (F) THF, EDCI. HCl, HOBt, Phenyl piperazine, rt, overnight

Synthesis of (6-chloro-1-phenyl-9*H*-pyrido-[3,4-*b*]-indol-3-yl) (4-phenylpiperazin-1-yl)-methanone derivatives

To a solution of the compound 4 (22.6 g, 0.10 mmol) in ethyl acetate (300 mL), a solution of *N*-chlorosuccinimide (15.7 g, 0.12 mmol) in ethyl acetate (300 mL) was added, and the mixture was refluxed for 18-20 h. Progress of the reaction was monitored by thin layer chromatography, after completion of the reaction, cooled to room temperature, the reaction mixture was washed with 0.1 M aq. NaOH (100 mL). The organic phase was collected and dried under vacuum to get the desired compound.

Characterized data for 6-chloro substituted compounds of scheme 3:

(6-chloro-1-phenyl-9*H*-pyrido-[3,4-*b*]-indol-3-yl) (4-(4-methoxyphenyl)-piperazin-1-yl)-methanone (33): Yellow solid, Yield 62 %, Melting point $187\text{--}189^\circ\text{C}$, IR $\nu_{\text{max}}/\text{cm}^{-1}$: 3213, 1652, 1518, 1431, 725, $^1\text{H NMR}$ (400 MHz, Chloroform-*d*) δ 8.41 (s, 1H), 8.03 – 7.95 (m, 2H), 7.69 – 7.62 (m, 2H), 7.59 (d, $J = 1.8$ Hz, 1H), 7.28 (s, 1H), 6.99 – 6.84 (m, 7H), 4.06 (t, $J = 5.1$ Hz, 2H), 3.79 (d, $J = 1.9$ Hz, 3H), 3.50 (q, $J = 7.0$ Hz, 2H), 3.16 (d, $J = 5.8$ Hz, 4H). ESI MS (m/z): calculated for $\text{C}_{29}\text{H}_{25}\text{ClN}_4\text{O}_2$, 496.17, found 497.13 $[\text{M}+\text{H}]^+$

(6-chloro-1-phenyl-9*H*-pyrido-[3,4-*b*]-indol-3-yl) (4-(2-fluorophenyl)-piperazin-1-yl)-methanone (34): Yellow solid, Yield 52 %, Melting point $167\text{--}169^\circ\text{C}$, IR $\nu_{\text{max}}/\text{cm}^{-1}$: 3214,

Chapter 5. Synthesis and Characterization of the designed analogues

1640, 1525, 725, ¹H NMR (400 MHz, Chloroform-*d*) δ 8.57 (s, 1H), 8.37 (s, 1H), 8.09 (d, *J* = 7.8, 1.0 Hz, 1H), 7.88 – 7.82 (m, 2H), 7.53 – 7.45 (m, 2H), 7.30 – 7.24 (m, 1H), 7.07 – 7.02 (m, 3H), 6.84 – 6.75 (m, 2H), 4.04 – 3.91 (m, 4H), 3.84 (s, 3H), 3.18. (d, *J* = 30.1 Hz, 2H). ESI MS (*m/z*): calculated for C₂₈H₂₂ClFN₄O, 484.15, found 485.78 [M+H]⁺, 486.56 [M+2]⁺

(6-chloro-1-phenyl-9H-pyrido-[3,4-*b*]-indol-3-yl) (4-(*p*-tolyl)-piperazin-1-yl)-methanone (35): Yellow solid, Yield 59 %, Melting point 187-189 °C, IR *v*_{max}/cm: 3219, 1650, 1529, 725, ¹H NMR (400 MHz, Chloroform-*d*) δ 8.82 (s, 1H), 8.47 (s, 1H), 8.17 (d, *J* = 7.9 Hz, 1H), 8.01-7.98 (m, 2H), 7.64-7.51 (m, 5H), 7.38-7.34 (m, 1H), 7.08-7.04 (m, 1H), 7.01-6.90 (m, 3H), 4.20- 4.10 (m, 4H), 3.25 (s, 3H). ¹³C NMR (101 MHz, Chloroform-*d*) δ 170.60, 152.20, 151.68, 147.26, 146.78, 142.12, 129.23, 126.64, 128.14, 115.35, 113.35, 55.80, 26.60, 49.65, 29.56. ESI MS (*m/z*): calculated for C₂₉H₂₅ClN₄O, 480.17, found 481.26 [M+H]⁺, 482.26 [M+2]⁺

(6-chloro-1-phenyl-9H-pyrido-[3,4-*b*]-indol-3-yl) (4-(2-methoxyphenyl)-piperazin-1-yl)-methanone (36): White solid, Yield 53%, Melting point 188-190 °C, IR *v*_{max}/cm: 3184, 1624, 1595, 750, ¹H NMR (400 MHz, Chloroform-*d*) δ 8.90 (s, 1H), 8.37 (s, 1H), 8.09 (d, *J* = 7.8, 1.0 Hz, 1H), 7.88 – 7.82 (m, 2H), 7.53 – 7.45 (m, 2H), 7.30 – 7.24 (m, 1H), 7.07 – 7.02 (m, 3H), 6.84 – 6.75 (m, 2H), 4.04 – 3.91 (m, 3H), 3.84 (s, 3H), 3.18. (d, *J* = 30.1 Hz, 4H), 2.21 (s, 3H). ESI MS (*m/z*): calculated for C₂₉H₂₅ClN₄O₂, 496.17, found 497.42 [M+H]⁺, 498.43 [M+2]⁺

(6-chloro-1-(4-methoxyphenyl)-9H-pyrido-[3,4-*b*]-indol-3-yl) (4-phenylpiperazin-1-yl)-methanone (37): White solid, Yield 59%, Melting point 187-189 °C, IR *v*_{max}/cm: 3163, 1642, 1545, 720, ¹H NMR (400 MHz, Chloroform-*d*) δ 9.25 (s, 1H), 8.44- 8.49 (m, 3H), 8.26-8.19 (m, 2H), 8.09-8.06 (m, 2H), 7.69-7.53 (m, 6H), 7.30-7.27 (m, 1H), 6.84 (t, *J* = 11.7 Hz, 2H), 4.03-3.93 (m, 4H), 3.80 (s, 3H), 3.57-3.51 (m, 4H). ESI MS (*m/z*): calculated for C₂₉H₂₅ClN₄O₂, 496.17, found 497.23 [M+H]⁺, 498.24 [M+2]⁺

(6-chloro-1-(4-methoxyphenyl)-9H-pyrido-[3,4-*b*]-indol-3-yl) (4-(2-fluorophenyl)-piperazin-1-yl)-methanone (38): White solid, Yield 60%, Melting point 165-167 °C, IR *v*_{max}/cm: 3153, 1645, 1555, 750, ¹H NMR (400 MHz, Chloroform-*d*) δ 8.85 (s, 1H), 8.64 (s, 1H), 8.12 (d, *J* = 7.8 Hz, 1H), 8.01-7.91 (m, 2H), 7.65-7.54 (m, 4H), 7.54 (t, *J* = 7.4 Hz, 1H), 7.38-7.31 (m, 1H), 7.22-7.20 (m, 2H), 7.11-7.00 (m, 2H), 4.10-4.00 (m, 4H), 3.38 (s, 3H), 3.10-3.01 (m, 3H). ESI MS (*m/z*): calculated for C₂₉H₂₄ClFN₄O₂, 514.16, found 515.56 [M+H]⁺, 516.58 [M+2]⁺

(6-chloro-1-(4-methoxyphenyl)-9H-pyrido-[3,4-*b*]-indol-3-yl) (4-(*p*-tolyl)-piperazin-1-yl)-methanone (39): White solid, Yield 65%, Melting point 177-179 °C, IR *v*_{max}/cm: 3159,

Chapter 5. Synthesis and Characterization of the designed analogues

1610, 1588, 723, ¹H NMR (400 MHz, Chloroform-*d*) δ 8.56 (s, 1H), 8.37 (s, 1H), 8.10 (d, *J* = 7.4, 1.0 Hz, 1H), 7.84 – 7.86 (m, 3H), 7.53 – 7.45 (m, 4H), 7.35 – 7.24 (m, 2H), 7.09 – 7.02 (m, 4H), 6.85 – 6.75 (m, 2H), 4.04 – 3.94 (m, 3H), 3.18. (d, *J* = 30.1 Hz, 4H). ESI MS (*m/z*): calculated for C₃₀H₂₇ClN₄O₂, 510.18, found 511.47 [M+H]⁺, 512.48 [M+2]⁺

(6-chloro-1-(4-methoxyphenyl)-9H-pyrido-[3,4-*b*]-indol-3-yl) (4-(4-methoxyphenyl)-piperazin-1-yl)-methanone (40): White solid, Yield 59%, Melting point 167-169 °C, IR *v*_{max}/cm: 3164, 1624, 1595, 725, ¹H NMR (400 MHz, Chloroform-*d*) δ 8.59 (s, 1H), 8.35 (s, 1H), 8.09 (d, *J* = 7.4, 1.0 Hz, 1H), 7.88 – 7.84 (m, 2H), 7.53 – 7.45 (m, 2H), 7.30 – 7.24 (m, 3H), 7.07 – 7.02 (m, 3H), 6.84 – 6.75 (m, 2H), 4.04 – 3.91 (m, 4H), 3.84 (s, 3H), 3.18. (d, *J* = 30.1 Hz, 4H). ¹³C NMR (101 MHz, Chloroform-*d*) δ 168.70, 152.30, 151.68, 147.25, 149.78, 132.12, 129.23, 125.54, 124.14, 115.35, 113.35, 55.80, 56.60, 50.75. ESI MS (*m/z*): calculated for C₃₀H₂₇ClN₄O₃, 526.18, found 527.13 [M+H]⁺, 528.78 [M+2]⁺

(6-chloro-1-(thiophen-2-yl)-9H-pyrido-[3,4-*b*]-indol-3-yl) (4-phenylpiperazin-1-yl)-methanone (41): Pale yellow solid, Yield 59%, Melting point 187-189 °C, IR *v*_{max}/cm: 3163, 1642, 1545, 750, ¹H NMR (400 MHz, Chloroform-*d*) δ 10.01 (s, 1H), 8.26-8.19 (m, 2H), 8.09-8.06 (m, 2H), 7.69-7.53 (m, 6H), 7.30-7.27 (m, 1H), 6.84 (t, *J* = 11.7 Hz, 2H), 4.03-3.93 (m, 4H), 3.57-3.51 (m, 4H). ESI MS (*m/z*): calculated for C₂₆H₂₁ClN₄OS, 472.11 found 473.59 [M+H]⁺, 474.89 [M+2]⁺

(6-chloro-1-(thiophen-2-yl)-9H-pyrido-[3,4-*b*]-indol-3-yl) (4-(*p*-tolyl)-piperazin-1-yl)-methanone (42): White solid, Yield 60%, Melting point 200-202 °C, IR *v*_{max}/cm: 3153, 1652, 1515, 720, ¹H NMR (400 MHz, Chloroform-*d*) δ 8.20 (s, 1H), 7.6 – 7.38 (m, 9H), 7.02 – 6.79 (m, 3H), 3.10-3.01 (m, 4H), 2.10 – 2.05 (m, 2H), 1.36 – 1.21 (s, 3H). ESI MS (*m/z*): calculated for C₂₇H₂₃ClN₄OS, 486.13, found 487.27 [M+H]⁺, 488.98 [M+2]⁺

(6-chloro-1-(thiophen-2-yl)-9H-pyrido-[3,4-*b*]-indol-3-yl) (4-(4-methoxyphenyl)-piperazin-1-yl)-methanone (43): White solid, Yield 50%, Melting point 177-179 °C, IR *v*_{max}/cm: 3159, 1614, 1550, 753, ¹H NMR (400 MHz, Chloroform-*d*) δ 8.54 (s, 1H), 8.37 (s, 1H), 8.05 (d, *J* = 7.8, 1.0 Hz, 1H), 7.88 – 7.84 (m, 2H), 7.53 – 7.46 (m, 2H), 7.32 – 7.24 (m, 1H), 7.09 – 7.02 (m, 3H), 6.84 – 6.78 (m, 2H), 4.04 – 3.91 (m, 4H), 3.80 (s, 3H), 3.18. (d, *J* = 30.1 Hz, 3H). ESI MS (*m/z*): calculated for C₂₇H₂₃ClN₄O₂S, 502.12, found 503.45 [M+H]⁺, 504.46 [M+2]⁺

(6-chloro-1-(thiophen-2-yl)-9H-pyrido-[3,4-*b*]-indol-3-yl) (4-(2-fluorophenyl)-piperazin-1-yl)-methanone (44): White solid, Yield 58%, Melting point 127-129 °C, IR *v*_{max}/cm: 3381, 1634, 1512, 760, ¹H NMR (400 MHz, Chloroform-*d*) δ 8.61 (s, 1H), 8.37 (s, 1H), 8.10 (d, *J* =

Chapter 5. Synthesis and Characterization of the designed analogues

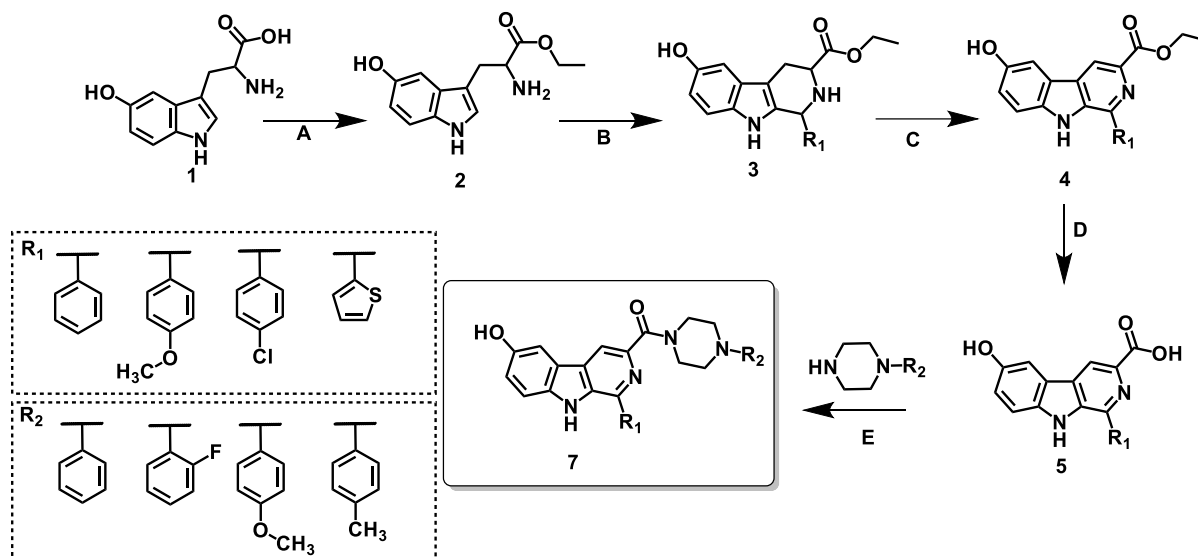
7.0, 1.0 Hz, 1H), 7.78 – 7.86 (m, 1H), 7.53 – 7.45 (m, 3H), 7.30 – 7.24 (m, 2H), 7.09 – 7.02 (m, 2H), 6.85 – 6.75 (m, 2H), 4.04 – 3.94 (m, 3H), 3.18. (d, $J = 30.1$ Hz, 4H). ESI MS (m/z): calculated for $C_{26}H_{20}ClFN_4OS$, 490.10, found 491.16 $[M+H]^+$, 492.14 $[M+2]^+$

(6-chloro-1-(thiophen-2-yl)-9H-pyrido-[3,4-b]-indol-3-yl) (4-(2-methoxyphenyl)-piperazin-1-yl)-methanone (45): Yellow solid, Yield 56%, Melting point 137-139 °C, IR ν_{max}/cm : 3203, 1610, 1588, 760, 1H NMR (400 MHz, Chloroform-*d*) δ 8.66 (s, 1H), 8.37 (s, 1H), 8.15 (d, $J = 7.3$, 1.0 Hz, 1H), 7.71 – 7.89 (m, 2H), 7.53 – 7.45 (m, 2H), 7.30 – 7.26 (m, 2H), 7.09 – 7.02 (m, 2H), 6.85 – 6.76 (m, 2H), 4.04 – 3.94 (m, 3H), 3.86 (s, 3H), 3.12. (d, $J = 30.1$ Hz, 4H). ESI MS (m/z): calculated for $C_{27}H_{23}ClN_4O_2S$, 502.12, found 503.79 $[M+H]^+$, 504.34 $[M+2]^+$

(6-chloro-1-(4-chlorophenyl)-9H-pyrido-[3,4-b]-indol-3-yl) (4-(2-fluorophenyl)-piperazin-1-yl)-methanone (46): White solid, Yield 69%, Melting point 187-189 °C, IR ν_{max}/cm : 3863, 1642, 1545, 720, 1H NMR (400 MHz, Chloroform-*d*) δ 9.22 (s, 1H), 8.44-8.49 (m, 3H), 8.25-8.19 (m, 2H), 8.09-8.06 (m, 2H), 7.69-7.53 (m, 6H), 7.30-7.27 (m, 1H), 6.84 (t, $J = 11.7$ Hz, 2H), 4.03-3.93 (m, 4H), 3.80 (s, 3H), 3.57-3.51 (m, 4H). ESI MS (m/z): calculated for $C_{28}H_{21}Cl_2FN_4O$, 518.11, found 519.46 $[M+H]^+$, 520.48 $[M+2]^+$, 522.78 $[M+4]^+$

(6-chloro-1-(4-chlorophenyl)-9H-pyrido-[3,4-b]-indol-3-yl) (4-(p-tolyl)-piperazin-1-yl)-methanone (47): White solid, Yield 79%, Melting point 177-179 °C, IR ν_{max}/cm : 3164, 1624, 1595, 725, 1H NMR (400 MHz, Chloroform-*d*) δ 8.59 (s, 1H), 8.35 (s, 1H), 8.09 (d, $J = 7.4$, 1.0 Hz, 1H), 7.88 – 7.84 (m, 2H), 7.53 – 7.45 (m, 2H), 7.30 – 7.24 (m, 3H), 7.07 – 7.02 (m, 3H), 6.84 – 6.75 (m, 2H), 4.04 – 3.91 (m, 4H), 3.84 (s, 3H), 3.18. (d, $J = 30.1$ Hz, 4H). ^{13}C NMR (101 MHz, Chloroform-*d*) δ 171.70, 156.30, 151.68, 147.25, 148.77, 132.12, 127.23, 125.54, 124.16, 115.35, 113.35, 55.10, 56.60, 50.77. ESI MS (m/z): calculated for $C_{29}H_{24}Cl_2N_4O$, 514.13, found 515.68 $[M+H]^+$, 516.56 $[M+2]^+$, 518.46 $[M+4]^+$

(6-chloro-1-(4-chlorophenyl)-9H-pyrido-[3,4-b]-indol-3-yl) (4-(4-methoxyphenyl)-piperazin-1-yl)-methanone (48): White solid, Yield 58%, Melting point 197-199 °C, IR ν_{max}/cm : 3381, 1634, 1512, 760, 1H NMR (400 MHz, Chloroform-*d*) δ 8.61 (s, 1H), 8.37 (s, 1H), 8.10 (d, $J = 7.0$, 1.0 Hz, 1H), 7.78 – 7.86 (m, 1H), 7.53 – 7.45 (m, 3H), 7.30 – 7.24 (m, 2H), 7.09 – 7.02 (m, 2H), 6.85 – 6.75 (m, 2H), 4.04 – 3.94 (m, 3H), 3.18. (d, $J = 30.1$ Hz, 4H). ESI MS (m/z): calculated for $C_{29}H_{24}Cl_2N_4O_2$, 530.13, found 531.47 $[M+H]^+$, 532.67 $[M+2]^+$, 534.67 $[M+4]^+$



Scheme 4: Reagents and conditions: (A) SOCl_2 , ethanol, 0 °C, reflux, 1 h (B) Aromatic aldehydes, trifluoroacetic acid, DCM, rt, 3 h (C) Sulfur, xylene, 100 C, reflux 24 h (D) NaOH, ethanol: water (1:1), rt, 45 min (E) THF, EDCI. HCl, HOBT, Phenyl piperazine, rt, overnight

Synthesis of (6-hydroxy-1-phenyl-9H-pyrido-[3,4-b]-indol-3-yl) (4-phenylpiperazin-1-yl)-methanone derivatives

For the synthesis of hydroxy substituted analogues, the starting material used was 5-hydroxy tryptophan instead of simple DL-tryptophan. The rest of the procedure was same as mentioned in the scheme 1.

Characterized data for 6-hydroxy substituted compounds of scheme 4:

(6-hydroxy-1-phenyl-9H-pyrido-[3,4-b]-indol-3-yl) (4-(p-tolyl)-piperazin-1-yl)-methanone (49): White solid, Yield 65%, Melting point 156-158 °C, IR $\nu_{\text{max}}/\text{cm}$: 3244, 1615, 1547, 1511, 1256, ^1H NMR (400 MHz, Chloroform-*d*) 8.65 (s, 1H), δ 7.5 – 7.38 (m, 10H), 7.02 – 6.89 (m, 3H), 3.82 (s, 3H), 2.10 – 2.05 (m, 1H), 1.36 – 1.21 (m, 8H). ^{13}C NMR (101 MHz, Chloroform-*d*) δ 170.60, 152.20, 151.68, 147.26, 146.78, 142.12, 129.23, 126.64, 128.14, 115.35, 113.35, 55.80, 26.60, 49.65, 29.56, ESI MS (*m/z*): calculated for $\text{C}_{29}\text{H}_{26}\text{N}_4\text{O}_2$, 462.21, found 463.25 $[\text{M}+\text{H}]^+$

(4-(2-fluorophenyl)-piperazin-1-yl) (6-hydroxy-1-phenyl-9H-pyrido-[3,4-b]-indol-3-yl)-methanone (50): White solid, Yield 61%, Melting point 166-168 °C, IR $\nu_{\text{max}}/\text{cm}$: 3220, 1612, 1558, 1520, 748, ^1H NMR (400 MHz, Chloroform-*d*) 8.57 (s, 1H), 8.09 (d, $J = 7.5$, 1.0 Hz, 1H), 7.88 – 7.82 (m, 2H), 7.53 – 7.45 (m, 2H), 7.30 – 7.24 (m, 1H), 7.07 – 7.02 (m, 3H), 6.84 – 6.75 (m, 2H), 4.04 – 3.91 (m, 4H), 3.84 (s, 3H), 3.18. (d, $J = 30.1$ Hz, 4H). ESI MS (*m/z*): calculated for $\text{C}_{28}\text{H}_{23}\text{FN}_4\text{O}_2$, 466.18, found 467.19 $[\text{M}+\text{H}]^+$

(6-hydroxy-1-phenyl-9H-pyrido-[3,4-b]-indol-3-yl) (4-(4-methoxyphenyl)-piperazin-1-yl)-methanone (51): White solid, Yield 58%, Melting point 155-157 °C, IR ν_{max} /cm: 3260, 1614, 1537, 1521, ^1H NMR (400 MHz, Chloroform-*d*) δ 8.54 (s, 1H), 7.45 – 7.30 (m, 9H), 7.05 – 6.98 (m, 4H), 3.8 (s, 3H), 2.10 – 2.05 (m, 3H), 1.37 – 1.28 (m, 5H). ESI MS (m/z): calculated for $\text{C}_{29}\text{H}_{26}\text{N}_4\text{O}_3$, 478.20, found 479.26 [M+H]⁺

(6-hydroxy-1-phenyl-9H-pyrido-[3,4-b]-indol-3-yl) (4-phenylpiperazin-1-yl)-methanone (52): White solid, Yield 61%, Melting point 155-157 °C, IR ν_{max} /cm: 3262, 1614, 1550, 1508, 1521, ^1H NMR (400 MHz, Chloroform-*d*) δ 8.82 (s, 1H), 8.47 (s, 1H), 8.17 (d, $J = 7.9$ Hz, 1H), 8.01-7.98 (m, 2H), 7.64-7.51 (m, 5H), 7.38-7.34 (m, 1H), 7.08-7.04 (m, 1H), 7.01-6.90 (m, 3H), 4.20- 4.10 (m, 4H), 3.25-3.16 (m, 4H). ESI MS (m/z): calculated for $\text{C}_{28}\text{H}_{24}\text{N}_4\text{O}_2$, 448.19, found 449.56 [M+H]⁺

(6-hydroxy-1-(4-methoxyphenyl)-9H-pyrido-[3,4-b]-indol-3-yl) (4-phenylpiperazin-1-yl)-methanone (53): White solid, Yield 59%, Melting point 145-147 °C, IR ν_{max} /cm: 3263, 1656, 1541, 1508, ^1H NMR (400 MHz, Chloroform-*d*) δ 8.85 (s, 1H), 8.64 (s, 1H), 8.12 (d, $J = 7.8$ Hz, 1H), 8.01-7.91 (m, 2H), 7.65-7.54 (m, 4H), 7.54 (t, $J = 7.4$ Hz, 1H), 7.38-7.31 (m, 1H), 7.22-7.20 (m, 2H), 7.11-7.00 (m, 2H), 4.10-4.00 (m, 4H), 3.38 (s, 3H), 3.10-3.01 (m, 4H). ESI MS (m/z): calculated for $\text{C}_{29}\text{H}_{26}\text{N}_4\text{O}_3$, 478.20, found 479.48 [M+H]⁺

(4-(2-fluorophenyl)-piperazin-1-yl) (6-hydroxy-1-(4-methoxyphenyl)-9H-pyrido-[3,4-b]-indol-3-yl)-methanone (54): White solid, Yield 62%, Melting point 134-136 °C, IR ν_{max} /cm: 3182, 1610, 1556, 1498, 750; ^1H NMR (400 MHz, Chloroform-*d*) 8.0 (s, 1H), 8.05- 8.09 (m, 2H), 7.88 – 7.82 (m, 2H), 7.53 – 7.45 (m, 2H), 7.30 – 7.24 (m, 1H), 7.07 – 7.02 (m, 3H), 6.84 – 6.75 (m, 2H), 4.04 – 3.91 (m, 4H), 3.84 (s, 3H), 3.18. (d, $J = 30.1$ Hz, 4H). ^{13}C NMR (101 MHz, Chloroform-*d*) δ 164.60, 153.28, 152.68, 145.27, 146.79, 131.18, 128.23, 122.54, 122.14, 115.75, 113.35, 55.80, 51.63, 48.67. ESI MS (m/z): calculated for $\text{C}_{29}\text{H}_{25}\text{FN}_4\text{O}_3$, 496.19, found 497.85 [M+H]⁺

(6-hydroxy-1-(4-methoxyphenyl)-9H-pyrido-[3,4-b]-indol-3-yl)(4-(p-tolyl)-piperazin-1-yl)-methanone (55): White solid, Yield 51%, Melting point 159-161 °C, IR ν_{max} /cm: 3172, 1620, 1540, 1440, ^1H NMR (400 MHz, Chloroform-*d*) 8.81 (s, 1H), 8.0- 8.10 (m, 3H), 7.88 – 7.86 (m, 2H), 7.43 – 7.48 (m, 2H), 7.30 – 7.24 (m, 3H), 7.07 – 7.02 (m, 3H), 6.84 – 6.75 (m, 2H), 4.00 – 3.81 (m, 4H), 3.80 (s, 3H), 3.18. (d, $J = 31.1$ Hz, 4H). ESI MS (m/z): calculated for $\text{C}_{30}\text{H}_{28}\text{N}_4\text{O}_3$, 492.22, found 493.45 [M+H]⁺

(6-hydroxy-1-(4-methoxyphenyl)-9H-pyrido-[3,4-b]-indol-3-yl)(4-(4-methoxyphenyl)piperazin-1-yl)-methanone (56): White solid, Yield 59%, Melting point 155-157 °C, IR

Chapter 5. Synthesis and Characterization of the designed analogues

ν_{\max}/cm : 3163, 1642, 1545, 1419, $^1\text{H NMR}$ (400 MHz, Chloroform-*d*) δ 11.70 (s, 1H), 8.44-8.49 (m, 3H), 8.26-8.19 (m, 2H), 8.09-8.06 (m, 2H), 7.69-7.53 (m, 6H), 7.30-7.27 (m, 1H), 6.84 (t, $J = 11.7$ Hz, 2H), 4.03-3.93 (m, 4H), 3.80 (s, 3H), 3.57-3.51 (m, 4H). ESI MS (m/z): calculated for $\text{C}_{30}\text{H}_{28}\text{N}_4\text{O}_4$, 508.21 found 509.12 $[\text{M}+\text{H}]^+$

(1-(4-chlorophenyl)-6-hydroxy-9H-pyrido-[3,4-*b*]-indol-3-yl) (4-phenylpiperazin-1-yl)-methanone (57): Pale yellow solid, Yield 62%, Melting point 177-179 °C, IR ν_{\max}/cm : 3153, 1652, 1515, 1469;720, $^1\text{H NMR}$ (400 MHz, Chloroform-*d*) δ 8.20 (s, 1H), 7.5 – 7.38 (m, 9H), 7.02 – 6.89 (m, 3H), 3.10-3.01 (m, 4H), 2.10 – 2.05 (m, 2H), 1.36 – 1.21 (m, 4H). ESI MS (m/z): calculated for $\text{C}_{28}\text{H}_{23}\text{ClN}_4\text{O}_2$, 482.15, found 483.75 $[\text{M}+\text{H}]^+$, 484.65 $[\text{M}+2]^+$

(1-(4-chlorophenyl)-6-hydroxy-9H-pyrido-[3,4-*b*]-indol-3-yl) (4-(2-fluorophenyl)-piperazin-1-yl)-methanone (58): Pale yellow solid, Yield 68%, Melting point 166-168 °C, IR ν_{\max}/cm : 3160, 1672, 1568, 1520, 760, $^1\text{H NMR}$ (400 MHz, Chloroform-*d*) 8.57 (s, 1H), 8.10-8.15 (m, 2H), 7.88 – 7.82 (m, 3H), 7.53 – 7.45 (m, 2H), 7.30 – 7.34 (m, 1H), 7.07 – 7.02 (m, 3H), 6.84 – 6.75 (m, 2H), 4.04 – 3.81 (m, 4H), 3.18. (d, $J = 30.1$ Hz, 4H). ESI MS (m/z): calculated for $\text{C}_{28}\text{H}_{22}\text{ClFN}_4\text{O}_2$, 500.14, found 501.78 $[\text{M}+\text{H}]^+$, 502.34 $[\text{M}+2]^+$

(6-hydroxy-1-(thiophen-2-yl)-9H-pyrido-[3,4-*b*]-indol-3-yl) (4-phenylpiperazin-1-yl)-methanone (59): White solid, Yield 58%, Melting point 125-127 °C, IR ν_{\max}/cm : 3381, 1634, 1512, 1481, 1257, $^1\text{H NMR}$ (400 MHz, Chloroform-*d*) δ 8.61 (s, 1H), 8.37 (s, 1H), 8.10 (d, $J = 7.0$, 1.0 Hz, 1H), 7.78 – 7.86 (m, 2H), 7.53 – 7.45 (m, 3H), 7.30 – 7.24 (m, 2H), 7.09 – 7.02 (m, 2H), 6.85 – 6.75 (m, 2H), 4.04 – 3.94 (m, 3H), 3.18. (d, $J = 30.1$ Hz, 4H). ESI MS (m/z): calculated for $\text{C}_{26}\text{H}_{22}\text{N}_4\text{O}_2\text{S}$, 454.15, found 455.86 $[\text{M}+\text{H}]^+$

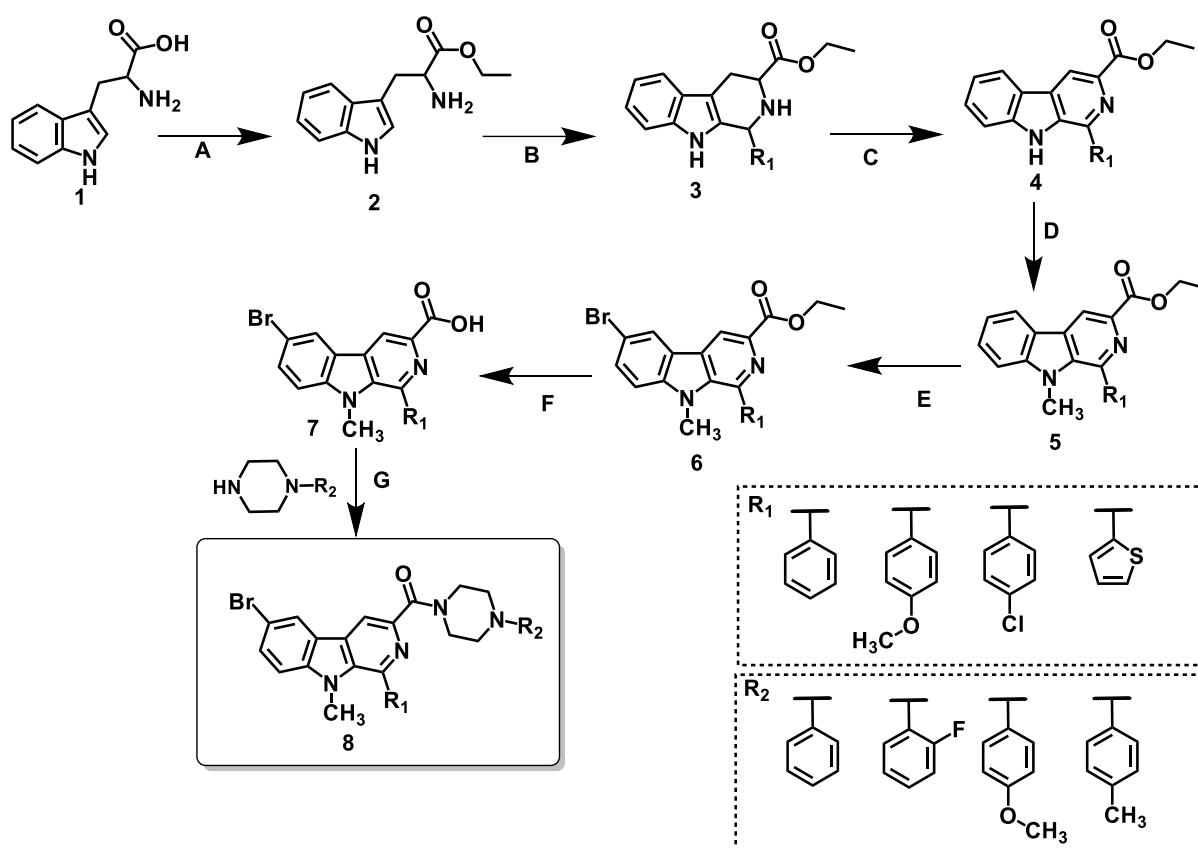
(6-hydroxy-1-(thiophen-2-yl)-9H-pyrido-[3,4-*b*]-indol-3-yl) (4-(*p*-tolyl)-piperazin-1-yl)-methanone (60): White solid, Yield 61%, Melting point 159-161 °C, IR ν_{\max}/cm : 3157, 1629, 1550, 1492, 1234, 740, $^1\text{H NMR}$ (400 MHz, Chloroform-*d*) δ 8.74 (s, 1H), 8.46 (s, 1H), 8.17 (d, $J = 7.9$ Hz, 1H), 7.98-7.89 (m, 2H), 7.64-7.54 (m, 2H), 7.38-7.34 (m, 1H), 7.27-7.23 (m, 2H), 7.17-7.12 (m, 2H), 6.92- 6.87 (m, 2H), 4.12-4.02 (m, 4H), 3.93 (s, 3H), 3.33-3.26 (m, 2H). ESI MS (m/z): calculated for $\text{C}_{27}\text{H}_{24}\text{N}_4\text{O}_2\text{S}$, 466.16, found 467.19 $[\text{M}+\text{H}]^+$

(4-(2-fluorophenyl)-piperazin-1-yl) (6-hydroxy-1-(thiophen-2-yl)-9H-pyrido-[3,4-*b*]-indol-3-yl)-methanone (61): White solid, Yield 59 %, Melting point 184-186 °C, IR ν_{\max}/cm : 3223, 1622, 1508, 1431, 1234, 744, $^1\text{H NMR}$ (400 MHz, Chloroform-*d*) δ 8.78 (s, 1H), 8.44 (s, 1H), 8.18 (d, $J = 7.6$ Hz, 1H), 7.80-7.84 (m 2H), 7.74 (d, $J = 7.8$ Hz, 1H), 7.62-7.56 (m, 2H), 7.38-7.34 (m, 2H), 7.15-7.08 (m, 2H), 7.03-6.97 (m, 2H), 4.19-4.00 (m, 3H), 3.26-3.17 (m, 4H). ESI MS (m/z): calculated for $\text{C}_{26}\text{H}_{21}\text{FN}_4\text{O}_2\text{S}$, 472.14, found 473.89 $[\text{M}+\text{H}]^+$

(6-hydroxy-1-(thiophen-2-yl)-9H-pyrido-[3,4-b]-indol-3-yl) (4-(4-methoxyphenyl) piperazin-1-yl)-methanone (62): Pale yellow solid, Yield 60%, Melting point 155-157 °C, IR $\nu_{\text{max}}/\text{cm}$: 3233, 1672, 1548, 1471, 750, ^1H NMR (400 MHz, Chloroform-*d*) 8.64 (s, 1H), 8.12 (s, 1H), 8.01-7.91 (m, 2H), 7.65-7.54 (m, 4H), 7.54 (t, $J = 7.4$ Hz, 1H), 7.38-7.31 (m, 1H), 7.22-7.20 (m, 2H), 7.11-7.00 (m, 2H), 4.10-4.00 (m, 4H), 3.38 (s, 3H), 3.10-3.01 (m, 3H). ESI MS (m/z): calculated for $\text{C}_{27}\text{H}_{24}\text{N}_4\text{O}_3\text{S}$, 484.16, found 485.56 $[\text{M}+\text{H}]^+$

(1-(4-chlorophenyl)-6-hydroxy-9H-pyrido-[3,4-b]-indol-3-yl) (4-phenylpiperazin-1-yl)-methanone (63): Yellow solid, Yield 68%, Melting point 134-136 °C, IR $\nu_{\text{max}}/\text{cm}$: 3164, 1672, 1568, 1540, 730, ^1H NMR (400 MHz, Chloroform-*d*) 8.54 (s, 1H), 8.10- 8.15 (m, 2H), 7.88 – 7.82 (m, 3H), 7.53 – 7.45 (m, 2H), 7.30 – 7.34 (m, 1H), 7.07 – 7.22 (m, 3H), 6.84 – 6.75 (m, 2H), 4.04 – 3.81 (m, 4H), 3.18. (d, $J = 30.1$ Hz, 4H). ^{13}C NMR (101 MHz, Chloroform-*d*) δ 173.64, 152.21, 151.68, 147.24, 146.78, 147.12, 129.23, 126.64, 128.14, 115.35, 113.35, 55.80, 56.60, 49.65, 29.5 ESI MS (m/z): calculated for $\text{C}_{28}\text{H}_{23}\text{ClN}_4\text{O}_2$, 482.15, found 483.78 $[\text{M}+\text{H}]^+$, 484.22 $[\text{M}+2]^+$

(1-(4-chlorophenyl)-6-hydroxy-9H-pyrido-[3,4-b]-indol-3-yl) (4-(4-methoxyphenyl) piperazin-1-yl)-methanone (64): Yellow solid, Yield 59%, Melting point 157-159 °C, IR $\nu_{\text{max}}/\text{cm}$: 3163, 1642, 1545, 1419, ^1H NMR (400 MHz, Chloroform-*d*) δ 11.70 (s, 1H), 8.26-8.19 (m, 2H), 8.09-8.06 (m, 2H), 7.69-7.53 (m, 5H), 7.30-7.27 (m, 1H), 6.84 (t, $J = 11.7$ Hz, 2H), 4.03-3.93 (m, 4H), 3.80 (s, 3H), 3.57-3.51 (m, 4H). ESI MS (m/z): calculated for $\text{C}_{29}\text{H}_{25}\text{ClN}_4\text{O}_3$, 512.16 found 513.49 $[\text{M}+\text{H}]^+$, 514.67 $[\text{M}+2]^+$



Scheme 5: Reagents and conditions: (A) SOCl₂, ethanol, 0 °C, reflux, 1 h (B) Aromatic aldehydes, trifluoroacetic acid, DCM, rt, 3 h (C) Sulfur, xylene, 100 C, reflux 24 h (D) Methyl iodide, KOH, DMSO, rt, 30 min (E) *N*-bromo succinimide, ethyl acetate, reflux, 24 h (F) NaOH, ethanol: water (1:1), rt, 45 min (G) THF, EDCI. HCl, HOBT, Phenyl piperazine, rt, overnight

Synthesis of 9-methyl-1-phenyl-9H-pyrido-[3,4-b]-indole-3-carboxylate (scheme-5) The general procedure was same for the above-mentioned scheme (scheme-5) except the fourth step (step-D). In this procedure, 100 mg of methyl iodide was taken in DMSO and KOH was added to it. The reaction mixture was stirred for 5 min and the reactant 1-phenyl-9H-pyrido-[3,4-b]-indole-3-carboxylate (500 mg) was added to it and allowed to stir for 30 min at room temperature. The progress of the reaction was monitored by TLC. The reaction mixture was added to ethyl acetate and extract the organic layer dried over Na₂SO₄ and concentrate under vacuum to get the desired product.

Characterized data for 6-bromo-9-methyl substituted compounds of scheme 5:

(6-bromo-9-methyl-1-phenyl-9H-pyrido-[3,4-b]-indol-3-yl) (4-(4-methoxyphenyl)-piperazin-1-yl)-methanone (65): Yellow solid, Yield 74%, Melting point 185-187 °C, IR v_{max}/cm: 3057, 1625, 1556, 1454, 1435, 1253, 701, ¹H NMR (400 MHz, Chloroform-*d*): δ 8.54 (s, 1H), 8.21 (d, J=7.8 Hz, 1H), 7.66–7.62 (m, 3H), 7.56–7.50 (m, 3H), 7.46 (d, J=8.3 Hz,

Chapter 5. Synthesis and Characterization of the designed analogues

1H), 7.36 (t, J=7.5 Hz, 1H), 7.20 (t, J=8.0 Hz, 1H), 6.62–6.48 (m, 3H), 4.13–4.07 (m, 4H), 3.80 (s, 3H), 3.52 (s, 3H), 3.36–3.26 (m, 3H). ESI MS (m/z): calculated for C₃₀H₂₇BrN₄O₂, 555.13 found 556.19 [M+H]⁺, 557.22 [M+2]⁺

(6-bromo-9-methyl-1-phenyl-9H-pyrido-[3,4-b]-indol-3-yl) (4-phenylpiperazin-1-yl)-methanone (66): White solid, Yield 69%, Melting point 135-137 °C, IR ν_{\max}/cm : 3047, 1655, 1546, 1444, 1243, 710, ¹H NMR (400 MHz, Chloroform-*d*): δ 8.05 (s, 1H), 8.01 (d, J=7.8 Hz, 1H), 7.69–7.62 (m, 3H), 7.56–7.59 (m, 3H), 7.49 (d, J=8.3 Hz, 1H), 7.39 (t, J=7.5 Hz, 1H), 7.20 (t, J=8.0 Hz, 1H), 6.67–6.48 (m, 3H), 4.16–4.07 (m, 3H), 3.80 (s, 3H), 3.37–3.26 (m, 4H). ¹³C NMR (101 MHz, Chloroform-*d*) δ 168.70, 152.30, 151.68, 147.25, 149.78, 132.12, 129.23, 125.54, 124.14, 115.35, 113.35, 55.80, 56.60, 50.75. ESI MS (m/z): calculated for C₂₉H₂₅BrN₄O, 524.12 found 525.46 [M+H]⁺, 526.33 [M+2]⁺

(6-bromo-9-methyl-1-phenyl-9H-pyrido-[3,4-*b*]-indol-3-yl) (4-(*p*-tolyl)-piperazin-1-yl)-methanone (67): White solid, Yield 69%, Melting point 166-168 °C, IR ν_{\max}/cm : 3047, 1655, 1546, 1444, 1243, 710, ¹H NMR (400 MHz, Chloroform-*d*): δ 8.05 (s, 1H), 8.03 (d, J=7.8 Hz, 1H), 7.69–7.62 (m, 3H), 7.56–7.59 (m, 3H), 7.49 (d, J=8.3 Hz, 1H), 7.39 (t, J=7.5 Hz, 1H), 7.20 (t, J=8.0 Hz, 1H), 6.67–6.48 (m, 3H), 4.16–4.07 (m, 3H), 3.84 (s, 3H), 3.56 (s, 3H), 3.37–3.26 (m, 4H). ESI MS (m/z): calculated for C₃₀H₂₇BrN₄O, 538.14 found 539.48 [M+H]⁺, 540.14 [M+2]⁺

(6-bromo-9-methyl-1-phenyl-9H-pyrido-[3,4-*b*]-indol-3-yl) (4-(2-fluorophenyl)-piperazin-1-yl)-methanone (68): White solid, Yield 72%, Melting point 147-145 °C, IR ν_{\max}/cm : 3049, 1659, 1548, 1454, 1243, 715, ¹H NMR (400 MHz, Chloroform-*d*) δ 8.51 (s, 1H), 8.21 (d, J=7.8 Hz, 1H), 7.65–7.62 (m, 3H), 7.56–7.44 (m, 4H), 7.46–7.44 (m, 2H), 7.24–7.20 (m, 1H), 7.05–6.97 (m, 2H), 4.04–4.10 (m, 4H), 3.51 (s, 3H), 3.19–3.08 (m, 3H). ESI MS (m/z): calculated for C₂₉H₂₄BrFN₄O, 542.11 found 543.78 [M+H]⁺, 544.23 [M+2]⁺

(6-bromo-1-(4-methoxyphenyl)-9-methyl-9H-pyrido-[3,4-*b*]-indol-3-yl) (4-(2-fluorophenyl)-piperazin-1-yl)-methanone (69): White solid, Yield 65%, Melting point 157-159 °C, IR ν_{\max}/cm : 3042, 1654, 1548, 1453, 1241, 710, ¹H NMR (400 MHz, Chloroform-*d*): δ 8.07 (s, 1H), 8.04–8.01 (m, 2H), 7.69–7.65 (m, 3H), 7.58–7.47 (m, 5H), 7.38 (t, J=7.5 Hz, 1H), 6.69–6.66 (m, 2H), 4.02-4.10 (m, 4H), 3.71–3.69 (m, 4H), 3.55 (s, 3H). ESI MS (m/z): calculated for C₃₀H₂₆BrFN₄O₂, 572.12 found 573.49 [M+H]⁺, 574.22 [M+2]⁺

(6-bromo-1-(4-methoxyphenyl)-9-methyl-9H-pyrido-[3,4-*b*]-indol-3-yl) (4-(2-methoxyphenyl)-piperazin-1-yl)-methanone (70): White solid, Yield 68%, Melting point 155-157 °C, IR ν_{\max}/cm : 3042, 1656, 1548, 1443, 1251, 713, ¹H NMR (400 MHz, Chloroform-

Chapter 5. Synthesis and Characterization of the designed analogues

d): δ 8.03 (s, 1H), 7.69–7.65 (m, 5H), 7.58–7.47 (m, 5H), 7.38 (t, $J=7.5$ Hz, 1H), 6.69–6.66 (m, 3H), 4.02–4.11 (m, 4H), 3.71 (s, 3H), 3.55 (s, 3H), 3.54 (s, 3H). ESI MS (m/z): calculated for $C_{31}H_{29}BrN_4O_3$, 584.14 found 585.47 $[M+H]^+$, 586.33 $[M+2]^+$

(6-bromo-1-(4-methoxyphenyl)-9-methyl-9H-pyrido-[3,4-*b*]-indol-3-yl)(4-(*p*-tolyl)-piperazin-1-yl)-methanone (71): White solid, Yield 63%, Melting point 148-150 °C, IR ν_{max}/cm : 3052, 1676, 1558, 723, 1H NMR (400 MHz, Chloroform-*d*): δ 8.06 (s, 1H), 7.65–7.61 (m, 6H), 7.53–7.48 (m, 5H), 7.48 (t, $J=7.5$ Hz, 1H), 6.69–6.61 (m, 3H), 4.12–4.16 (m, 5H), 3.71 (s, 3H), 3.55 (s, 3H), 2.55 (s, 3H). ESI MS (m/z): calculated for $C_{31}H_{29}BrN_4O_2$, 568.15 found 569.76 $[M+H]^+$, 570.22 $[M+2]^+$

(6-bromo-1-(4-methoxyphenyl)-9-methyl-9H-pyrido-[3,4-*b*]-indol-3-yl) (4-(4-methoxyphenyl)-piperazin-1-yl)-methanone (72): Pale yellow solid, Yield 59%, Melting point 155-157 °C, IR ν_{max}/cm : 3072, 1676, 1568, 713, 1H NMR (400 MHz, Chloroform-*d*): δ 8.08 (s, 1H), 8.04–8.00 (m, 2H), 7.69–7.65 (m, 3H), 7.58–7.49 (m, 5H), 7.38 (t, $J=7.5$ Hz, 1H), 6.69–6.68 (m, 2H), 4.02–4.17 (m, 2H), 3.71–3.69 (m, 4H), 3.88 (s, 3H), 3.71 (s, 3H), 3.55 (s, 3H). ESI MS (m/z): calculated for $C_{31}H_{29}BrN_4O_3$, 584.14 found 585.13 $[M+H]^+$, 586.35 $[M+2]^+$

(6-bromo-1-(4-chlorophenyl)-9-methyl-9H-pyrido-[3,4-*b*]-indol-3-yl) (4-(*p*-tolyl)-piperazin-1-yl)-methanone (73): White solid, Yield 58%, Melting point 155-157 °C, IR ν_{max}/cm : 3054, 1678, 1558, 718, 1H NMR (400 MHz, Chloroform-*d*): δ 8.11 (s, 1H), 7.66–7.62 (m, 3H), 7.56–7.50 (m, 5H), 7.46 (d, $J=8.3$ Hz, 1H), 7.36 (t, $J=7.5$ Hz, 1H), 7.20 (t, $J=8.0$ Hz, 1H), 6.62–6.48 (m, 4H), 4.13–4.07 (m, 4H), 3.80 (s, 3H), 2.80 (s, 3H). ^{13}C NMR (101 MHz, Chloroform-*d*) δ 168.70, 152.30, 151.68, 147.25, 149.78, 132.12, 129.23, 125.54, 124.14, 115.35, 113.35, 55.80, 56.60, 50.75. ESI MS (m/z): calculated for $C_{30}H_{26}BrClN_4O$, 572.10 found 573.46 $[M+H]^+$, 574.34 $[M+2]^+$, 576.45 $[M+4]^+$

(6-bromo-1-(4-chlorophenyl)-9-methyl-9H-pyrido-[3,4-*b*]-indol-3-yl) (4-(4-methoxyphenyl)-piperazin-1-yl)-methanone (74): Pale yellow solid, Yield 68%, Melting point 166-168 °C, IR ν_{max}/cm : 3052, 1676, 1548, 723, 1H NMR (400 MHz, Chloroform-*d*): δ 8.15 (s, 1H), 7.66–7.61 (m, 3H), 7.53–7.50 (m, 5H), 7.46 (d, $J=8.3$ Hz, 1H), 7.46 (t, $J=7.5$ Hz, 1H), 7.26 (t, $J=8.0$ Hz, 1H), 6.63–6.48 (m, 4H), 4.13–4.04 (m, 4H), 3.80 (s, 3H), 3.50 (s, 3H). ESI MS (m/z): calculated for $C_{30}H_{26}BrClN_4O_2$, 588.09 found 589.16 $[M+H]^+$, 590.34 $[M+2]^+$, 592.56 $[M+4]^+$

(6-bromo-1-(4-chlorophenyl)-9-methyl-9H-pyrido-[3,4-*b*]-indol-3-yl) (4-(2-fluorophenyl)-piperazin-1-yl)-methanone (75): Pale yellow solid, Yield 62%, Melting point 165-167 °C, IR

Chapter 5. Synthesis and Characterization of the designed analogues

$\nu_{\text{max}}/\text{cm}$: 3042, 1666, 1538, 713, ^1H NMR (400 MHz, Chloroform-*d*): δ 8.06 (s, 1H), 7.65–7.61 (m, 5H), 7.53–7.48 (m, 5H), 7.48 (t, $J=7.5$ Hz, 1H), 6.69–6.61 (m, 4H), 4.12–4.16 (m, 5H), 3.71 (s, 3H). ESI MS (m/z): calculated for $\text{C}_{29}\text{H}_{23}\text{BrClFN}_4\text{O}$, 576.07 found 577.13 $[\text{M}+\text{H}]^+$, 578.43 $[\text{M}+2]^+$, 580.34 $[\text{M}+2]^+$

(6-bromo-1-(4-chlorophenyl)-9-methyl-9H-pyrido-[3,4-*b*]-indol-3-yl) (4-(2-methoxyphenyl)-piperazin-1-yl)-methanone (76): Pale yellow solid, Yield 53%, Melting point 160-162 °C, IR $\nu_{\text{max}}/\text{cm}$: 3058, 1678, 1578, 729, ^1H NMR (400 MHz, Chloroform-*d*): δ 8.03 (s, 1H), 7.69–7.65 (m, 6H), 7.58–7.47 (m, 5H), 7.38 (t, $J=7.5$ Hz, 1H), 6.69–6.66 (m, 3H), 4.02–4.11 (m, 4H), 3.71 (s, 3H), 3.55 (s, 3H). ESI MS (m/z): calculated for $\text{C}_{30}\text{H}_{26}\text{BrClN}_4\text{O}_2$, 588.09 found 589.40 $[\text{M}+\text{H}]^+$, 590.34 $[\text{M}+2]^+$, 592.34 $[\text{M}+4]^+$

(6-bromo-9-methyl-1-(thiophen-2-yl)-9H-pyrido-[3,4-*b*]-indol-3-yl) (4-(2-methoxyphenyl)-piperazin-1-yl)-methanone (77): Yellow solid, Yield 63%, Melting point 155-157 °C, IR $\nu_{\text{max}}/\text{cm}$: 3052, 1676, 1558, 723, ^1H NMR (400 MHz, Chloroform-*d*): δ 8.50 (s, 1H), 7.69-7.53 (m, 6H), 7.30-7.27 (m, 5H), 6.84 (t, $J = 11.7$ Hz, 2H), 4.03-3.93 (m, 5H), 3.77 (s, 3H), 3.72 (s, 3H). ESI MS (m/z): calculated for $\text{C}_{28}\text{H}_{25}\text{BrN}_4\text{O}_2\text{S}$, 560.09 found 561.79 $[\text{M}+\text{H}]^+$, 562.67 $[\text{M}+2]^+$

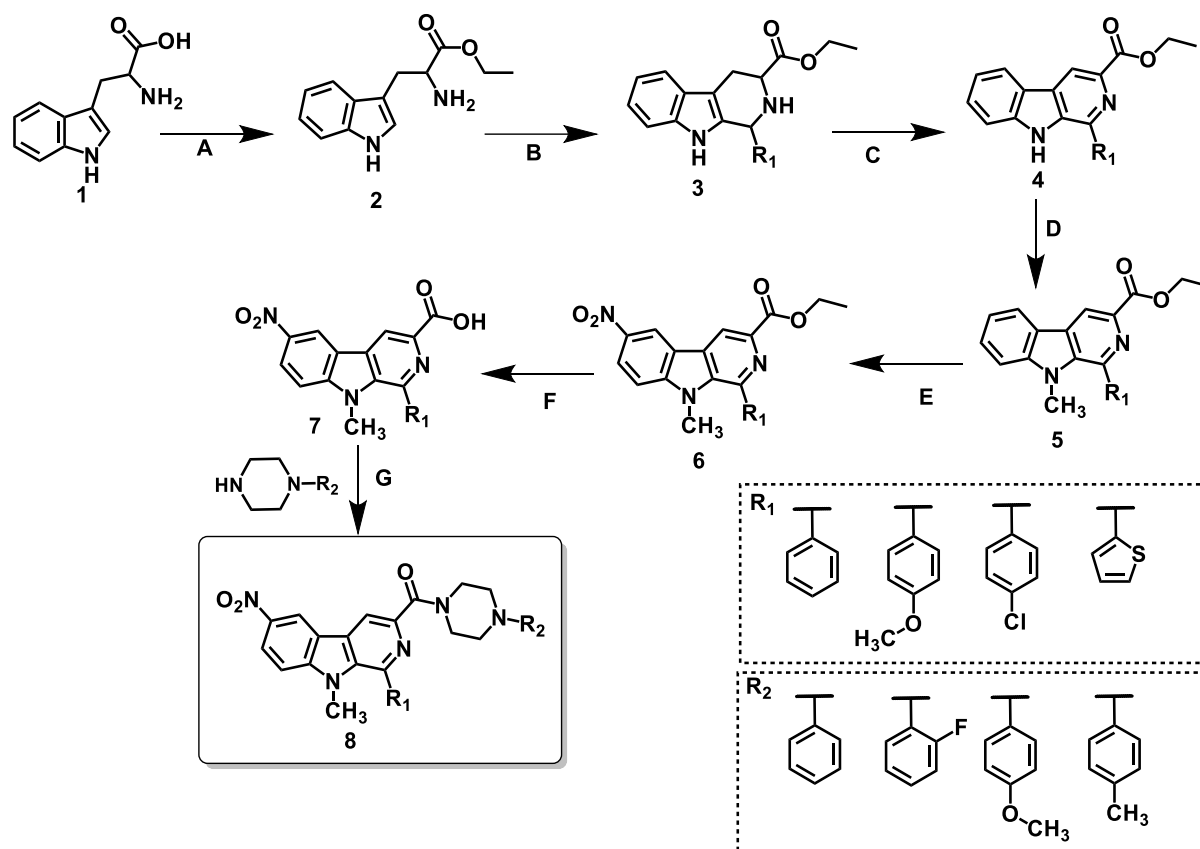
(6-bromo-9-methyl-1-(thiophen-2-yl)-9H-pyrido-[3,4-*b*]-indol-3-yl) (4-(2-fluorophenyl)-piperazin-1-yl)-methanone (78): Yellow solid, Yield 73%, Melting point 145-147 °C, IR $\nu_{\text{max}}/\text{cm}$: 3110, 1626, 1588, 719, ^1H NMR (400 MHz, Chloroform-*d*): δ 8.20 (s, 1H), 7.69-7.57 (m, 6H), 7.40-7.37 (m, 5H), 6.84 (t, $J = 11.7$ Hz, 2H), 4.03-3.83 (m, 5H), 3.77 (s, 3H). ESI MS (m/z): calculated for $\text{C}_{27}\text{H}_{22}\text{BrFN}_4\text{OS}$, 548.07 found 549.47 $[\text{M}+\text{H}]^+$, 550.45 $[\text{M}+2]^+$

(6-bromo-9-methyl-1-(thiophen-2-yl)-9H-pyrido-[3,4-*b*]-indol-3-yl) (4-(*p*-tolyl)-piperazin-1-yl)-methanone (79): Yellow solid, Yield 73%, Melting point 134-136 °C, IR $\nu_{\text{max}}/\text{cm}$: 3052, 1676, 1558, 728, ^1H NMR (400 MHz, Chloroform-*d*): δ 8.24 (s, 1H), 7.69-7.47 (m, 6H), 7.40-7.30 (m, 5H), 6.84 (t, $J = 11.7$ Hz, 2H), 4.03-3.86 (m, 5H), 3.77 (s, 3H), 2.32(s, 3H). ESI MS (m/z): calculated for $\text{C}_{28}\text{H}_{25}\text{BrN}_4\text{OS}$, 544.09 found 545.19 $[\text{M}+\text{H}]^+$, 546.33 $[\text{M}+2]^+$

(6-bromo-9-methyl-1-(thiophen-2-yl)-9H-pyrido-[3,4-*b*]-indol-3-yl) (4-(4-methoxyphenyl)-piperazin-1-yl)-methanone (80): Yellow solid, Yield 53%, Melting point 155-157 °C, IR $\nu_{\text{max}}/\text{cm}$: 3042, 1656, 1538, 719, ^1H NMR (400 MHz, Chloroform-*d*): δ 8.14 (s, 1H), 7.79-7.57 (m, 6H), 7.40-7.30 (m, 5H), 6.74 (t, $J = 11.7$ Hz, 2H), 4.03-3.87 (m, 5H), 3.77 (s, 3H), 3.52(s, 3H). ^{13}C NMR (101 MHz, Chloroform-*d*) δ 168.70, 152.30, 151.68, 147.25,

Chapter 5. Synthesis and Characterization of the designed analogues

149.78, 132.12, 129.23, 125.54, 124.14, 115.35, 113.35, 55.80, 56.60, 50.75. ESI MS (m/z): calculated for $C_{28}H_{25}BrN_4O_2S$, 560.09 found 561.79 $[M+H]^+$, 562.33 $[M+2]^+$



Scheme 6: Reagents and conditions: (A) $SOCl_2$, ethanol, 0 °C, reflux, 1 h (B) Aromatic aldehydes, trifluoroacetic acid, DCM, rt, 3 h (C) Sulfur, xylene, 100 C, reflux 24 h (D) Methyl iodide, KOH, DMSO, rt, 30 min (E) Trifluoro acetic acid, sodium nitrite, 0 °C, 24 h (F) NaOH, ethanol: water (1:1), rt, 45 min (G) THF, EDCI. HCl, HOBT, Phenyl piperazine, rt, overnight

Characterized data for 6-nitro-9-methyl substituted compounds of scheme 6:

(4-(4-methoxyphenyl)-piperazin-1-yl) (9-methyl-6-nitro-1-phenyl-9H-pyrido-[3,4-b]-indol-3-yl)-methanone (81): Yellow solid, Yield 64%, Melting point 160-162 °C, IR ν_{max}/cm : 3052, 1676, 1558, 723, 1H NMR (400 MHz, Chloroform-*d*): δ 8.37 (s, 1H), 8.09 (d, $J = 7.8$, 1.0 Hz, 1H), 7.88 – 7.82 (m, 2H), 7.30 – 7.24 (m, 3H), 7.07 – 7.02 (m, 4H), 6.84 – 6.75 (m, 2H), 4.04 – 3.91 (m, 4H), 3.18. (d, $J = 30.1$ Hz, 4H), 3.87 (s, 3H), 3.72 (s, 3H). ESI MS (m/z): calculated for $C_{30}H_{27}N_5O_4$, 521.21 found 522.46 $[M+H]^+$

(4-(2-methoxyphenyl)-piperazin-1-yl) (9-methyl-6-nitro-1-phenyl-9H-pyrido-[3,4-b]-indol-3-yl)-methanone (82): Yellow solid, Yield 68%, Melting point 160-162 °C, IR ν_{max}/cm : 3043, 1668, 1547, 720, 1H NMR (400 MHz, Chloroform-*d*): δ 8.39 (s, 1H), 8.29 (d, $J = 7.8$, 1.0 Hz, 1H), 7.88 – 7.82 (m, 2H), 7.30 – 7.24 (m, 3H), 7.07 – 7.02 (m, 3H), 6.84 – 6.75 (m, 2H),

Chapter 5. Synthesis and Characterization of the designed analogues

4.04 – 3.91 (m, 4H), 3.18. (d, $J = 30.1$ Hz, 4H), 3.87 (s, 3H), 3.72(s, 3H). ESI MS (m/z): calculated for $C_{30}H_{27}N_5O_4$, 521.21 found 522.79 [M+H]⁺

(9-methyl-6-nitro-1-phenyl-9H-pyrido-[3,4-b]-indol-3-yl) (4-(p-tolyl)-piperazin-1-yl)-methanone (83): Yellow solid, Yield 62%, Melting point 154-156 °C, IR ν_{max}/cm : 3032, 1676, 1578, 723, ¹H NMR (400 MHz, Chloroform-*d*): δ 8.49 (s,1H), 8.29 (d, $J = 7.5, 1.5$ Hz, 1H), 7.88 – 7.72 (m, 2H), 7.30 – 7.24 (m, 1H), 7.17 – 7.12 (m, 3H), 6.74 – 6.65 (m, 4H), 4.04 – 3.91 (m, 4H), 3.18. (d, $J = 30.1$ Hz, 4H), 3.87 (s, 3H), 2.32(s, 3H). ESI MS (m/z): calculated for $C_{30}H_{27}N_5O_3$, 550.10 found 551.16 [M+H]⁺

(4-(2-fluorophenyl)-piperazin-1-yl) (9-methyl-6-nitro-1-phenyl-9H-pyrido-[3,4-b]-indol-3-yl)-methanone (84): Yellow solid, Yield 69%, Melting point 160-162 °C, IR ν_{max}/cm : 3052, 1666, 1588, 713, ¹H NMR (400 MHz, Chloroform-*d*): δ 8.59 (s,1H), 8.39 (d, $J = 7.5, 1.5$ Hz, 1H), 7.68 – 7.72 (m, 3H), 7.30 – 7.24 (m, 1H), 7.17 – 7.12 (m, 4H), 6.94 – 6.65 (m, 3H), 4.15 – 3.91 (m, 4H), 3.84 (s, 3H), 3.18. (d, $J = 30.1$ Hz, 4H). ESI MS (m/z): calculated for $C_{29}H_{24}FN_5O_3$, 509.19 found 510.46 [M+H]⁺

(4-(2-fluorophenyl)-piperazin-1-yl) (1-(4-methoxyphenyl)-9-methyl-6-nitro-9H-pyrido-[3,4-b]-indol-3-yl)-methanone (85): Yellow solid, Yield 50%, Melting point 152-154 °C, IR ν_{max}/cm : 3072, 1676, 1578, 713, ¹H NMR (400 MHz, Chloroform-*d*): δ 8.69 (s,1H), 8.59 (d, $J = 7.5, 1.5$ Hz, 1H), 7.78 – 7.72 (m, 2H), 7.40 – 7.44 (m, 2H), 7.17 – 7.12 (m, 3H), 6.64 – 6.55 (m, 3H), 4.04 – 3.91 (m, 4H), 3.87 (s, 3H), 3.72(s, 3H), 3.18. (d, $J = 30.1$ Hz, 4H). ¹³C NMR (101 MHz, Chloroform-*d*) δ 168.70, 152.30, 151.68, 147.25, 149.78, 132.12, 129.23, 125.54, 124.14, 115.35, 113.35, 55.80, 56.60, 50.75. ESI MS (m/z): calculated for $C_{30}H_{26}FN_5O_4$, 539.20 found 540.28 [M+H]⁺

(1-(4-methoxyphenyl)-9-methyl-6-nitro-9H-pyrido-[3,4-b]-indol-3-yl) (4-(2-methoxyphenyl)-piperazin-1-yl)-methanone (86): Yellow solid, Yield 59%, Melting point 160-162 °C, IR ν_{max}/cm : 3052, 1676, 1558, 723, ¹H NMR (400 MHz, Chloroform-*d*): δ 8.79 (s,1H), 8.59 (d, $J = 7.5, 1.5$ Hz, 1H), 7.78 – 7.74 (m, 2H), 7.68 – 7.64 (m, 2H), 7.27 – 7.30 (m, 3H), 6.64 – 6.59 (m, 3H), 4.06 – 3.91 (m, 4H), 3.88 (s, 3H), 3.74 (s, 3H), 3.62(s, 3H), 3.18. (d, $J = 30.1$ Hz, 4H). ESI MS (m/z): calculated for $C_{31}H_{29}N_5O_5$, 551.22 found 552.47 [M+H]⁺

(1-(4-methoxyphenyl)-9-methyl-6-nitro-9H-pyrido-[3,4-b]-indol-3-yl) (4-(p-tolyl)-piperazin-1-yl)-methanone (87): Yellow solid, Yield 71%, Melting point 160-162 °C, IR ν_{max}/cm : 3059, 1686, 1548, 727, ¹H NMR (400 MHz, Chloroform-*d*): δ 8.89 (s,1H), 8.59 (d, $J = 7.5, 1.5$ Hz, 1H), 7.78 – 7.74 (m, 2H), 7.68 – 7.64 (m, 2H), 7.27 – 7.40 (m, 3H), 6.69 – 6.59

Chapter 5. Synthesis and Characterization of the designed analogues

(m, 3H), 4.07 – 3.91 (m, 4H), 3.88 (s, 3H), 3.74 (s, 3H), 2.62(s, 3H), 3.18. (d, $J = 30.1$ Hz, 4H).

ESI MS (m/z): calculated for $C_{31}H_{29}N_5O_4$, 535.22 found 536.89 [M+H]⁺

(1-(4-methoxyphenyl)-9-methyl-6-nitro-9H-pyrido-[3,4-b]-indol-3-yl) (4-(4-methoxyphenyl)-piperazin-1-yl)-methanone (88): White solid, Yield 79%, Melting point

162-164 °C, IR ν_{max}/cm : 3052, 1663, 1538, 725, ¹H NMR (400 MHz, Chloroform-*d*): δ 8.79 (s,1H), 8.63 (d, $J = 7.5, 1.5$ Hz, 1H), 7.70 – 7.64 (m, 2H), 7.68 – 7.64 (m, 2H), 7.37 – 7.40 (m, 3H), 6.69 – 6.59 (m, 3H), 4.06 – 3.91 (m, 4H), 3.88 (s, 3H), 3.74 (s, 3H), 2.62 (s, 3H), 3.18. (d, $J = 30.1$ Hz, 4H). ESI MS (m/z): calculated for $C_{31}H_{29}N_5O_5$, 551.22 found 552.46 [M+H]⁺

(1-(4-chlorophenyl)-9-methyl-6-nitro-9H-pyrido-[3,4-b]-indol-3-yl) (4-(2-methoxyphenyl)-piperazin-1-yl)-methanone (89): White solid, Yield 49%, Melting point

160-162 °C, IR ν_{max}/cm : 3062, 1655, 1550, 728, ¹H NMR (400 MHz, Chloroform-*d*): δ 8.79 (s,1H), 8.59 (d, $J = 7.5, 1.5$ Hz, 1H), 7.78 – 7.74 (m, 2H), 7.68 – 7.64 (m, 2H), 7.27 – 7.30 (m, 3H), 6.64 – 6.59 (m, 3H), 4.06 – 3.91 (m, 4H), 3.88 (s, 3H), 3.74 (s, 3H), 3.18. (d, $J = 30.1$ Hz, 4H). ESI MS (m/z): calculated for $C_{30}H_{26}ClN_5O_4$, 555.17 found 556.49 [M+H]⁺, 557.33 [M+2]⁺

(1-(4-chlorophenyl)-9-methyl-6-nitro-9H-pyrido-[3,4-b]-indol-3-yl) (4-(4-methylphenyl)-piperazin-1-yl)-methanone (90): White solid, Yield 59%, Melting point 160-162 °C, IR

ν_{max}/cm : 3022, 1696, 1558, 727, ¹H NMR (400 MHz, Chloroform-*d*): δ 8.69 (s,1H), 8.59 (d, $J = 7.5, 1.5$ Hz, 1H), 7.78 – 7.72 (m, 2H), 7.40 – 7.44 (m, 2H), 7.17 – 7.12 (m, 3H), 6.64 – 6.55 (m, 3H), 4.04 – 3.91 (m, 4H), 3.87 (s, 3H), 3.72(s, 3H), 3.18. (d, $J = 30.1$ Hz, 4H). ESI MS (m/z): calculated for $C_{30}H_{26}ClN_5O_3$, 539.17 found 540.45 [M+H]⁺, 541.22 [M+2]⁺

(1-(4-chlorophenyl)-9-methyl-6-nitro-9H-pyrido-[3,4-b]-indol-3-yl) (4-(2-fluorophenyl)-piperazin-1-yl)-methanone (91): White solid, Yield 69%, Melting point 145-147 °C, IR

ν_{max}/cm : 3044, 1677, 1548, 720, ¹H NMR (400 MHz, Chloroform-*d*): δ 8.79 (s,1H), 8.63 (d, $J = 7.5, 1.5$ Hz, 1H), 7.70 – 7.68 (m, 2H), 7.68 – 7.54 (m, 2H), 7.39 – 7.40 (m, 3H), 6.69 – 6.58 (m, 3H), 4.06 – 3.91 (m, 4H), 3.88 (s, 3H), 3.18. (d, $J = 30.1$ Hz, 4H). ESI MS (m/z): calculated for $C_{29}H_{23}ClFN_5O_3$, 543.15 found 544.23 [M+H]⁺, 545.22 [M+2]⁺

(1-(4-chlorophenyl)-9-methyl-6-nitro-9H-pyrido-[3,4-b]-indol-3-yl) (4-(p-tolyl)-piperazin-1-yl)-methanone (92): White solid, Yield 63%, Melting point 160-162 °C, IR

ν_{max}/cm : 3053, 1676, 1558, 721, ¹H NMR (400 MHz, Chloroform-*d*): δ 8.79 (s,1H), 8.66 (d, $J = 7.5, 1.5$ Hz, 1H), 7.70 – 7.69 (m, 2H), 7.68 – 7.64 (m, 2H), 7.37 – 7.39 (m, 3H), 6.69 – 6.59 (m, 3H), 4.06 – 3.81 (m, 4H), 3.74 (s, 3H), 2.68 (s, 3H), 3.18. (d, $J = 30.1$ Hz, 4H). ¹³C NMR (101 MHz, Chloroform-*d*) δ 168.70, 152.30, 151.68, 147.25, 149.78, 132.12, 129.23, 125.54,

Chapter 5. Synthesis and Characterization of the designed analogues

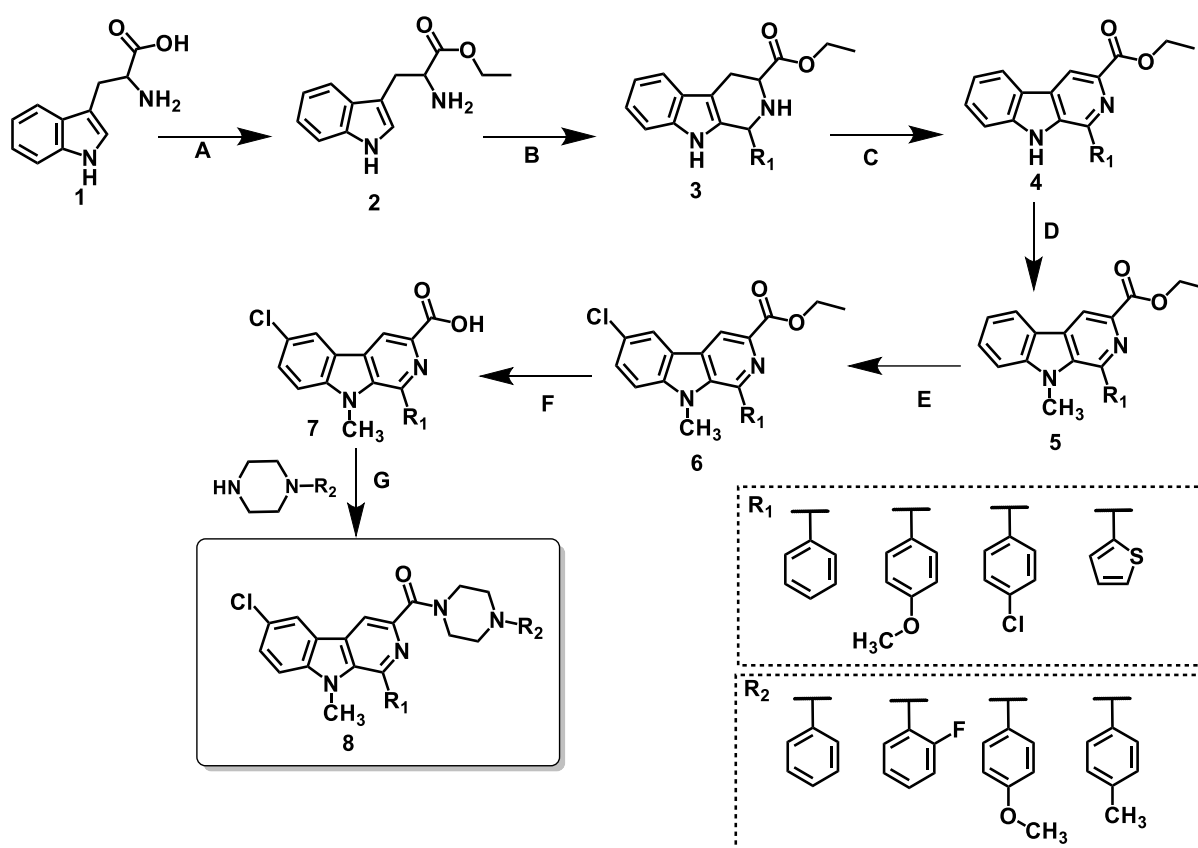
124.14, 115.35, 113.35, 55.80, 56.60, 50.75. ESI MS (m/z): calculated for C₃₀H₂₆ClN₅O₃, 539.17 found 540.79 [M+H]⁺, 541.45 [M+2]⁺

(4-(2-methoxyphenyl)-piperazin-1-yl) (9-methyl-6-nitro-1-(thiophen-2-yl)-9H-pyrido-[3,4-b]-indol-3-yl)-methanone (93): White solid, Yield 64%, Melting point 150-152 °C, IR v_{max}/cm: 3052, 1672, 1558, 723, ¹H NMR (400 MHz, Chloroform-*d*): δ 8.60 (s, 1H), 7.69-7.49 (m, 6H), 7.34-7.27 (m, 5H), 6.89 (t, J = 11.7 Hz, 2H), 4.03-3.98 (m, 5H), 3.77 (s, 3H), 3.72 (s, 3H). ESI MS (m/z): calculated for C₂₈H₂₅N₅O₄S, 527.16 found 528.43 [M+H]⁺

(4-(2-fluorophenyl)-piperazin-1-yl) (9-methyl-6-nitro-1-(thiophen-2-yl)-9H-pyrido-[3,4-b]-indol-3-yl)-methanone (94): White solid, Yield 68%, Melting point 158-160 °C, IR v_{max}/cm: 3059, 1676, 1558, 720, ¹H NMR (400 MHz, Chloroform-*d*): δ 8.72 (s, 1H), 7.89-7.59 (m, 6H), 7.44-7.27 (m, 5H), 6.89 (t, J = 11.7 Hz, 2H), 4.13-3.98 (m, 5H), 3.77 (s, 3H). ESI MS (m/z): calculated for C₂₇H₂₂FN₅O₃S, 515.14 found 516.48 [M+H]⁺

(9-methyl-6-nitro-1-(thiophen-2-yl)-9H-pyrido-[3,4-b]-indol-3-yl) (4-(p-tolyl)-piperazin-1-yl)-methanone (95): White solid, Yield 69%, Melting point 180-182 °C, IR v_{max}/cm: 3452, 1686, 1598, 729, ¹H NMR (400 MHz, Chloroform-*d*): δ 8.24 (s, 1H), 7.69-7.47 (m, 6H), 7.40-7.30 (m, 6H), 6.84 (t, J = 11.7 Hz, 2H), 4.03-3.86 (m, 6H), 3.77 (s, 3H), 2.32(s, 3H). ESI MS (m/z): calculated for C₂₈H₂₅N₅O₃S, 511.17 found 512.48 [M+H]⁺

(4-(4-methoxyphenyl)-piperazin-1-yl) (9-methyl-6-nitro-1-(thiophen-2-yl)-9H-pyrido-[3,4-b]-indol-3-yl)-methanone (96): White solid, Yield 60%, Melting point 170-172 °C, IR v_{max}/cm: 3052, 1676, 1558, 723, ¹H NMR (400 MHz, Chloroform-*d*): δ 8.14 (s, 1H), 7.39-7.27 (m, 6H), 7.48-7.32 (m, 5H), 6.74 (t, J = 11.7 Hz, 2H), 4.03-3.87 (m, 5H), 3.76 (s, 3H), 3.52(s, 3H). ESI MS (m/z): calculated for C₂₈H₂₅N₅O₄S, 527.16 found 528.17 [M+H]⁺



Scheme 7: Reagents and conditions: (A) SOCl₂, ethanol, 0 °C, reflux, 1 h (B) Aromatic aldehydes, trifluoroacetic acid, DCM, rt, 3 h (C) Sulfur, xylene, 100 °C, reflux 24 h (D) Methyl iodide, KOH, DMSO, rt, 30 min (E) *N*-chloro succinimide, ethyl acetate, reflux, 24 h (F) NaOH, ethanol: water (1:1), rt, 45 min (G) THF, EDCI. HCl, HOBT, Phenyl piperazine, rt, overnight

Characterized data for 6-chloro-9-methyl substituted compounds of scheme 7:

(6-chloro-9-methyl-1-phenyl-9*H*-pyrido-[3,4-*b*]-indol-3-yl) (4-(4-methoxyphenyl)-piperazin-1-yl)-methanone (97): White solid, Yield 69%, Melting point 135-136 °C, IR ν_{max} /cm: 3057, 1625, 1556, 1454, 1435, 1253, 701, ¹H NMR (400 MHz, Chloroform-*d*): δ 8.54 (s, 1H), 8.27 (d, *J*=7.8 Hz, 1H), 7.69–7.62 (m, 3H), 7.56–7.50 (m, 3H), 7.44 (d, *J*=8.3 Hz, 1H), 7.38 (t, *J*=7.5 Hz, 1H), 7.20 (t, *J*=8.0 Hz, 1H), 6.62–6.48 (m, 3H), 4.13–4.07 (m, 4H), 3.80 (s, 3H), 3.52 (s, 3H), 3.36–3.26 (m, 3H). ESI MS (*m/z*): calculated for C₃₀H₂₇ClN₄O₂, 510.18 found 511.48 [M+H]⁺, 512.33 [M+2]⁺

(6-chloro-9-methyl-1-phenyl-9*H*-pyrido-[3,4-*b*]-indol-3-yl) (4-phenylpiperazin-1-yl)-methanone (98): White solid, Yield 71%, Melting point 136-138 °C, IR ν_{max} /cm: 3067, 1655, 1546, 1474, 1243, 710, ¹H NMR (400 MHz, Chloroform-*d*): δ 8.15 (s, 1H), 8.11 (d, *J*=7.8 Hz, 1H), 7.49–7.32 (m, 3H), 7.56–7.59 (m, 3H), 7.49 (d, *J*=8.3 Hz, 1H), 7.39 (t, *J*=7.5 Hz, 2H), 7.10

Chapter 5. Synthesis and Characterization of the designed analogues

(t, $J=8.0$ Hz, 1H), 6.57–6.48 (m, 3H), 4.66–4.57 (m, 3H), 3.84 (s, 3H), 3.37–3.26 (m, 4H). ESI MS (m/z): calculated for $C_{29}H_{25}ClN_4O$, 480.17 found 481.46 $[M+H]^+$, 482.34 $[M+2]^+$

(6-chloro-9-methyl-1-phenyl-9H-pyrido-[3,4-b]-indol-3-yl) (4-(p-tolyl)-piperazin-1-yl)-methanone (99): White solid, Yield 67%, Melting point 137-139 °C, IR ν_{max}/cm : 3077, 1655, 1546, 1494, 1243, 720, 1H NMR (400 MHz, Chloroform-*d*): δ 8.05 (s, 1H), 8.03 (d, $J=7.8$ Hz, 1H), 7.69–7.82 (m, 3H), 7.56–7.59 (m, 3H), 7.49 (d, $J=8.3$ Hz, 1H), 7.39(t, $J=7.5$ Hz, 1H), 7.20 (t, $J=8.0$ Hz, 1H), 6.67–6.48 (m, 3H), 4.16–4.07 (m, 3H), 3.84 (s, 3H), 2.56 (s, 3H), 3.34–3.28 (m, 4H). ESI MS (m/z): calculated for $C_{30}H_{27}ClN_4O$, 494.19 found 495.20 $[M+H]^+$, 496.33 $[M+2]^+$

(6-chloro-9-methyl-1-phenyl-9H-pyrido-[3,4-b]-indol-3-yl) (4-(2-fluorophenyl)-piperazin-1-yl)-methanone (100): White solid, Yield 66%, Melting point 132-134 °C, IR ν_{max}/cm : 3149, 1669, 1548, 1454, 715, 1H NMR (400 MHz, Chloroform-*d*) δ 8.51 (s, 1H), 8.31 (d, $J=7.8$ Hz, 1H), 7.65–7.62 (m, 3H), 7.56–7.44 (m, 4H), 7.46–7.44 (m, 2H), 7.34–7.20 (m, 1H), 7.05–6.97 (m, 2H), 4.04–4.19 (m, 4H), 3.57 (s, 3H), 3.19–3.08 (m, 3H). ESI MS (m/z): calculated for $C_{29}H_{24}ClFN_4O$, 498.16 found 499.43 $[M+H]^+$, 450.13 $[M+2]^+$

(6-chloro-1-(4-methoxyphenyl)-9-methyl-9H-pyrido-[3,4-b]-indol-3-yl) (4-(2-fluorophenyl)-piperazin-1-yl)-methanone (101): White solid, Yield 57%, Melting point 135-136 °C, IR ν_{max}/cm : 3076, 1636, 1578, 723, 1H NMR (400 MHz, Chloroform-*d*): δ 8.49 (s, 1H), 8.39 (d, $J = 7.5, 1.5$ Hz, 1H), 7.78 – 7.72 (m, 2H), 7.39 – 7.44 (m, 2H), 7.20 – 7.17 (m, 3H), 6.64 – 6.52 (m, 3H), 4.04 – 3.92 (m, 4H), 3.87 (s, 3H), 3.74(s, 3H), 3.15. (d, $J = 30.1$ Hz, 4H). ESI MS (m/z): calculated for $C_{30}H_{26}ClFN_4O_2$, 528.17 found 529.46 $[M+H]^+$, 530.33 $[M+2]^+$

(6-chloro-1-(4-methoxyphenyl)-9-methyl-9H-pyrido-[3,4-b]-indol-3-yl)(4-phenylpiperazin-1-yl)-methanone (102): Pale yellow solid, Yield 58%, Melting point 138-140 °C, IR ν_{max}/cm : 3032, 1656, 1568, 1443, 733, 1H NMR (400 MHz, Chloroform-*d*): δ 8.03 (s, 1H), 7.69–7.65 (m, 6H), 7.58–7.47 (m, 5H), 7.38 (t, $J=7.5$ Hz, 1H), 6.69–6.66 (m, 3H), 4.02–4.11 (m, 4H), 3.71 (s, 3H), 3.67 (s, 3H), 3.55 (s, 3H). ^{13}C NMR (101 MHz, Chloroform-*d*) δ 167.70, 162.30, 151.67, 147.25, 149.78, 132.12, 129.23, 125.54, 124.14, 115.35, 113.35, 55.80, 56.60, 50.75. ESI MS (m/z): calculated for $C_{30}H_{27}ClN_4O_2$, 510.18 found 512.47 $[M+2]^+$

(6-chloro-1-(4-methoxyphenyl)-9-methyl-9H-pyrido-[3,4-b]-indol-3-yl) (4-(p-tolyl)-piperazin-1-yl)-methanone (103): White solid, Yield 65%, Melting point 153-155 °C, IR ν_{max}/cm : 3052, 1656, 1558, 723, 1H NMR (400 MHz, Chloroform-*d*): δ 8.09 (s, 1H), 7.65–7.71 (m, 6H), 7.53–7.48 (m, 5H), 7.48 (t, $J=7.5$ Hz, 1H), 6.69–6.61 (m, 3H), 4.12–4.16(m, 4H),

Chapter 5. Synthesis and Characterization of the designed analogues

3.71 (s, 3H), 3.55 (s, 3H), 2.55 (s, 3H). ESI MS (m/z): calculated for C₃₁H₂₉ClN₄O₂, 524.20 found 525.43 [M+H]⁺, 526.33 [M+2]⁺

(6-chloro-1-(4-methoxyphenyl)-9-methyl-9H-pyrido-[3,4-b]-indol-3-yl) (4-(4-methoxyphenyl)-piperazin-1-yl)-methanone (104): White solid, Yield 68%, Melting point 135-136 °C, IR ν_{max} /cm: 3042, 1663, 1538, 775, ¹H NMR (400 MHz, Chloroform-*d*): δ 8.70 (s, 1H), 8.63 (d, *J* = 7.5, 1.5 Hz, 1H), 7.70 – 7.64 (m, 2H), 7.65 – 7.55 (m, 2H), 7.37 – 7.40 (m, 3H), 6.69 – 6.59 (m, 3H), 4.06 – 3.91 (m, 4H), 3.88 (s, 3H), 3.74 (s, 3H), 2.62 (s, 3H), 3.18. (d, *J* = 30.1 Hz, 4H). ESI MS (m/z): calculated for C₃₁H₂₉ClN₄O₃, 540.19 found 541.53 [M+H]⁺, 542.33 [M+2]⁺

(6-chloro-1-(4-chlorophenyl)-9-methyl-9H-pyrido-[3,4-b]-indol-3-yl) (4-(p-tolyl)-piperazin-1-yl)-methanone (105): White solid, Yield 52%, Melting point 131-133 °C, IR ν_{max} /cm: 3034, 1678, 1558, 728, ¹H NMR (400 MHz, Chloroform-*d*): δ 8.16 (s, 1H), 7.66–7.62 (m, 3H), 7.56–7.54 (m, 5H), 7.46 (d, *J*=8.3 Hz, 1H), 7.36 (t, *J*=7.5 Hz, 1H), 7.25 (t, *J*=8.0 Hz, 1H), 6.62–6.48 (m, 4H), 4.13–4.07 (m, 4H), 3.80 (s, 3H), 2.80 (s, 3H). ESI MS (m/z): calculated for C₃₀H₂₆Cl₂N₄O, 528.15 found 529.17 [M+H]⁺, 530.33 [M+2]⁺, 532.23 [M+4]⁺

(6-chloro-1-(4-chlorophenyl)-9-methyl-9H-pyrido-[3,4-b]-indol-3-yl) (4-(4-methoxyphenyl)-piperazin-1-yl)-methanone (106): White solid, Yield 66%, Melting point 135-136 °C, IR ν_{max} /cm: 3022, 1626, 1558, 737, ¹H NMR (400 MHz, Chloroform-*d*): δ 8.60 (s, 1H), 8.59 (d, *J* = 7.0, 1.5 Hz, 1H), 7.78 – 7.72 (m, 2H), 7.40 – 7.40 (m, 2H), 7.17 – 7.10 (m, 3H), 6.64 – 6.55 (m, 3H), 4.04 – 3.91 (m, 4H), 3.87 (s, 3H), 3.72 (s, 3H), 3.18. (d, *J* = 30.1 Hz, 4H). ESI MS (m/z): calculated for C₃₀H₂₆Cl₂N₄O₂, 544.14 found 545.16 [M+H]⁺, 546.11 [M+2]⁺, 548.33 [M+4]⁺

(6-chloro-1-(4-chlorophenyl)-9-methyl-9H-pyrido-[3,4-b]-indol-3-yl) (4-(2-fluorophenyl)-piperazin-1-yl)-methanone (107): White solid, Yield 62%, Melting point 146-148 °C, IR ν_{max} /cm: 3042, 1666, 1538, 713, ¹H NMR (400 MHz, Chloroform-*d*): δ 8.06 (s, 1H), 7.65–7.61 (m, 5H), 7.53–7.48 (m, 5H), 7.48 (t, *J*=7.5 Hz, 1H), 6.69–6.61 (m, 4H), 4.12–4.16 (m, 5H), 3.71 (s, 3H). ESI MS (m/z): calculated for C₂₉H₂₃Cl₂FN₄O, 532.12 found 533.47 [M+H]⁺, 534.55 [M+2]⁺, 536.43 [M+4]⁺

(6-chloro-1-(4-chlorophenyl)-9-methyl-9H-pyrido-[3,4-b]-indol-3-yl) (4-phenylpiperazin-1-yl)-methanone (108): White solid, Yield 63%, Melting point 138-140 °C, IR ν_{max} /cm: 3053, 1676, 1558, 721, ¹H NMR (400 MHz, Chloroform-*d*): δ 8.79 (s, 1H), 8.66 (d, *J* = 7.5, 1.5 Hz, 1H), 7.70 – 7.69 (m, 3H), 7.68 – 7.64 (m, 2H), 7.37 – 7.39 (m, 3H), 6.69 – 6.59 (m, 3H), 4.06

Chapter 5. Synthesis and Characterization of the designed analogues

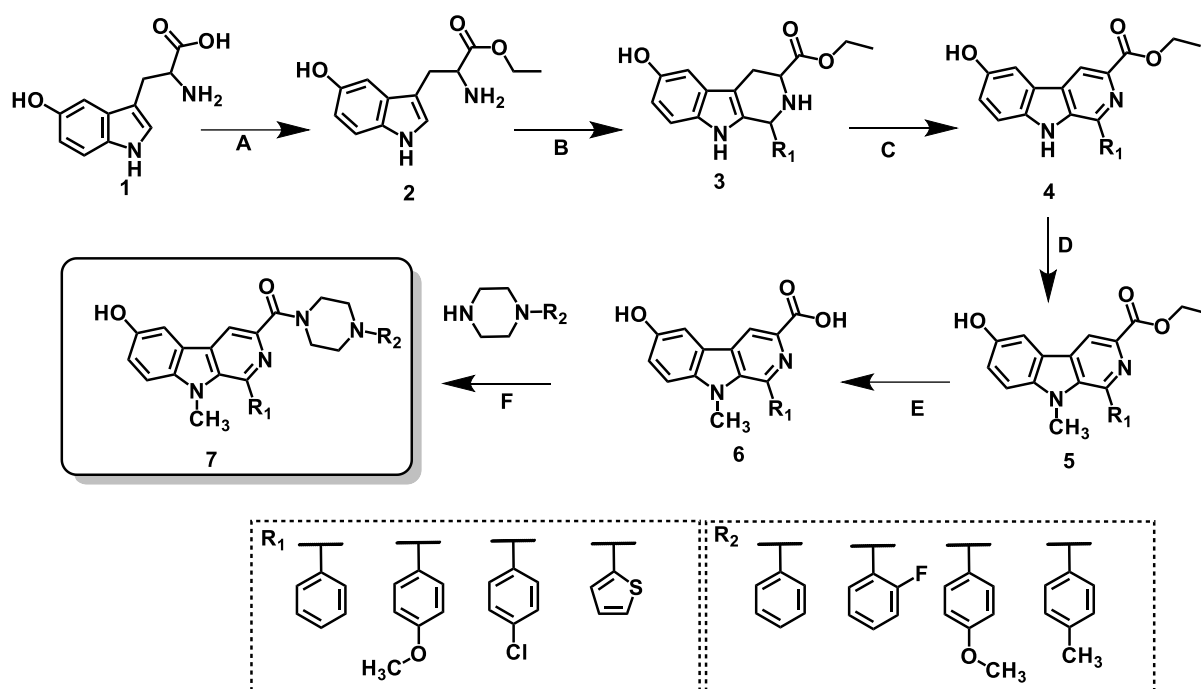
– 3.81 (m, 4H), 2.68 (s, 3H), 3.18. (d, $J = 30.1$ Hz, 4H). ESI MS (m/z): calculated for $C_{29}H_{24}Cl_2N_4O$, 514.13 found 515.47 $[M+H]^+$, 516.34 $[M+2]^+$

(6-chloro-9-methyl-1-(thiophen-2-yl)-9H-pyrido-[3,4-b]-indol-3-yl)(4-phenylpiperazin-1-yl)-methanone (109): White solid, Yield 59%, Melting point 137-139 °C, IR ν_{max}/cm : 3152, 1676, 1558, 723, 1H NMR (400 MHz, Chloroform-*d*): δ 8.58 (s, 1H), 7.79-7.53 (m, 6H), 7.30-7.27 (m, 5H), 6.74 (t, $J = 11.7$ Hz, 2H), 4.03-3.93 (m, 5H), 3.78 (s, 3H), 3.72 (s, 3H). ESI MS (m/z): calculated for $C_{27}H_{23}ClN_4OS$, 486.13 found 487.20 $[M+H]^+$, 488.23 $[M+2]^+$

(6-chloro-9-methyl-1-(thiophen-2-yl)-9H-pyrido-[3,4-b]-indol-3-yl) (4-(2-fluorophenyl)-piperazin-1-yl)-methanone (110): White solid, Yield 63%, Melting point 155-157 °C, IR ν_{max}/cm : 3120, 1636, 1588, 719, 1H NMR (400 MHz, Chloroform-*d*): δ 8.25 (s, 1H), 7.67-7.57 (m, 6H), 7.42-7.37 (m, 5H), 6.87 (t, $J = 11.7$ Hz, 2H), 4.63-3.83 (m, 5H), 3.77 (s, 3H). ESI MS (m/z): calculated for $C_{27}H_{22}ClFN_4OS$, 504.12 found 505.40 $[M+H]^+$, 506.66 $[M+2]^+$

(6-chloro-9-methyl-1-(thiophen-2-yl)-9H-pyrido-[3,4-b]-indol-3-yl)(4-(p-tolyl)-piperazin-1-yl)-methanone (111): White solid, Yield 68%, Melting point 137-139 °C, IR ν_{max}/cm : 3462, 1676, 1598, 729, 1H NMR (400 MHz, Chloroform-*d*): δ 8.24 (s, 1H), 7.69-7.49 (m, 6H), 7.40-7.33 (m, 6H), 6.86 (t, $J = 11.7$ Hz, 2H), 4.03-3.86 (m, 6H), 3.76 (s, 3H), 2.32(s, 3H). ESI MS (m/z): calculated for $C_{28}H_{25}ClN_4OS$, 500.14 found 501.48 $[M+H]^+$, 502.23 $[M+2]^+$

(6-chloro-9-methyl-1-(thiophen-2-yl)-9H-pyrido-[3,4-b]-indol-3-yl) (4-(4-methoxyphenyl)-piperazin-1-yl)-methanone (112): White solid, Yield 73%, Melting point 147-149 °C, IR ν_{max}/cm : 3042, 1656, 1538, 719, 1H NMR (400 MHz, Chloroform-*d*): δ 8.18 (s, 1H), 7.89-7.57 (m, 6H), 7.48-7.30 (m, 5H), 6.79 (t, $J = 11.7$ Hz, 2H), 4.05-3.87 (m, 5H), 3.79 (s, 3H), 3.52(s, 3H). ESI MS (m/z): calculated for $C_{28}H_{25}ClN_4O_2S$, 516.14 found 517.48 $[M+H]^+$, 518.44 $[M+2]^+$



Scheme 8: Reagents and conditions: (A) SOCl_2 , ethanol, 0 °C, reflux, 1 h (B) Aromatic aldehydes, trifluoroacetic acid, DCM, rt, 3 h (C) Sulfur, xylene, 100 °C, reflux 24 h (D) Methyl iodide, KOH, DMSO, rt, 30 min (E) NaOH, ethanol: water (1:1), rt, 45 min (F) THF, EDCI, HCl, HOBt, Phenyl piperazine, rt, overnight

Characterized data for 6-hydroxy-9-methyl substituted compounds of scheme 8:

(6-hydroxy-9-methyl-1-phenyl-9H-pyrido-[3,4-b]-indol-3-yl) (4-(p-tolyl)piperazin-1-yl)-methanone (113): White solid, Yield 65%, Melting point 160-162 °C, IR $\nu_{\text{max}}/\text{cm}$: 3244, 1615, 1547, 1511, 1256, $^1\text{H NMR}$ (400 MHz, Chloroform-*d*) 8.65 (s, 1H), δ 7.5 – 7.38 (m, 9H), 7.02 – 6.89 (m, 3H), 3.82 (s, 3H), 3.79 (s, 3H) 2.10 – 2.05 (m, 1H), 1.36 – 1.21 (m, 8H). ESI MS (*m/z*): calculated for $\text{C}_{30}\text{H}_{28}\text{N}_4\text{O}_2$, 462.21, found 463.25 $[\text{M}+\text{H}]^+$

(4-(2-fluorophenyl)-piperazin-1-yl) (6-hydroxy-9-methyl-1-phenyl-9H-pyrido-[3,4-b]-indol-3-yl)-methanone (114): Yellow solid, Yield 61%, Melting point 150-152 °C, IR $\nu_{\text{max}}/\text{cm}$: 3220, 1612, 1558, 1520, 748, $^1\text{H NMR}$ (400 MHz, Chloroform-*d*) 8.57 (s, 1H), 8.09 (d, $J = 7.5, 1.0$ Hz, 1H), 7.88 – 7.82 (m, 2H), 7.53 – 7.45 (m, 3H), 7.30 – 7.24 (m, 1H), 7.07 – 7.02 (m, 3H), 6.84 – 6.75 (m, 2H), 4.04 – 3.91 (m, 4H), 3.84 (s, 3H), 3.18. (d, $J = 30.1$ Hz, 4H). ESI MS (*m/z*): calculated for $\text{C}_{29}\text{H}_{25}\text{FN}_4\text{O}_2$, 480.20, found 481.29 $[\text{M}+\text{H}]^+$

(6-hydroxy-9-methyl-1-phenyl-9H-pyrido-[3,4-b]-indol-3-yl) (4-(4-methoxyphenyl)-piperazin-1-yl)-methanone (115): Pale yellow solid, Yield 58%, Melting point 160-162 °C, IR $\nu_{\text{max}}/\text{cm}$: 3260, 1614, 1537, 1521, $^1\text{H NMR}$ (400 MHz, Chloroform-*d*) δ 8.54 (s, 1H), 7.45 – 7.30 (m, 9H), 7.05 – 6.98 (m, 4H), 3.90 (s, 3H), 3.8 (s, 3H), 2.10 – 2.05 (m, 3H), 1.37 – 1.28 (m, 5H). ESI MS (*m/z*): calculated for $\text{C}_{30}\text{H}_{28}\text{N}_4\text{O}_3$, 492.22, found 493.47 $[\text{M}+\text{H}]^+$

(6-hydroxy-9-methyl-1-phenyl-9H-pyrido-[3,4-b]-indol-3-yl) (4-phenylpiperazin-1-yl)-methanone (116): White solid, Yield 61%, Melting point 158-160 °C, IR $\nu_{\text{max}}/\text{cm}$: 3262, 1614, 1550, 1508, 1521, ^1H NMR (400 MHz, Chloroform-*d*) δ 8.82 (s, 1H), 8.47 (s, 1H), 8.17 (d, $J = 7.9$ Hz, 1H), 8.01-7.98 (m, 2H), 7.64-7.51 (m, 5H), 7.38-7.34 (m, 1H), 7.08-7.04 (m, 1H), 7.01-6.90 (m, 3H), 4.20- 4.10 (m, 4H), 3.85 (s, 3H), 3.25-3.16 (m, 4H). ^{13}C NMR (101 MHz, Chloroform-*d*) δ 173.64, 152.21, 151.68, 147.24, 146.78, 147.12, 129.23, 126.64, 128.14, 115.35, 113.35, 55.80, 26.60. ESI MS (m/z): calculated for $\text{C}_{29}\text{H}_{26}\text{N}_4\text{O}_2$, 462.21, found 463.78 $[\text{M}+\text{H}]^+$

(6-hydroxy-1-(4-methoxyphenyl)-9-methyl-9H-pyrido-[3,4-b]-indol-3-yl) (4-phenylpiperazin-1-yl)-methanone (117): White solid, Yield 59%, Melting point 168-170 °C, IR $\nu_{\text{max}}/\text{cm}$: 3263, 1656, 1541, 1508, ^1H NMR (400 MHz, Chloroform-*d*) δ 8.85 (s, 1H), 8.64 (s, 1H), 8.12 (d, $J = 7.8$ Hz, 1H), 8.01-7.91 (m, 3H), 7.65-7.54 (m, 4H), 7.54 (t, $J = 7.4$ Hz, 1H), 7.38-7.31 (m, 1H), 7.22-7.20 (m, 2H), 7.11-7.00 (m, 3H), 4.10-4.00 (m, 4H), 3.38 (s, 3H), 3.10-3.01 (m, 4H). ESI MS (m/z): calculated for $\text{C}_{30}\text{H}_{28}\text{N}_4\text{O}_3$, 492.22, found 493.46 $[\text{M}+\text{H}]^+$

(4-(2-fluorophenyl)-piperazin-1-yl) (6-hydroxy-1-(4-methoxyphenyl)-9-methyl-9H-pyrido-[3,4-b]-indol-3-yl)-methanone (118): White solid, Yield 62%, Melting point 160-162 °C, IR $\nu_{\text{max}}/\text{cm}$: 3182, 1610, 1556, 1498, 750, ^1H NMR (400 MHz, Chloroform-*d*) 8.0 (s, 1H), 8.05- 8.09 (m, 2H), 7.88 – 7.82 (m, 2H), 7.53 – 7.45 (m, 2H), 7.30 – 7.24 (m, 1H), 7.07 – 7.02 (m, 3H), 6.84 – 6.75 (m, 4H), 4.04 – 3.91 (m, 5H), 3.84 (s, 3H), 3.18. (d, $J = 30.1$ Hz, 4H). ESI MS (m/z): calculated for $\text{C}_{30}\text{H}_{27}\text{FN}_4\text{O}_3$, 510.21, found 511.47 $[\text{M}+\text{H}]^+$

(6-hydroxy-1-(4-methoxyphenyl)-9-methyl-9H-pyrido-[3,4-b]-indol-3-yl)(4-(p-tolyl)piperazin-1-yl)-methanone (119): White solid, Yield 51%, Melting point 148-150 °C, IR $\nu_{\text{max}}/\text{cm}$: 3172, 1620, 1540, 1440, ^1H NMR (400 MHz, Chloroform-*d*) 8.81 (s, 1H), 8.0- 8.10 (m, 3H), 7.88 – 7.86 (m, 2H), 7.43 – 7.48 (m, 2H), 7.30 – 7.24 (m, 3H), 7.07 – 7.02 (m, 3H), 6.84 – 6.75 (m, 2H), 4.00 – 3.81 (m, 4H), 3.80 (s, 3H), 3.84 (s, 3H), 3.18. (d, $J = 31.1$ Hz, 4H). ESI MS (m/z): calculated for $\text{C}_{31}\text{H}_{30}\text{N}_4\text{O}_3$, 506.23, found 507.46 $[\text{M}+\text{H}]^+$

(6-hydroxy-1-(4-methoxyphenyl)-9-methyl-9H-pyrido-[3,4-b]-indol-3-yl) (4-(4-methoxyphenyl)-piperazin-1-yl)-methanone (120): White solid, Yield 59%, Melting point 161-163 °C, IR $\nu_{\text{max}}/\text{cm}$: 3163, 1642, 1545, 1419, ^1H NMR (400 MHz, Chloroform-*d*) δ 11.70 (s, 1H), 8.44- 8.49 (m, 3H), 8.26-8.19 (m, 2H), 8.09-8.06 (m, 2H), 7.69-7.53 (m, 6H), 7.30-7.27 (m, 1H), 6.84 (t, $J = 11.7$ Hz, 2H), 4.03-3.93 (m, 4H), 3.80 (s, 3H), 3.85 (s, 3H), 3.57-3.51 (m, 3H). ESI MS (m/z): calculated for $\text{C}_{31}\text{H}_{30}\text{N}_4\text{O}_4$, 522.13 found 523.47 $[\text{M}+\text{H}]^+$

(1-(4-chlorophenyl)-6-hydroxy-9-methyl-9H-pyrido-[3,4-b]-indol-3-yl) (4-phenylpiperazin-1-yl)-methanone (121): White solid, Yield 62%, Melting point 159-161 °C, IR $\nu_{\text{max}}/\text{cm}$: 3153, 1652, 1515, 1469;720, $^1\text{H NMR}$ (400 MHz, Chloroform-*d*) δ 8.20 (s, 1H), 7.5 – 7.38 (m, 8H), 7.02 – 6.89 (m, 3H), 3.10-3.01 (m, 4H), 3.80 (s, 3H), 2.10 – 2.05 (m, 2H), 1.36 – 1.21 (m, 4H). ESI MS (m/z): calculated for $\text{C}_{29}\text{H}_{25}\text{ClN}_4\text{O}_2$, 496.17, found 497.26 $[\text{M}+\text{H}]^+$, 498.44 $[\text{M}+2]^+$

(1-(4-chlorophenyl)-6-hydroxy-9-methyl-9H-pyrido-[3,4-b]-indol-3-yl) (4-(2-fluorophenyl)-piperazin-1-yl)-methanone (122): White solid, Yield 68%, Melting point 165-167 °C, IR $\nu_{\text{max}}/\text{cm}$: 3160, 1672, 1568, 1520,760, $^1\text{H NMR}$ (400 MHz, Chloroform-*d*) 8.57 (s, 1H), 8.10- 8.15 (m,2H), 7.88 – 7.82 (m, 3H), 7.53 – 7.45 (m, 2H), 7.30 – 7.34 (m, 1H), 7.07 – 7.02 (m, 3H), 6.84 – 6.75 (m, 2H), 4.04 – 3.81 (m, 3H), 3.85 (s, 3H), 3.18. (d, $J = 30.1$ Hz, 4H). ESI MS (m/z): calculated for $\text{C}_{29}\text{H}_{24}\text{ClFN}_4\text{O}_2$, 514.12, found 515.46 $[\text{M}+\text{H}]^+$, 516.33 $[\text{M}+2]^+$

(6-hydroxy-9-methyl-1-(thiophen-2-yl)-9H-pyrido-[3,4-b]-indol-3-yl) (4-phenylpiperazin-1-yl)-methanone (123): White solid, Yield 58%, Melting point 160-162 °C, IR $\nu_{\text{max}}/\text{cm}$: 3381, 1634, 1512, 1481, 1257, $^1\text{H NMR}$ (400 MHz, Chloroform-*d*) δ 8.61 (s, 1H), 8.37 (s,1H), 8.10 (d, $J = 7.0, 1.0$ Hz, 1H), 7.78 – 7.86 (m, 2H), 7.53 – 7.45 (m, 3H), 7.30 – 7.24 (m, 2H), 7.09 – 7.02 (m, 2H), 6.85 – 6.75 (m, 2H), 4.04 – 3.94 (m, 3H), 3.85 (s, 3H), .18. (d, $J = 30.1$ Hz, 4H). ESI MS (m/z): calculated for $\text{C}_{27}\text{H}_{24}\text{N}_4\text{O}_2\text{S}$, 468.16, found 469.15 $[\text{M}+\text{H}]^+$

(6-hydroxy-9-methyl-1-(thiophen-2-yl)-9H-pyrido-[3,4-b]-indol-3-yl) (4-(p-tolyl)-piperazin-1-yl)-methanone (124): White solid, Yield 61%, Melting point 170-172 °C, IR $\nu_{\text{max}}/\text{cm}$: 3157, 1629, 1550, 1492, 1234, 740, $^1\text{H NMR}$ (400 MHz, Chloroform-*d*) δ 8.74 (s, 1H), 8.46 (s, 1H), 8.17 (d, $J = 7.9$ Hz, 1H), 7.98-7.89 (m, 2H), 7.64-7.54 (m, 2H), 7.38-7.34 (m, 1H), 7.27-7.23 (m, 2H), 7.17-7.12 (m, 2H), 6.92- 6.87 (m, 2H), 4.12-4.02 (m, 4H), 3.93 (s, 3H), 3.89 (s, 3H), 3.33-3.26 (m, 2H). ESI MS (m/z): calculated for $\text{C}_{28}\text{H}_{26}\text{N}_4\text{O}_2\text{S}$, 482.18 found 483.49 $[\text{M}+\text{H}]^+$

(4-(2-fluorophenyl)-piperazin-1-yl) (6-hydroxy-9-methyl-1-(thiophen-2-yl)-9H-pyrido-[3,4-b]-indol-3-yl)-methanone (125): White solid, Yield 59 %, Melting point 140-142 °C, IR $\nu_{\text{max}}/\text{cm}$: 3223, 1622, 1508, 1431, 1234, 744, $^1\text{H NMR}$ (400 MHz, Chloroform-*d*) δ 8.78 (s, 1H), 8.44 (s, 1H), 8.18 (d, $J = 7.6$ Hz, 1H), 7.80-7.84 (m 2H), 7.74 (d, $J = 7.8$ Hz, 1H), 7.62-7.56 (m, 2H), 7.38-7.34 (m, 2H), 7.15-7.08 (m, 2H), 7.03-6.97 (m, 2H), 4.19-4.00 (m, 3H), 3.95 (s, 3H), 3.26-3.17 (m, 4H). ESI MS (m/z): calculated for $\text{C}_{27}\text{H}_{23}\text{FN}_4\text{O}_2\text{S}$, 486.15, found 487.46 $[\text{M}+\text{H}]^+$

(6-hydroxy-9-methyl-1-(thiophen-2-yl)-9H-pyrido-[3,4-b]-indol-3-yl) (4-(4-methoxyphenyl)-piperazin-1-yl)-methanone (126): White solid, Yield 60%, Melting point 170-172 °C, IR $\nu_{\text{max}}/\text{cm}$: 3233, 1672, 1548, 1471, 750, ^1H NMR (400 MHz, Chloroform-*d*) 8.64 (s, 1H), 8.12 (s, 1H), 8.01-7.91 (m, 2H), 7.65-7.54 (m, 4H), 7.54 (t, $J = 7.4$ Hz, 1H), 7.38-7.31 (m, 1H), 7.22-7.20 (m, 2H), 7.11-7.00 (m, 2H), 4.10-4.00 (m, 4H), 3.38 (s, 3H), 3.29 (s, 3H), 3.10-3.01 (m, 3H). ESI MS (m/z): calculated for $\text{C}_{28}\text{H}_{26}\text{N}_4\text{O}_3\text{S}$, 498.17, found 499.76 $[\text{M}+\text{H}]^+$

(1-(4-chlorophenyl)-6-hydroxy-9-methyl-9H-pyrido-[3,4-b]-indol-3-yl) (4-phenylpiperazin-1-yl)-methanone (127): White solid, Yield 68%, Melting point 165-167 °C, IR $\nu_{\text{max}}/\text{cm}$: 3164, 1672, 1568, 1540, 730, ^1H NMR (400 MHz, Chloroform-*d*) 8.54 (s, 1H), 8.10- 8.15 (m, 2H), 7.88 – 7.82 (m, 3H), 7.53 – 7.45 (m, 2H), 7.30 – 7.34 (m, 1H), 7.07 – 7.22 (m, 3H), 6.84 – 6.75 (m, 2H), 4.04 – 3.81 (m, 4H), 3.38 (s, 3H), 3.18. (d, $J = 30.1$ Hz, 4H). ESI MS (m/z): calculated for $\text{C}_{29}\text{H}_{25}\text{ClN}_4\text{O}_2$, 496.17, found 497.26 $[\text{M}+\text{H}]^+$, 498.44 $[\text{M}+2]^+$

(1-(4-chlorophenyl)-6-hydroxy-9-methyl-9H-pyrido-[3,4-b]-indol-3-yl) (4-(4-methoxyphenyl)-piperazin-1-yl)-methanone (128): White solid, Yield 59%, Melting point 180-182 °C, IR $\nu_{\text{max}}/\text{cm}$: 3163, 1642, 1545, 1419, ^1H NMR (400 MHz, Chloroform-*d*) δ 11.70 (s, 1H), 8.26-8.19 (m, 2H), 8.09-8.06 (m, 2H), 7.69-7.53 (m, 5H), 7.30-7.27 (m, 1H), 6.84 (t, $J = 11.7$ Hz, 2H), 4.03-3.93 (m, 4H), 3.80 (s, 3H), 3.57-3.51 (m, 4H) 3.48 (s, 3H). ^{13}C NMR (101 MHz, Chloroform-*d*) δ 169.64, 156.81, 151.62, 146.23, 145.79, 142.11, 128.23, 120.64, 120.14, 115.23, 111.35, 58.90, 58.60. ESI MS (m/z): calculated for $\text{C}_{30}\text{H}_{27}\text{ClN}_4\text{O}_3$, 526.18 found 527.49 $[\text{M}+\text{H}]^+$, 528.44 $[\text{M}+2]^+$

Chapter 5. Synthesis and Characterization of the designed analogues

References:

- (1) Ashok penta, T. *Synthesis, Study of Some Novel β -Carboline Derivatives as Potential Agents Against HIV and Associated Infections*; 2015. Ph. D thesis.
- (2) Ashok, P.; Chander, S.; Smith, T. K.; Sankaranarayanan, M. Design, Synthesis and Biological Evaluation of Piperaziny- β -Carbolinederivatives as Anti-Leishmanial Agents Penta. *European Journal of Medicinal Chemistry* **2018**, *150*, 559–566. <https://doi.org/10.1016/j.ejmech.2018.03.022>.
- (3) Ashok, P.; Chander, S.; Chow, L. M. C.; Wong, I. L. K.; Singh, R. P.; Jha, P. N.; Sankaranarayanan, M. Synthesis and In-Vitro Anti-Leishmanial Activity of (4-Arylpiperazin-1-Yl)(1-(Thiophen-2-Yl)-9H-Pyrido[3,4-b]Indol-3-Yl)Methanone Derivatives. *Bioorganic Chemistry* **2017**, *70*, 100–106. <https://doi.org/10.1016/j.bioorg.2016.11.013>.
- (4) Kumar, B. K.; Faheem; Fouce, R. B.; Melcon-Fernandez, E.; Yolanda, Y. P.-P.; Reguera, R. M.; Adinarayana, N.; Sekhar, K. V. G. C.; Vanaparthi, S.; Murugesan, S. Design, Synthesis and Evaluation of Novel β -Carboline Ester Analogues as Potential Anti-Leishmanial Agents. *Journal of Biomolecular Structure and Dynamics* **2022**, *40* (23), 12592–12607. <https://doi.org/10.1080/07391102.2021.1973564>.



**Chapter 6. Anti-leishmanial, Cell viability and
Trypanothione reductase inhibition assay**



Anti-Leishmanial screening

Experimental and Methodology:

All the synthesized compounds were *in-vitro* evaluated for their potency against leishmaniasis. In the first stage, the compounds were tested against Promastigote forms of *L. infantum* BCN150 iRFP (iRFP-*L. infantum*), this was the first stage in the life cycle of leishmaniasis. Secondly, the same compounds were also screened against Amastigote forms as well. This stage plays a vital role in the replication of leishmaniasis and its fatal nature. Finally, the titled test compounds were causing any damage to the normal cells or not were confirmed by Cell viability screening against standard human hepatocarcinoma cell HepG2 line (ATCC HB-8065). The detailed methodology is described below

6.1. Promastigotes proliferation assay:

All compounds were assayed *in vitro* against *L. infantum* BCN150 iRFP promastigotes (iRFP-*L. infantum*), a genetically modified strain that constitutively produces the infrared fluorescent protein (iRFP) for near infrared detection ¹. Promastigotes were cultured in M199 medium (Gibco), supplemented with 25 mM HEPES pH 6.9, 7.6 mM hemin, 10 mM glutamine, 0.1 mM adenosine, 0.01 mM folic acid, 1xRPMI 1640 vitamin mix (Sigma), 10% (v/v) heat inactivated foetal bovine serum (FBS) (Gibco) and antibiotic cocktail (50 U/mL penicillin and 50 µg/mL streptomycin). Cultures of iRFP-*L. infantum* promastigotes with a density of 1×10^6 cells/mL, were dispensed into 96-well optical bottom black plates (Thermo Scientific), 180 µL per well. Each compound was tested adding 20 µL of different stock solutions to the inoculated wells. Stock solutions were prepared in DMSO and serially diluted in M199 media (0.01-200 µM final concentrations). The viability of promastigotes to calculate the 50% effective concentration (EC₅₀) values was assessed measuring their fluorescence at 713 nm in an Odyssey (Li-Cor) infrared imaging system after 72 h exposure at 26 °C. All compounds and controls were assayed by triplicate. Plots were fitted by non-linear analysis using Sigma Plot 10.1 statistical package ².

6.2. *Ex vivo* murine splenic explant cultures (Amastigotes assay):

Primary infected splenic explants were obtained inoculating intraperitoneally 10^8 iRFP-*L. infantum* metacyclic promastigotes to female BALB/c mice. After five weeks, mice were humanely sacrificed and spleens were aseptically dissected, washed with cold phosphate-buffered saline (PBS), cut into small pieces and incubated with 5 mL of 2 mg/mL collagenase D (Sigma) prepared in buffer (10 mM HEPES, pH 7.4, 150 mM NaCl, 5 mM KCl, 1 mM MgCl₂ and 1.8 mM CaCl₂) for 20 min, to obtain a cell suspension. The cell suspension was

Chapter 6. Anti-leishmanial, Cell viability, and Trypanothione reductase assay

passed through a 100 μM -mesh cell strainer, harvested by centrifugation (500 \times g for 7 min at 4 °C), washed twice with PBS and re-suspended in RPMI medium (Gibco), supplemented with 10 mM HEPES, 1 mM sodium pyruvate, 1xRPMI 1640 vitamin mix, 10% (v/v) FBS and antibiotics cocktail. Different concentrations of the tested compounds (0.01–200 μM) were added to these cultures seeded in 384-well black optical bottom plates at 37 °C under 5% CO₂ atmosphere. The viability of iRFP-*L. infantum* amastigotes infecting macrophages was calculated by recording the fluorescence at 713 nm by an Odyssey (Li- Cor) infrared imaging system. The EC₅₀ value was calculated by plotting the infrared fluorescence emitted by viable amastigotes against different concentrations of the tested compounds after 72 h of exposure. Plots were fitted by non-linear analysis using the Sigma Plot 10.1 statistical package ².

6.3. Cell viability and selectivity index (SI) determination:

To determine the selectivity of the tested compounds, BALB/c splenocytes obtained from uninfected animals and isolated as described above has been used. On the other hand, the cell viability of each compound was tested on standard human hepatocarcinoma cell HepG2 lines (ATCC HB-8065) as a suitable *in vitro* toxicity model system of human hepatocytes. HepG2 cells were seeded in 96-well plates at 37 °C under 5% CO₂ atmosphere. The Glutamax Dulbecco's Modified Eagle's Medium (DMEM, Gibco) was used as cultured medium, supplemented with 10% (v/v) FBS and antibiotics cocktail. Serial dilutions of each compound ranging from 0.01 to 200 μM were added to the cultures of both mouse splenocytes and HepG2 cells, after 72 h of exposure, the reading was measured using Alamar Blue staining method, according to manufacturer's recommendations (Invitrogen). The resulting plots of cell viability vs concentration of each compound was adjusted by non-linear analysis using Sigma Plot 10.1 statistical package and used to calculate the 50% cytotoxic concentration (CC₅₀). Selectivity index (SI) for both promastigotes (Selectivity index of Promastigotes (SIP)) and amastigotes (Selectivity index of Amastigotes (SIA)) for each compound was calculated as the ratio between CC₅₀ values obtained to that of EC₅₀ values for promastigotes and obtained EC₅₀ values with *ex vivo* murine splenic explant cultures, respectively².

6.4. Experimental procedure for TR inhibition assay:

Trypanothione (TS2) was purchased from Bachem, Switzerland. Glutathione sepharose-4B resin and thrombin were purchased from GE Healthcare Bio-Sciences Ltd. All other chemicals of the highest purity were purchased from Sigma Chemical Co. Stock solutions (10 mM) of the inhibitors were made in DMSO and stored at -20 °C.

Chapter 6. Anti-leishmanial, Cell viability, and Trypanothione reductase assay

Recombinant *L. infantum* trypanothione reductase (LITR) was expressed in *E. coli* BL21 (DE3) and purified to homogeneity. Purity was checked by SDS-PAGE method. Enzyme activity was measured according to the method of Hamilton et al.³ in presence of oxidized trypanothione (TS₂). Briefly, the reaction mixture contained *L. infantum* TR (1 m-unit), 40 mM HEPES pH 7.5, 1 mM EDTA, 0.15 mM NADPH, 25 μM DTNB and 5 Mm TS₂. The reaction was initiated by the addition of oxidized trypanothione and the change in optical density (OD) was monitored at 412 nm using SpectraMax M2 (Molecular Devices) microplate reader. The protein concentration was determined by Bradford method⁴ using bovine serum albumin (BSA) as the standard. Primary screening of compounds for their inhibitory activity against LITR was performed at varied concentrations (10 – 100 μM) of the compound(s). The compounds were added to enzyme in reaction mixture 5 min prior to the addition of substrate. Control assays containing the respective amount of DMSO were carried out where appropriate. The compounds exhibiting dose dependent inhibition were evaluated further for their type of inhibition and inhibitory constant⁵. The effect of test compounds on the enzyme activity was determined at two substrate concentrations (50 and 100 μM) and over a range of inhibitor concentrations.

β-carbolines are known to exert their antileishmanial activity via the following mechanisms.

6.5. Inhibition of trypanothione reductase (amastigote forms):

The leishmanial parasite proliferates inside the macrophage cells and still protects itself from the wrathful effects of free radicals generated by macrophage cells. Like the host's glutathione / glutathione reductase redox system, the parasite utilizes trypanothione / trypanothione reductase peroxidase system to neutralize the free radicals. Trypanothione TS₂ that has been synthesized from two substrates glutathione and spermidine using the enzyme trypanothione synthetase (TS). The trypanothione (TS₂) is kept in its reduced form T(SH)₂ by Trypanothione Reductase (TR). T(SH)₂ is, in turn, used to reduce tryparedoxin (TXNSH) into its reduced form TXN(SH)₂. Tryparedoxin peroxidase (TXNP) neutralizes the free radicals generated by the macrophage cells, thus providing a favourable environment for the growth of the parasite.

Trypanothione reductase is a homodimer in which each subunit is formed by three domains, namely NADPH binding domain, FAD-binding domain, and interface domain. The trypanothione binding site is placed at the interface between FAD-binding domain and interface domain. The active site of trypanothione reductase has an overall net negative charge to attract the positively charged trypanothione and repel the negatively charged glutathione.

Chapter 6. Anti-leishmanial, Cell viability, and Trypanothione reductase assay

CYS52, CYS57, HIS461 and GLU466 are the essential conserved amino acid residues that are involved in the catalytic process. Chauhan et al. designed a series of **β -carboline**-quinazoline hybrids as inhibitors of trypanothione reductase ⁵.

6.6. Alterations in the cell division cycle (promastigote forms):

Barea et al. synthesized and evaluated novel **β -carboline**-1,3,5-triazine hybrids against both promastigote and amastigote forms of the leishmanial parasite (Barea et al., 2018). The titled compounds were found to exhibit potent activity against amastigote forms of the parasite. Further studies were conducted to elucidate the mechanism of action of compounds. Electron microscopic analysis of promastigotes following 72 h of treatment with one of the compounds showed an increase in lipid-storage bodies, alterations in mitochondria and plasma membrane. The authors postulated that the increase in lipid-storage level may be because of cellular stress and mitochondrial dysfunction, which ultimately culminated in cell death via apoptotic pathways ⁶.

Findings and discussions:

The biological screening including anti-leishmanial evaluation of the synthesized analogues was performed in the following stages:

- A. Promastigote screening
- B. Amastigote screening
- C. Cell viability determination
- D. Selectivity index determination
- E. Structure Activity Relationship (SAR) studies
- F. Trypanothione reductase inhibition assay

Anti-leishmanial screening conclusions:

The anti-leishmanial screening results of the titled compounds showed a significant inhibition activity against both promastigote forms of *L. infantum* (BCN150 iRFP (iRFP-*L. infantum*) and amastigote forms. The results were quite interesting that some of the compounds screened revealed the best results when compared to the standard drug Miltefosine.



Miltefosine

EC₅₀ against *L. Infantum*
EC₅₀ = 12.6 ± 1.1 μM (Promastigotes)
EC₅₀ = 4.8 ± 0.8 μM (Amastogotes)

A. Promastigote screening results:

Parasites of the genus *Leishmania* are dimorphic, existing in two forms: the flagellated (promastigote) form that lives and multiplies in the digestive tracts of sand flies and the aflagellated (amastigote) form that replicates in the cells of mammals. After the sandflies bite, the promastigotes make it to a puncture wound and macrophages and other mononuclear phagocytic cells engulf them.

The synthesized molecules were used in the first phase of screening against promastigote forms of *L. infantum*. Around 128 different analogues were screened, and out of those, some of the molecules showed significant inhibition against promastigotes of *L. infantum*. Promastigotes were the first stage of the screening process to determine whether the molecules could inhibit, as was mentioned earlier in the context. The other molecules were not that much effective as described in **table 6.1**. The critical investigation was further carried out to find a suitable molecule among the tested analogues. These were segregated into potent molecules (equipotent or equal to that of standard drug $EC_{50} < 12.60 \mu\text{M}$), significantly active molecules and moderately active molecules in order to find out the potentially active hit molecules. The cut-off value for the selection of significant compounds were EC_{50} in the range between 13 to 25 μM against promastigotes (standard drug Miltefosine exhibited $12.60 \mu\text{M}$ (Double the value of standard)). In the same way the moderately active molecules were also found with the cut-off value EC_{50} between 25 to 50 μM .

Among the series of (6-bromo-1-phenyl-9*H*-pyrido-[3,4-*b*]-indol-3-yl) (4-phenylpiperazin-1-yl)-methanone derivatives (**1-16**), around three compounds exhibited potent activity with EC_{50} of compound **12** - $8.26 \pm 0.97 \mu\text{M}$, compound **4** - $10.17 \pm 1.11 \mu\text{M}$, compound **9** - $12.68 \pm 8.171 \mu\text{M}$ which is comparable to that of standard drug Miltefosine (EC_{50} $12.60 \mu\text{M}$). Three compounds were found significantly active with EC_{50} of compound **5** - $17.57 \pm 8.92 \mu\text{M}$, compound **13** - $23.00 \pm 0.96 \mu\text{M}$ and compound **15** - $25.32 \pm 10.59 \mu\text{M}$. Another series of compounds (6-nitro-1-phenyl-9*H*-pyrido-[3,4-*b*]-indol-3-yl) (4-phenylpiperazin-1-yl)-methanone derivatives (**17-32**), around three compounds possessed potent activity with EC_{50} of compound **29** - $10.85 \pm 0.81 \mu\text{M}$, compound **19** - $12.19 \pm 0.9 \mu\text{M}$, compound **20** - $12.48 \pm 0.61 \mu\text{M}$ and two compounds showed significant activity with EC_{50} of compound **22** - $13.30 \pm 4.22 \mu\text{M}$, compound **27** - $23.42 \pm 5.96 \mu\text{M}$. In the search of potential promastigote inhibitory compounds from the series of (6-chloro-1-phenyl-9*H*-pyrido-[3,4-*b*]-indol-3-yl) (4-phenylpiperazin-1-yl)-methanone derivatives (**33-48**), only one compound, compound **35** - $24.41 \pm 10.38 \mu\text{M}$ found significantly active. The screening was also carried out on the series of

Chapter 6. Anti-leishmanial, Cell viability, and Trypanothione reductase assay

molecules containing hydroxyl group at 6th position (6-hydroxy-1-phenyl-9*H*-pyrido-[3,4-*b*]-indol-3-yl) (4-phenylpiperazin-1-yl)-methanone derivatives (**49-64**). Out of sixteen analogues from this series, four molecules were found potent in the promastigote assay. The molecules were, compound **60** - 7.59±2.96 μM, compound **51** - 8.42±0.76 μM, compound **56** - 12.32±0.51 μM, compound **54** - 12.83±1.14 μM and two compounds showed significant activity with EC₅₀ of compound **52** - 18.20±3.91 μM and compound **64** - 24.41±10.38 μM with their respective EC₅₀ values.

The nitrogen atom of the β-carboline nucleus was also modified with methyl group in the series of **65-128** analogues. The compounds with the series of **65-80** belongs to the (6-bromo-9-methyl-1-phenyl-9*H*-pyrido-[3,4-*b*]-indol-3-yl) (4-(4-methoxyphenyl)-piperazin-1-yl)-methanone derivatives. In this series of analogues, only one compound **72** - 5.20±0.54 μM showed potent and compound **80** - 47.27±13.35 μM showed moderate activity against promastigotes among all the tested derivatives. The rest other derivative of the series (4-(4-methoxyphenyl)-piperazin-1-yl) (9-methyl-6-nitro-1-phenyl-9*H*-pyrido-[3,4-*b*]-indol-3-yl)-methanone (**81-96 series**), (6-chloro-9-methyl-1-phenyl-9*H*-pyrido-[3,4-*b*]-indol-3-yl) (4-(4-methoxyphenyl)-piperazin-1-yl)-methanone (**97-112 series**), (6-hydroxy-9-methyl-1-phenyl-9*H*-pyrido-[3,4-*b*]-indol-3-yl) (4-(*p*-tolyl)-piperazin-1-yl)-methanone (**113-128 series**) showed EC₅₀ value in the range of 50-100 μM against the tested promastigotes of *L. infantum*. The outcome of the screening against promastigotes revealed 37 promising molecules. In that 12 molecules were potent than the standard drug Miltefosine. The compound **72** - 5.20±0.54 μM and compound **60** - 7.59±2.96 μM were potent active molecules (Fig 6.1). After finding the potent molecules, the significantly active molecules were also Identified. A total of 8 molecules were found significant with EC₅₀ in the range between 13 to 25 μM (Fig 6.2). Around 17 moderately active molecules were also identified with EC₅₀ in the range of 25-50 μM (Fig 6.3).

Chapter 6. Anti-leishmanial, Cell viability, and Trypanothione reductase assay

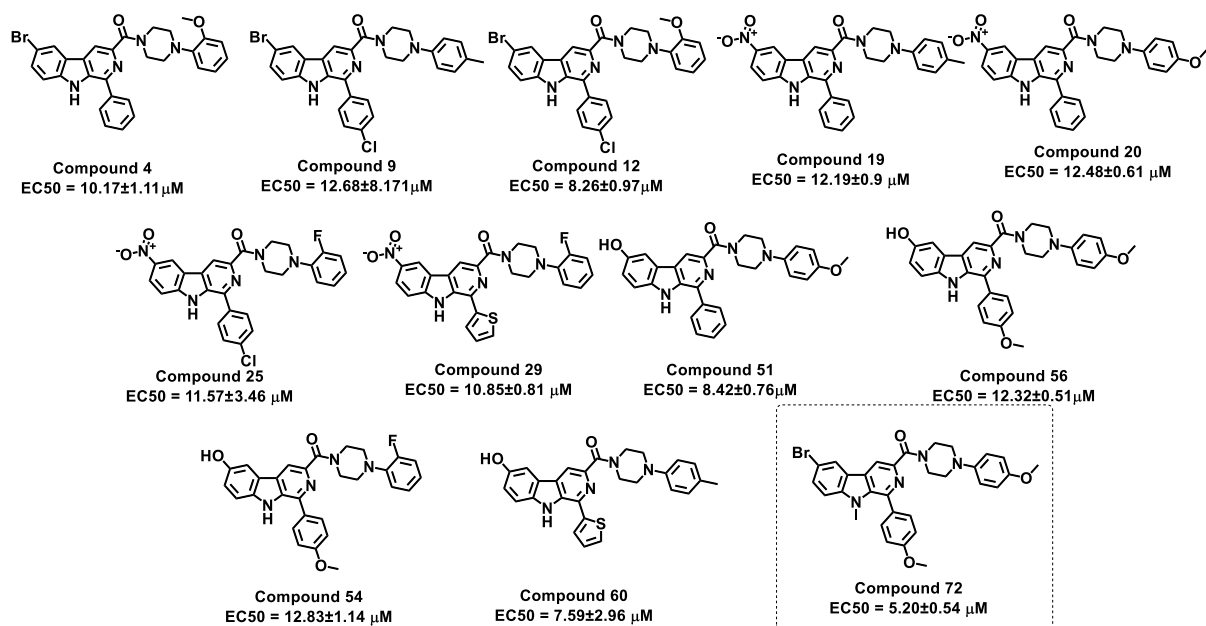


Figure 6.1. Structure of the potent active molecules against promastigotes

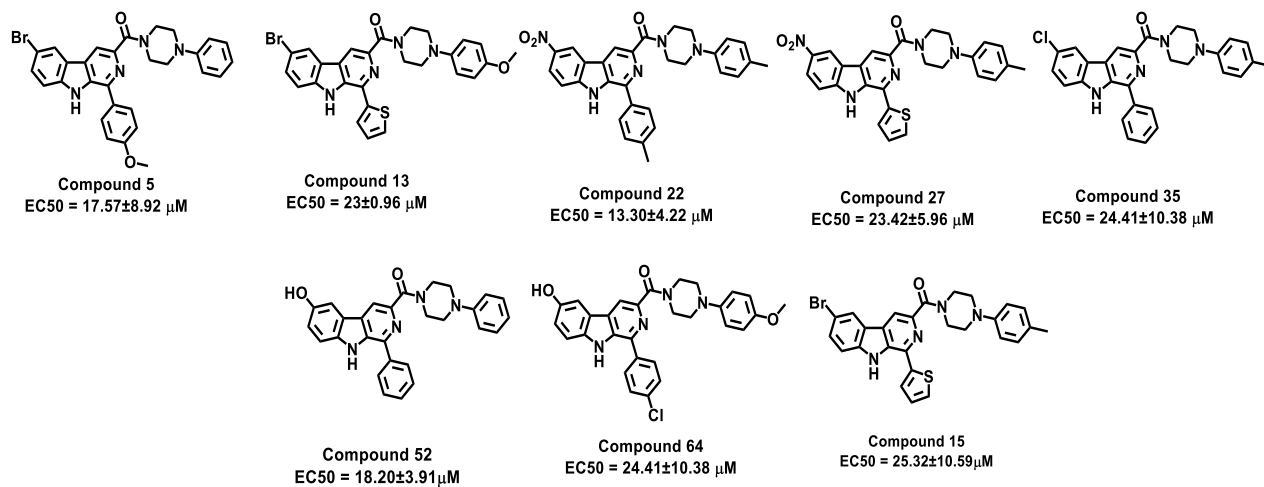


Figure 6.2. Structure of the significantly active molecules against promastigotes

Chapter 6. Anti-leishmanial, Cell viability, and Trypanothione reductase assay

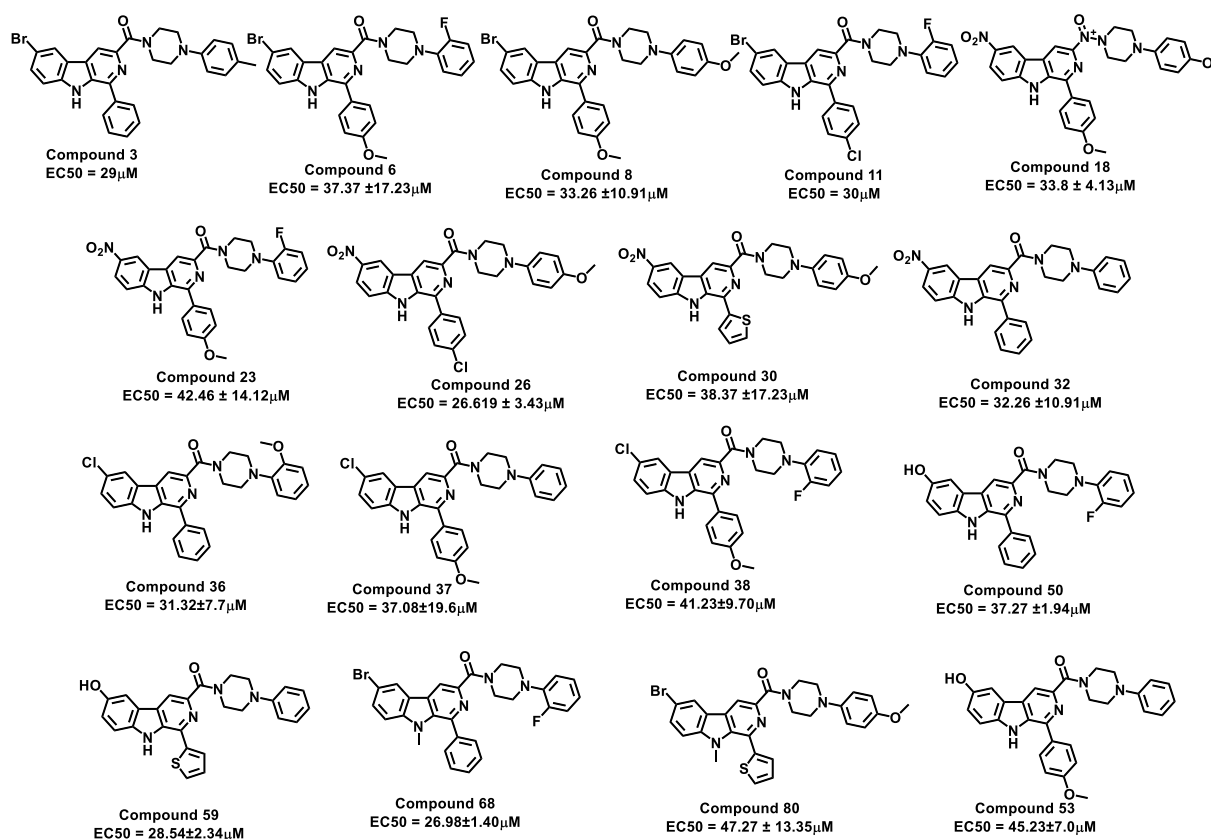


Figure 6.3. Structure of the moderately active molecules against promastigotes

B. Amastigote screening results:

This is a term commonly used to describe an intracellular stage of the life cycle of Leishmanial parasite. A single cell of a protist that does not have visible flagella or cilia is called an amastigote. To keep the infection alive inside their vertebrate hosts, amastigotes replicate in the Parasitophorous vacuole, which ultimately leads to death of host cells and the introduction of new macrophages. Amastigote forms are the virulence stage of the parasite. The screening against amastigote forms was carried out in a manner that was comparable to the screening that was carried out on the promastigotes. The screening was performed on the same **128** series of analogues. In the similar manner of the promastigotes, the amastigotes were also separated. These were segregated into potent molecules (equipotent or equal to that of standard drug EC₅₀ < 4.80 μM), significantly active molecules and moderately active molecules to find out the potentially active hit molecules. The cut-off value for the selectin of significant active compounds were EC₅₀ in the range of 5 to 10 μM against Amastigotes (standard drug Miltefosine exhibited 4.80 μM (Double the value of standard)). In the same way the moderately active molecules were also found with the cut-off value EC₅₀ 10 to 25 μM. The results were depicted in the **table 6.2**.

Chapter 6. Anti-leishmanial, Cell viability, and Trypanothione reductase assay

The screening results of (6-bromo-1-phenyl-9*H*-pyrido-[3,4-*b*]-indol-3-yl) (4-phenylpiperazin-1-yl)-methanone derivatives (**1-16**) showed two compounds exhibited significant activity with EC₅₀ compound **9** - 8.52±0.66 μM, compound **15** - 8.89±0.65 μM against amastigotes. Four compounds showed moderate inhibition with EC₅₀ compound **6** - 13.04±0.60 μM, compound **5** - 13.08±1.43 μM, compound **12** - 17.83±1.51 μM and compound **1** - 22.81±6.66 μM against amastigotes. Another series of compounds (6-nitro-1-phenyl-9*H*-pyrido-[3,4-*b*]-indol-3-yl) (4-phenylpiperazin-1-yl)-methanone derivatives (**17-32**) were also screened. Among the tested series of **17-32**, one compound showed moderate inhibition with EC₅₀ compound **23** - 19.48±1.47 μM against amastigotes. The amastigote inhibitory assay for other series of (6-chloro-1-phenyl-9*H*-pyrido-[3,4-*b*]-indol-3-yl) (4-phenylpiperazin-1-yl)-methanone derivatives (**33-48**) was also carried out to find the potential hit form this series of analogues. Among the series screened, one compound exhibited significant inhibition with EC₅₀ compound **41** - 7.32±1.34 μM. This was the first hit molecule identified from the above-mentioned series of compounds. In the hydroxy molecule series (6-hydroxy-1-phenyl-9*H*-pyrido-[3,4-*b*]-indol-3-yl) (4-phenylpiperazin-1-yl)-methanone derivatives (**49-64**), one compound showed moderate inhibition with EC₅₀ compound **55** - 11.18±0.98 μM against amastigotes.

It was a prominent piece of evidence that the amastigote activity has been increased by the incorporation of methyl group in place of simple nitrogen-containing hydrogen of the β-carboline ring. This may be considered as the most successful of all the β-carboline analogues and the series thereof. Within the context of the series **65-128**, the nitrogen of the β-carboline nucleus was modified by the addition of methyl group. The compounds with serial number between **65** and **80** are members of the (6-bromo-9-methyl-1-phenyl-9*H*-pyrido-[3,4-*b*]-indol-3-yl) (4-(4-methoxyphenyl)-piperazin-1-yl)-methanone derivatives. A total of 11 molecules were found most significantly active in this series of analogues. Out of all the series, the EC₅₀ ranged < 1 μM in this series of analogues. This was the prominent series of analogues that the compounds were more potent than the standard drug **Miltefosine**. The five compounds showed potent EC₅₀ were the compound **68** - 0.54±0.03 μM, compound **70** - 0.46±0.06 μM, compound **72** - 1.28±0.19 μM, compound **75** - 0.81±0.11 μM and compound **77** - 0.45±0.03 μM against amastigotes.

These findings provided a lot of motivation for us to move forward with the additional research that needs to be done. In point of fact, the results were very much satisfying, and the obstacles that we had to overcome have been eliminated. The rest other derivatives of the series (4-(4-

Chapter 6. Anti-leishmanial, Cell viability, and Trypanothione reductase assay

methoxyphenyl)-piperazin-1-yl) (9-methyl-6-nitro-1-phenyl-9*H*-pyrido-[3,4-*b*]-indol-3-yl)-methanone (**81-96 series**), around 11 molecules were prominent in this series. In this series also some of the interesting molecules were found. The EC₅₀ values ranged from 1.51 to 23.86 μM. Two molecules were found potent active with EC₅₀ of compound **88** - 1.51±0.20 μM and compound **89** - 1.62±0.09 μM. In the (6-chloro-9-methyl-1-phenyl-9*H*-pyrido-[3,4-*b*]-indol-3-yl) (4-(4-methoxyphenyl)-piperazin-1-yl)-methanone (**97-112 series**), only 6 molecules were found prominent with EC₅₀ values ranged from 9.39 to 29.27 μM. The EC₅₀ compound **100** – 1.65±0.03 μM showed potent activity against amastigotes and was the best in this series. The last series of compound (6-hydroxy-9-methyl-1-phenyl-9*H*-pyrido-[3,4-*b*]-indol-3-yl) (4-(*p*-tolyl)-piperazin-1-yl)-methanone (**113-128 series**), only one compound **119** - 11.98±0.15 μM was found moderately active when compared with other tested compounds.

In light of the increased amastigote inhibitory activity, the significance of the methyl group has been significantly boosted.

The findings of the amastigote screening revealed **47** promising molecules. In that 12 molecules were potent than the standard drug Miltefosine. The compound **70** – 0.46±0.06 μM and compound **77** – 0.45±0.03 μM were most potent active molecules (Fig 6.4) among the tested series of compounds. After finding the potent molecules, the significantly active molecules were also identified. A total of 9 molecules were found significant with the EC₅₀ less than 10 μM (Fig 6.5). Around 26 moderately active molecules were also identified with EC₅₀ within the range of 10-25 μM (**Fig 6.6**). This was the most promising study results showed that the molecules were more effective than the existing standard drug Miltefosine.

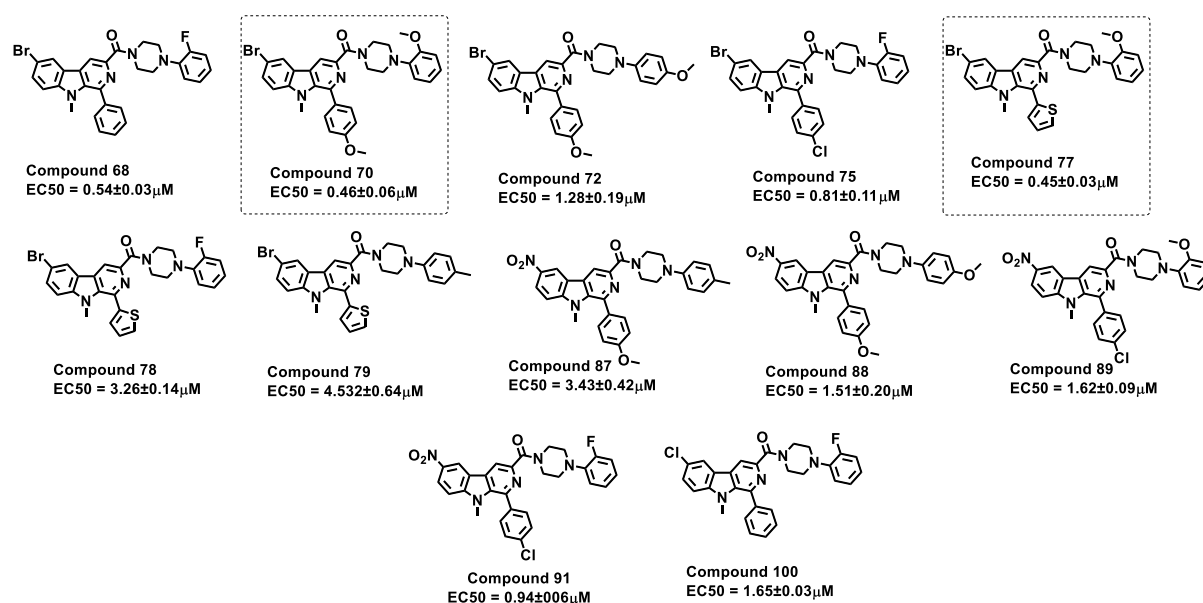


Figure 6.4. Structure of the potent active molecules against amastigotes

Chapter 6. Anti-leishmanial, Cell viability, and Trypanothione reductase assay

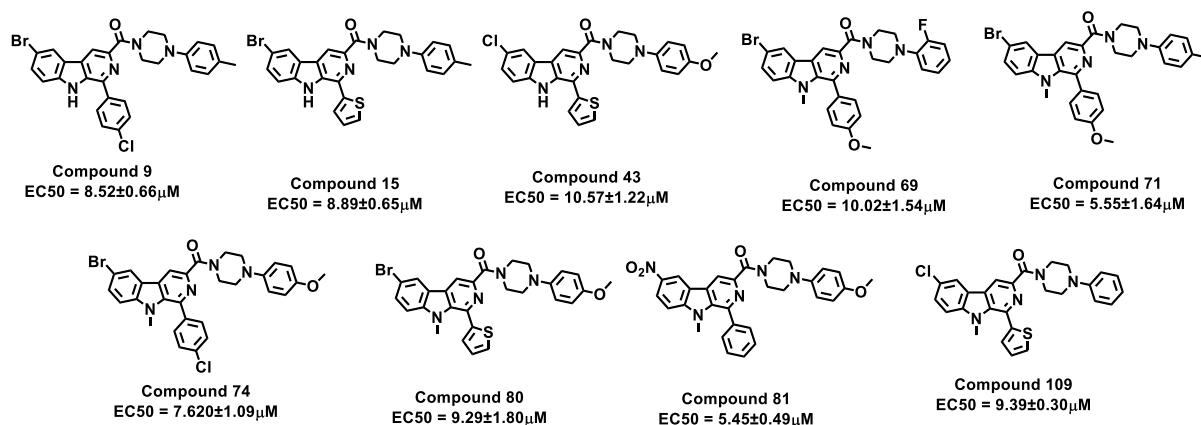


Figure 6.5. Structure of the significantly active molecules against amastigotes

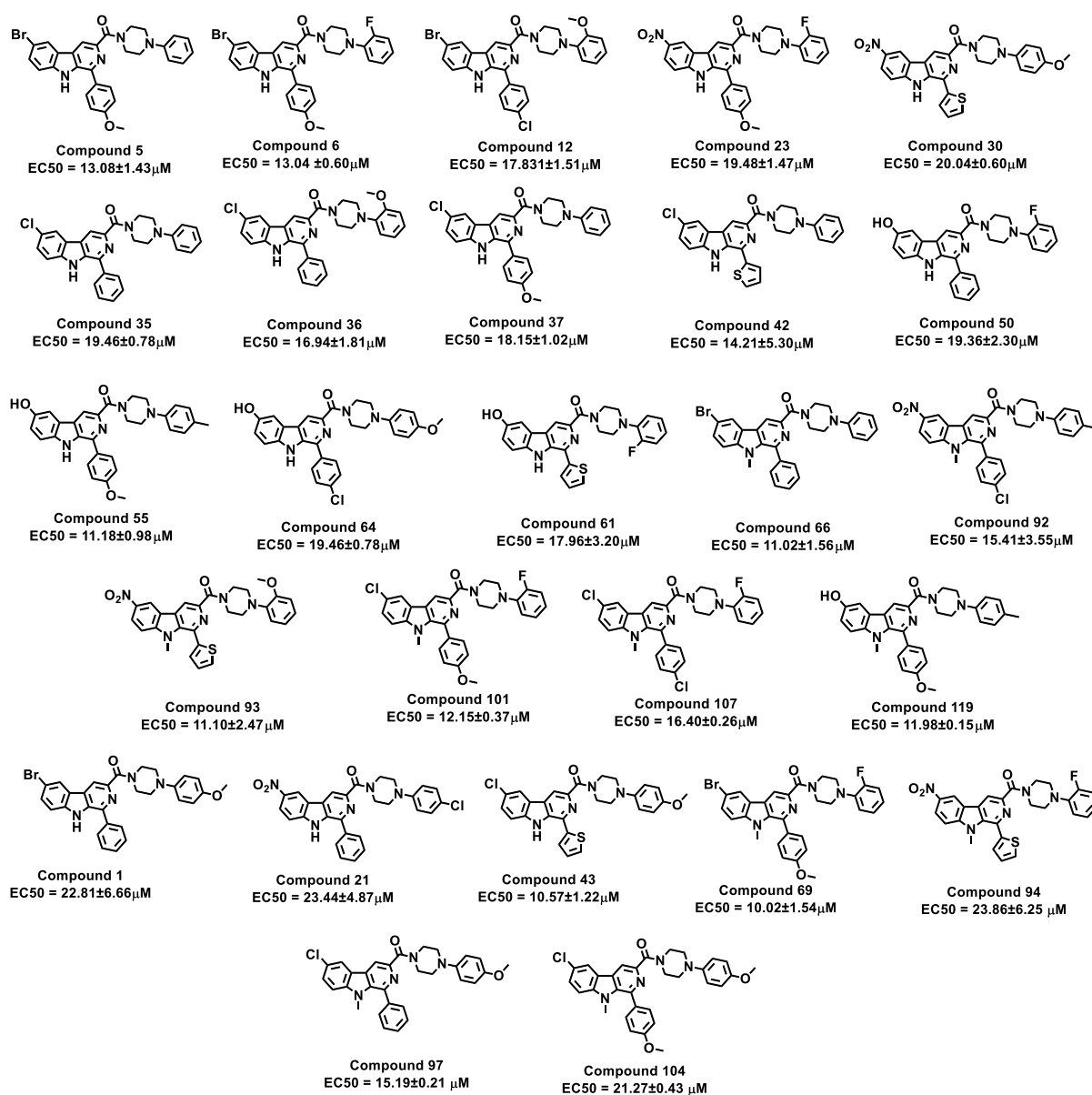


Figure 6.6. Structure of the moderately active molecules against amastigotes

Chapter 6. Anti-leishmanial, Cell viability, and Trypanothione reductase assay

In the search of duly potent molecules among the series of 128 analogues, it has been found that around 15 molecules showed dual inhibition of both promastigotes as well as amastigotes. Among these 15 molecules, compound **9** showed EC_{50} -12.68±8.171 μ M (promastigotes), EC_{50} - 8.52±0.66 μ M (amastigotes) and compound **72** with EC_{50} -5.20±0.54 μ M (promastigotes), EC_{50} - 1.28±0.19 μ M (amastigotes) (**Fig 6.7**).

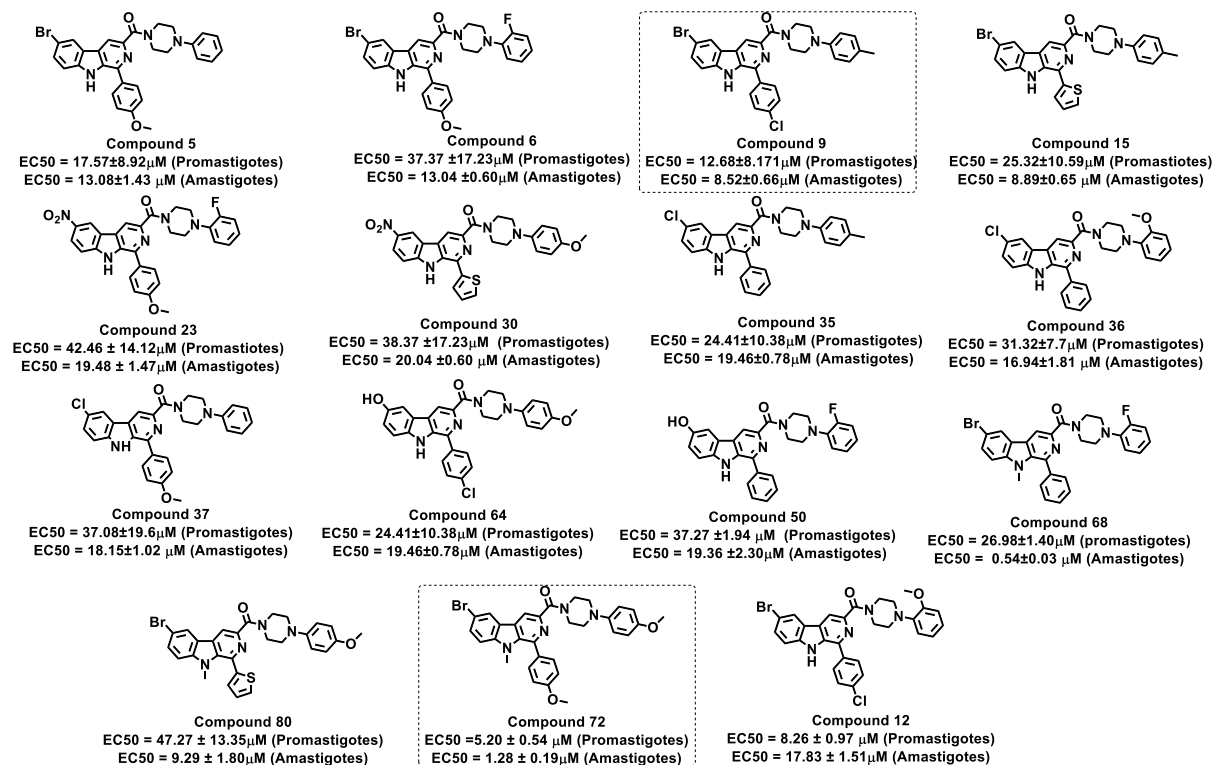


Figure 6.7. Structure of the duly active molecules against both promastigotes and amastigotes

C. Cell viability determination

The most common applications for human hepatoma known as HepG2 include research on drug metabolism and hepatotoxicity. HepG2 cells are non-cancerous cells that have high rate of proliferation, a morphology like epithelial cells and the ability to perform a wide variety of differentiated hepatic functions. The investigation was carried out to determine whether or not any of the synthesized analogues (1-128) were cytotoxic to normal cells. The HepG2 liver cells was specially selected because the VL forms effect more on liver and spleen cells. The screened compounds should not cause any damage to the normal liver cells. If it causes damage to liver cells, then it is not possible to show selective inhibition. Around 29 molecules out of 128 analogues displayed CC_{50} values in the range of 1.9 to greater than 100 μ M (the highest concentration used in the assay).

Chapter 6. Anti-leishmanial, Cell viability, and Trypanothione reductase assay

The potentially identified hit molecules were found to be non-hepatotoxic in nature (**Fig 6.8**). This was given a clear insight that the hit molecules were safe without any hepatotoxicity. Out of 128 molecules 73 molecules exhibited the CC_{50} more than $50\ \mu\text{M}$. This indicates the screened analogues did not reveal any hepatotoxicity.

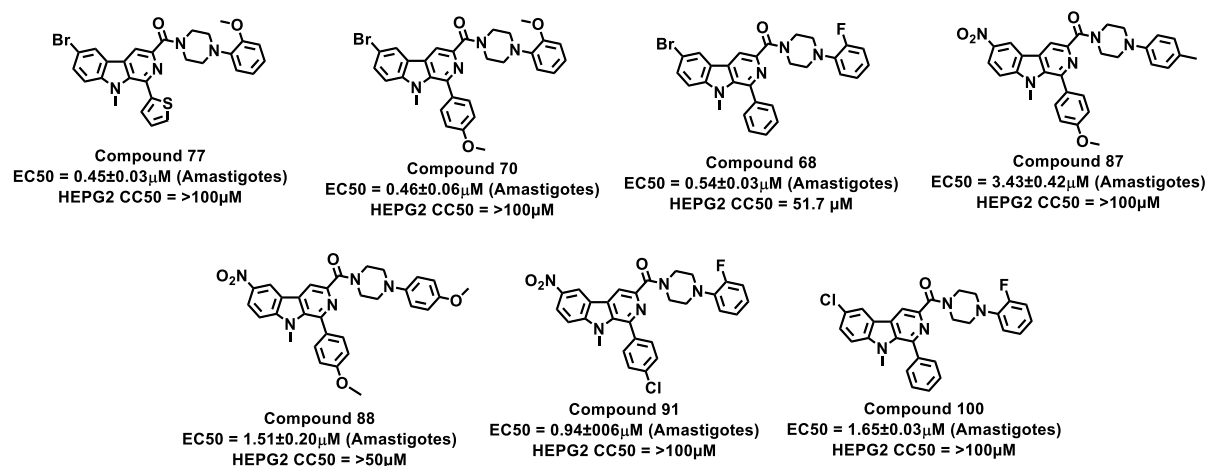


Figure 6.8. Structure of the potent active molecules against amastigotes with their cell viability value

Selectivity index (SI) determination

The selectivity index (SI) is a ratio that divides Cell viability and antileishmanial activity to measure the window of opportunity between the two. In theory, a drug's *in vivo* treatment for a specific infection would be more successful while reducing the risk of adverse effects if it had a higher SI ratio. As described in section 6.3, the SI of the tested analogues was determined for both promastigotes (SIP) and amastigotes (SIA). In the earlier context, the higher the values are the higher the therapeutic potential of the respective compound.

The purpose of this study was to determine whether any of the synthesized analogues (**1-128**) exhibited potentially useful therapeutic activity against leishmaniasis or not. More than one SI value was found for around 47 tested analogues against promastigotes, which account for 36% of the total tested compounds. Additionally, around 78 molecules were discovered, against the promastigotes, **compound 100** was found to have a SI value of 10 and against amastigotes, **compound 77** was found to have a higher SI (218.96). The compound **77** exhibited the highest significant therapeutic index against amastigotes among the tested analogues. According to the data (**table 6.4**), sixty percent of the molecules do not exhibit any toxic properties in their natural state.

Chapter 6. Anti-leishmanial, Cell viability, and Trypanothione reductase assay

Table 18. Results of *L. infantum* promastigotes inhibition assay

| Comp. code | <i>L. infantum</i> Promastigotes (EC ₅₀ (μM)) | Comp. code | <i>L. infantum</i> Promastigotes (EC ₅₀ (μM)) | Comp. code | <i>L. infantum</i> Promastigotes (EC ₅₀ (μM)) | Comp. code | <i>L. infantum</i> Promastigotes (EC ₅₀ (μM)) |
|------------|--|------------|--|------------|--|------------|--|
| 1 | >100 | 33 | >155 | 65 | >100 | 97 | >50 |
| 2 | -- | 34 | >111 | 66 | -- | 98 | >50 |
| 3 | 29 | 35 | 24.41±10.38 | 67 | -- | 99 | >50 |
| 4 | 10.17±1.11 | 36 | 31.32±7.7 | 68 | 26.98±1.40 | 100 | >10 |
| 5 | 17.57±8.92 | 37 | 37.08±19.6 | 69 | -- | 101 | >50 |
| 6 | 37.37±17.23 | 38 | 41.23±9.70 | 70 | >50 | 102 | >50 |
| 7 | >100 | 39 | -- | 71 | >100 | 103 | >25 |
| 8 | 33.26±10.91 | 40 | -- | 72 | 5.20±0.54 | 104 | >50 |
| 9 | 12.68±8.171 | 41 | -- | 73 | -- | 105 | >100 |
| 10 | -- | 42 | -- | 74 | -- | 106 | >50 |
| 11 | 30 | 43 | >100 | 75 | >50 | 107 | >50 |
| 12 | 8.26±0.97 | 44 | >100 | 76 | -- | 108 | >50 |
| 13 | 23±0.96 | 45 | >100 | 77 | >50 | 109 | >50 |
| 14 | >100 | 46 | 33 | 78 | -- | 110 | >50 |
| 15 | 25.32±10.59 | 47 | >100 | 79 | >50 | 111 | >50 |
| 16 | -- | 48 | 31 | 80 | 47.27±13.35 | 112 | >50 |
| 17 | 52.02±7.21 | 49 | >100 | 81 | >50 | 113 | >50 |
| 18 | 33.8±4.13 | 50 | 37.27±1.94 | 82 | >50 | 114 | >50 |
| 19 | 12.19±0.9 | 51 | 8.42±0.76 | 83 | >60 | 115 | >50 |
| 20 | 12.48±0.61 | 52 | 18.20±3.91 | 84 | >50 | 116 | >50 |
| 21 | >100 | 53 | 45.23±7.0 | 85 | >50 | 117 | >50 |
| 22 | 13.30±4.22 | 54 | 12.83±1.14 | 86 | >50 | 118 | >50 |
| 23 | 42.46±14.12 | 55 | -- | 87 | >100 | 119 | >50 |
| 24 | 82.7±9.79 | 56 | 12.32±0.51 | 88 | >50 | 120 | >25 |
| 25 | 11.57±3.46 | 57 | 70 | 89 | >50 | 121 | >50 |
| 26 | 26.619±3.43 | 58 | >100 | 90 | >50 | 122 | >50 |
| 27 | 23.42±5.96 | 59 | 28.54±2.34 | 91 | >50 | 123 | >50 |
| 28 | >100 | 60 | 7.59±2.96 | 92 | >60 | 124 | >50 |
| 29 | 10.85±0.81 | 61 | >100 | 93 | >50 | 125 | >50 |
| 30 | 38.37±17.23 | 62 | >155 | 94 | >50 | 126 | >50 |
| 31 | >100 | 63 | >111 | 95 | >50 | 127 | >50 |
| 32 | 32.26±10.91 | 64 | 24.41±10.38 | 96 | >50 | 128 | >50 |

Chapter 6. Anti-leishmanial, Cell viability, and Trypanothione reductase assay

Table 19. Results of *L. infantum* amastigotes inhibition assay

| Comp. code | <i>L. infantum</i> Amastigotes (EC ₅₀ (μM)) | Comp. code | <i>L. infantum</i> Amastigotes (EC ₅₀ (μM)) | Comp. code | <i>L. infantum</i> Amastigotes (EC ₅₀ (μM)) | Comp. code | <i>L. infantum</i> Amastigotes (EC ₅₀ (μM)) |
|------------|--|------------|--|------------|--|------------|--|
| 1 | 22.81±6.66 | 33 | -- | 65 | -- | 97 | 15.19±0.21 |
| 2 | -- | 34 | -- | 66 | 11.02±1.56 | 98 | >50 |
| 3 | -- | 35 | 19.46±0.78 | 67 | >25 | 99 | >50 |
| 4 | 33.78±3.08 | 36 | 16.94±1.81 | 68 | 0.54±0.03 | 100 | 1.65±0.03 |
| 5 | 13.08±1.43 | 37 | 18.15±1.02 | 69 | 10.02±1.54 | 101 | 12.15±0.37 |
| 6 | 13.04±0.60 | 38 | 28.45±6.96 | 70 | 0.46±0.06 | 102 | >50 |
| 7 | 28.09±3.00 | 39 | 35.66±3.08 | 71 | 5.55±1.64 | 103 | >25 |
| 8 | 30.57±5.05 | 40 | 26.43±1.40 | 72 | 1.28±0.19 | 104 | 21.27±0.43 |
| 9 | 8.52±0.66 | 41 | 7.32±1.34 | 73 | >20 | 105 | >100 |
| 10 | -- | 42 | 14.21±5.30 | 74 | 7.620±1.09 | 106 | >50 |
| 11 | -- | 43 | 10.57±1.22 | 75 | 0.81±0.11 | 107 | 16.40±0.26 |
| 12 | 17.831±1.51 | 44 | 28.48±2.05 | 76 | >20 | 108 | >50 |
| 13 | -- | 45 | -- | 77 | 0.45±0.03 | 109 | 9.39±0.30 |
| 14 | 32.49±3.51 | 46 | -- | 78 | 3.26±0.14 | 110 | >50 |
| 15 | 8.89±0.65 | 47 | 24.21±1.20 | 79 | 4.532±0.64 | 111 | >50 |
| 16 | -- | 48 | -- | 80 | 9.29±1.80 | 112 | >50 |
| 17 | -- | 49 | 62.55±21.83 | 81 | 5.45±0.49 | 113 | >50 |
| 18 | >50 | 50 | 19.36±2.30 | 82 | >25 | 114 | >50 |
| 19 | >10 | 51 | 72.65±4.13 | 83 | >30 | 115 | >50 |
| 20 | >50 | 52 | >100 | 84 | >50 | 116 | >50 |
| 21 | 23.44±4.87 | 53 | >100 | 85 | >50 | 117 | >50 |
| 22 | 31.41±6.3 | 54 | 82.21±8.09 | 86 | >25 | 118 | >50 |
| 23 | 19.48±1.47 | 55 | 11.18±0.98 | 87 | 3.43±0.42 | 119 | 11.98±0.15 |
| 24 | >100 | 56 | >100 | 88 | 1.51±0.20 | 120 | >25 |
| 25 | 42.56±6.92 | 57 | -- | 89 | 1.62±0.09 | 121 | >50 |
| 26 | >100 | 58 | 53.22±3.3 | 90 | >25 | 122 | >50 |
| 27 | 32.60±3.18 | 59 | >100 | 91 | 0.94±0.06 | 123 | >50 |
| 28 | >100 | 60 | 47.61±0.43 | 92 | 15.41±3.55 | 124 | >50 |
| 29 | >100 | 61 | 17.96±3.20 | 93 | 11.10±2.47 | 125 | >50 |
| 30 | 20.04±0.60 | 62 | -- | 94 | 23.86±6.25 | 126 | >50 |
| 31 | 28.09±3.00 | 63 | -- | 95 | 8.55±1.29 | 127 | >50 |
| 32 | 30.57±5.05 | 64 | 19.46±0.78 | 96 | 7.33±0.47 | 128 | >50 |

Chapter 6. Anti-leishmanial, Cell viability, and Trypanothione reductase assay

Table 20. Results of cell viability assay using human hepatoma (HepG2) cells

| Comp. code | HEPG2 CC ₅₀ (μM) | Comp. code | HEPG2 CC ₅₀ (μM) | Comp. code | HEPG2 CC ₅₀ (μM) | Comp. code | HEPG2 CC ₅₀ (μM) |
|------------|-----------------------------|------------|-----------------------------|------------|-----------------------------|------------|-----------------------------|
| 1 | >100 | 33 | -- | 65 | >100 | 97 | >50 |
| 2 | -- | 34 | -- | 66 | >100 | 98 | >50 |
| 3 | -- | 35 | 51.78±2.61 | 67 | >100 | 99 | >50 |
| 4 | >100 | 36 | 50.89±0.0 | 68 | 51.76±13.49 | 100 | >10 |
| 5 | 54.45±0.0 | 37 | 50.39±0.0 | 69 | | 101 | >50 |
| 6 | >100 | 38 | >100 | 70 | >100 | 102 | >50 |
| 7 | >100 | 39 | >100 | 71 | >50 | 103 | >25 |
| 8 | >100 | 40 | 52.61±0.0 | 72 | 7.77±0.33 | 104 | >50 |
| 9 | 77.72±3.46 | 41 | 56.36±0.0 | 73 | >20 | 105 | >100 |
| 10 | -- | 42 | -- | 74 | >20 | 106 | >50 |
| 11 | -- | 43 | -- | 75 | 3.41±0.11 | 107 | >50 |
| 12 | 59.30±8.19 | 44 | >100 | 76 | | 108 | >50 |
| 13 | -- | 45 | -- | 77 | >100 | 109 | >50 |
| 14 | >100 | 46 | -- | 78 | >20 | 110 | >50 |
| 15 | 71.04±2.88 | 47 | 54.03±0.0 | 79 | 6.24±0.19 | 111 | >50 |
| 16 | -- | 48 | -- | 80 | >50 | 112 | >50 |
| 17 | 56.28±3.93 | 49 | 56.10±0.0 | 81 | >25 | 113 | >50 |
| 18 | >100 | 50 | 56.45±6.11 | 82 | >25 | 114 | >50 |
| 19 | >100 | 51 | 52.70±0.0 | 83 | >30 | 115 | >50 |
| 20 | >100 | 52 | >100 | 84 | 21.39±0.09 | 116 | >50 |
| 21 | >100 | 53 | >100 | 85 | 32.87±3.24 | 117 | >50 |
| 22 | >100 | 54 | >100 | 86 | >25 | 118 | >50 |
| 23 | >100 | 55 | 97.77±3.51 | 87 | >100 | 119 | >50 |
| 24 | >100 | 56 | 50.98±0.0 | 88 | >50 | 120 | >25 |
| 25 | 25.93±4.47 | 57 | -- | 89 | 1.91±0.04 | 121 | >50 |
| 26 | >100 | 58 | 54.73±16.8 | 90 | >25 | 122 | >50 |
| 27 | 81.80±4.82 | 59 | 48.96±2.3 | 91 | >100 | 123 | >50 |
| 28 | >100 | 60 | 46.55±2.18 | 92 | >30 | 124 | >50 |
| 29 | >100 | 61 | 44.52±8.69 | 93 | >25 | 125 | >50 |
| 30 | >100 | 62 | >100 | 94 | >25 | 126 | >50 |
| 31 | >100 | 63 | >100 | 95 | >25 | 127 | >50 |
| 32 | >100 | 64 | >100 | 96 | >50 | 128 | >50 |

Chapter 6. Anti-leishmanial, Cell viability, and Trypanothione reductase assay

Table 21. Results of selectivity index of the antileishmanial activities

| Comp. code | SIP | SIA | Comp. code | SIP | SIA | Comp. code | SIP | SIA | Comp. code | SIP | SIA |
|------------|------|-------|------------|------|------|------------|------|--------|------------|-------|-------|
| 1 | 1.00 | 1.00 | 33 | 0.65 | 1.00 | 65 | 1.00 | 1.00 | 97 | 1.00 | 3.29 |
| 2 | 1.00 | 2.00 | 34 | 0.90 | 1.00 | 66 | 1.00 | 9.07 | 98 | 1.00 | 1.00 |
| 3 | 3.45 | 0.87 | 35 | 2.12 | 2.66 | 67 | 1.00 | 4.00 | 99 | 1.00 | 1.00 |
| 4 | 9.83 | 0.41 | 36 | 1.62 | 3.00 | 68 | 1.92 | 95.46 | 100 | 10.00 | 60.61 |
| 5 | 3.10 | 1.61 | 37 | 1.36 | 2.78 | 69 | 1.00 | 9.98 | 101 | 1.00 | 4.12 |
| 6 | 2.68 | 2.24 | 38 | 2.43 | 3.51 | 70 | 2.00 | 215.98 | 102 | 1.00 | 1.00 |
| 7 | 1.00 | 7.00 | 39 | 1.00 | 2.80 | 71 | 0.50 | 9.01 | 103 | 1.00 | 1.00 |
| 8 | 3.01 | 2.66 | 40 | 0.53 | 1.99 | 72 | 1.49 | 6.07 | 104 | 1.00 | 2.35 |
| 9 | 6.13 | 1.47 | 41 | 0.56 | 7.70 | 73 | 0.20 | 1.00 | 105 | 1.00 | 1.00 |
| 10 | 1.00 | 10.00 | 42 | 1.00 | 7.04 | 74 | 0.20 | 2.62 | 106 | 1.00 | 1.00 |
| 11 | 3.33 | 3.30 | 43 | 1.00 | 9.46 | 75 | 0.07 | 4.21 | 107 | 1.00 | 3.05 |
| 12 | 7.18 | 1.67 | 44 | 1.00 | 3.51 | 76 | 1.00 | 5.00 | 108 | 1.00 | 1.00 |
| 13 | 4.35 | 2.99 | 45 | 1.00 | 1.00 | 77 | 2.00 | 218.96 | 109 | 1.00 | 5.32 |
| 14 | 1.00 | 14.00 | 46 | 3.03 | 1.00 | 78 | 0.20 | 6.12 | 110 | 1.00 | 1.00 |
| 15 | 2.81 | 5.35 | 47 | 0.54 | 2.23 | 79 | 0.12 | 1.38 | 111 | 1.00 | 1.00 |
| 16 | 1.00 | 16.00 | 48 | 3.23 | 1.00 | 80 | 1.06 | 5.38 | 112 | 1.00 | 1.00 |
| 17 | 1.08 | 15.71 | 49 | 0.56 | 0.90 | 81 | 0.50 | 4.58 | 113 | 1.00 | 1.00 |
| 18 | 2.96 | 6.08 | 50 | 1.51 | 2.92 | 82 | 0.50 | 1.00 | 114 | 1.00 | 1.00 |
| 19 | 8.20 | 2.32 | 51 | 6.26 | 0.73 | 83 | 0.42 | 0.83 | 115 | 1.00 | 1.00 |
| 20 | 8.01 | 2.50 | 52 | 5.49 | 1.00 | 84 | 0.43 | 0.43 | 116 | 1.00 | 1.00 |
| 21 | 1.00 | 21.00 | 53 | 2.21 | 1.00 | 85 | 0.66 | 0.66 | 117 | 1.00 | 1.00 |
| 22 | 7.52 | 2.93 | 54 | 7.79 | 1.22 | 86 | 0.50 | 1.00 | 118 | 1.00 | 1.00 |
| 23 | 2.36 | 9.77 | 55 | 0.98 | 8.75 | 87 | 1.00 | 29.15 | 119 | 1.00 | 4.17 |
| 24 | 1.21 | 19.85 | 56 | 4.14 | 0.51 | 88 | 1.00 | 33.11 | 120 | 1.00 | 1.00 |
| 25 | 2.24 | 11.16 | 57 | 1.43 | 1.00 | 89 | 0.04 | 1.18 | 121 | 1.00 | 1.00 |
| 26 | 3.76 | 6.92 | 58 | 0.55 | 1.03 | 90 | 0.50 | 1.00 | 122 | 1.00 | 1.00 |
| 27 | 3.49 | 7.73 | 59 | 1.72 | 0.49 | 91 | 2.00 | 106.16 | 123 | 1.00 | 1.00 |
| 28 | 1.00 | 28.00 | 60 | 6.13 | 0.98 | 92 | 0.50 | 1.95 | 124 | 1.00 | 1.00 |
| 29 | 9.22 | 3.15 | 61 | 0.45 | 2.48 | 93 | 0.50 | 2.25 | 125 | 1.00 | 1.00 |
| 30 | 2.61 | 11.51 | 62 | 0.65 | 1.00 | 94 | 0.50 | 1.05 | 126 | 1.00 | 1.00 |
| 31 | 1.00 | 31.00 | 63 | 0.90 | 1.00 | 95 | 0.50 | 2.92 | 127 | 1.00 | 1.00 |
| 32 | 3.10 | 10.32 | 64 | 4.10 | 5.14 | 96 | 1.00 | 6.82 | 128 | 1.00 | 1.00 |

SIP – Selectivity index of promastigotes; SIA – Selectivity index of amastigotes

E. Structure Activity Relationship (SAR) studies for antileishmanial activity

The connection between a molecule's chemical group and its biological effect is known as structure-activity relationship (SAR). In 1865, Crum-Brown and Fraser first put forward this theory. It is possible to identify the class of chemicals that causes a desired biological response by using SAR analysis. As a result, the chemical structure of a bioactive compound (typically a drug) can be altered to change its effect or potency. The outcomes were segregated into significantly active molecules, molecules that are more potent than the standard drug Miltefosine.

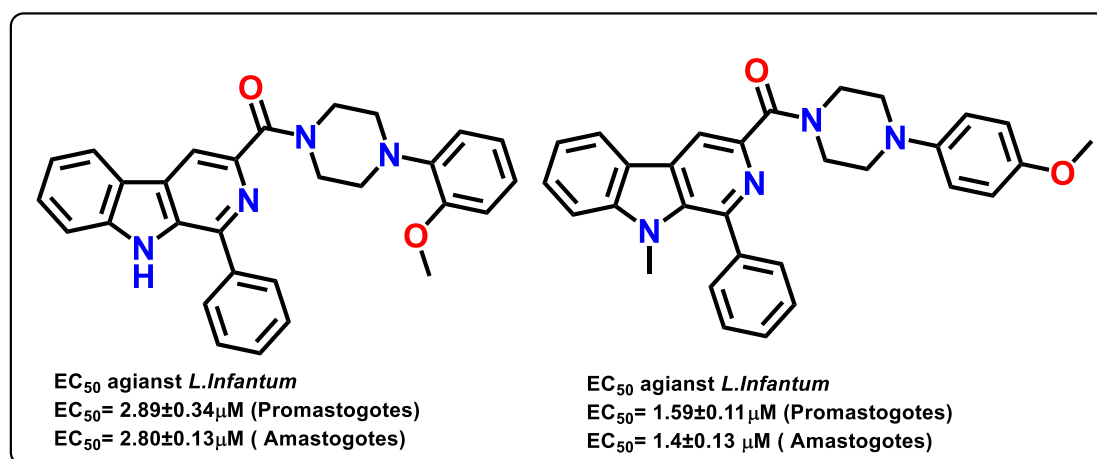


Figure 6.9. Lead compound identified from the past studies

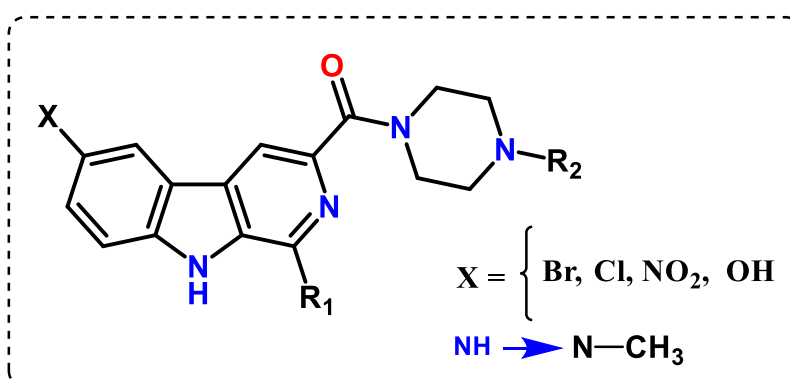


Figure 6.10. Structure Activity Relationship (SAR) studies of the β -carboline analogues. Substitutions were made in different positions of the 9H-pyrido-[3,4-b]-indole scaffold in the lead compound (**Figure 6.9**) to boost its activity against Amastigotes of *L. infantum*. When the R1 was substituted with phenyl ring and R2 with 4-methoxy phenyl, on the 6-bromo substituted molecule, the EC_{50} was found to be 22.81 μM (compound 1). To the same scaffold, when R2 substituted with 2-fluoro phenyl or p-tolyl group, the compounds did not show any activity (compounds 2, 3). Further, 2-methoxy phenyl substitution led to the decreased activity (compound 4). Replacing R1 with 4-methoxy phenyl and R2 with phenyl ring had increased the activity to 13.08 μM (compound 5). Similar result was shown upon removal of fluoro on

Chapter 6. Anti-leishmanial, Cell viability, and Trypanothione reductase assay

the ring at R2 position (**Figure 6.10**), indicating, addition of fluoro group decreased the activity against amastigotes (compound **6**). Addition of 4-methyl (compound **7**) or 4-methoxy (compound **8**) on compound **5** had drastically decreased the activity. When methoxy group of compound **7** was replaced with a halogen (chlorine) (compound **9**), or thiophene group (compound **15**) the activity was drastically increased to 8.52 μM and 8.89 μM , respectively being the most potent compounds of the 6-bromo series. Additionally, compound **9** was also found to show potent inhibition against promastigotes (EC_{50} 12.68 μM). Compound **12** with R1 having 4-chloro phenyl and R2 with 2-methoxy phenyl substitution exhibited potent inhibition on promastigotes (EC_{50} 8.26 μM) while it showed moderate inhibition against amastigotes (EC_{50} 17.83 μM). When 6th position was modified with nitro and various substitutions made at R1 and R2 position, the activity did not increase (compound **17-32** series). However, when substitutions were made on 6th position by replacing with chlorine, R1 was substituted with thiophene and R2 with p-tolyl, the activity was slightly lower than compound **15** with EC_{50} of 10.57 μM (compound **43**). Upon removal of 4-methyl from compound **43** drastically increased the activity than compound **15** and the EC_{50} was found to be 7.32 μM (compound **41**). Further, when hydroxyl group was substituted at 6th position, the activity was decreased in all the compounds of series **49-64**. However, compounds **51**, **54** and **56** were shown to have potent inhibition against promastigotes with their EC_{50} of 8.42 μM , 12.83 μM and 12.32 μM , respectively. Replacement of hydrogen of N1 with methyl group on 6-bromo series has improved the activity drastically. Around four molecules of compound **65-80** series that has *N*-methyl on 9th position exhibited EC_{50} between 0.4 to 1.0 μM concentrations. The molecules include compound **68**, **70**, **75** and **77**. Compounds **68** and **75** had 2-fluoro substitution on R2 position, while R1 was phenyl and 4-chloro phenyl substitutions, respectively. Whereas compound **70** and **77** had 2-methoxy phenyl on R2 position, while R1 position was 4-methoxy and thiophene ring, respectively. EC_{50} value of compounds **68**, **70**, **75** and **77** were 0.54 μM , 0.46 μM , 0.81 μM and 0.45 μM , respectively. The molecules **69**, **71**, **72**, **79** and **80** had EC_{50} values ranging between 1 – 10 μM concentration. In the **65-80** series of compounds, 6th position was modified using chloro-, nitro- and hydroxyl-groups. With 6-nitro substitution (**81-96** series), compounds **88**, **89**, **91**, **95** and **96** were shown to have significant inhibition against amastigotes. Among these, compound **91** was found to be potent with EC_{50} value of 0.94 μM , while the other active molecules had EC_{50} ranging from 1 – 9 μM concentration. Similarly, in the **65-80** series of compounds, 6th position substitution was altered by replacing with chlorine and the results were like that of **97-112** series

Chapter 6. Anti-leishmanial, Cell viability, and Trypanothione reductase assay

compounds. These compounds were active against amastigotes and showed high EC₅₀ values in case of promastigotes. The potent compound in this series includes **100** and **109** with their EC₅₀ values 1.65 μ M and 9.39 μ M, respectively. When, the 6th position of compound **113-128** series was substituted with hydroxyl group, all the molecules had EC₅₀ values > 50 μ M except compound **119** with EC₅₀ of 11.98 μ M. However, these series of compounds did not show potent inhibition against amastigotes. From the SAR analysis of the synthesized molecules, *N*-methyl substitution on the 9th position may be responsible for decrease in activity of the compounds that has substitution on 6th position with nitro or hydroxyl group.

Although, compounds containing halogen group at position 6 showed notable inhibitory properties, those containing bromo at position 6th and *N*1-methyl group are extremely effective. These findings sheds light on the requirement for 6th-halo substitution and *N*1-methyl group to produce potent inhibitory activity compounds against amastigotes of *L. infantum*.

F. Trypanothione reductase (TR) inhibition assay

Trypanothione reductase, often known as TR, is widely regarded as one of the most promising targets for the development of novel anti-leishmanial medications. This enzyme is essential for the survival of parasite within the host because it is responsible for the reduction of trypanothione. Trypanothione is a molecule that has been used by the tryparedoxin / tryparedoxin peroxidase system of *Leishmania* to neutralise the hydrogen peroxide that was produced by host macrophages during infection. Trypanothione reductase is an obligate homodimer with each of the two individual subunits, related by two-fold symmetry, comprising an FAD-binding domain (residues 1–160 and 289–360), an NADPH-binding domain (residues 161–288) and an interface domain (residues 361–488)⁷.

The protein catalyses the reduction of dithiol trypanothione (from TS2 to T(SH)₂) at the expense of the co-substrate NADPH. NADPH and TS2 binds at different cavities facing opposite sides of the isoalloxazine ring of FAD. The TS2 site, located at the interface between the two subunits, is shaped by residues belonging to both subunits. The reaction mechanism relies on the transfer of two electrons from NADPH to two catalytic cysteines (CYS52 and CYS57), via the FAD co-factor. Once the cysteines were reduced, the oxidized TS2 binds to the protein and CYS52, deprotonated by the couple HIS461-GLU466, attacks the disulfide bridge of the substrate, resulting in the formation of a mixed disulfide. Finally, the attack of CYS57 on CYS52 enables the release of the reduced T(SH)₂⁸.

Initially, we conducted an *in-silico* pilot analysis against prospective targets, including Leishmanial Trypanothione oxidase, *N*-Myristyl transferase, Pteridine reductase and

Chapter 6. Anti-leishmanial, Cell viability, and Trypanothione reductase assay

Spermidine synthase using designed prototype compounds before deciding that the TR would be the probable target for the titled molecules to go. During molecular docking and molecular dynamics investigation, we discovered a problem that was associated with other targets that were named above. The β -carboline molecules did not fit into the active sites, and in some targets, they were completely outside of the active site, which resulted in lower docking scores. These problems were found to be associated with the other targets. According to the findings of the pilot experiments that were carried out, only TR was capable of binding at the active site and also provided an insightful docking score. Because of this as well as the available literature, we reasoned that the trypanothione reductase would be a possible target for the titled compounds and the experimental studies were carried out.

In light of the findings regarding antileishmanial activity, all the compounds (the ones with an EC_{50} less than 10 μ M against amastigotes) were subjected to additional testing to determine whether or not they inhibited the activity of trypanothione reductase (TR) enzyme. As a result, the structure-activity relationship (SAR) was also computed.

At the concentrations of 50 and 100 μ M that were tested, it was discovered that the synthesized compounds were able to inhibit the enzymatic activity of TR. Under the experimental procedure chosen for the TR inhibition assay (6.4. Experimental Procedures for TR inhibition assay), compound **78**, at a concentration of 100 μ M, showed an inhibition of TS2 (trypanothione disulfide) reduction that was as high as 100 ± 2 % when compared to the standard thioridazine (95.99 ± 1 %) (Table 6.5).

Based on these findings, the TR inhibition potential of compounds **78**, **68**, **81**, **70**, **96** and **88** revealed the TR inhibition at 50 μ M were 50 ± 1 %, 43 ± 1 %, 38 ± 5 %, 36 ± 5 %, 33 ± 3 % and 31 ± 2 %, respectively. At 100 μ M concentration, the compounds **78**, **68**, **81**, **15** and **109** exhibited TR inhibition of 100 ± 2 %, 63 ± 1 %, 61 ± 1 %, 57 ± 2 % and 47 ± 1 %, respectively. As mentioned in the previous context, the findings were quite interesting.

It was established as a closing point following the TR experimental studies that the compound **78** was the only one that was found to be more effective in preventing TR. Due to the above-mentioned findings, it has become evident that the TR is not the only target that the β -carboline derivatives are attempting to hit. Hence, further detailed investigations will be required against other possible available targets of leishmaniasis in order to determine the exact molecular target on which the anti-leishmanial β -carboline analogues will act..

Chapter 6. Anti-leishmanial, Cell viability, and Trypanothione reductase assay

Table 22. Results of Trypanothione reductase inhibition assay

| S. No | Comp. code | % TR inhibition (50 μ M) | % TR inhibition (100 μ M) |
|-----------|---------------------|------------------------------|-------------------------------|
| 1 | 9 | 17 \pm 1 | 39 \pm 4 |
| 2 | 15 | 23 \pm 3 | 57 \pm 2 |
| 3 | 41 | 9 \pm 2 | 2 \pm 3 |
| 4 | 43 | 18 \pm 3 | 17 \pm 1 |
| 5 | 68 | 43 \pm 1 | 63 \pm 1 |
| 6 | 69 | 8 \pm 2 | 22 \pm 5 |
| 7 | 70 | 36 \pm 5 | 32 \pm 2 |
| 8 | 71 | 3 \pm 4 | 9 \pm 2 |
| 9 | 72 | 12 \pm 1 | 15 \pm 3 |
| 10 | 74 | 2 \pm 2 | 4 \pm 1 |
| 11 | 77 | 2 \pm 1 | 1 \pm 3 |
| 12 | 79 | 1 \pm 1 | 11 \pm 4 |
| 13 | 78 | 50\pm1 | 100\pm2 |
| 14 | 80 | 8 \pm 1 | 13 \pm 3 |
| 15 | 81 | 38 \pm 5 | 61 \pm 1 |
| 16 | 87 | 16 \pm 5 | 19 \pm 3 |
| 17 | 88 | 31 \pm 2 | 16 \pm 2 |
| 18 | 89 | 11 \pm 3 | 6 \pm 4 |
| 19 | 91 | 1 \pm 1 | 34 \pm 1 |
| 20 | 95 | 10 \pm 3 | 4 \pm 3 |
| 21 | 96 | 33 \pm 3 | 35 \pm 2 |
| 22 | 100 | 22 \pm 1 | Yellow precipitate |
| 23 | 109 | 7 \pm 2 | 47 \pm 1 |
| 24 | 119 | 2 \pm 1 | Yellow precipitate |
| 25 | Thioridazine | 95\pm1 | 99\pm1 |

Structure Activity Relationship (SAR) studies for Trypanothione reductase inhibition

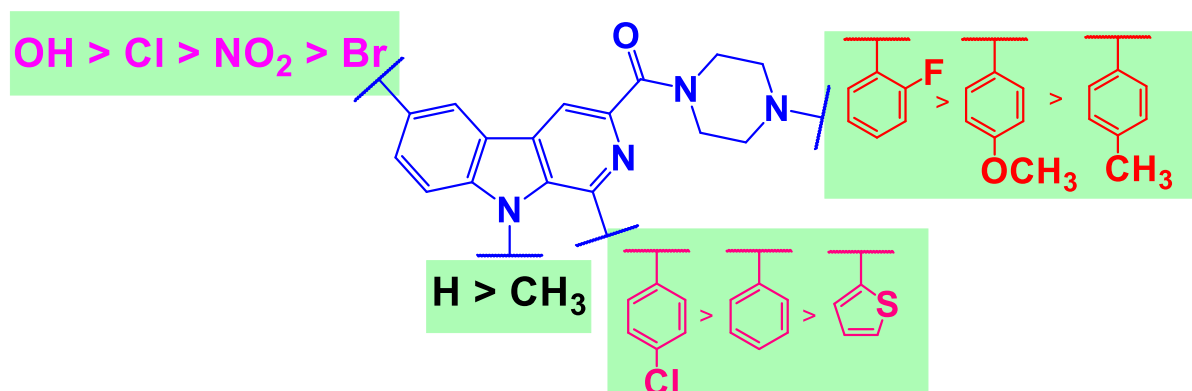


Figure 6.11. Structure activity relationship study of β -carboline associated with its Trypanothione reductase inhibitory activity

- In order to gain an understanding of the trypanothione reductase activity spectrum of the compounds that were screened, simple structure-activity relationship studies were carried out. The goal of these studies was to conclude the impact of variation of substitution at various positions of the β -carboline scaffold (**Figure 6.11**).
- As a direct result of the research that was outlined earlier, it is now plainly evident that the *N*-methyl substituted β -carboline is the more potent molecules.
- The same thing was found here, and it revealed that TR inhibition of the *N*-methyl substituted β -carboline showed 100% inhibition at 100 μ M tested concentration when compared to the standard drug thioridazine (99%) at the same concentration.
- After making substitution with hydroxyl group at the sixth position, the activity spectrum decreased. The addition of chlorine, followed by addition of nitro groups at the 6th position, led to an increase in the TR inhibition.
- Upon bromine was substituted, the results showed a significant increase in the TR inhibition. The piperazines were modified so that they possessed phenyl rings instead, which resulted in various differences in TR inhibition activity.
- The activity spectrum of compound with 4-methyl benzene substitution at phenyl piperazine showed increase in activity when compared with 2-fluoro benzene substitution at phenyl piperazine moiety.
- The TR inhibition was significantly aided by contributions of the substituted aldehydes. When compared to benzaldehyde, the inhibition was not significantly altered upon chlorobenzaldehyde substitution.

Chapter 6. Anti-leishmanial, Cell viability, and Trypanothione reductase assay

- An enormous boost in TR inhibition was provided by heterocycle aldehyde thiophene. In general, the halogens such as bromine along with heterocyclic aldehyde substitution were responsible for major modifications in the TR inhibition.

References

- (1) Calvo-Álvarez, E.; Stamatakis, K.; Punzón, C.; Álvarez-Velilla, R.; Tejería, A.; Escudero-Martínez, J. M.; Pérez-Pertejo, Y.; Fresno, M.; Balaña-Fouce, R.; Reguera, R. M. Infrared Fluorescent Imaging as a Potent Tool for in Vitro, Ex Vivo and in Vivo Models of Visceral Leishmaniasis. *PLoS Neglected Tropical Diseases* **2015**, *9* (3), e0003666. <https://doi.org/10.1371/journal.pntd.0003666>.
- (2) Pérez-Pertejo, Y.; Escudero-Martínez, J. M.; Reguera, R. M.; Balaña-Fouce, R.; García, P. A.; Jambrina, P. G.; San Feliciano, A.; Castro, M. Á. Antileishmanial Activity of Terpenylquinones on *Leishmania Infantum* and Their Effects on *Leishmania* Topoisomerase IB. *International Journal for Parasitology: Drugs and Drug Resistance* **2019**, *11*, 70–79. <https://doi.org/10.1016/j.ijpddr.2019.10.004>.
- (3) Hamilton, C. J.; Saravanamuthu, A.; Eggleston, I. M.; Fairlamb, A. H. Ellman's-Reagent-Mediated Regeneration of Trypanothione in Situ: Substrate-Economical Microplate and Time-Dependent Inhibition Assays for Trypanothione Reductase. *The Biochemical Journal* **2003**, *369* (Pt 3), 529–537. <https://doi.org/10.1042/BJ20021298>.
- (4) Bradford, M. M. A Rapid and Sensitive Method for the Quantitation of Microgram Quantities of Protein Utilizing the Principle of Protein-Dye Binding. *Analytical Biochemistry* **1976**, *72*, 248–254. <https://doi.org/10.1006/abio.1976.9999>.
- (5) Chauhan, S. S.; Pandey, S.; Shivahare, R.; Ramalingam, K.; Krishna, S.; Vishwakarma, P.; Siddiqi, M. I.; Gupta, S.; Goyal, N.; Chauhan, P. M. S. Novel β -Carboline-Quinazolinone Hybrid as an Inhibitor of *Leishmania Donovanii* Trypanothione Reductase: Synthesis, Molecular Docking and Bioevaluation. *MedChemComm* **2015**, *6* (2), 351–356. <https://doi.org/10.1039/c4md00298a>.
- (6) Baréa, P.; Barbosa, V. A.; Bidóia, D. L.; de Paula, J. C.; Stefanello, T. F.; da Costa, W. F.; Nakamura, C. V.; Sarragiotto, M. H. Synthesis, Antileishmanial Activity and Mechanism of Action Studies of Novel β -Carboline-1,3,5-Triazine Hybrids. *European Journal of Medicinal Chemistry* **2018**, *150*, 579–590. <https://doi.org/10.1016/j.ejmech.2018.03.014>.
- (7) Battista, T.; Colotti, G.; Ilari, A.; Fiorillo, A. Targeting Trypanothione Reductase, a Key Enzyme in the Redox Trypanosomatid Metabolism, to Develop New Drugs against Leishmaniasis and Trypanosomiasis. *Molecules* **2020**, *25* (8). <https://doi.org/10.3390/molecules25081924>.
- (8) Turcano, L.; Torrente, E.; Missineo, A.; Andreini, M.; Gramiccia, M.; Di Muccio, T.;

Chapter 6. Anti-leishmanial, Cell viability, and Trypanothione reductase assay

Genovese, I.; Fiorillo, A.; Harper, S.; Bresciani, A.; Colotti, G.; Ilari, A. Identification and Binding Mode of a Novel Leishmania Trypanothione Reductase Inhibitor from High Throughput Screening. *PLoS Neglected Tropical Diseases* **2018**, *12* (11), 1–21. <https://doi.org/10.1371/journal.pntd.0006969>.



Chapter 7. Computational investigations



Material and methods for the computational investigations

Molecular docking:

Computational sources: Xenon W3565 processor, Ubuntu 18.04

Software and version: Schrodinger software, version 2018-1¹ (Glide module for docking).

Retrieval of the proteins: RCSB protein data bank²

(PDB-2JK6 <https://www.rcsb.org/structure/2JK6>)

Docking method: Extra precession mode

Results analysis: XP visualizer (Schrodinger)

Docking workflow: The Ligprep module of the software (Version 2018-1, Schrodinger)³ was used to minimize the energy with Optimized Potentials for Liquid Simulations 3 (OPLS3) force fields. The minimization process enables the allocation of bond orders, addition of hydrogens to ligands and conversion of 2D into 3D structures to improve docking performance. Further docking studies were conducted using the output file (Best conformations of the ligands)³.

In Schrodinger, the protein preparation wizard (version 2019-1, Schrodinger)⁴ is the primary application for preparing proteins and minimizing their energy content. It adds hydrogen atoms to protein and assign charges to them. The Het states were generated using Epik at pH 7.0 ± 2.0. Using workspace analysis, the protein was refined, modified and the heteroatoms in the water were removed. The crucial water molecules stayed the same, but all other molecules apart from the water were removed except the co-crystal ligand. The OPLS3 force field was then used to minimize the protein. An active site grid was generated by considering co-crystal ligands, which are included in the active site of the selected protein target (PDB-2JK6). To validate the protein, root mean square deviation (RMSD) was calculated after docking with the co-crystal ligand in XP mode, which came out to be 0.20 Å.

Molecular mechanics with generalised Born and surface area solvation (MMGBSA)

studies: The extra precession (XP) mode docking output was selected as input for MMGBSA analysis. The raw files were executed using Prime module of Schrodinger to calculate the Binding free energy of each docked complexes.

Molecular dynamics workflow: Simulation of Molecular Dynamics (MD) helps visualize the action of Protein-Ligand complexes (PLC) at the target's binding site region under physiological conditions. MD was performed using Desmond module of Schrödinger developed by D.E Shaw research group (Academic license, Version 2020-1)⁵ through the system's builder panel. The orthorhombic simulation box was prepared with TIP3P water model in such a way that the minimum distance between protein surface and solvent surface is 10 Å⁶. Neutralization of the solvated system was accomplished by using counterions and

limiting the salt concentration in the physiological system to 0.15 M. The PLC system was designated with the all-atom Optimized Potentials for Liquid Simulations (OPLS4) force field ⁷.

Two seconds of relaxation time was used for the Reversible reference System Propagator Algorithms (RESPA) integrator ⁸, Nose-Hoover chain thermostat ⁹ and Martyna-Tobias-Klein barostat. The final production of MD simulation was performed using the equilibrated system. This MD simulation was set to run for 100 ns with 310 K temperatures at 1.0 bar pressure, with the NPT (Isothermal-Isobaric ensemble, constant number of particles (N), constant pressure (P), constant temperature (T)) ensemble at default settings ¹⁰ for relaxation before simulation. The MD simulation was performed with MD simulation tool, with the simulation time set to 100 ns. Furthermore, the `_out` file was used to view the trajectories and create a movie. The `out.cms` file was imported and the movie was exported at higher resolution (1280x1024) with better quality. The trajectory was written with 1000 frames during the entire MD simulation. The protein backbone frames were aligned to backbone of the initial frame to better understand the complex's stability during MD simulation. Finally, after loading the `.out` file and selected the Root Mean Square Deviation (RMSD), Root Mean Square Fluctuation (RMSF) in the analysis type to oblique, the simulation interaction diagram and the results were analysed ^{11,12}.

Findings from molecular docking study

The molecular docking method can be used to model the interaction between small molecule and target protein at the atomic level. This gives us the ability to characterize the behavior of small molecules in the binding site of target proteins as well as to shed light on fundamental biochemical processes. The molecular docking and molecular dynamics workflow were already described in the methodology section of chapter 4. The molecular docking was initially started with downloading of the appropriate PDB from the RCSB website. The PDB – 2JK6 was selected based on the Classification: oxidoreductase Organism(s): *Leishmania infantum* Expression System: *Escherichia coli* Method: X-ray diffraction, Resolution: 2.95 Å, R-Value Free: 0.264, R-Value Work: 0.235, R-Value Observed: 0.237 and some of the previously reported literature. It was the first PDB available in the RCSB for leishmanial Trypanothione reductase. It contains 2 chains of homodimer with 511 amino acid residues. The validation of the selected PDB was done by checking the Root Mean Square Deviation and found to be 0.20 Å (**Figure 7.1**). Trypanothione reductase (TR) is perceived as one of the significant strategic targets for discovering new leishmaniasis therapeutic agents. It is an enzyme indispensable for the host's parasite sustenance because it reduces trypanothione, a molecule sent to neutralize hydrogen peroxide host macrophages during the infection in Leishmaniasis. To investigate the

putative binding pattern of the titled compounds against TR, molecular docking studies was performed.

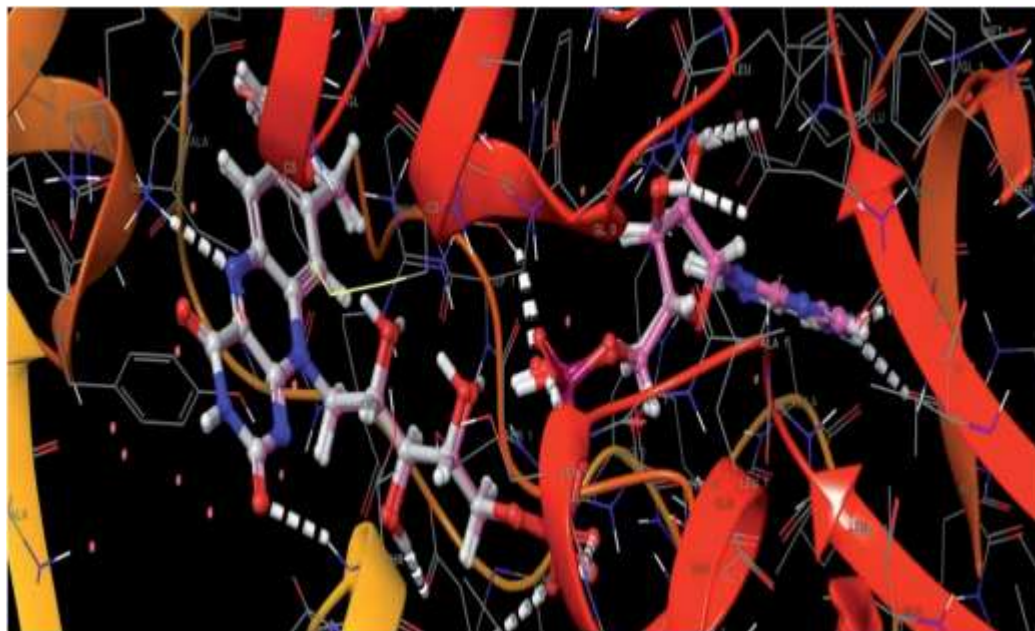


Figure 7.1. Superimposed view of the FAD molecule in the active site of the target PDB-2JK6 and its re-docked pose in the same target (RMSD – 0.20 °A)

The results obtained and analysis are shown in **table 7.1**, after the investigative process of molecular docking studies. The binding score of the standard TR inhibitor (SQD) was found to be -6.6 Kcal/mol and from the standard's docked orientation, MET365, CYS52, TYR198, GLU202 and ALA365 are actively implicated at the binding pocket of the TR target. In complex **72**, the compound formed hydrophobic interactions with LYS60 and TYR198 at the distance of 5.79 Å and 3.24 Å, respectively (-5.19 Kcal/mol), while ALA365, PHE230, MET365 and ASP327 residues coordinated with compound **72** through aromatic bond of length less than 3 Å, as shown in **table 7.1**. In complex **75**, the active compound showed three aromatic hydrogen bonds with TYR198 (2.32 Å), ASP327 (2.41 Å) and ALA365 (2.34 Å) with docking score of -6.81 Kcal/mol. Also, pi-pi stacking contact with TYR198 (3.93 Å) and pi-cation contact with LYS60 (5.07 Å) of the binding pocket. Similarly, complex **77** is stabilized by aromatic hydrogen bonds with MET365 (2.37 Å), ASP327 (2.65 Å), PRO435 (2.57 Å, 2.69 Å), one strong hydrogen bond interaction with ALA365 (2.05 Å) and hydrophobic contacts with PHE367 (5.29 Å, 5.46 Å, 5.12 Å) and LYS61 (4.04 Å) at the binding pocket of TR enzyme (**Figure 7.2**). Docked complexes of compounds **68** and **78** showed similar type of binding pattern with THR335 and PHE367 at the active site with the docking score of -5.8 and -6.36 Kcal/mol, respectively. Another active complex **70** is supported by hydrophobic interactions with LYS60 (6.02 Å) and TYR198 (5.27 Å). Additionally, the compound forms a halogen bond

with SER178 (2.4 Å) and an aromatic hydrogen bond with ALA159 (2.39 Å) at the TR's active site. The low docking score (-2.80 Kcal/mol) of compound **70** could be due to the additional bond interaction with the enzyme at the binding site. Similarly, the significant compounds **91** and **78** exhibited strong aromatic hydrogen bond linkage with amino acid PRO435 with docking scores of -4.60 Kcal/mol and -4.92 Kcal/mol, respectively (**Figure 7.3**). Moreover, compound **78** was further stabilized by hydrogen and pi-pi stacking interaction with PHE367 and TYR198 at the active site of TR target. Another compound **100** revealed three pi interactions with PHE 367 and one hydrogen bond with ALA 367 (**Figure 7.3**) residue with docking score of -4.92 Kcal/mol.

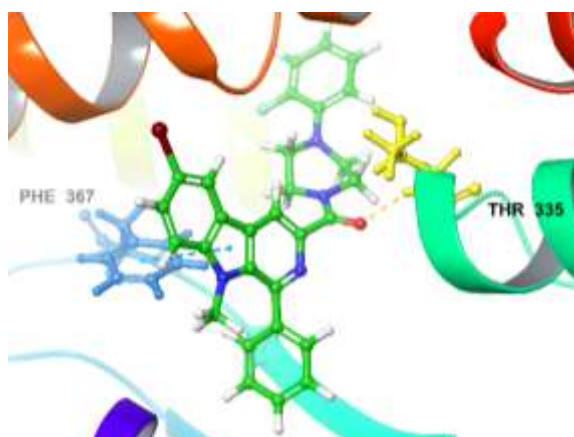
All the active compounds interact with the surrounding amino acid residues as discussed previously in order to establish a constant connection between the compound atoms and the TR target. Further, these studies were validated by molecular dynamics studies of all the docked complexes in the active site of the TR target.

Table 23. Results of molecular docking studies of test compounds at the active site of target protein (PDB-2JK6)

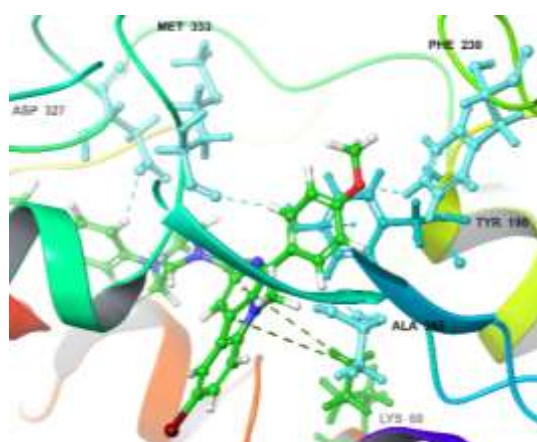
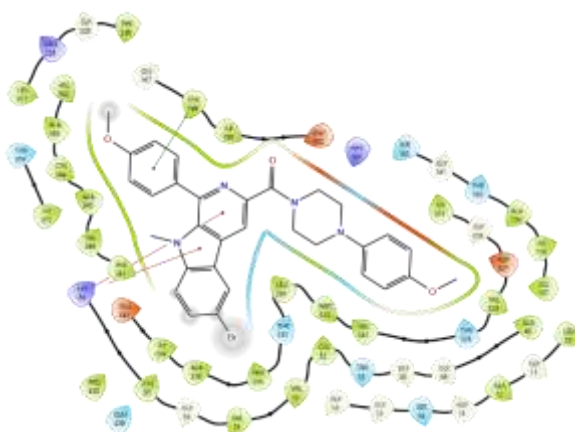
| Comp. code | Docking score (kcal/mol) | Amino acid involved in interactions | Distance (Å) | Type of bond |
|------------|--------------------------|-------------------------------------|--------------|-----------------|
| 68 | -5.82 | THR335 | 2.18 | H-Bond |
| | | PHE367 | 5.37 | Pi-pi Stacking |
| 72 | -5.19 | LYS60 | 5.79 | Pi-Cation |
| | | ALA365 | 2.56 | Aromatic H-Bond |
| | | TYR198 | 3.24 | Pi-pi Stacking |
| | | PHE230 | 2.46 | Aromatic H-Bond |
| | | MET333 | 2.54 | Aromatic H-Bond |
| | | ASP327 | 2.38 | Aromatic H-Bond |
| 75 | -6.36 | TYR198 | 3.93 | Pi-pi Stacking |
| | | | 2.32 | Aromatic H-Bond |
| | | LYS60 | 5.07 | Pi-Cation |
| | | ASP327 | 2.41 | Aromatic H-Bond |
| | | ALA365 | 2.34 | Aromatic H-Bond |
| 77 | -5.43 | MET333 | 2.37 | Aromatic H-Bond |
| | | ASP327 | 2.65 | Aromatic H-Bond |
| | | ALA365 | 2.05 | H-Bond |
| | | PRO435 | 2.57 | Aromatic H-Bond |
| | | | 2.69 | Aromatic H-Bond |
| | | PHE367 | 5.29 | Pi-pi Stacking |
| | | | 5.46 | Pi-pi Stacking |
| | | | 5.12 | Pi-pi Stacking |
| LYS61 | 4.04 | Pi-Cation | | |
| 78 | -6.81 | PHE367 | 5.31 | Pi-pi Stacking |
| | | THR335 | 1.99 | H-Bond |
| 70 | -2.81 | LYS60 | 6.02 | Pi-Cation |
| | | TYR198 | 5.27 | Pi-pi Stacking |
| | | ALA159 | 2.39 | Aromatic H-Bond |
| | | SER178 | 2.4 | Halogen-Bond |
| 91 | -4.69 | PRO435 | 2.51 | Aromatic H-Bond |
| 100 | -4.92 | PHE367 | 5.35 | Pi-pi Stacking |
| | | | 5.31 | Pi-pi Stacking |

Chapter 7. Computational investigations

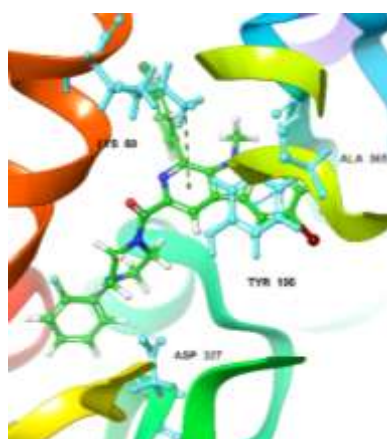
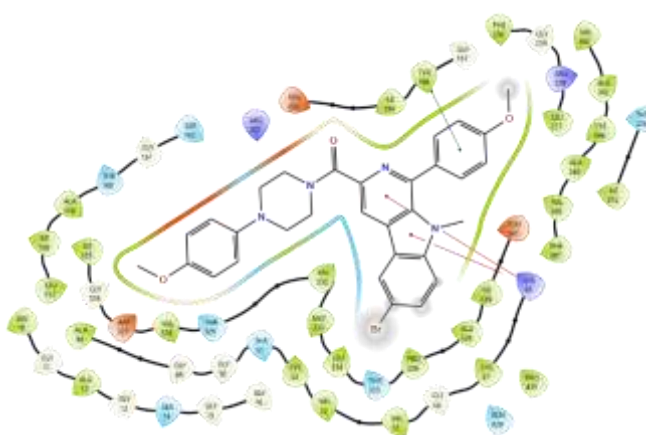
| | | | | |
|------------------------------|-------|---------|------|-----------------|
| | | | 5.03 | Pi-pi Stacking |
| | | ALA365 | 2.4 | H-Bond |
| | | TYR198 | 5.46 | Pi-pi Stacking |
| | | PRO435 | 2.3 | Aromatic H-Bond |
| Standard TR (SQD) | -6.67 | CYS 52 | 2.64 | Hydrogen bond |
| | | MET333 | 2.23 | Hydrogen bond |
| | | TYR198 | 3.71 | Pi stacking |
| | | TYR198 | 5.32 | Pi stacking |
| | | TYR198 | 5.5 | Pi stacking |
| | | GLU 202 | 2.73 | Aromatic bond |
| | | ALA365 | 2.32 | Aromatic bond |
| | | ALA365 | 2.34 | Aromatic bond |



Structure Code: 68



Structure Code: 72



Structure Code: 75

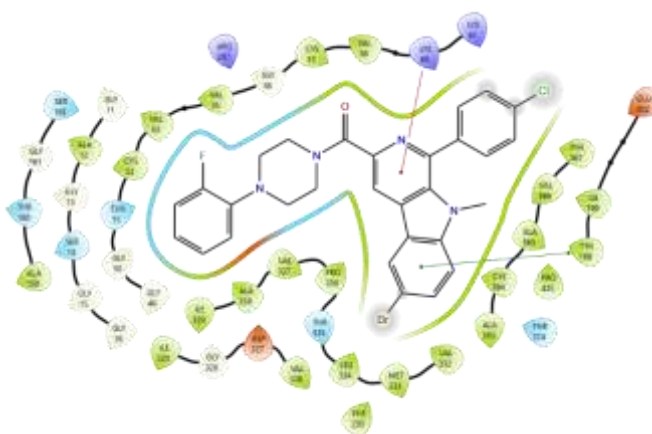
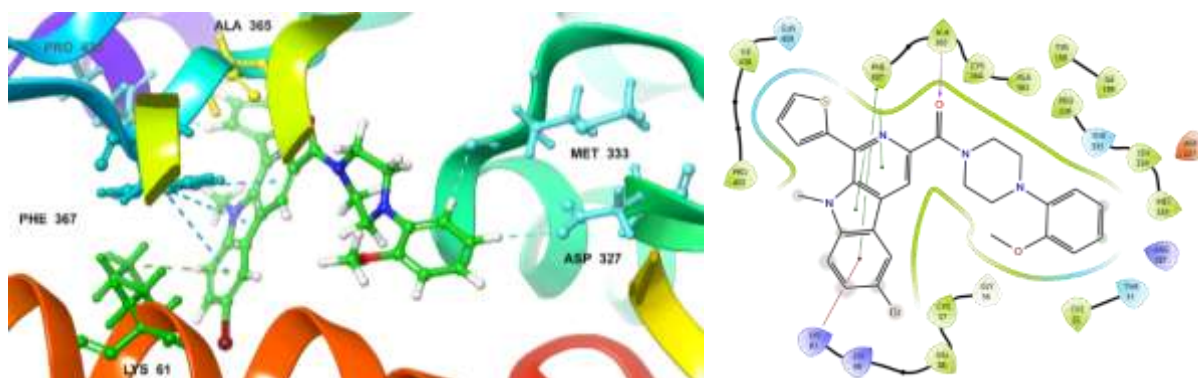
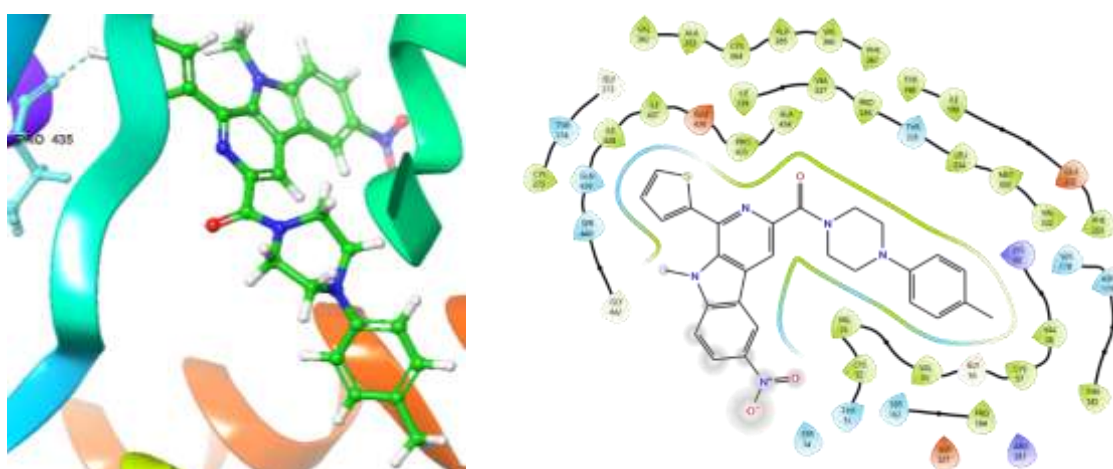


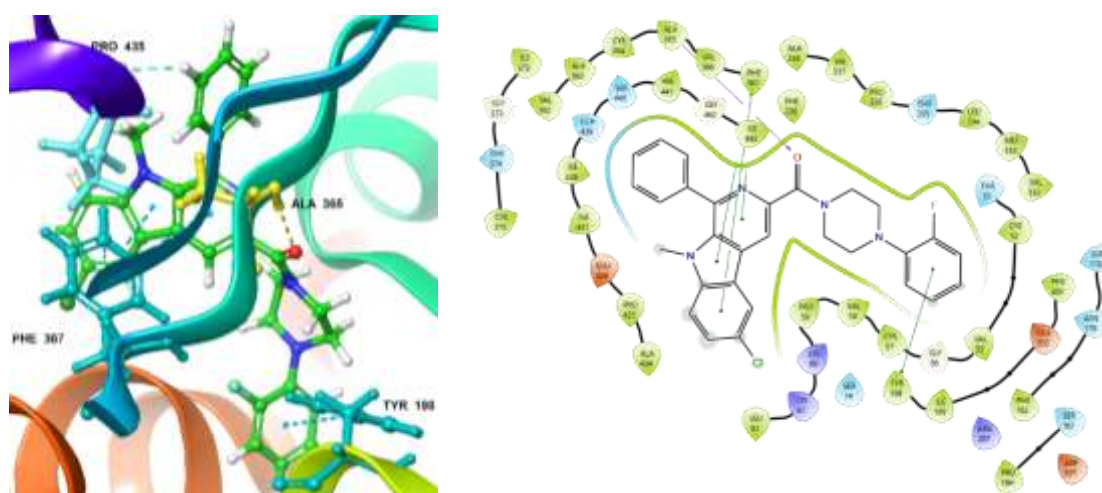
Figure 7.2. Exposed amino-acid residue interactions (3D and 2D) of the significantly active compounds **68**, **72** and **75** in the active site of the target protein (PDB:2JK6)



Structure Code: 77

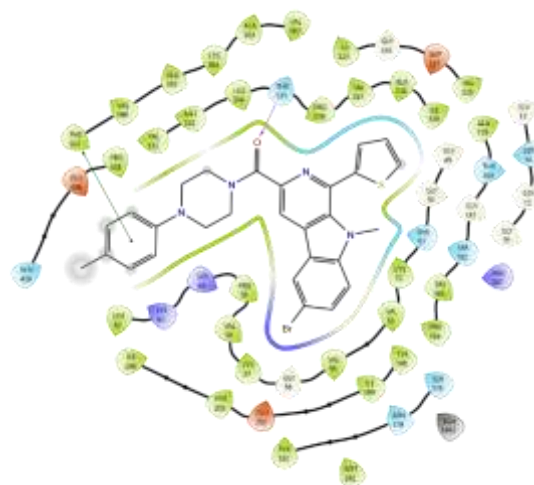
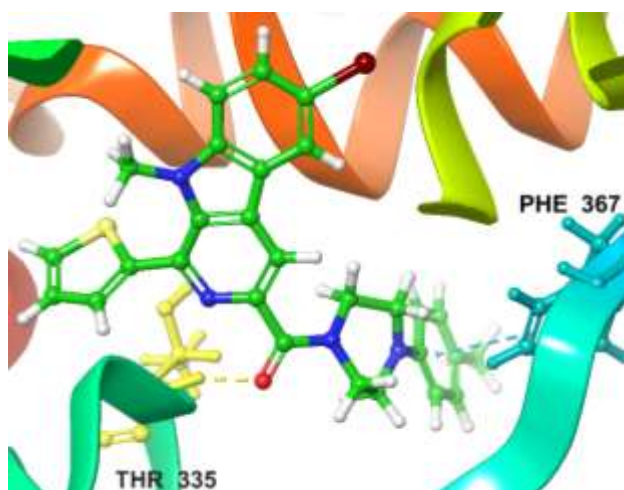


Structure Code: 91

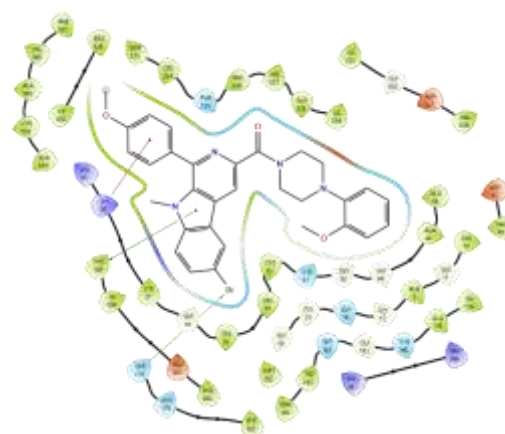
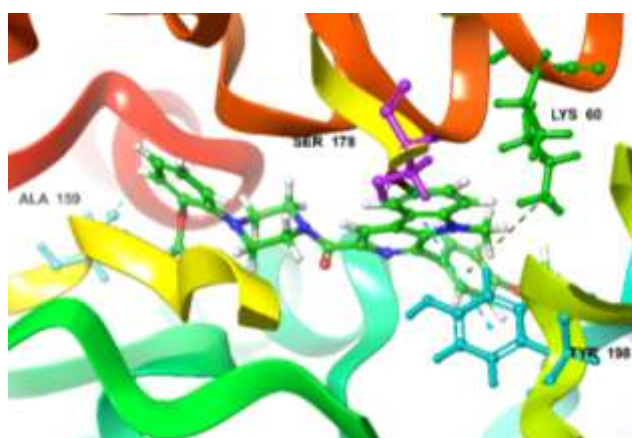


Structure Code: 100

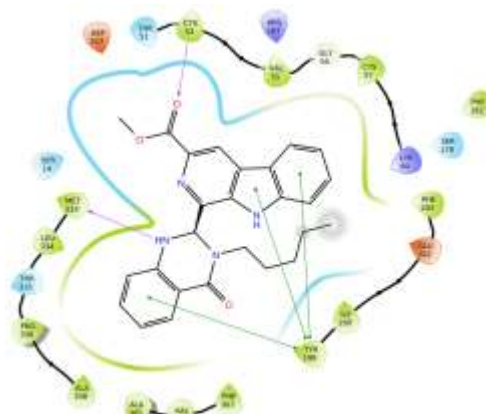
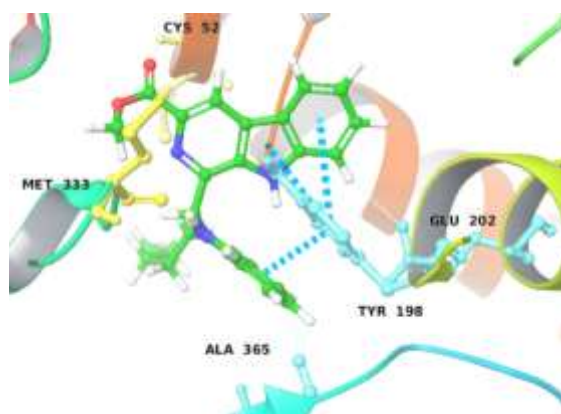
Figure 7.3. Exposed amino-acid residue interactions (3D and 2D) of the significantly active compounds **77**, **91** and **100** in the active site of the target protein (PDB:2JK6)



Structure Code 78



Structure Code 70



Structure Code: Standard TR (SQD)

Figure 7.4. Exposed amino-acid residue interactions (3D and 2D) of the significantly active compounds **78**, **70** and standard TR (SQD) in the active site of the target protein (PDB:2JK6)

Findings from MMGBSA analysis

Molecular mechanics with generalized Born and surface area (MM/GBSA) solvation is a popular method to calculate the free energy of binding of ligand to protein. The binding free energy is the total energy of all interactions between ligand and target molecule. When compared with the scores obtained from molecular docking, the binding free energies of the identified hit molecules (compound codes **72**, **68**, **70**, **75**, **77**, **78**, **91** and **100**) showed encouraging results. These results were rushed so that a molecular dynamics simulation could be carried out. **Figure 7.5** provides visual evidence that the binding free energy are relatively high and the scores vary from -72.75 to -103.45 Kcal/mol. When contrasted to the findings of the docking studies, these are highly encouraging signs. The compound **78** showed a score of -103.45 Kcal/mol, which made it the winner of MMGBSA competition. Based on these results, it was hypothesized that the compounds that were found hold potential for trypanothione reductase inhibition.

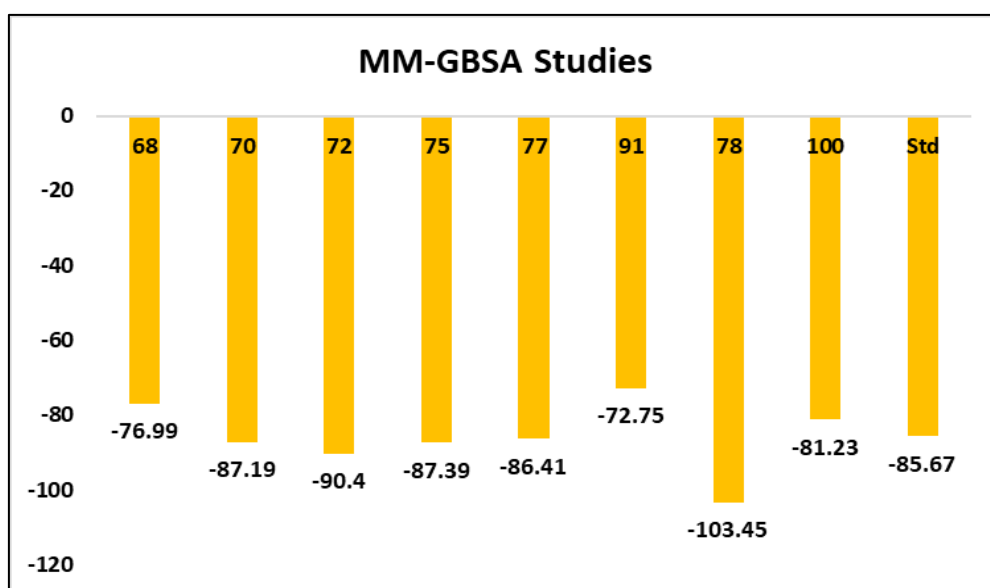


Figure 7.5. MMGBSA plot of topmost identified hit molecules (compound codes **72**, **68**, **70**, **75**, **77**, **78**, **91** and **100**)

Findings from molecular dynamics studies

Root Mean Square Deviation (RMSD)

The study about the motion that atoms and molecules make in real life using a method called molecular dynamics (MD), which is a type of computer simulation based analysis. The atoms and molecules were given a pre-determined amount of time in order to interact with one another, which provides a glimpse into "evolution" of the dynamic nature of the system. Using MD simulation to analyze how a bio-molecular system will react to a change in its environment is one of the most important applications of this technique. In every scenario, an individual

should run multiple simulations of both the perturbed and unperturbed systems in order to determine whether there are discernible differences in the outcomes.

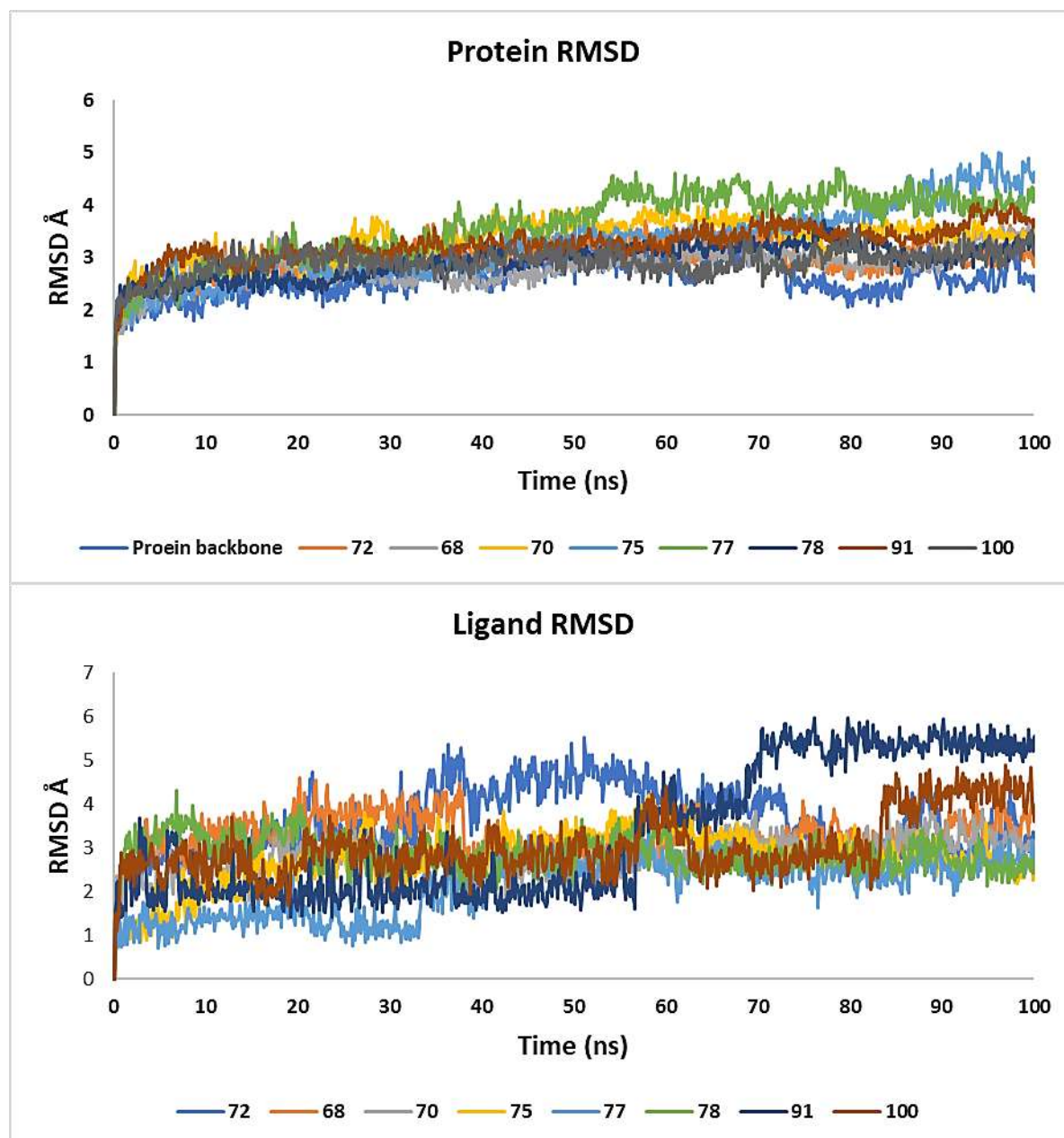


Figure 7.6. RMSD plot of protein and topmost identified hit molecules (compound codes **72, 68, 70, 75, 77, 78, 91** and **100**)

The MD simulation was performed for the best 8 molecules which showed significant activity against amastigotes and TR inhibition with the target protein (**PDB: 2JK6**). From the dynamics results, the ligands attained equilibrium with the protein during the simulation runs. **Figure 7.6.** represents the RMSD of ligands during the simulation time which clearly signifies that all the ligands had RMSD below 5.0 Å except for compound **91** that fluctuated up to 6.0 Å. Despite fluctuations, the ligands never moved out of the active site pocket. Further, to see the variation

in the protein structure, an RMSD plot of protein backbone against each ligand was also plotted and the results showed similar fluctuating pattern of the protein with all the ligands during simulation and the RMSD fluctuated between 2.0 - 5.0 Å.

Root Mean Square Fluctuation (RMSF)

Additionally, the RMSF plot determines the fluctuating residues during the simulation period. As shown in **figure 7.7**, most of the residues showed lower RMSF values of < 2.0 Å. The common residues that formed multiple interactions with the ligands include LYS60, LYS61, GLU202, ARG287, THR335, ALA365 and PHE367 (**table 7.2, 7.3**). In compound **68**, THR335 and ALA365 contributed majorly (52% and 45%, respectively) in interactions during the complete simulation. In compound **70**, the major contributing residues were LYS60 and ARG287 with contributions of 34% and 31%, respectively. Similarly, compound **72** exhibited interactions with LYS60 (52% contribution), ARG287 (52% contribution) and in addition, GLY15 also interacted with the ligand and contributed for 44% of the interactions during the simulation. Strong interactions were observed with compound **75** and **77**. The residue CYS57 and LYS60 interacted for most of the simulation time with compound **75** and their contributions were 79% and 84%, respectively, while in compound **77** highly contributing residue was ALA365 (85%) followed by LYS60 and LYS61 (30% and 34%, respectively). The residue GLU202 formed moderate interaction with compound **78** (33%), compound **91** (56%) and compound **100** (41%). Apart from this, ALA368 contributed for 50% of interactions with

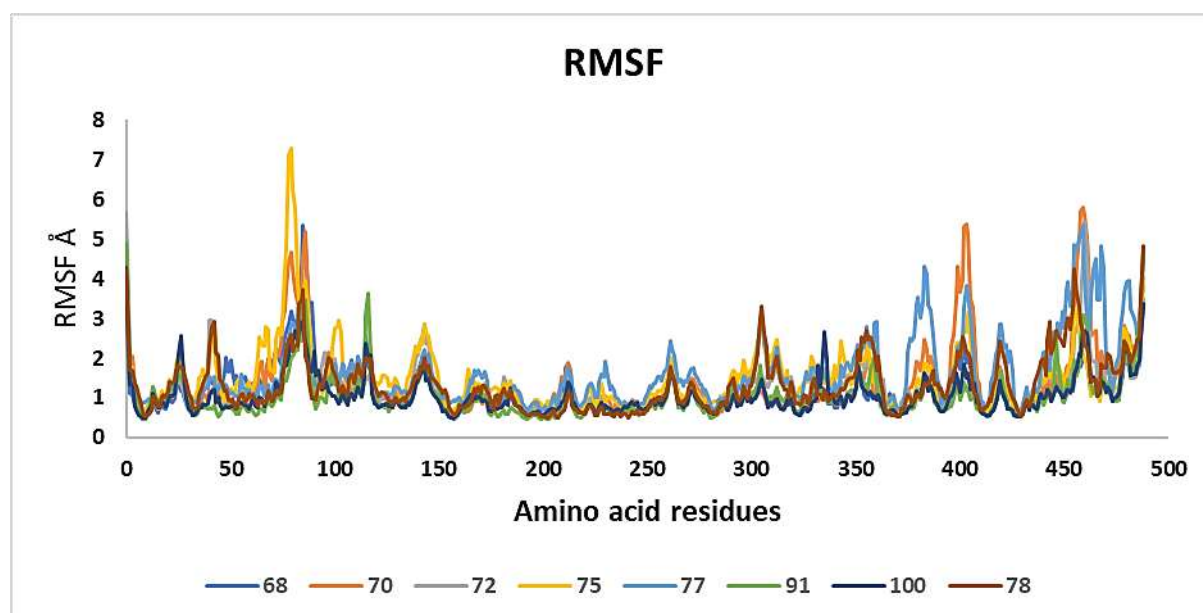


Figure 7.7. RMSF plot of topmost identified hit molecules (compound codes **72, 68, 70, 75, 77, 78, 91** and **100**)

compound **78** and ALA365, PHE367 contributed for 59% and 33% interactions, respectively with compound **100**.

Radius of gyration (RGY)

The rotatable bonds present in the test compounds are usually responsible for high fluctuations during the simulation run. Hence, in order to observe their impact on the target protein, radius of gyration is keenly observed. **Figure 7.6** shows the root mean square deviation (RMSD), which suggests that the torsion of rotatable bonds in the simulation did not cause significant RMSD variation. It's a sign that the target was not deviated. If the RMSD was smaller, then the radius of gyration must have been smaller too (**Figure 7.8**). This indicates that the intended amino acids are bonded firmly to one another and have not been displaced from their original position. This gives an insight of the stability of the ligands within the active site of the target protein.

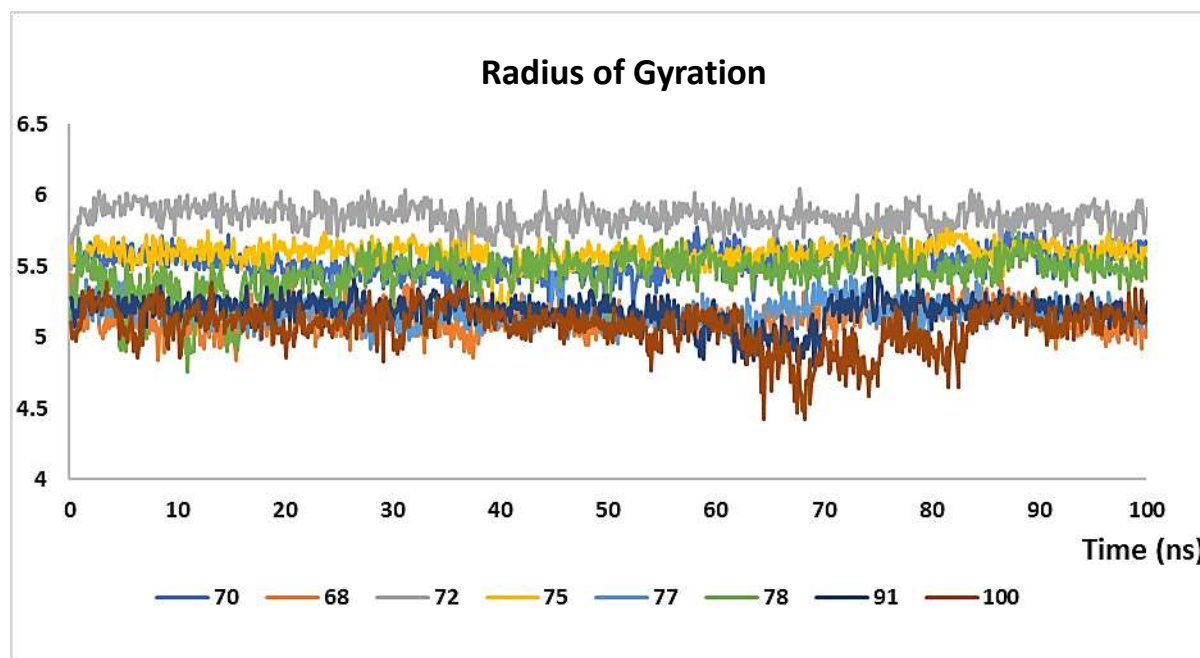


Figure 7.8. RGY plot of topmost identified hit molecules (compound codes **72, 68, 70, 75, 77, 78, 91 and 100**)

Amino acid interaction analysis

The investigations focused on the essential amino acids engaged in interactions with the hit compounds **72, 68, 70, 75, 77, 78, 91 and 100**. It was revealed that some of the surrounding amino acid residues were involved in interactions with the compounds, which gave some useful information. The hydrogen bond contact between compound **68** and ALA365 amino acid was found to be 45 %, whereas the interaction between compound **68** and THR335 was found to be 52 %. This suggests that over the entirety of 100 ns simulation, this was actively participating

in the development of bonds. The percentage of the amino acid involved in the interactions were depicted in **Table 7.2**

In comparison to compound **68**, compound **70** exhibited high number of contacts, but the percentages were still quite low. The LYS60 showed highest percentage in it (34 %), while SER14 had the lowest (7 %). In addition to this, compound **70** exhibited five interactions that were mediated by water.

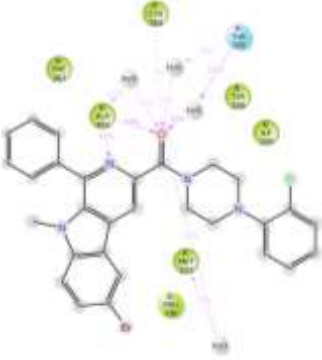


The investigation was continued all the way up to the compound **72**. In this instance, LYS60 and ARG287 revealed that there were 52% of bonds. GLY15 was engaged in 44% of all the interactions that include hydrogen bonds as well. Only one water-mediated interaction was observed in compound **72**. The LYS60 in combination with compound **75** produced the highest number, which was 84 %. This represented the largest percentage of amino acids that had been contributed up to this point. The amino acid CYS57 is involved in the formation of hydrogen bond with 79% and there was no evidence of any water-mediated interactions. The bar graph representations of the same were represented in **table 7.3**.


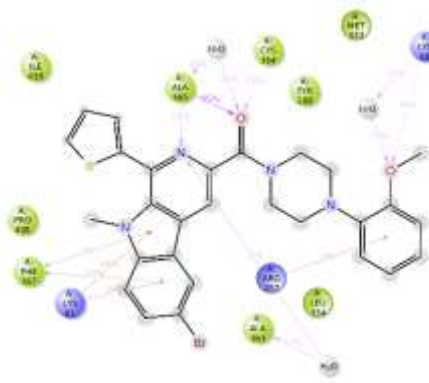
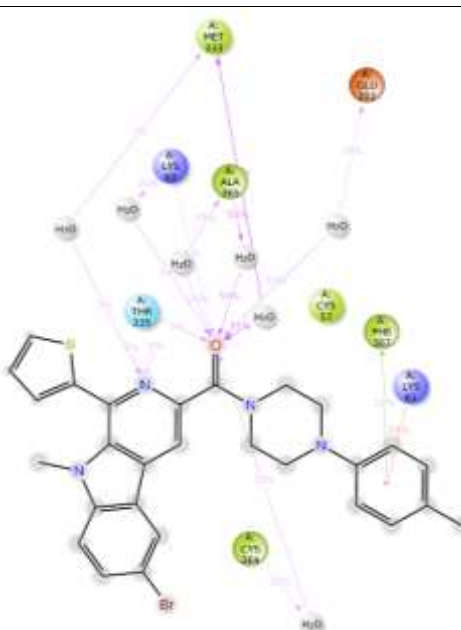
With 85 % of the communication taking place with ALA365 amino acid, compound **77** was involved with hydrogen bond. Other amino acids, such as LYS60, LYS61 and PHE367 was involved in the formation of bond to the extent of thirty percent, thirty-four percent and sixteen percent, respectively. One interaction involving water as a mediator was also seen with ALA365.

A number of amino acids, including LYS60 and LYS61, GLU202, THR335, MET333 and ALA365 were occupied the compound **78**. Only one of these amino acids, ALA365 was found to be involved in highest proportion of the hydrogen bond interactions and water-mediated interactions with compound **78**. This was the case out of all amino acids that were found to be involved in active contacts. The LYS60 was engaged with 24 % of interactions that were mainly carried out with water. The compound **91** also makes use of the same amino acid in its construction. Within this, the amino acid GLU202 contributed significantly with compound **91**, accounting for 56% of the total contribution. In addition to this, this was involved in interactions that were mediated by water as well. Amino acid LYS61 was responsible for smaller portion (10%) of contribution.

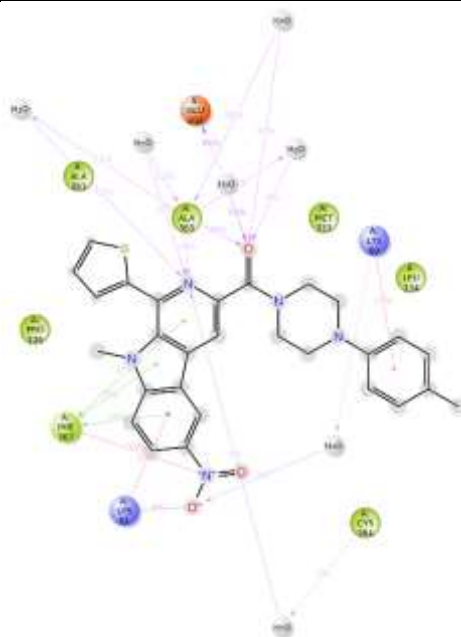
Including the six amino acids LYS61, TYR198, GLY202, ALA365, PHE367 and LYS60, all of which are encircled by compound **100**. Within these amino acids, ALA365 was responsible for 59 % of hydrogen bond interactions, while GLU365 was responsible for 41 % of water-mediated interactions.

Table 24. 2D interaction of protein-ligand contacts of the potent molecules with target protein (PDB:2JK6)

| S. No | Comp. code | Interacting image | Contributing residues | | |
|-------|------------|---|-----------------------|---------------|----------------|
| | | | Residue name | Contributions | Water mediated |
| 1. | 68 |  | MET333 | 15% | Yes |
| | | | THR335 | 52% | Yes |
| | | | CYS364 | 7% | No |
| | | | ALA365 | 45% | No |
| 2. | 70 |  | SER14 | 7% | Yes |
| | | | GLY15 | 7% | Yes |
| | | | LYS60 | 34% | No |
| | | | ARG287 | 31% | No |
| | | | ILE325 | 3% | Yes |
| | | | ASP327 | 17% | Yes |
| | | | ALA338 | 13% | Yes |
| 3. | 72 |  | GLY15 | 44% | No |
| | | | GLY16 | 11% | Yes |
| | | | LYS60 | 52% | No |
| | | | ARG287 | 52% | No |
| | | | CYS364 | 7% | No |
| | | | ALA365 | 9% | No |

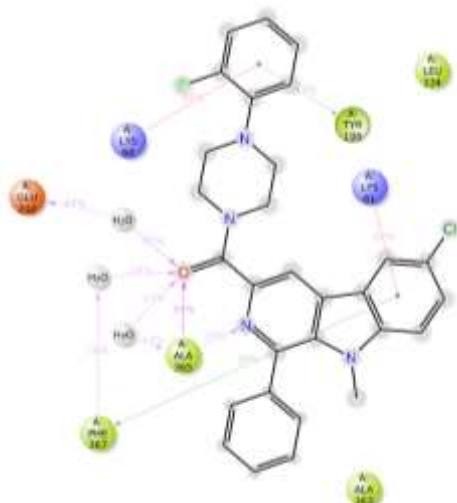
| | | | | | |
|----|----|---|-------|-----|-----|
| | | PHE367 | 18% | No | |
| 4. | 75 |  | CYS57 | 79% | No |
| | | LYS60 | 84% | No | |
| | | TYR198 | 18% | No | |
| | | ARG287 | 5% | No | |
| 5. | 77 |  | LYS60 | 30% | No |
| | | LYS61 | 34% | No | |
| | | ARG287 | 17% | No | |
| | | ALA363 | 17% | Yes | |
| | | ALA365 | 85% | No | |
| | | CYS364 | 13% | No | |
| | | PHE367 | 16% | No | |
| 6. | 78 |  | LYS60 | 24% | Yes |
| | | LYS61 | 14% | No | |
| | | GLU202 | 33% | Yes | |
| | | MET333 | 2% | Yes | |
| | | THR335 | 2% | No | |
| | | CYS364 | 22% | Yes | |
| | | ALA365 | 50% | Yes | |
| | | PHE367 | 11% | No | |

7. 91



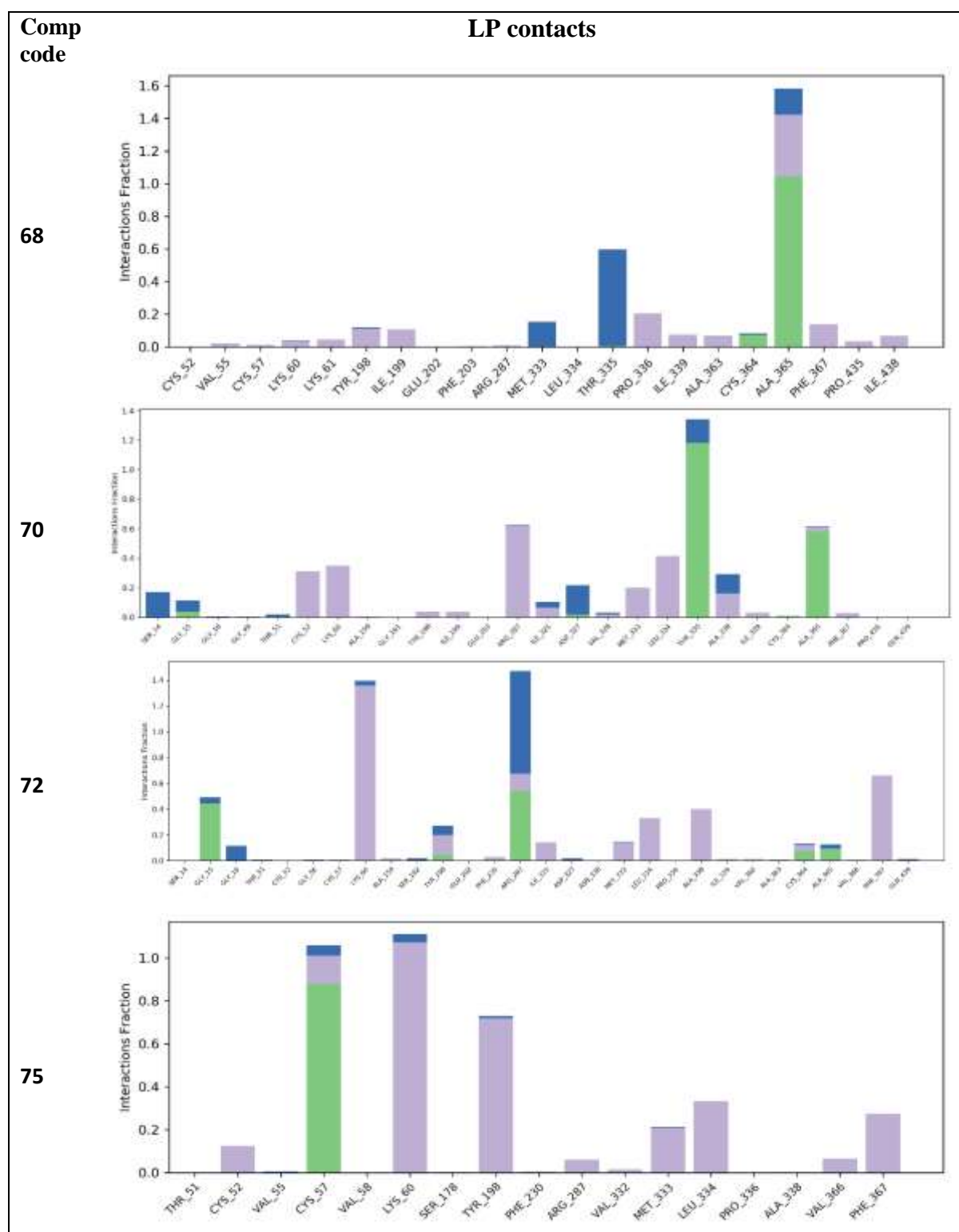
| | | |
|--------|-----|-----|
| LYS60 | 13% | No |
| LYS61 | 10% | No |
| GLU202 | 56% | Yes |
| ALA363 | 15% | Yes |
| ALA365 | 14% | No |
| PHE367 | 17% | No |

8. 100

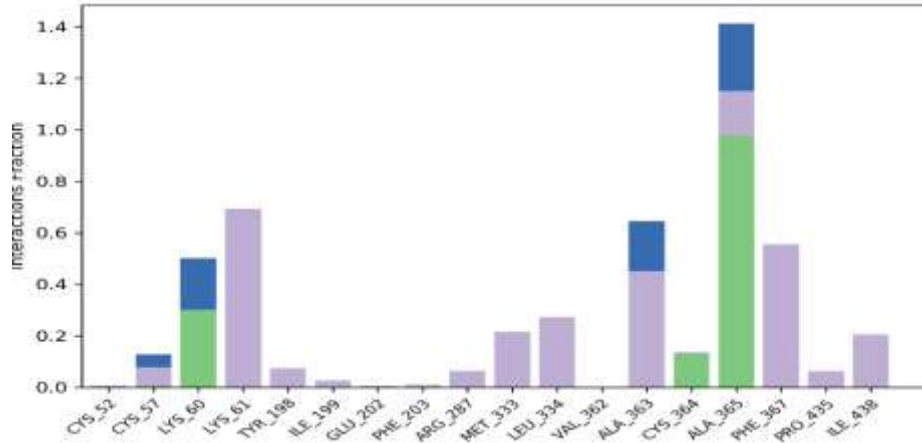


| | | |
|--------|-----|-----|
| LYS60 | 16% | No |
| LYS61 | 22% | No |
| TYR198 | 13% | No |
| GLU202 | 41% | Yes |
| ALA365 | 59% | No |
| PHE367 | 33% | No |

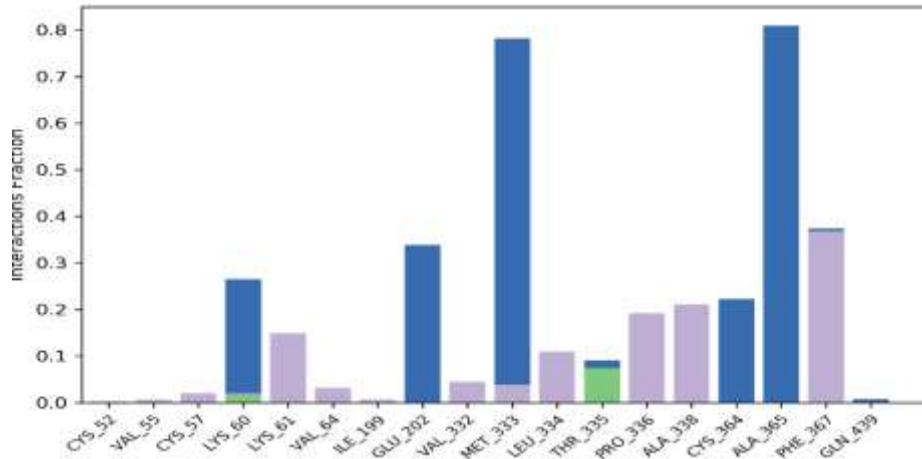
Table 25. Plot of potent ligands protein contacts



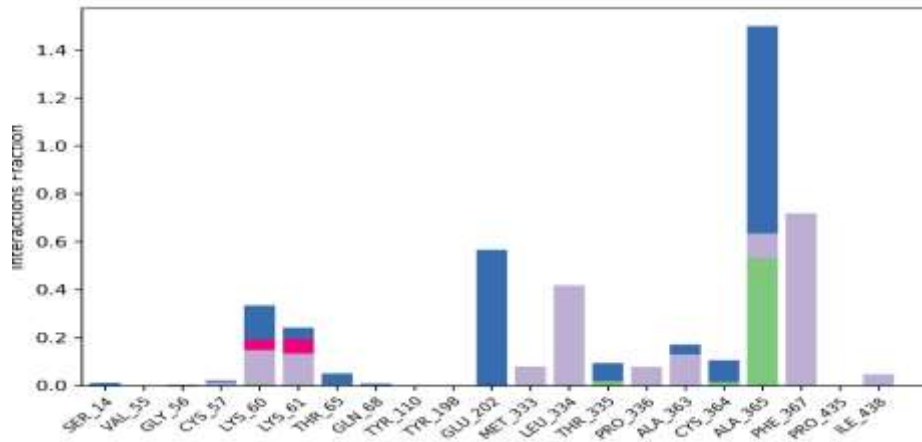
77

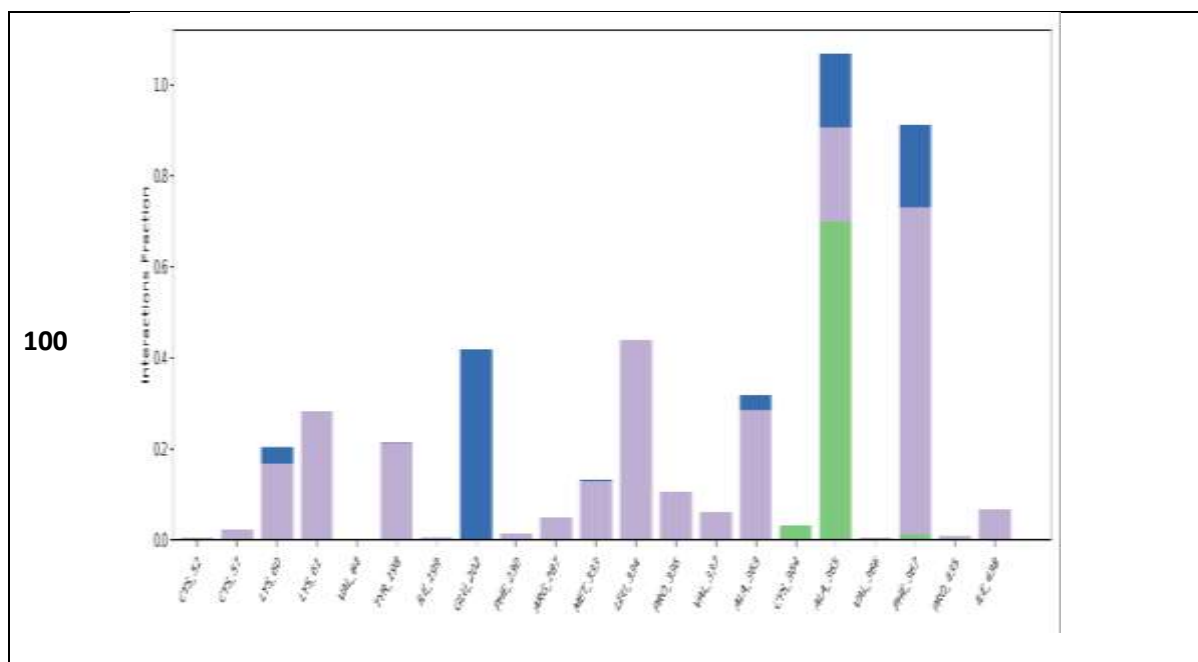


78



91





Trajectory frame analysis (Time frame analysis)

Compound 68

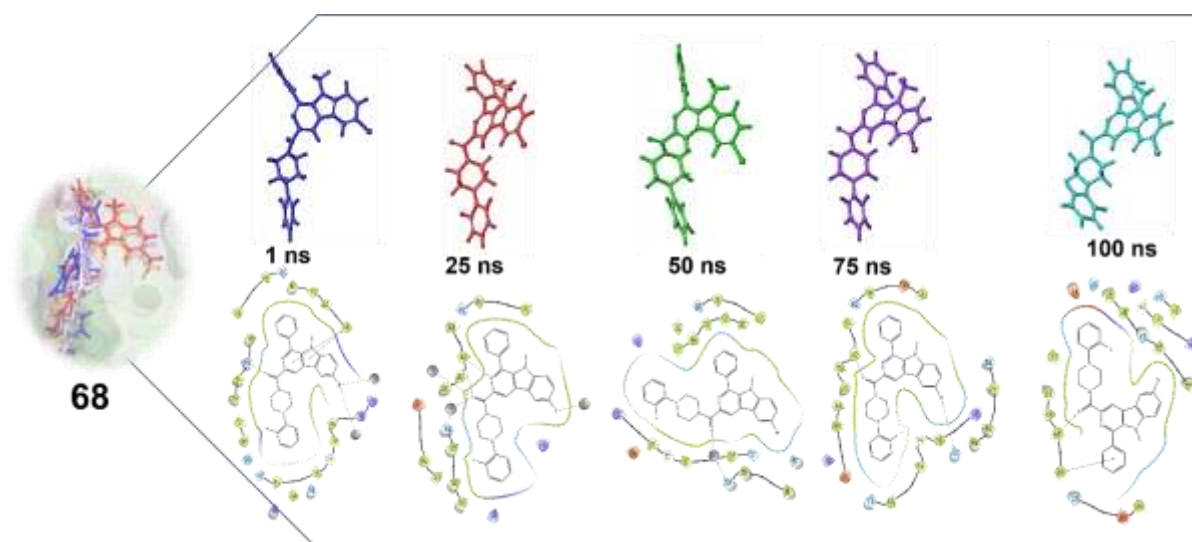


Figure 7.9. Time frame analysis of compound **68** at 1, 25, 50, 75 and 100 ns during the Molecular dynamics simulation

To assess the conformational behavior of molecule at the target location during 100 ns simulation, a time frame analysis was performed on compound **68**. To determine the orientation of ligands in the target's active site, the trajectory time frame analysis was performed for all the compounds for which MD were studied. The trajectories were exported into individual 25 ns time frames (**Figure 7.9**). Observing the interactions of the compound **68** with pyrido indole scaffold at 1 ns, PHE367 reveals pi-pi stacking interaction. It was discovered that two water molecules were involved in bromine-halogen bond interaction of the same scaffold. Hydrogen

bond interaction with an oxygen atom of keto group was observed with THR335. At 25 ns, it was discovered that two water molecules and ALA365 was formed a hydrogen bond with the same oxygen atom. The nitrogen of the pyrido indole scaffold forms a hydrogen bond with the same residue as well. Up to 50 ns, the interactions remain unchanged. At 75 ns, SER14 and bromine formed a halogen bond, ALA365 and oxygen of the propan-2-one linkage established a hydrogen bond. With other orientations of compound **68** at 100 ns, the study was continued. Up to 100 ns, no substantial changes were observed.

Compound 72

The methoxy phenyl of pyrido indole scaffold and TYR198 formed pi-pi stacking interaction with each other in the MD simulation of compound **72** at 1 ns, according to the time frame analysis. Amino acid LYS60 showed salt bridge mediated interaction while GLY15 formed a hydrogen bond with an oxygen atom. With the bromine of pyrido indole scaffold, one water molecule formed a halogen bond. Two water molecules were also involved in interaction at 25 ns (**Figure 7.10**); one was hydrogen bond with nitrogen of the pyrido indole scaffold and the other was a bond with oxygen of the methoxy phenyl in the same scaffold.

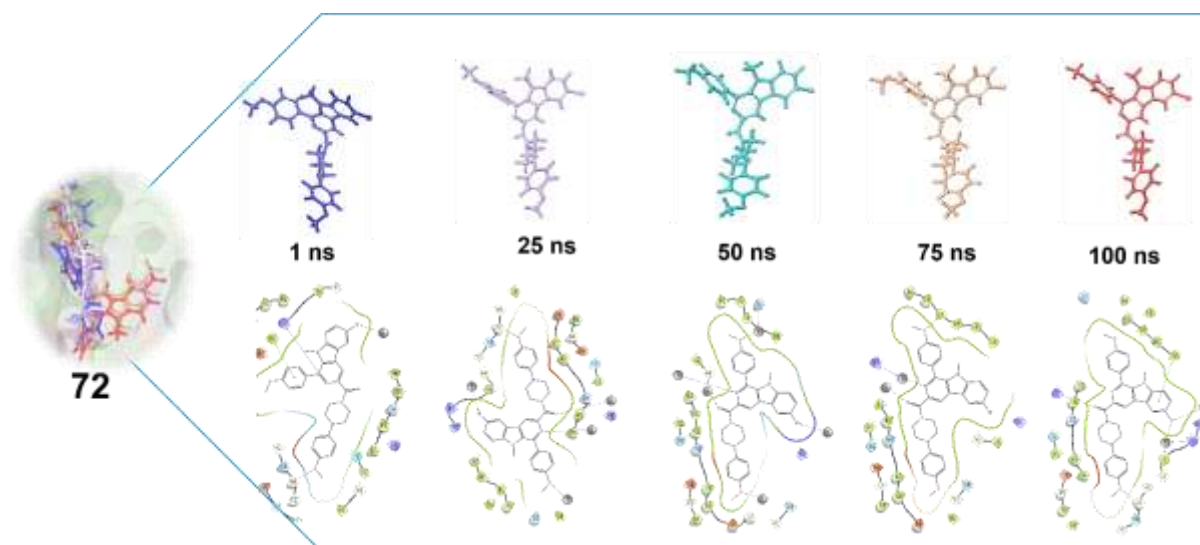


Figure 7.10. Time frame analysis of compound **72** at 1, 25, 50, 75 and 100 ns during the Molecular dynamics simulation

Until 25 ns, the remaining interactions was consistent. The amino acid residue GLN439 formed a hydrogen bond with water molecule at 50 ns time frame and some additional water molecules were also identified to be involved in interaction at that time. At 75 ns, CYS364 bonded to oxygen of methoxy phenyl in the scaffold of pyrido indole nucleus. The other interactions were unchanged. Two water molecules contacted the bromine of pyrido indole scaffold through

halogen bond at a time of 100 ns. Amino acid residues LYS60 and CYS57 with the same water molecule and ARG287 with an oxygen atom exhibited hydrogen bond interactions as well.

Compound 70

The pi-cation interaction between LYS60 and methoxy phenyl of pyrido indole scaffold was seen in the time frame analysis of compound **70** at 1 ns. The amino acid residues ALA365 and THR335 with the oxygen atom of methoxy group, respectively, formed hydrogen bond interaction (**Figure 7.11**). Three water molecules were evident in the interaction at 25 ns and all formed hydrogen bonds with one another. Amino acid ARG287 has established pi-cation interaction with pyrido indole scaffold. Amino acid ALA365 showed the same hydrogen bonding interaction with oxygen at 25 ns. Up to 50 ns, the interactions remain unchanged. Amino acid residues such as LYS60 & ARG287 showed several pi-cation interactions at 75 ns. In compound **70**, amino acid THR335 was found to form hydrogen bonds with oxygen and nitrogen atoms. At 100 ns, no significant changes were noticed.

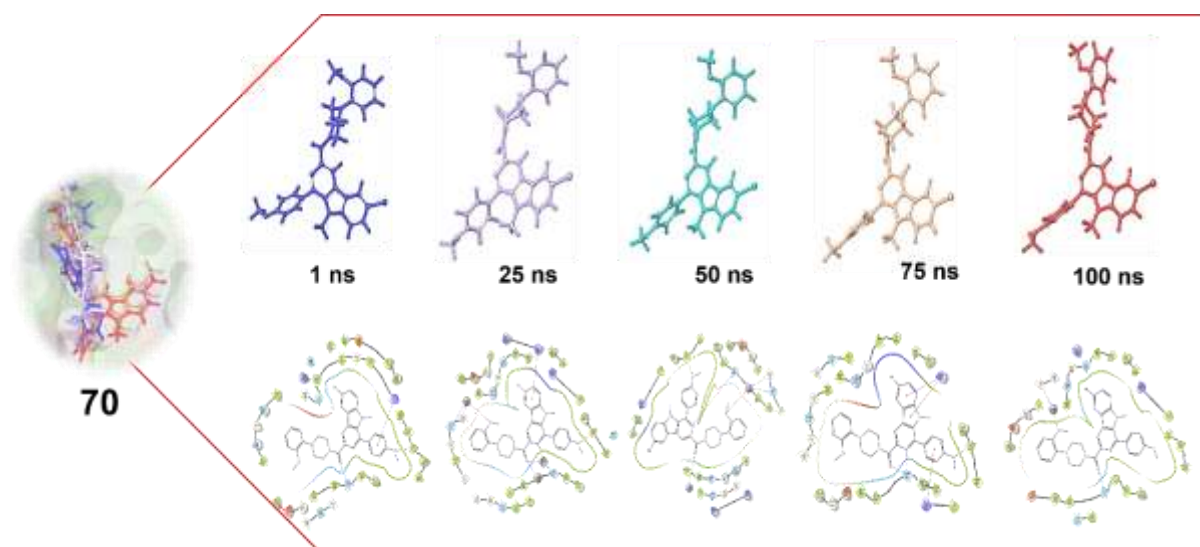


Figure 7.11. Time frame analysis of compound **70** at 1, 25, 50, 75 and 100 ns during the Molecular dynamics simulation

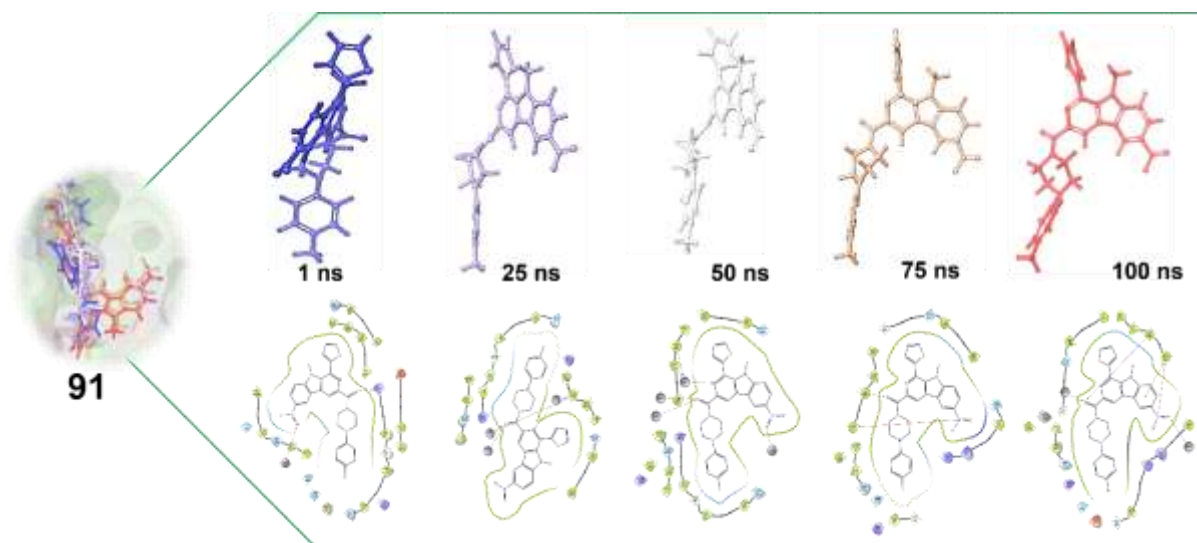
Compound 91

Figure 7.12. Time frame analysis of compound **91** at 1, 25, 50, 75 and 100 ns during the Molecular dynamics simulation

At 1 ns, the water molecule and amino acid residue LYS60 formed hydrogen bond interaction with oxygen atom. Multiple water molecules mediated hydrogen bonds were observed at 25 ns. At 50 ns, another water molecule contributed to the hydrogen bond, and all other interactions remain constant until 50 ns. At 75 ns, amino acid PHE367 established pi-cation interaction with nitro group of the pyrido indole scaffold and ALA365 formed a hydrogen bond with oxygen of ketone. Compound **91** exhibited hydrogen bond interactions at 100 ns between ALA365 and water molecules with the same oxygen atom of the propan-2-one linker. The PHE367 exhibited pi-pi and pi-cation interactions with pyrido indole scaffold and nitrogen atom, respectively (**Figure 7.12**).

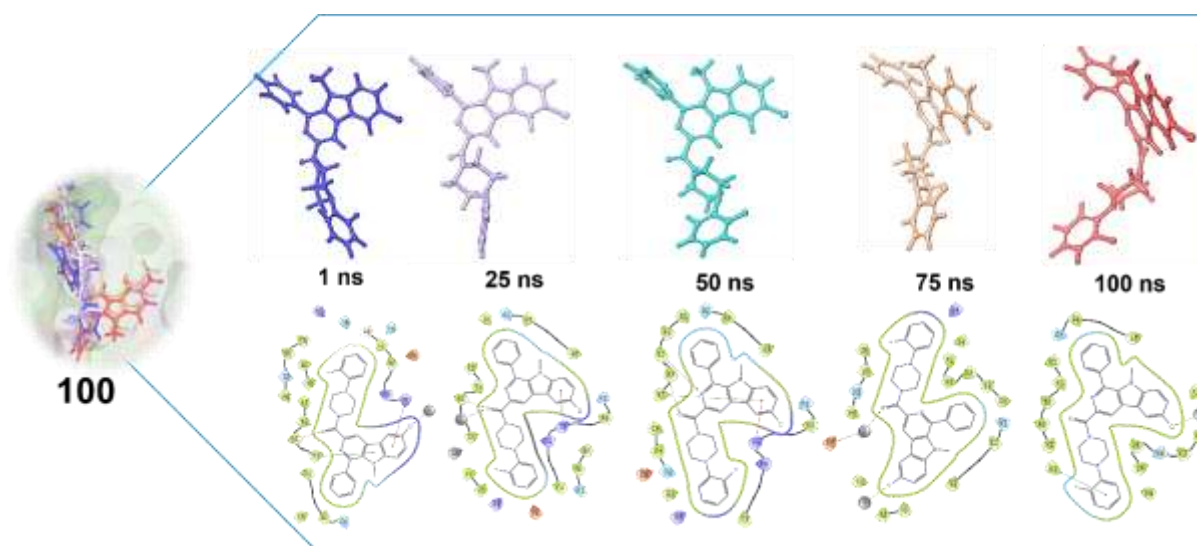
Compound 100

Figure 7.13. Time frame analysis of compound **100** at 1, 25, 50, 75 and 100 ns during the Molecular dynamics simulation

Amino acids PHE367 and LYS61 showed pi-pi stacking and pi-cation interactions with pyrido indole scaffold in **compound 100**. At 25 ns, amino acid ALA365 and one water molecule exhibited hydrogen bonding, while all other interactions remain unchanged. Amino acid ALA365 formed a hydrogen bond with nitrogen of the pyrido indole scaffold at 50 ns (**Figure 7.13**). At 75 ns, two water molecules were seen, one formed halogen bond interaction with chlorine of pyrido indole scaffold, the other hydrogen bond interaction with GLU202 and the oxygen atom of the propan-2-one linker. Amino acid TYR198 formed pi-pi interactions with fluorobenzene, while one water molecule formed halogen bond interactions with chlorine of the pyrido indole scaffold. At 100 ns, no additional substantial alterations were seen for compound **100**.

Compound 77

The amino acid residues PHE367, ALA365 and LYS60 are all actively implicated in hydrogen bond interactions with the molecule **77**. At a timescale of 1 ns, the oxygen atom that is part of the keto group formed a hydrogen bond with ALA365. At a time of 25 ns, the bromine atom was a participant in the hydrogen bond contact. The duration of other exchanges was always 1 ns. In addition, the pyrido indole scaffold demonstrated Pi interactions with LYS61 when the time resolution was raised to 50 ns (**Figure 7.14**). Amino acid PHE367 was engaged in Pi cationic interactions that took place. The formation of hydrogen bond between ALA365 and oxygen atom of the keto group, which was implicated in water-mediated interactions at 75 ns. When compared to the first-time frames, the number of interactions that occurred at 100 ns was significantly lower and only one hydrogen bond was formed with ALA365.

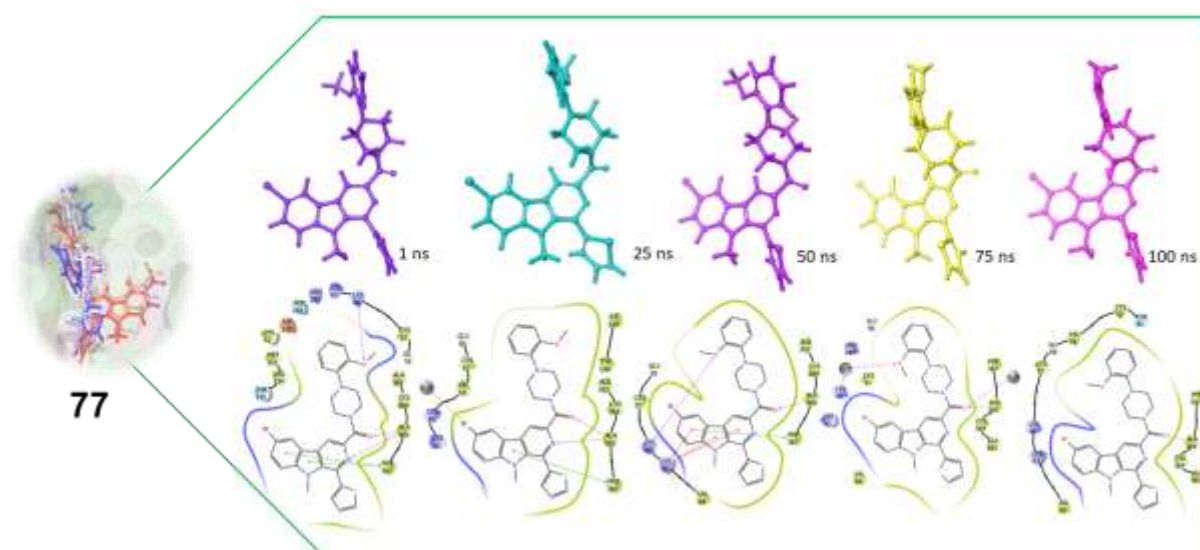


Figure 7.14. Time frame analysis of compound **77** at 1, 25, 50, 75 and 100 ns during the Molecular dynamics simulation

Compound 75

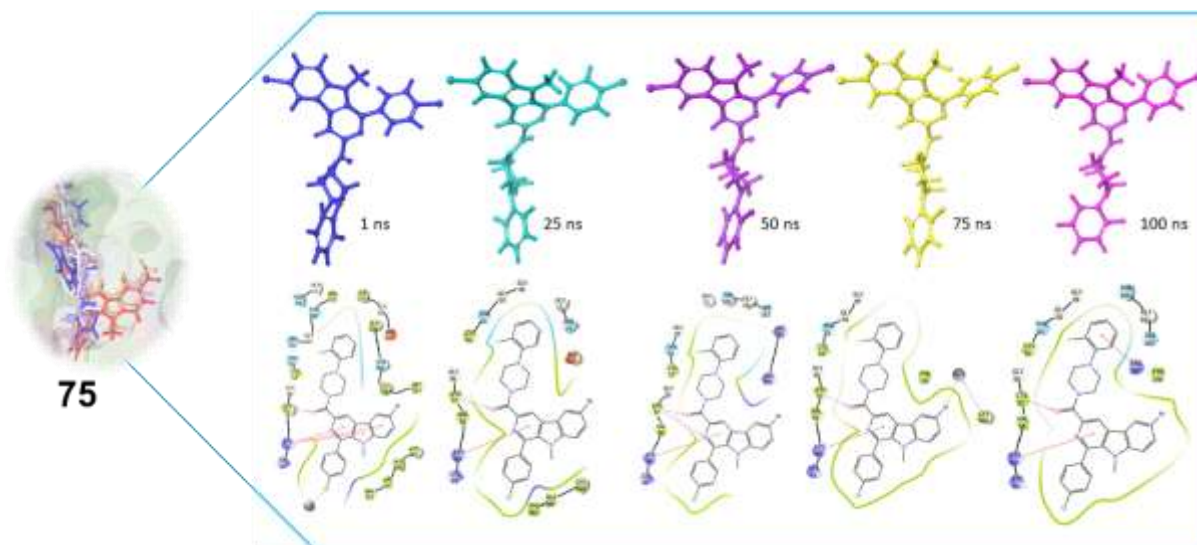


Figure 7.15. Time frame analysis of compound **75** at 1, 25, 50, 75 and 100 ns during the Molecular dynamics simulation

Halogens such as bromine, chlorine and fluorine are the building blocks of the chemical compound **75** (**Figure 7.15**). At 1 ns, there was a full participation of pyrido indole scaffold in the pi cationic interaction that took place with LYS60. Within 25 ns, the number of the same pi connections has been reduced to one. The CYS57 and oxygen atom of the keto group were participated in hydrogen bonding. At 50 ns, one more hydrogen bond was formed with CYS57, while the other interactions remained the same. At a timescale of 75 ns, the same collaborations were maintained, and in addition, one water-mediated connection was also observed between bromine atom. At 100 ns, there was no evidence of any additional charges, except for ARG287, which was implicated in the fluorobenzene pi cationic interactions.

Compound 78

The nitrogen atom of the pyridine ring was involved in hydrogen bond interactions with THR 335 at 1 ns. At a timescale of 25 ns, it was seen that two water-mediated interactions had taken place between the oxygen atom of the keto group. Amino acid PHE365 played a significant role in pi interaction with the benzene ring that contained the methyl group (**Figure 7.16**). At a timescale of 50 ns, no interactions were discovered. At a timescale of 75 ns, the connections with the water molecules were successfully re-established. At 100 ns time scale, the compound **78** attracted more attention due to the largest number of connections it had with the surrounding

amino acid residues. SER178 was involved in the formation of halogen bond with bromine atom. The oxygen atom that was involved in the interactions were mediated by water.

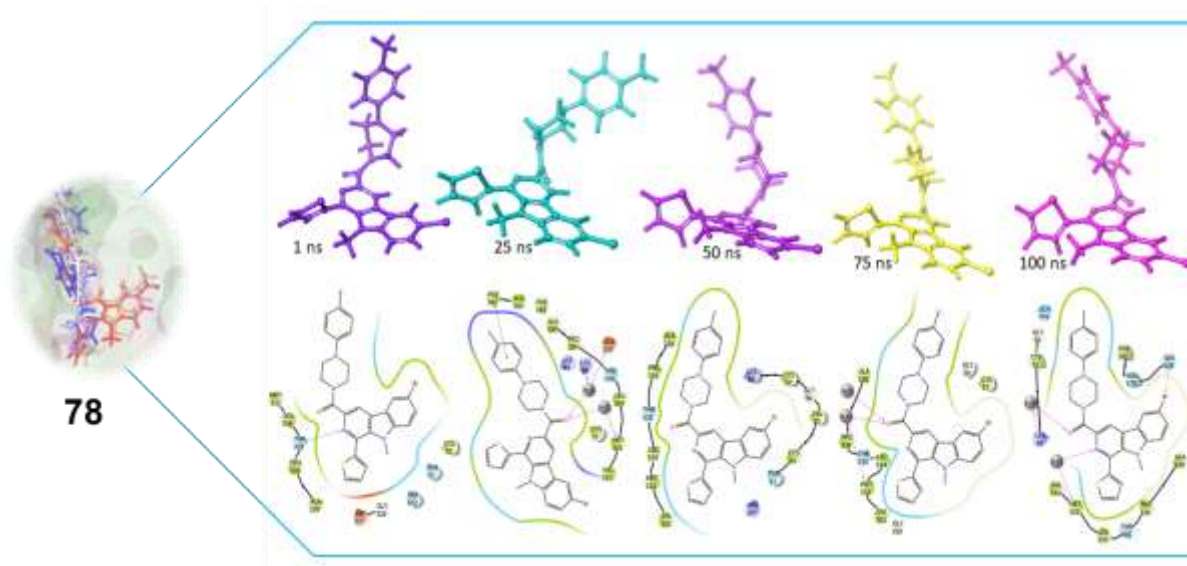


Figure 7.16. Time frame analysis of compound **78** at 1, 25, 50, 75 and 100 ns during the Molecular dynamics simulation

Amino acids such as PHE365, THR335, CYS57, LYS60, ALA365, PHE367 and ARG287 were actively involved in tight holding of the hit molecules at the active site of trypanothione reductase. This is a concluding comment that has obtained from the output of time frame analysis. These amino acids uncovered several contacts with the hit molecules, including hydrogen bonds, aromatic bonds, pi interactions and halogen bonds. In addition to this, several interactions that were mediated by water were also engaged in the process of tightly holding the molecules in the active site of the target protein.

References

- (1) Schrödinger Release 2019-1: Maestro, Schrödinger, LLC, New York, NY, 2019.
- (2) Conners, R.; Schambach, F.; Read, J.; Cameron, A.; Sessions, R. B.; Vivas, L.; Easton, A.; Croft, S. L.; Brady, R. L. Mapping the Binding Site for Gossypol-like Inhibitors of Plasmodium Falciparum Lactate Dehydrogenase. *Molecular and Biochemical Parasitology* **2005**, *142* (2), 137–148. <https://doi.org/10.1016/j.molbiopara.2005.03.015>.
- (3) Schrödinger Release 2019-1: LigPrep, Schrödinger, LLC, New York, NY, 2019.
Schrödinger Release 2019-1: LigPrep, Schrödinger, LLC, New York, NY, 2019.
- (4) Schrödinger Release 2019-1: Schrödinger Suite 2019-1 Protein Preparation Wizard; Epik, Schrödinger, LLC, New York, NY, 2019.
- (5) Schrödinger Release 2020-4: Desmond Molecular Dynamics System, D. E. Shaw Research, New York, NY, 2020. Maestro-Desmond Interoperability Tools, Schrödinger, New York, NY, 2020.
- (6) Mark, P.; Nilsson, L. Structure and Dynamics of the TIP3P, SPC, and SPC/E Water Models at 298 K. *Journal of Physical Chemistry A* **2001**, *105* (43), 9954–9960. <https://doi.org/10.1021/jp003020w>.
- (7) Jorgensen, W. L.; Maxwell, D. S.; Tirado-Rives, J. Development and Testing of the OPLS All-Atom Force Field on Conformational Energetics and Properties of Organic Liquids. *Journal of the American Chemical Society* **1996**, *118* (45), 11225–11236. <https://doi.org/10.1021/ja9621760>.
- (8) Berne, M. T. and B. J. G. J. M. Reversible Multiple Time Scale Molecular Dynamics. *The Journal of Physical Chemistry* **1993**, *97* (51), 13429–13434. <https://doi.org/10.1021/j100153a002>.
- (9) Cheng, A.; Merz, K. M. Application of the Nosé–Hoover Chain Algorithm to the Study of Protein Dynamics. *The Journal of Physical Chemistry* **1996**, *100* (5), 1927–1937. <https://doi.org/10.1021/jp951968y>.
- (10) Kalibaeva, G.; Ferrario, M.; Ciccotti, G. Constant Pressure–Constant Temperature Molecular Dynamics: A Correct Constrained NPT Ensemble Using the Molecular Virial. *Molecular Physics* **2003**, *101* (6), 765–778. <https://doi.org/10.1080/0026897021000044025>.
- (11) Kumar, B. K.; Faheem; Sekhar, K. V. G. C.; Ojha, R.; Prajapati, V. K.; Pai, A.; Murugesan, S. Pharmacophore Based Virtual Screening, Molecular Docking, Molecular Dynamics and MM-GBSA Approach for Identification of Prospective SARS-CoV-2

- Inhibitor from Natural Product Databases. *Journal of Biomolecular Structure and Dynamics* **2022**, 40 (3), 1363–1386. <https://doi.org/10.1080/07391102.2020.1824814>.
- (12) Karan Kumar, B.; Faheem; Balana Fouce, R.; Melcon-Fernandez, E.; Perez-Pertejo Yolanda, Y.; Reguera, R. M.; Adinarayana, N.; Chandra Sekhar, K. V. G.; Vanaparthi, S.; Murugesan, S. Design, Synthesis and Evaluation of Novel β -Carboline Ester Analogues as Potential Anti-Leishmanial Agents. *Journal of Biomolecular Structure and Dynamics* **2022**, 40 (23), 12592–12607. <https://doi.org/10.1080/07391102.2021.1973564>.



Chapter 8. Conclusion and future perspectives



Conclusion and future perspectives

In several countries, leishmaniasis is one of the most frequently found infectious disease affecting larger population. At present there are no vaccines proven to be successful, so the treatment of leishmaniasis is mainly depends on decade old chemotherapy.

β -carboline has a wide range of pharmacological effects, earning it an important place in the field of medicinal chemistry. This dissertation was aimed to investigate the anti-leishmanial potential of β -carboline derivatives. The research was conducted to identify a potentially useful candidate for the treatment of leishmaniasis, the β -carboline molecules were conceived of, constructed and evaluated.

When considered the research that had been previously published, the screening results led to the discovery of some exciting new information. The synthesized compounds were tested for their *in-vitro* anti-leishmanial promastigote activity (using *L. infantum* BCN150 iRFP promastigotes (iRFP-*L. infantum*)), *in-vitro* anti-leishmanial amastigote activity (using *L. infantum* BCN150), cell viability (using the human hepatocarcinoma cell line ATCC HB-8065), TR inhibition and molecular modeling studies. Several noteworthy conclusions gleaned from the screening results were supplied by the findings.

The findings were summarized as follows,

- The investigation begins with the previously identified hit molecules named (4-(2-methoxyphenyl)-piperazin-1-yl) (1-phenyl-9*H*-pyrido-[3,4-*b*]-indol-3-yl)-methanone which revealed EC₅₀ of 2.80 μ M, and the other hit (4-(4-methoxyphenyl)-piperazin-1-yl) (9-methyl-1-phenyl-9*H*-pyrido-[3,4-*b*]-indol-3-yl)-methanone revealed an EC₅₀ of 1.4 μ M against amastigotes.
- The investigation was further proceeded with the modification of β -carboline with substitutions like Nitro, Bromo, Chloro and hydroxy at the 6th position as there were no reports available.
- The β -carboline was synthesized by pictet-spengler reaction followed by acid amide coupling reaction with various substituted phenyl piperazines. The synthesized molecules (Total 128) were characterized by IR, NMR and Mass spectroscopic analytical methods. The molecules were segregated into following series,
- (6-bromo-1-phenyl-9*H*-pyrido-[3,4-*b*]-indol-3-yl) (4-phenylpiperazin-1-yl)-methanone derivatives (**1-16**)
- (6-nitro-1-phenyl-9*H*-pyrido-[3,4-*b*]-indol-3-yl) (4-phenylpiperazin-1-yl)-methanone derivatives (**17-32**)

- (6-chloro-1-phenyl-9*H*-pyrido-[3,4-*b*]-indol-3-yl) (4-phenylpiperazin-1-yl)-methanone derivatives (**33-48**)
- (6-hydroxy-1-phenyl-9*H*-pyrido-[3,4-*b*]-indol-3-yl) (4-phenylpiperazin-1-yl)-methanone derivatives (**49-64**)
- (6-bromo-9-methyl-1-phenyl-9*H*-pyrido-[3,4-*b*]-indol-3-yl) (4-(4-methoxyphenyl)-piperazin-1-yl)-methanone (**65-80**)
- (4-(4-methoxyphenyl)-piperazin-1-yl) (9-methyl-6-nitro-1-phenyl-9*H*-pyrido-[3,4-*b*]-indol-3-yl)-methanone (**81-96**)
- (6-chloro-9-methyl-1-phenyl-9*H*-pyrido-[3,4-*b*]-indol-3-yl) (4-(4-methoxyphenyl)-piperazin-1-yl)-methanone (**97-112**)
- (6-hydroxy-9-methyl-1-phenyl-9*H*-pyrido-[3,4-*b*]-indol-3-yl) (4-(*p*-tolyl)-piperazin-1-yl)-methanone (**113-128**)
- Initially, the titled compounds were designed, predicted for their pharmacokinetic parameters such as Absorption, Distribution, Metabolism, Excretion and Toxicity (ADMET) profiles. The findings of the investigation of 128 compounds were carried out, and it was observed that β -carboline analogues possessed better drug likeness profile and non-toxic in nature (No violations of Lipinski's rule of five and Jorgenson rule of three was observed).
- The titled β -carboline piperazine derivatives were synthesized using DL-Tryptophan as starting material. 5-hydroxy tryptophan was used as starting material for hydroxy substituted analogues. Initial esterification of DL-Tryptophan using thionyl chloride was followed by Pictet-Spengler reaction. Apart from this, nitration, bromination and chlorination at 6th position was also performed.
- The esterified product was oxidized with sulfur and xylene and continued by 9*N*-methylation with methyl iodide in presence of potassium hydroxide. The carboxylic acid key intermediate was treated with appropriate amines (aryl-substituted piperazines) in presence of coupling agent 1-ethyl-3-(3-dimethylaminopropyl)-carbodiimide hydrochloride (EDCI) and hydroxy benzotriazole (HOBt) to obtain the desired products.
- The anti-leishmanial screening of the synthesized analogues was performed in the stages like promastigote, amastigote assays, cell viability assay, selectivity index determination, Trypanothione reductase inhibition assay followed by computational investigations.

Chapter 8. Conclusion and future perspective

- The outcomes of the promastigote inhibitory assay revealed 37 promising molecules. In that 12 molecules were potent than the standard drug Miltefosine. The EC_{50} of compound **72** - $5.20 \pm 0.54 \mu\text{M}$, and compound **60** - $7.59 \pm 2.96 \mu\text{M}$ were potent active molecules. After finding the potent molecules, the significantly active molecules were also identified. A total of 8 molecules were found significant with EC_{50} in the range of 13 to $25 \mu\text{M}$. Around 17 moderately active molecules were also identified with EC_{50} in the range of 25- $50 \mu\text{M}$.
- The consequences of the amastigote inhibitory assay also revealed 47 promising molecules. In that around 12 molecules were potent than the standard drug Miltefosine. The EC_{50} of these compounds were compound **68** - $0.54 \pm 0.039 \mu\text{M}$, compound **70** - $0.46 \pm 0.06 \mu\text{M}$, compound **72** - $1.28 \pm 0.19 \mu\text{M}$, compound **75** - $0.81 \pm 0.11 \mu\text{M}$, compound **77** - $0.45 \pm 0.03 \mu\text{M}$, compound **78** - $3.26 \pm 0.14 \mu\text{M}$, compound **79** - $4.53 \pm 0.64 \mu\text{M}$, compound **87** - $3.43 \pm 0.42 \mu\text{M}$, compound **88** - $1.51 \pm 0.20 \mu\text{M}$, compound **89** - $1.62 \pm 0.09 \mu\text{M}$, compound **91** - $0.94 \pm 0.06 \mu\text{M}$, compound **100** - $1.65 \pm 0.03 \mu\text{M}$ were potent active molecules. After finding the potent molecules, the significantly active molecules were also identified. A total of 9 molecules were found significant with the EC_{50} in the range of 5 to $10 \mu\text{M}$. Around 26 moderately active molecules were also identified with EC_{50} in the range of 10- $25 \mu\text{M}$. This was the most promising study results showed that the molecules were more effective than the existing standard drug Miltefosine.
- In search of dual inhibitors among the series of 128 analogues, around 15 molecules showed dual inhibition against both promastigotes as well as amastigotes. Among these 15 molecules, compound **9** showed EC_{50} - $12.68 \pm 8.171 \mu\text{M}$ (promastigotes), EC_{50} - $8.52 \pm 0.66 \mu\text{M}$ (amastigotes) and compound **72** with EC_{50} - $5.20 \pm 0.54 \mu\text{M}$ (promastigotes), EC_{50} - $1.28 \pm 0.19 \mu\text{M}$ (amastigotes) exhibited notable inhibitory activities.
- The potentially identified hit molecules were found to be non-hepatotoxic in nature. This gave a lucid insight that the hit molecules were safe without any hepatotoxicity. Out of 128 molecules, around 73 molecules exhibited CC_{50} more than $50 \mu\text{M}$. This indicates the screened analogues did not reveal any hepatotoxicity.
- Against promastigotes, compound **100** was discovered to have SI value of 10, however against amastigotes, compound **77** was found to have significant SI value of 218.96.
- The compounds substituted with halogen at 6th position exhibited significant inhibitory properties. The most potent are the ones that have bromine at position 6th and *N*-methyl

group. These findings provided new insight about the necessity of 6th-halo substitution as well as *NI*-methyl group in order to generate potent inhibitors against *L. infantum* amastigotes.

- TR inhibitory activity spectrum of the compounds **78**, **68**, **81**, **70**, **96** and **88** revealed the TR inhibition at 50 μ M were 50 \pm 1 %, 43 \pm 1 %, 38 \pm 5 %, 36 \pm 5 %, 33 \pm 3 % and 31 \pm 2 %, respectively at the tested 50 μ M concentration. At 100 μ M concentration, the compounds **78**, **68**, **81**, **15** and **109** exhibited TR inhibition of 100 \pm 2 %, 63 \pm 1 %, 61 \pm 1 %, 57 \pm 2 % and 47 \pm 1 %, respectively. From the obtained results, it has been presumed that TR is not the only target that the β -carboline derivatives are attempting to hit. Hence, further detailed investigations will be required against other possible available targets of leishmaniasis in order to determine the exact molecular target on which the anti-leishmanial β -carboline analogues will act.
- The molecular docking analysis of the identified hits made it clear that the molecule was potentially bound with the conserved amino acid residues of the Trypanothione reductase target protein.
- The MMGBSA scores vary from -72.75 to -103.45 Kcal/mol. When contrasted to the findings of the docking studies, these are highly encouraging signs.
- Molecular dynamics RMSD plot of protein backbone against each ligand was also plotted and the results showed similar fluctuating patterns of the protein with all the ligands during simulation and the RMSD fluctuated between 2.0 - 5.0 Å.
- From time frame analysis, it has been observed that amino acids such as PHE365, THR335, CYS57, LYS60, ALA365, PHE367 and ARG287 were actively involved in the tight holding of hit molecules against trypanothione reductase. These amino acids uncovered several contacts with the studied hit molecules, including hydrogen bonds, aromatic bonds, pi interactions and halogen bonds. In addition to this, several water mediated interactions were also engaged in the process of tightly holding the hit molecules in the active site of the target protein.

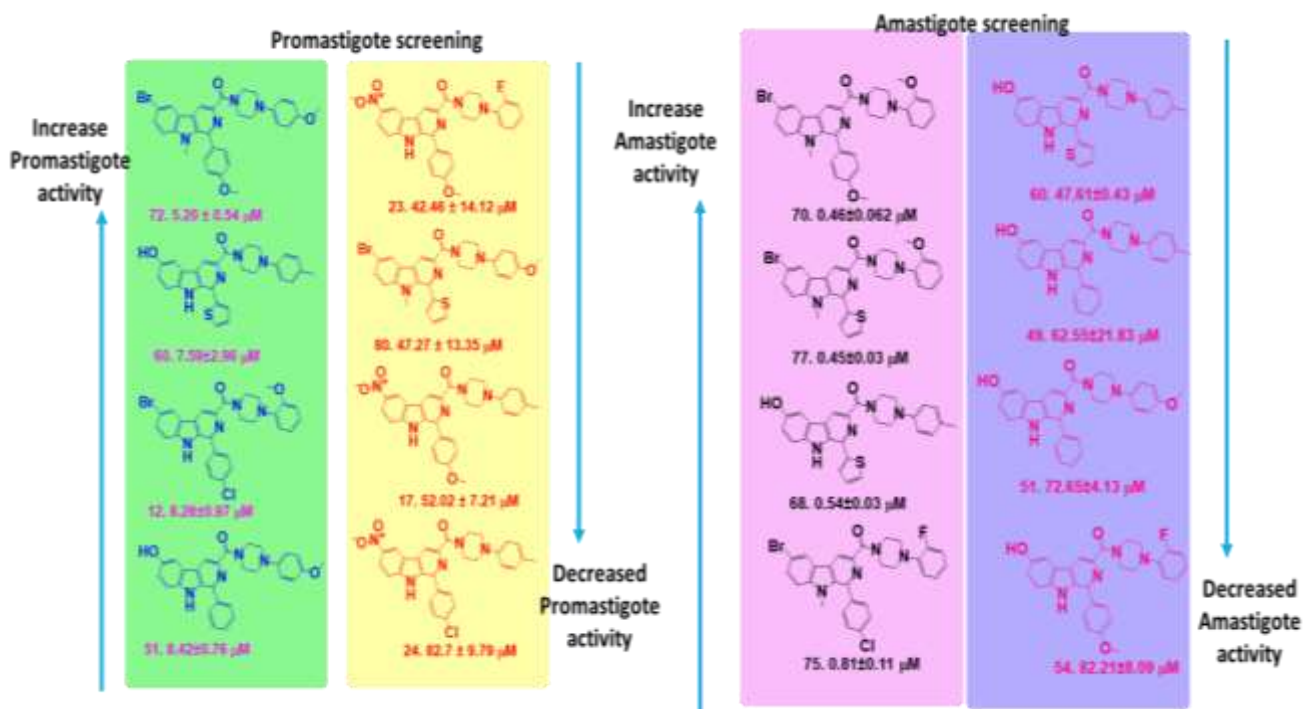


Figure 8.1. Pictorial representation of summarized β-carboline analogues with their promastigote and amastigote activity spectrum

Future perspectives

- ✓ In the realm of study about leishmaniasis, the current examination for the potential antileishmanial effects has discovered some intriguing possibilities.
- ✓ The compounds showed significant EC_{50} against amastigotes were compound **68** - $0.54 \pm 0.039 \mu\text{M}$, compound **70** - $0.46 \pm 0.06 \mu\text{M}$, compound **72** - $1.28 \pm 0.19 \mu\text{M}$, compound **75** - $0.81 \pm 0.11 \mu\text{M}$, compound **77** - $0.45 \pm 0.03 \mu\text{M}$, compound **78** - $3.26 \pm 0.14 \mu\text{M}$, compound **79** - $4.53 \pm 0.64 \mu\text{M}$, compound **87** - $3.43 \pm 0.42 \mu\text{M}$, compound **88** - $1.51 \pm 0.20 \mu\text{M}$, compound **89** - $1.62 \pm 0.09 \mu\text{M}$, compound **91** - $0.94 \pm 0.06 \mu\text{M}$, compound **100** - $1.65 \pm 0.03 \mu\text{M}$. These activity values were significantly potent than the standard drug Miltefosine. These identified compounds were amenable to further modification with a wide variety of substitutions, including methyl, amino and fluoro groups at 6th position which can be used to test their activity spectrum against leishmaniasis.
- ✓ Apart from Trypanothione reductase (TR) as a possible target for the titled β -carboline, molecular mechanistic investigation on other suitable available targets may be performed in order to find out the exact potential target of the tested β -carboline.
- ✓ In order to generate more effective TR inhibitors, BREED technique may be utilised for the designing of newer analogues with enhanced potency and lesser side effects.
- ✓ The above identified lead compounds can be studied for their pharmacokinetic (PK), pharmacodynamics (PD) and safety pharmacological evaluation.
- ✓ The above identified lead compounds can be subjected to developmental studies like pre-formulation, dosage form design and evaluation.
- ✓ The selected lead compounds can be tested for their effectiveness against various allied opportunistic infections such as malaria, tuberculosis and other parasitic diseases for their dual inhibitory potential.



Chapter 9. List of Publications and Conferences



Patent

Title: Discovery of β -carboline molecules to inhibit Trypanothione reductase – A significant development in the treatment of Leishmaniasis

Inventor: Sankaranarayanan Murugesan, Banoth Karan Kumar, Rafael Balana Fouce Kondapalli Venkata Gowri ChandraSekhar (Under submission stage)

List of Publications (Research and Review) from the thesis:

1. **Banoth Karan Kumar**, Faheem, Kondapalli Venkata Gowri ChandraSekhar, Nandikolla Adinarayana, and Sankaranarayanan Murugesan. 2020. “Recent Evolution on Synthesis Strategies and Anti-Leishmanial Activity of β -Carboline Derivatives – An Update.” *Heliyon* 6 (9): e04916. <https://doi.org/10.1016/j.heliyon.2020.e04916>.
2. **Banoth Karan Kumar**, Faheem, Kondapalli Venkata Gowri Chandra Sekhar, Selvaraj Kunjiappan, Joazaizulfazli Jamalis, Rafael Balaña-Fouce and Murugesan Sankaranarayanan. 2021. “Recent Update on the Anti-Infective Potential of β -Carboline Analogs.” *Mini-Reviews in Medicinal Chemistry* 21 (4): 398–425. <https://doi.org/10.2174/1389557520666201001130114>.
3. **Banoth Karan Kumar**, Tewari, Upasana, Divya Sharma, Shrey Srivastava, Faheem, and Sankaranarayanan Murugesan. 2021. “Anti-Tubercular Insights of Carbolines – A Decade Critique.” *ChemistrySelect* 6 (9): 2428–45. <https://doi.org/10.1002/slct.202100181>.
4. **Banoth Karan Kumar**, Faheem, Rafael Balana Fouce, Estela Melcon-Fernandez, Yolanda Perez-Pertejo Yolanda, Rosa M. Reguera, Nandikolla Adinarayana, K. V.G. Chandra Sekhar, Satheeshvarma Vanaparathi, and Sankaranarayan Murugesan. 2022. “Design, Synthesis and Evaluation of Novel β -Carboline Ester Analogues as Potential Anti-Leishmanial Agents.” *Journal of Biomolecular Structure and Dynamics* 40 (23): 12592–12607. <https://doi.org/10.1080/07391102.2021.1973564>.
5. **Banoth Karan Kumar**, Abirami M, Faheem, Sanchita Dey, Samridhi Johri, Rosa M. Reguera, Rafael Balaña-Fouce and Kondapalli Venkata Gowri Chandra Sekhar, Sankaranarayanan Murugesana, Molecular-level strategic goals and repressors in Leishmaniasis – Integrated data to accelerate target-based heterocyclic scaffolds (*Under review in Medicinal Research Reviews*)

List of Publications (Research and Review) other than thesis during the Ph.D. tenure

1. Johri, S.; **Banoth Karan Kumar**, Dey, S.; Faheem; Balana-Fouce, R.; Gowri Chandra Sekhar, K. V.; Kunjiappan, S.; Murugesan, S. Inspection of In-House Designed Novel Thiochromone Amino-Acid Conjugate Derivatives as Lm-NMT Inhibitor – An in-Silico Analysis. *Journal of Molecular Graphics and Modelling* **2023**, *119* (November 2022), 108397. <https://doi.org/10.1016/j.jmgm.2022.108397>.
2. Dey, S.; **Banoth Karan Kumar**, Johri, S.; Faheem; Murugesan, S. Design and Study of Novel Chromone and Thiochromone Derivatives as PflLDH Inhibitors — Computational Approach. *Structural Chemistry* **2022**, *33* (6), 2063–2082. <https://doi.org/10.1007/s11224-022-01974-4>.
3. **Banoth Karan Kumar**, Faheem; Sekhar, K. V. G. C.; Ojha, R.; Prajapati, V. K.; Pai, A.; Murugesan, S. Pharmacophore Based Virtual Screening, Molecular Docking, Molecular Dynamics and MM-GBSA Approach for Identification of Prospective SARS-CoV-2 Inhibitor from Natural Product Databases. *Journal of Biomolecular Structure and Dynamics* **2022**, *40* (3), 1363–1386. <https://doi.org/10.1080/07391102.2020.1824814>.
4. Mandal, S. **Banoth Karan Kumar**, B. K.; Sharma, P. K.; Murugesan, S.; Deepa, P. R. In Silico and in Vitro Analysis of PPAR – α / γ Dual Agonists: Comparative Evaluation of Potential Phytochemicals with Anti-Obesity Drug Orlistat. *Computers in Biology and Medicine* **2022**, *147* (June), 105796. <https://doi.org/10.1016/j.compbiomed.2022.105796>.
5. Chitti, S.; Van Calster, K.; Cappoen, D.; Nandikolla, A.; Khetmalis, Y. M.; Cos, P.; **Banoth Karan Kumar**, Murugesan, S.; Gowri Chandra Sekhar, K. V. Design, Synthesis and Biological Evaluation of Benzo-[d]-Imidazo-[2,1- b]-Thiazole and Imidazo-[2,1- b]-Thiazole Carboxamide Triazole Derivatives as Antimycobacterial Agents. *RSC Advances* **2022**, *12* (35), 22385–22401. <https://doi.org/10.1039/D2RA03318F>.
6. Chitti, S.; Nandikolla, A.; Khetmalis, Y. M.; Van Calster, K.; Kumar, B. V. S.; **Banoth Karan Kumar**, Murugesan, S.; Cappoen, D.; Sekhar, K. V. G. C. Design, Synthesis and Biological Evaluation of Novel Spiro-[Chroman-2,4'-Piperidin]-4-One Analogs as Anti-Tubercular Agents. *Chemistry & Biodiversity* **2022**, *19* (8), 1–9. <https://doi.org/10.1002/cbdv.202200304>.
7. Chitti, S.; Pulya, S.; Nandikolla, A.; Patel, T. K.; **Banoth Karan Kumar**,

- Murugesan, S.; Ghosh, B.; Chandra Sekhar Kondapalli, V. G. Design, Synthesis and Structure–Activity Relationship Studies of Novel Spirochromanone Hydrochloride Analogs as Anticancer Agents. *Future Medicinal Chemistry* **2022**, *14* (5), 325–342. <https://doi.org/10.4155/fmc-2021-0237>.
8. Dessai, P. G.; Dessai, S. P.; Dabholkar, R.; Pednekar, P.; Naik, S.; Mamledesai, S.; Gopal, M.; Pavadai, P.; **Banoth Karan Kumar**, Murugesan, S.; Chandavarkar, S.; Theivendren, P.; Selvaraj, K. Design, Synthesis, Graph Theoretical Analysis and Molecular Modelling Studies of Novel Substituted Quinoline Analogues as Promising Anti-Breast Cancer Agents. *Molecular Diversity* **2022**, No. 0123456789. <https://doi.org/10.1007/s11030-022-10512-7>.
 9. Faheem; Dey, S.; Johri, S.; Abirami, M.; **Banoth Karan Kumar**, Taramelli, D.; Basilico, N.; Balana-Fouce, R.; Gowri Chandra Sekhar, K. V.; Murugesan, S. Search for Structurally Diverse Heterocyclic Analogs as Dual-Acting Antimalarial and Antileishmanial Agents: An Overview. *European Journal of Medicinal Chemistry Reports* **2022**, *4* (2021), 100031. <https://doi.org/10.1016/j.ejmcr.2022.100031>.
 10. Jupudi, S.; Rajagopal, K.; Murugesan, S.; **Banoth Karan Kumar**, Raman, K.; Byran, G.; Chennaiah, J.; Muthiah, V. pillai; Dasan P, B.; Sankaran, S. Identification of Papain-Like Protease Inhibitors of SARS CoV-2 through HTVS, Molecular Docking, MMGBSA and Molecular Dynamics Approach. *South African Journal of Botany* **2022**, *151*, 82–91. <https://doi.org/10.1016/j.sajb.2021.11.033>.
 11. Khetmalis, Y. M.; Chitti, S.; Umarani Wunnava, A.; **Banoth Karan Kumar**, Murali Krishna Kumar, M.; Murugesan, S.; Chandra Sekhar, K. V. G. Design, Synthesis and Anti-Mycobacterial Evaluation of Imidazo[1,2-a]Pyridine Analogues. *RSC Medicinal Chemistry* **2022**, *13* (3), 327–342. <https://doi.org/10.1039/d1md00367d>.
 12. Nandikolla, A.; Mahadu Khetmalis, Y.; Mahalakshmi Naidu, K.; **Banoth Karan Kumar**, Murugesan, S.; Chandra Sekhar, K. V. G. Discovery of Potent Antitubercular Agents: Design, Synthesis and Biological Evaluation of 4-(3-(4-Substitutedpiperazin-1-Yl)-Quinoxalin-2-Yl)-Naphthalen-1-Ol Analogues. *Toxicology in Vitro* **2022**, *82*, 105370. <https://doi.org/10.1016/j.tiv.2022.105370>.
 13. Nandikolla, A.; Singireddi, S.; **Banoth Karan Kumar**, Murugesan, S.; Aggarwal, H.; Balaña-Fouce, R.; Estela, M.-F.; Chandra Sekhar Kondapalli, V. G. Design, Synthesis and Evaluation of Novel Phenanthridine Triazole Analogs as Potential Antileishmanial Agents. *Future Medicinal Chemistry* **2022**, *14* (12), 867–880.

- <https://doi.org/10.4155/fmc-2021-0354>.
14. Rosy, J. C.; Babkiewicz, E.; Maszczyk, P.; Mrówka, P.; **Banoth Karan Kumar**, Murugesan, S.; Kunjiappan, S.; Sundar, K. L-Ornithine-N5-Monooxygenase (PvdA) Substrate Analogue Inhibitors for Pseudomonas Aeruginosa Infections Treatment: Drug Repurposing Computational Studies. *Biomolecules* **2022**, *12* (7), 887. <https://doi.org/10.3390/biom12070887>.
 15. Faheem; **Banoth Karan Kumar**, Chandra Sekhar, K. V. G.; Chander, S.; Kunjiappan, S.; Murugesan, S. Medicinal Chemistry Perspectives of 1,2,3,4-Tetrahydroisoquinoline Analogs – Biological Activities and SAR Studies. *RSC Advances* **2021**, *11* (20), 12254–12287. <https://doi.org/10.1039/D1RA01480C>.
 16. Faheem; **Banoth Karan Kumar**, Venkata Gowri Chandra Sekhar, K.; Chander, S.; Kunjiappan, S.; Murugesan, S. 1,2,3,4-Tetrahydroisoquinoline (THIQ) as Privileged Scaffold for Anticancer de Novo Drug Design. *Expert Opinion on Drug Discovery* **2021**, *16* (10), 1119–1147. <https://doi.org/10.1080/17460441.2021.1916464>.
 17. Ganesan, M. S.; Raja, K.K , Murugesan, S.; **Banoth Karan Kumar**, Faheem, F.; Thirunavukkarasu, S.; Shetye, G.; Ma, R.; Franzblau, S. G.; Wan, B.; Rajagopal, G. Quinoline-Proline, Triazole Hybrids: Design, Synthesis, Antituberculosis, Molecular Docking, and ADMET Studies. *Journal of Heterocyclic Chemistry* **2021**, *58* (4), 952–968. <https://doi.org/10.1002/jhet.4229>.
 18. Kunjiappan, S.; Sankaranarayanan, M.; **Banoth Karan Kumar**, Pavadai, P.; Babkiewicz, E.; Maszczyk, P.; Glodkowska-Mrowka, E.; Arunachalam, S.; Ram Kumar Pandian, S.; Ravishankar, V.; Baskararaj, S.; Vellaichamy, S.; Arulmani, L.; Panneerselvam, T. Capsaicin-Loaded Solid Lipid Nanoparticles: Design, Biodistribution, in Silico Modeling and in Vitro Cytotoxicity Evaluation. *Nanotechnology* **2021**, *32* (9), 095101. <https://doi.org/10.1088/1361-6528/abc57e>.
 19. Nandikolla, A.; Srinivasarao, S.; **Banoth Karan Kumar**, Murugesan, S.; Aggarwal, H.; Balaña-Fouce, R.; Melcón-Fernandez, E.; Pérez-Pertejo, Y.; Chandra Sekhar, K. V. G. Novel Phenanthridine Amide Analogs as Potential Anti-Leishmanial Agents: In Vitro and in Silico Insights. *Bioorganic Chemistry* **2021**, *117*, 105414. <https://doi.org/10.1016/j.bioorg.2021.105414>.
 20. Nandikolla, A.; Srinivasarao, S.; Khetmalis, Y. M.; **Banoth Karan Kumar**, Murugesan, S.; Shetye, G.; Ma, R.; Franzblau, S. G.; Sekhar, K. V. G. C. Design, Synthesis and Biological Evaluation of Novel 1,2,3-Triazole Analogues of Imidazo-

- [1,2-a]-Pyridine-3-Carboxamide against Mycobacterium Tuberculosis. *Toxicology in Vitro* **2021**, *74*, 105137. <https://doi.org/10.1016/j.tiv.2021.105137>.
21. Ashoka, P.; Faheem; **Banoth Karan Kumar**, Chander, S.; Chandra Sekhar, K. V. G.; Sankaranarayanan, M. Anti-Infective Potential of Manzamine Alkaloids - A Review. *Medicinal Chemistry* **2021**, *18* (6), 629–654. <https://doi.org/10.2174/1573406417666210803101740>.
 22. Chitti, S.; Pulya, S.; Nandikolla, A.; Patel, T. K.; **Banoth Karan Kumar**, Murugesan, S.; Ghosh, B.; Sekhar, K. V. G. C. Design, Synthesis and Biological Evaluation of 7-(5-((Substituted – Amino)-Methyl)-Thiophen-2-Yl)-Spiro-[Chroman-2,4'-Piperidin]-4-One Hydrochloride Analogues as Anticancer Agents. *Bioorganic Chemistry* **2021**, *112*, 104865. <https://doi.org/10.1016/j.bioorg.2021.104865>.
 23. Kharkwal, H.; **Banoth Karan Kumar**, Murugesan, S.; Singhvi, G.; Avasthi, P.; Goyal, A.; Jamalis, J.; Chander, S. Search for New Therapeutics against HIV-1 via Dual Inhibition of RNase H and Integrase: Current Status and Future Challenges. *Future Medicinal Chemistry* **2021**, *13* (3), 269–286. <https://doi.org/10.4155/fmc-2020-0257>.
 24. Faheem; **Banoth Karan Kumar**, Sekhar, K. V. G. C.; Kunjiappan, S.; Jamalis, J.; Balaña-Fouce, R.; Tekwani, B. L.; Sankaranarayanan, M. Druggable Targets of SARS-CoV-2 and Treatment Opportunities for COVID-19. *Bioorganic Chemistry* **2020**, *104*, 104269. <https://doi.org/10.1016/j.bioorg.2020.104269>.
 25. Ganesan, M. S.; Raja, K. K.; Murugesan, S.; **Banoth Karan Kumar**, Rajagopal, G.; Thirunavukkarasu, S. Synthesis, Biological Evaluation, Molecular Docking, Molecular Dynamics and DFT Studies of Quinoline-Fluoroproline Amide Hybrids. *Journal of Molecular Structure* **2020**, *1217*, 128360. <https://doi.org/10.1016/j.molstruc.2020.128360>.
 26. Ganesan, M. S.; Raja, K. K.; Narasimhan, K.; Murugesan, S.; **Banoth Karan Kumar**. Design, Synthesis, α -Amylase Inhibition and in Silico Docking Study of Novel Quinoline Bearing Proline Derivatives. *Journal of Molecular Structure* **2020**, *1208*, 127873. <https://doi.org/10.1016/j.molstruc.2020.127873>.
 27. Kamat, V.; Santosh, R.; Poojary, B.; Nayak, S. P.; **Banoth Karan Kumar**, Sankaranarayanan, M.; Faheem; Khanapure, S.; Barretto, D. A.; Vootla, S. K. Pyridine- and Thiazole-Based Hydrazides with Promising Anti-Inflammatory and

- Antimicrobial Activities along with Their In Silico Studies. *ACS Omega* **2020**, *5* (39), 25228–25239. <https://doi.org/10.1021/acsomega.0c03386>.
- 28.** Nandikolla, A.; Srinivasarao, S.; **Banoth Karan Kumar**, Murugesan, S.; Aggarwal, H.; Major, L. L.; Smith, T. K.; Chandra Sekhar, K. V. G. Synthesis, Study of Antileishmanial and Antitrypanosomal Activity of Imidazo Pyridine Fused Triazole Analogues. *RSC Advances* **2020**, *10* (63), 38328–38343. <https://doi.org/10.1039/D0RA07881F>.
- 29.** Pola, S.; **Banoth Karan Kumar**, Sankaranarayanan, M.; Ummani, R.; Garlapati, A. Design, Synthesis, in Silico Studies, and Evaluation of Novel Chalcones and Their Pyrazoline Derivatives for Antibacterial and Antitubercular Activities. *Medicinal Chemistry Research* **2020**, *29* (10), 1819–1835. <https://doi.org/10.1007/s00044-020-02602-8>.
- 30.** Srinivasarao, S.; Nandikolla, A.; Suresh, A.; Ewa, A.-K.; Głogowska, A.; Ghosh, B.; **Banoth Karan Kumar**, Murugesan, S.; Pulya, S.; Aggarwal, H.; Sekhar, K. V. G. C. Discovery of 1,2,3-Triazole Based Quinoxaline-1,4-Di-N-Oxide Derivatives as Potential Anti-Tubercular Agents. *Bioorganic Chemistry* **2020**, *100*, 103955. <https://doi.org/10.1016/j.bioorg.2020.103955>.

Book chapter published during the Ph.D. tenure

1. Gourav Rakshit, Sheikh Murtuja, **Banoth Karan Kumar**, Sankaranarayanan Murugesan, and V. J. *Structure-Based Drug Design Structure-Based Drug Design*, Mithun Rud.; Elsevier, 2022; Vol. 384.

List of conferences (presented and attended) during the Ph.D. tenure

1. **Banoth Karan Kumar**, Faheem, Kondapalli Venkata Gowri Chandra Sekhar, Murugesan Sankaranarayanan. Paper entitled "Preliminary investigation of drug repurposing as a direction towards anti-Leishmanial drug discovery" presented at International Conference on Drug Discovery ICDD-2020, BITS-Pilani, Hyderabad campus, Telangana. Feb-29th-Mar-2nd 2020.
2. **Banoth Karan Kumar**, Faheem, Suraj Pyarelal Gupta, K.V.G. Chandrashekar, Murugesan Sankaranarayanan. Paper entitled "In-silico target identification of novel anti-leishmanial β -carboline analogues" presented at 26th Indian Society for Chemists and Biologists Conference jointly organized with 5th Nirma Institute of Pharmacy International Conference, Ahmedabad. January 22-24, 2020.
3. Shivani Pola, **Banoth Karan Kumar**, Murugesan Sankaranarayanan, Ramesh Ummani, Achaiah Garlapati Paper entitled "Design, Synthesis, In-Silico Studies and Screening of Novel Chalcones and Their Pyrazoline Derivatives Against Mycobacterium Tuberculosis" presented at International Conference on Drug Discovery ICDD-2020, BITS-Pilani, Hyderabad campus, Telangana. Feb-29th-Mar-2nd 2020.
4. Komal Daipule, Mallika Alvala, **Banoth Karan Kumar**, Murugesan Sankaranarayanan, Yong-Tang Zheng Paper entitled "In-vitro anti-HIV evaluation of novel amide and ether conjugates of 2, 3-diaryl thiazolidin-4-ones" " presented at International Conference on Drug Discovery ICDD-2020, BITS-Pilani, Hyderabad campus, Telangana. Feb-29th-Mar-2nd 2020.
5. Faheem, Suraj Pyarelal Gupta, **Banoth Karan Kumar**, K.V.G. Chandrashekar, Murugesan Sankaranarayanan. Paper entitled "Design and In-Silico study of novel Isatin analogues as potential anti-HIV agents with extended activity against mutant strains" presented at 26th Indian Society for Chemists and Biologists Conference jointly organized with 5th Nirma Institute of Pharmacy International Conference, Ahmedabad. January 22-24, 2020.

6. Suraj Pyarelal Gupta, Faheem, **Banoth Karan Kumar**, Murugesan Sankaranarayanan. Paper entitled "In Silico Target Identification Study of Novel Anti-Leishmanial Agents" presented at 26th Indian Society for Chemists and Biologists Conference jointly organized with 5th Nirma Institute of Pharmacy International Conference, Ahmedabad. January 22-24, 2020.
7. **Banoth Karan Kumar**, Faheem, Suraj Gupta, Moorthiamma Sarathy Ganesan, Sankaranarayanan Murugesan, paper entitled "In-silico design and study of novel proline derivatives as a potential inhibitor of α -amylase" accepted for presentation at 3rd National Conference on New Frontiers in Chemistry-From Fundamentals to Applications-III, organized by Department of Chemistry, BITS Pilani, K.K. Birla Goa Campus, Goa, Zuari Nagar, Goa-403726, December 20-22, 2019.
8. D. Mounika, **Banoth Karan Kumar**, S. Murugesan. Paper entitled "Design and study of novel Isatin analogues as potential anti-HIV agents" presented at International Conference on Life Science Research & its Interface with Engineering and Allied Sciences (LSRIEAS 2018) organized by Department of Biological Sciences, BITS Pilani, Pilani Campus, Pilani-333031. Rajasthan. India. November 1-3, 2018.
9. **Banoth Karan Kumar**, K. Ratnakar reddy, G. Achaiah, S. Murugesan. Paper entitled "3-Styryl-4H-Chromen-4-One Derivatives as Novel Cytotoxic Agents" presented at National Conference on Emerging Trends in Computational Drug Discovery organized by KIET Group of Institutions, Ghaziabad-201206. Uttar Pradesh, India. August 16-17, 2018. (Got second prize in technical oral presentation).

List of conference proceedings during the Ph.D. tenure

1. Sankaranaayanan Murugesan, **Banoth Karan Kumar**, Faheem and Kondapalli Venkata Gowri Chandrasekhar. Preliminary investigation of drug re-purposing as a direction towards anti-Leishmanial drug discovery (January 31, 2020). Proceedings of International Conference on Drug Discovery (ICDD) 2020, <http://dx.doi.org/10.2139/ssrn.3529249>.
2. Daipule Komal, Alvalaa Mallika, **Banoth Karan Kumar**, Sankaranarayanan, Murugesan, Zheng Yong-Tang and Shilkar Deepak. In-Vitro Anti-Hiv Evaluation of Novel Amide and Ether Conjugates of 2, 3-Diaryl-1, 3-Thiazolidin-4-Ones (February 9, 2020). Proceedings of International Conference on Drug Discovery (ICDD) 2020, SSRN: <https://ssrn.com/abstract=3534912>.

Bibliography

Prof. S. Murugesan is currently working as an Associate Professor in the Department of Pharmacy, BITS Pilani, Pilani Campus, Pilani, Rajasthan. He completed his graduation in Pharmacy from Dr. M.G.R Medical University, Tamilnadu, in the year 1999. He obtained his master 's degree in Pharmacy from BITS Pilani, Pilani Campus, Pilani, Rajasthan, India, in 2002. Later, in the year 2006, he got enrolled in Ph. D. under the guidance of Dr. Swastika Ganguly and acquired his doctorate in the year 2009 from Birla Institute of Technology, Mesra, Ranchi, India. During the doctoral study, he worked in the area of design, synthesis and biological evaluation of novel benzopiperidine analogues as anti-HIV agents; in addition, he also studied the anti-infective activity of synthesized compounds against various bacterial and fungal strains. Then, he joined the Department of Pharmacy, BITS Pilani, Pilani Campus, Pilani as an assistant professor in the year 2010 and pursuing his teaching activity for B. Pharmacy and M. Pharmacy programs till date. In parallel, Dr. Murugesan is actively involved in computer-aided drug design and drug synthesis against HIV and allied opportunistic infections. He had more than 15 years of teaching and research experience. He has guided more than 30 B. Pharm, 25 M. Pharm students to fulfil their dissertation work. Two scholars have already completed a full-time doctorate, while eight are pursuing under his guidance. He has completed 3 research projects, including two as major projects from DST-SERB and DBT, India. Dr. Murugesan has published more than 100 research papers in various peer-reviewed journals of international and national repute and presented more than 100 papers / posters in various international and national conferences. He also published six book chapters in well renowned publishers.

Banoth Karan Kumar is currently pursuing his Ph.D. under Prof. S. Murugesan in the Department of Pharmacy, Birla Institute of Technology and Science Pilani, Pilani Campus, Pilani, Rajasthan. Mr. Karan has Pharmaceutical Chemistry background in his master's degree and graduated from University College of Pharmaceutical Sciences, Kakatiya University, Warangal. He published 40 research and review articles in various peer-reviewed journals of international and national repute to his credit. In addition to that, he also presented 15 papers / posters at various international and national conferences. His current research area includes design, synthesis, molecular docking and dynamics studies for infectious diseases like leishmaniasis, malaria and tuberculosis.